MODELLING THE DYNAMIC REPONSE OF EMERGENCY SHUT-DOWN VALVES FOLLOWING FULL BORE RUPTURE OF LONG PIPELINES

A thesis submitted to the University of London for the degree of Doctor of Philosophy

by

Pratik Saha

Department of Chemical and Biochemical Engineering
University College London
Torrington Place
London WC1E 7JE
December 1997

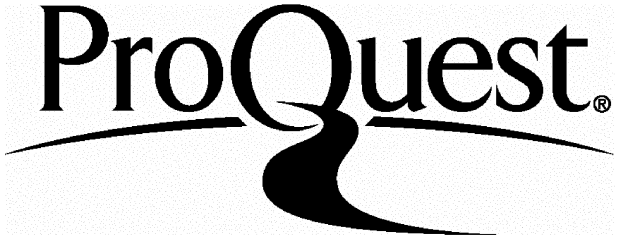

ABSTRACT

This thesis describes the development of a numerical simulation based on the method of characteristics (MOC) for full bore rupture (FBR) of long pipelines containing high pressure hydrocarbons. The Peng-Robinson equation of state coupled with the assumption of thermal equilibrium and homogeneous flow are used to generate the appropriate vapour/liquid equilibrium data. A variety of solution techniques including the use of a second order MOC in conjunction with a nested grid system have been developed in order to investigate their effects on computation run times and accuracy.

The above, together with the use of a DEC Workstation, has allowed for the first time, the validation of a MOC model by comparison with intact end pressure data logged for 20,000s following FBR of the Piper-Alpha main riser. Excellent agreement is obtained. Comparison with field data obtained following FBR of LPG pipelines also gives good agreement.

The main part of the thesis describes the application of the simulation for the study of the dynamic response of ball valves and check valves following hypothetical FBR of a long pipeline containing either gas or a two-phase mixture. A variety of scenarios including the effects of valve proximity to the rupture plane and the delay in closure on the total amount of inventory released prior to pipeline isolation are analysed. The accompanying pressure oscillations and surges are also accounted for. The results are in turn used to recommend guidelines regarding the appropriate choice of emergency shut-down valve depending on the failure scenario.

To my wife
for everything

ACKNOWLEDGMENTS

A special thank you to Dr. Haroun Mahgerefteh for his invaluable support, constant encouragement and guidance throughout this work.

Many thanks also to my family for always believing it was possible and for their constant motivation.

Sincerest thanks to my dear friend Renee Boerefijn without whose help, this work would not have realised its just conclusion.

Finally, I wish to express my gratitude to all my colleagues for creating the right atmosphere for informed discussions and providing the wit and humour necessary to survive a PhD.

LIST OF CONTENTS

CHAPTER 5: DEVELOPMENT AND VALIDATION OF THE CNGS-HEM MODEL AND ITS APPLICATION IN PREDICTING ESDV OR SSIV RESPONSE

CHAPTER 1: INTRODUCTION

Long pipelines are frequently used for the transport of large quantities of hydrocarbons under high pressure. In the case of a typical offshore platform in the North Sea for example, the amount of gas present in a 150 km pipeline at 100 bar is 637,000 kg. This represents an enormous source of energy release which in the event of full bore pipeline rupture (FBR) poses the risks of general and extreme fire exposure to all personnel in 'open platform' areas, and also undermines platform integrity. The Piper Alpha tragedy (Cullen, 1990) clearly demonstrated the catastrophic nature of this type of accident.

The risk of FBR is of course not confined to offshore installations. Table 4.1.1 lists some of the documented cases (Bond, 1996) of pipeline rupture in the past two decades which have resulted in numerous fatalities and damage to the environment.

In order to isolate and thereby limit the amount of inventory which may be released as a result of pipeline rupture, it is now a statutory requirement (HMSO, 1989) that for offshore marine pipelines, riser ESDV's have to be provided. They are always driven thus excluding certain types of valve such as check valves which are non-automatic. In addition to riser ESDV's, protection can also be provided by subsea isolation valves (SSIV's) although this is as yet, free of any statutory requirement. SSIV's can be either automatic or non-automatic.

In offshore operations, the responsibility is then placed upon the operators of the platform to demonstrate, through the Safety Case (HMSO, 1992), that all hazards arising from pipeline rupture are addressed and satisfactorily accommodated. Central to this type of analysis is the evaluation of the release rate and its variation with time in the event of FBR during isolated (ESDV operating) and un-isolated (ESDV disabled) release. Such data have an important bearing on almost every safety aspect of the platform including the survival time of the temporary safe refuge.

DATE	LOCATION	NATURE OF ACCIDENT	DAMAGE CAUSED
9 December 1970	Port Hudson; Missouri; USA	Rupture of 20.32cm propane pipeline releasing 60 tonnes of gas	Ignition of gas caused explosion and a firestorm. 10 injured.
24 October 1978	Brookside Village; Texas; USA	76.2cm natural gas pipeline ruptured and caused extensive damage	41 injured and 6 deaths
28 July 1988	San Juan De Los Reyes; Mexico	Oil pipeline explosion	10000 people had to be evacuated, 80 injured and 11 deaths
28 August 1988	Juan Diaz Covarrubias; Mexico	76.2 inch pipeline ruptured along 4 km length. Caused fire of 4.8 km radius	Fire burned for 5 hours and 20000 barrels of crude oil lost. 80 injured and 12 deaths
9 November 1988	Mahul; Bombay; India	Naptha pipeline ruptured and spilt inventory caught fire	Structural damage. 40 injured and 12 deaths
30 January 1992	Baku Area; Azerbaijan	Crude oil pipeline ruptured	Spilt crude oil entered water pumping system
March 1992	Penza Oblast; Russia	Druzhba oil pipeline ruptured leading to the loss of 6000m^3 oil	Massive pollution of local river
29 September 1993	Caracas; Miranda State; Venezuela	Rupture of natural gas pipeline	60 deaths as a result of the blast
October 1994	Usinsk Area; Russia	Major crude oil pipeline rupture	Leakage over 14400m^2 occurred. 120000 tonnes of oil spilt over Tundra river Pechora

Table 4.1.1: A listing of some of the major accidents relating to pipeline rupture (Bond, 1996).

Basically, there are two types of valves which may be employed for emergency shutdown. These include ball valves which are self-activating on sensing a drop in pressure, or check valves which serve the function of emergency block valve when the rupture flow is the reverse of the normal direction of flow. Associated with each valve, there are two characteristic time domains which govern their performance. The first, here defined as the activation time t_a, is dictated by the time lapsed for fluid disturbances initiated as a result of FBR to be transmitted from the rupture plane to the location of the ESDV. The other, defined as the closure time, t_c is a design parameter and corresponds to the time it takes for the valve to close from the moment it is activated until its complete closure. The valve response time, t_r is the summation of the two.

The choice of the appropriate valve presents design and safety engineers with a dilemma.

The advantage of a check valve is its low t_c, thus minimising the amount of inventory loss following FBR. This may however be at a cost of dangerously high pressure surges resulting from bringing the high velocity escaping fluid to rest (Wylie and Streeter, 1978); Thorley, 1989; Perko, 1986; Koetzier et. al., 1986). Although such problems are normally insignificant in the case of a ball valve due to its gradual closure, significant amounts of inventory may escape during this period. This effect becomes particularly important near the rupture plane where massive amounts of inventory are released in a very short space of time. In addition ball valves, particularly those suitable for offshore applications are very expensive and normally duplicated.

This thesis describes the development of a mathematical model based on the Method of Characteristics (MOC) for simulating fluid dynamic effects following FBR of long pipelines containing high pressure gas or two phase mixtures. A variety of solution techniques including the use of nested grid systems in conjunction with second order characteristics are employed. Their effects on CPU and accuracy are investigated. This is then followed by application of the model in predicting the dynamic response of ESDV's subsequent to FBR.

The development process for a transient two-phase fluid flow model entails three main steps. Firstly, the basic equations governing the flow, the thermodynamics, and the initial and boundary conditions need to be formulated. Secondly, an efficient and accurate method of resolving these equations needs to be chosen and implemented. Finally validation of the model with experimental data or actual records is necessary.

Chapter 2 deals entirely with the first step. The basic partial differential equations of flow are derived for unsteady quasi-one-dimensional flow of fluids through a rigid constant cross-section area of pipe. The various assumptions made in their derivations are explained. The derived partial differential equations pertaining to conservation of mass, momentum and energy together with an equation of state (EOS) constitute a system of equations that are essentially Euler equations with stiff source terms due to the friction term in the momentum equation and the heat transfer term in the energy equation. The thermodynamic relationships that are needed to deal effectively with the presence of a real fluid (single and two phase) are also presented.

The appropriate vapour liquid equilibrium data are obtained using the HTSFLASH programme developed by Michelsen (1982, 1987) incorporating Peng-Robinson equation of state (Peng and Robinson, 1976).

In chapter 3, a mathematical description of the hyperbolic nature of the Euler equations is described. This is followed by a review of all available approaches to the numerical resolution of the Euler equations including the method of characteristics (MOC) which is the preferred method in this study. This is then followed by a description of the methods used by various authors to model fluid dynamic effects during FBR.

Chapter 4 describes the development of a methodology based on the MOC for the solution of the conservation equations in conjunction with an ideal gas. This involves:

- transformation of the partial differential equations, derived in Chapter 2, to particular total differential equations called the compatibility equations,
- solution of the compatibility equations based on a new modification to the classical method of specified time intervals (ST), and using the Euler predictor-

corrector technique (Zucrow and Hoffman, 1976) to enhance accuracy of the numerical analysis. This technique utilises first order finite difference discretisation of the compatibility equations for the predictor step followed by a second order discretisation for the corrector step.

Various procedures with the primary objective of reducing the CPU run times without compromising accuracy in order to produce an optimised model are also discussed. These include the application of a nested grid system (CNGS) as well as the use of curved characteristics.

Accuracy of the simulation is assessed by comparing output data with measurements taken during the Piper Alpha tragedy, and by making comparisons with results obtained by the models of Chen et. al (1992).

Some workers such as Flatt (1985), and Olorunmaiye and Imide (1993) respectively make the assumption of adiabatic and isothermal flow following FBR. The deficiencies of these approaches with respect to accurate prediction over long depressurisation times, and the influence of fire on the rate of heat transfer to the fluid are also highlighted.

The optimised model is then used to simulate the dynamic response of emergency shutdown of both ball and check valves subsequent to FBR. The principal aim is to demonstrate the importance of predicting the rapid variations in the fluid dynamics within the pipeline during FBR and their influence on the appropriate choice of ESDV. Of particular interest are the evaluations of lost inventory and resulting pressure surges as a function of valve proximity to the rupture plane and its response time. Pipelines containing gases whose behaviour may be approximated as ideal are considered here.

In chapter 5, the CNGS coupled with the Homogeneous Equilibrium Model, (CNGS-HEM) is used to derive the relevant characteristic and compatibility equations for simulating FBR of pipelines containing two-phase multi-component hydrocarbon mixtures.

In solving these equations, particular areas of attention, primarily due to the highly non-linear variation of the physical properties of such fluids are:

- use of a flash calculation procedure for accurate prediction of fluid properties such as ρ, a and P at each node, and at each interpolation point during the numerical discretisation
- accurate prediction of the 'wall' friction factor as it is shown that this parameter has an important effect on fluid dynamics
- the calculation for the initial conditions (t=0) at the broken end
- direct use of the method of characteristics to calculate fluid conditions at the boundaries between the coarse and fine grids. Linear interpolation is not deemed to be sufficiently accurate for this purpose
- use of curved characteristics near the rupture plane
- use of smaller than maximum permissible Δt, according to the CFL condition, for accurate simulation of the choking condition, thus avoiding numerical instability.

The above is followed by optimisation and validation of the model by comparison with various field data. The modifications to the classical ST method and access to a DEC workstation has meant that the MOC, as used in CNGS-HEM, has been used for the first time to validate two-phase transient flow in long pipelines over a long duration (> 30 minutes). Validations of the CNGS-HEM model are performed in conjunction with measured data taken after the accidental rupture of Piper-Alpha, and also with data regarding the Isle of Grain pipeline depressurisation tests conducted by Shell and BP.

The validated model is then used to predict the dynamic response of ESDV's or SSIV's following FBR of a pipeline containing a condensable gas mixture and comparisons are made in terms of the general trends observed in chapter 4 for pipelines containing permanent gases.

Chapter 6 deals with general conclusions and suggestions for future work.

CHAPTER 2: THEORETICAL MODELLING OF PIPELINE RUPTURE

2.1 INTRODUCTION

Full-bore rupture (FBR) of a high pressure pipeline can be described by a massive release at the rupture plane followed immediately by a large drop in pressure and highly transient flow within the pipeline. The development of a transient two-phase fluid model entails three main steps. Firstly, the basic equations governing the flow, the thermodynamics, and the initial and boundary conditions need to be formulated. Secondly, an efficient and accurate method of resolving these equations needs to be chosen and implemented. Finally validation of the model with experimental data is needed.

This chapter deals entirely with the first step. The numerical discretisation techniques available to solve these equations will then be reviewed in Chapter 3 followed by a review of methods used by past researchers to solve this problem.

Many models exist for the analysis of fluid transients in closed conduit circuits but only a few are applicable to FBR scenarios. A considerable difficulty has existed in modelling the fast transient behaviour of the fluid that occurs at the ruptured end, specifically the choking or critical flow condition that inevitably follows rupture of a high pressure pipeline. The physical choking condition for a gas states that the flow velocity equals the local speed of sound which imposes a stiff boundary condition (Picard & Bishnoi, 1989, Chen, J.R. 1993, Flatt, 1986). This condition is very rare for liquid flows since the speed of sound for liquids is usually more than 1500 m/s. For gas flows however, comparatively low local sound speeds (usually about 400 m/s) mean that the choking condition is quickly reached.

The unsteady flow of compressible fluids in pipelines is described by a set of three partial differential equations derived from the principles of conservation of mass (continuity equation), conservation of momentum or Newton's second law of motion (equation of motion or momentum equation) and conservation of energy or first law

of thermodynamics (energy equation). The fluid properties can be described by an appropriate equation of state. These together with appropriate auxiliary conditions, determine the mathematical state of the fluid. The most complete formulation to describe any fluid flow situation are the Navier-Stokes equations which allow for variation of fluid property in four dimensions, i.e. the three dimensions of space, x,y, and z, and also time, t. In order to resolve these equations numerically closure relations need to be provided to account for both the diffusive and source terms, thus yielding a system of equations that is extremely complicated.

Solving the full system is the ultimate goal of a numerical flow simulation but the numerical discretisation necessary to accomplish this for a whole range of fluid flows is extremely difficult and requires substantial computer resources. In fact, only very simplified flow systems are computed at present to such a high level of approximation. It is always necessary to ask the question if it is necessary to resolve every term in the Navier-Stokes equation. Depending on the type of flow scenario that needs resolving, certain terms in the equations will have a negligible outcome on the final solution anyway and can therefore effectively be ignored without any serious loss of accuracy.

The final form of these equations, ready for numerical discretisation, can be arrived at through many assumptions and simplifications. Based on the above, the equations may, in the more general classification, be linear, quasi-linear or non-linear, parabolic or hyperbolic, and first- or second-order.

Great simplifications to the governing equations can greatly reduce computer run times, but this might well be at a cost to accuracy of the final solution. For example, Bell (1978) used a simple exponential model that approximated the mass flowrate by the sum of two exponentials. This however took no account of either the highly non-linear nature of the discharge, or the type of flow or the length of the pipeline which has important frictional effects on the flow. The nature of FBR modelling, especially for two-phase flows when thermodynamic computations such as vapour liquid equilibria are important, demands powerful computing resources.

In most of the studies reviewed, researchers have made various assumptions and simplifications, in order to suit a particular method of solution or application. Suwan and Anderson (1992) argued that alternative formulations, interpolations, friction force representation, or time integration, which may be appropriate for parabolic problems, will all violate the basic wave like characteristics of a hyperbolic problem. Most cases of unsteady one-dimensional flow where disturbance propagation velocities do not vary significantly, are characterised by quasi-linear hyperbolic partial differential equations for continuity and momentum. On the other hand, complex phenomena such as stratified and intermittent stratified-bubble (slug) flows require a two-dimensional transient analysis for a complete treatment of the problem.

Various analytical techniques have been used to reduce the number of equations before employing the relevant numerical procedure. Van Deen and Reintsema (1983), for example, introduced a technique which reduces the energy equation to a single parameter-in-mass equation without the assumption of isothermal or isentropic flow.

There has been much research activity in many publications in the field of theoretical modelling of fluid transients. Much of this literature is reviewed in this study. Following this review, a new methodology based on an approach first proposed by Picard and Bishnoi (1989) is implemented.

The basic partial differential equations of flow are derived for unsteady quasi-one-dimensional flow of fluids through a rigid constant cross-section area of pipe. The various assumptions made in their derivation is explained.

Any two-phase flow model needs accurate vapour liquid equilibrium predictions for the multi-component fluids and in this study, this is done using the HTSFLASH programme first developed by Michelsen (1982, 1987). The Peng-Robinson equation of state (Peng and Robinson, 1976) is used to perform the flash calculations.

Numerical solution of the basic equations is effected using the method of characteristics which is described in Chapter 3.

2.2 REVIEW OF THE MATHEMATICAL APPROACHES AVAILABLE FOR THE DERIVATION OF THE CONSERVATION LAWS

A review of mathematical techniques used to date to derive fluid flow equations is presented in this section. There are three basic methods by which fluid flow problems are formulated namely, the control volume integral analysis, infinitesimal system differential analysis, and experimental or dimensional analysis. In all these cases, the equations of dynamics and thermodynamics must be satisfied.

In the control volume approach, a balance is made between the incoming and outgoing fluid, and the resultant changes within the control volume and details of the flow are normally ignored.

In the infinitesimal approach, the conservation laws are written for an infinitesimal system of fluid in motion and become the basic differential equations of fluid flow. To apply them to a specific problem it is necessary to integrate these equations mathematically over the volume, subject to the boundary conditions of the particular problem. Exact analytical solutions are often possible only for very simple geometries and boundary conditions, otherwise a numerical solution is needed.

The dimensional analysis approach can be applied to any problem but its inherent generality makes this type of approach undesirable.

The control-volume analysis is considered the most useful of all the three approaches as far as practical engineering applications are concerned. It gives results in a reasonable amount of time with accuracy depending on the assumptions made in setting up the model.

In fluid flow problems the dependent variables i.e. p, ρ, u etc. are functions of the independent variables i.e. t and x in the case of one-dimensional flow. In any given flow situation, the determination by experiment or theory of the fluid properties as a function of position and time is considered to be the solution to the problem. There are two distinct fundamental ways of specifying the flow field, namely the eulerian and the lagrangian descriptions.

In the Eulerian form the independent space variables refer to a co-ordinate system assumed to be fixed or translating in space and through which the fluid is moving. The flow is characterised by a time-dependent velocity field which is to be found by solving the initial value problem.

In Lagrangian form, the independent space variables refer to a co-ordinate system fixed in the fluid and undergoing all the motion and distortion of the fluid, so that the particles of the fluid are permanently identified by their Lagrangian variables, while their actual positions in space are among the dependent variables that need to be solved.

Although the Eulerian and Lagrangian forms are essentially equivalent, the Lagrangian form gives more information i.e. it tells where each volume of fluid came from initially and has the virtue that conservation of mass is automatic. This results in considerably greater accuracy in some problems.

Ritchmyer (1967) stated that for the above reasons, the Lagrangian form is generally preferred for some problems in a one space variable. For problems in two or more space variables and time, the Lagrangian method encounters serious difficulties. In particular, the accuracy usually decreases seriously as time goes on, due to distortions, unless a new Lagrangian point-net is defined from time to time, which requires cumbersome and usually rather inaccurate interpolations. From this point of view, the Eulerian form is more attractive. However, the Eulerian form is less adept at handling interfaces between fluids having different thermodynamic properties because it provides no simple mechanism to distinguish which kind of fluid is existent at a given space-time grid point (for problems in one space variable, such a mechanism can easily be provided). Many schemes have been tried, some combining the features of the Lagrangian and Eulerian forms but there is no satisfactory universal method that has been found for general multi-dimensional problems.

Fashbaugh and Widawsky (1972) stated that the Eulerian formulation is usually used in steady-state fluid flow problems and the Lagrangian formulation is used more extensively in unsteady flow and is more desirable for the solution of shock propagation problems. Also the fact that the Lagrangian formulation yields more

information, facilitates easy location of temperature contact surface propagation within the pipe. The study by Fashbaugh and Widawsky (1972) compared two methods, namely the pseudo-viscosity and the Lax-Wendroff numerical method in modelling the effects of duct area change on shock strength in one-dimensional viscous air flow. It was concluded that a one-dimensional variable area Lagrange analysis is adequate for predicting shock flow through a duct area increase ratio of at least 10 to 1.

Ames(1977) stated that until the early 1960's, the only known stable difference approximations for the Eulerian form were less accurate than those for the Lagrangian form. Consequently, the Lagrangian forms are preferred. Both systems have approximately the same complexity. The major disadvantage of the Eulerian system arises when interfaces (shocks) occur separating fluids of different density. The Lagrangian form does not have the spatial co-ordinate mesh fixed in advance and may require refinement of the mesh as computation advances. This possibility of re-gridding arises since the Lagrange form is constructed so that mass between two successive mesh points is approximately conserved.

White (1988) stated that certain numerical analyses of sharply bounded fluid flow, such as the motion of isolated fluid droplets are very conveniently computed in Lagrangian co-ordinates.

Other more recent writers, including Batchelor (1992) argued that the Lagrangian type of specification is useful in certain special contexts but it leads to rather cumbersome analysis and in general is at a disadvantage in not giving directly the spatial gradients of velocity in the fluid.

In fluid dynamics measurements, the Eulerian method is the most suitable. To simulate a Lagrangian measurement, the probe would have to move downstream at the fluid particle speeds. The Eulerian formulation has almost exclusively been used in all recent studies and literature, even in such cases where according to the above discussion, the Lagrangian description would seem more appropriate.

In this study, both descriptions are used depending on circumstance, with the Eulerian concept being denoted by ($\partial a/\partial t$) or ($\partial a/\partial x$), and the Lagrangian concept being denoted by (Da/Dt). The relationship between the two is given by,

$$\frac{Da}{Dt} = \frac{\partial a}{\partial t} + u\frac{\partial a}{\partial x} \qquad (2.2.1)$$

In the following section the mathematical model used to simulate the transient flow in a pipeline following FBR is developed. The equations will be derived from first principles and any assumptions or simplifications will be fully accounted for.

Conservation laws are time-dependent systems of partial differential equations (usually non-linear or quasi linear) and have a simple structure when in one space dimension (variation in the y and z directions are neglected). They take the form,

$$\frac{\partial}{\partial t}v(x,t) + \frac{\partial}{\partial x}f(v(x,t)) = Q_s \qquad (2.2.2)$$

where v denotes the generic function that is being computed with some numerical method and Q_s is the source term. Here $v(x, t) \in R^m$ is an m-dimensional vector of conserved quantities, or state variables which will be the mass, momentum and energy terms. More properly, v_j is the density function for the j'th state variable, with the interpretation that $\int_{x_1}^{x_2} v_j(x,t)dx$ is the total quantity of this state variable in the interval $[x_1, x_2]$ at time t.

The fact that these state variables are conserved means that $\int_{-\infty}^{\infty} v_j(x,t)dx$ should be constant with respect to t. The functions v_j themselves, representing the spatial distribution of the state variables with time t, will generally change as time progresses. The main assumption underlying equation 2.2.2 is that knowing the value of v(x, t) at a given point and time allows determination of flow or flux of each state variable at (x, t). The flux of the j'th component is given by some function $f_j(v(x, t))$. The vector-valued function f(v) with j'th component $f_j(v)$ is therefore the flux function for the system of conservation laws.

To see how the conservation laws arise from physical principles, the equation for conservation of mass in a one-dimensional fluid flow problem is first derived. The equations derived henceforth will be the full system of Navier-Stokes equations which are applicable to any flow. The Euler equations which are a simplified version of the Navier-Stokes equations are then derived with the relevant justifications explained. The Euler equations of fluid dynamics are used in this study.

2.3 DERIVATION OF THE CONSERVATION LAWS

This section deals with the mathematical derivation of the conservation laws of mass, momentum and energy. The assumptions or simplifications made in the following derivations of the Navier-Stokes equations are,

- one-dimensional flow
- homogeneous equilibrium fluid flow
- negligible minor losses and constant cross section area of pipe
- horizontal pipeline with no vertical elevation
- negligible fluid structure interaction

2.3.1 One-Dimensional Flow Assumption

A flow can be assumed to be one-dimensional if the rate of change of fluid properties normal to the streamline direction is negligible compared with the rate of change along the streamline. This means that over any cross-section of the pipe all the gas properties may be assumed to be uniform. The assumption of one-dimensional flow gives satisfactory solutions to many problems where either the cross-section area changes slowly along the path of the stream of gas, the radius of curvature of the pipe is large compared with its diameter or the shape of the velocity and temperature profiles are approximately constant along the pipe. For one-dimensional flow of a fluid, p, ρ, u etc. are only functions of t and x. The one-dimensional model enables simpler derivation of the basic equations of pipeline flow.

In real fluid flow situations, especially in the case of high-pressure natural gas flow in pipelines, the flow cannot be truly one-dimensional because viscous effects will produce a velocity profile across the pipe with the local velocity zero at the pipe wall and reaching a maximum in the centre. Moreover, the flow is turbulent so that there are random motions superimposed upon the mean flow.

Ansari (1972) investigated the influence of including radial flow on the solution of unsteady pipe flow equations. It was shown that neglecting the radial velocity can lead to substantial error in the determination of the axial velocity of flow. The effect of the assumption of negligible radial flow was also investigated in relation to another assumption which is commonly made, i.e. the gradient of the axial velocity in the axial direction, in viscous flow, is negligible compared to the gradient in the radial direction. It was found that for slow transients the latter assumption is valid while the former is not and vice versa for the case of rapid transients The departure from the one-dimensional flow assumption will be even more pronounced where there are bends and fittings in the pipeline. Nevertheless, despite the foregoing, the one-dimensional approximation in gas transmission systems has been shown to be very good for steady and slowly varying flows.

When the variations in flow are large and rapid, such as in high pressure gas pipeline ruptures, larger discrepancies are expected from the one-dimensional approximation. A more rigorous approach is to apply the integrated equation method used in the turbulent boundary layer theory.

There are many studies and computer models developed for multi-dimensional flow analysis. A few computer programmes based on multi-dimensional flow models such as FLOW-3D are commercially available. However, these models can only be applied to some special cases with confidence.

Shin (1978) discussed the extension of the one-dimensional method of characteristics to two space dimensions. The extended method uses the same simplifications and retains the similar simplicity and efficiency as in the conventional one. The two-dimensional method is applicable to both the Cartesian and axi-symmetric systems and includes the conventional method as a special case.

Wylie (1983) presented a similar numerical method for analysis of low-velocity two-dimensional transient fluid flow problems. The method contains similarities to the one-dimensional method of characteristics but does not follow the traditional characteristics theory for two-dimensional problems.

The most up to date and comprehensive study is that by Bendiksen and Moe (1993) and Bendiksen et. al. (1991), which presented the physical basis of a new type of multi-dimensional two-fluid model, particularly suited for transient flow problems. A basic difference between this model and the other models is in the solution procedure, aiming in particular at improved predictions of transient problems. The numerical scheme is based on an extension of an earlier one-dimensional model and employs an implicit finite difference scheme.

It follows from the above discussion that the three dimensional solution is the natural method for the FBR problem being modelled if a two-fluid model is to be employed. As shown in the above mentioned studies, the extension of one dimensional models to two-and three-dimensional models could, in principle, be achieved especially if caution is made in representation of the other terms in the equations.

2.3.2 Homogeneous Equilibrium Flow Assumption

Transient flows encountered in pipeline rupture problems are frequently two-phase flow even if the initial state of the fluid is single phase. The two phases occur either from liquid condensation due to low temperatures at the rupture plane which then propagates through the pipeline or for liquid flows, vapour flashing due to low pressure. A complicated multi-phase flow situation is therefore likely to be encountered, especially for a multi-component mixture. Convenient classification into two types of flow regimes would be dispersed (particles, bubbles and droplets), and separated (stratified, annular and elongated bubbles) flows. More complex flow regimes often occur as combinations of these, such as stratified and annular flows with entrainment and slug flow. Flow regimes commonly experienced are stratified (wavy or smooth), annular dispersed, intermittent (slug) and dispersed bubble flows. In relatively long pipelines, with possibly large pressure losses, several of these flow regimes may exist simultaneously as a result of changing in situ flow rates and physical properties of the fluids.

Dispersed flow regimes have been quite extensively studied recently using two and three-dimensional models. For two-phase flow, however, at least four general

purpose codes are available. They include FLUENT and RAMPANT, developed by Fluent Inc., FLOW-3D developed by Flow Science Inc., and PHOENICS developed by CHAM consultancy. For separated or stratified flow, there has been several studies, including those by Oliemans (1987); Stadtke and Holtbecker (1991), Philbin and Govan (1990), and Bendiksen and Moe (1993).

Oliemans (1987) investigated the accuracy of two-phase flow trunk line predictions by a one-dimensional steady model for stratified wavy flow in horizontal and inclined pipes.

Stadtke and Holtbecker (1991) proposed a two-fluid model, i.e. including slip velocity between the two phases, for transient fluid flow. The complexity associated with a two-fluid model is that the characteristic equations that define the flow do not have a simple analytical form. The characteristics in Stadtke and Holtbecker's model is derived based on analytical trials rather than physical modelling.

The effect of concentration stratification in multi-component two-phase flow as a result of slip, and mass transfer between the two phases is taken into account by the computer programmes, PLAC and OLGA developed by Philbin and Govan (1990) and Bendiksen and Moe(1993) respectively. However neither incorporte proper phase behavior during the transient flow process due to inherent limitations in the numerical methods employed.

In the multi-dimensional Moe-Bendiksen model (OLGA), the general two-fluid equations have been applied with the assumption of a single pressure field. The modelling of constitutive laws at the interface is not general but focused on separated or stratified flows. A volume equation is applied for the pressure, enabling a direct two-step solution procedure.

In analysing pressure transients in bubbly air-water mixtures Padmanabhan et. al. (1978) used a homogeneous model which consists of one-dimensional equations of conservation of mass for each of the phases and conservation of momentum for the mixture.

Bhallamudi and Chaudhry (1990) developed a third-order accurate explicit finite-difference scheme for transient flows in one-dimensional homogeneous gas-liquid mixtures in pipes. The gas-liquid mixture was treated as a pseudo-liquid.

Chen et. al. (1995) used a two-fluid model (MSM), in which the local instantaneous conservation equations are formulated for each phase. The hyperbolicity of the equations is achieved by forcing the flow to be marginally stable. Under this condition, all information related to the structure of the flow that is not considered to be non-dissipative, inviscid flow is embedded in an inertial coupling constant. To obtain correct and real sonic characteristics an expression for the inertial coupling constant is obtained based on critical flow data. The thermodynamic equilibrium assumption is used as the closure criterion for interfacial mass and energy transfer.

A gas-liquid mixture may be treated as a pseudo-fluid, if the mixture and its motion may be treated as homogeneous. In the homogeneous equilibrium model (HEM), the two phases are assumed to move at the same velocity and are always in thermodynamic equilibrium. The major advantage of HEM is that it has a relatively simpler mathematical structure and clearly defined characteristic equations are assured for all flow situations.

Chen et al. (1993, 1995) showed that for long pipelines (length $\geq$ 100m) the HEM gave very good agreement with data obtained for full-bore rupture from tests performed by British Gas on the Isle of Grain. The predicted release rate of HEM and the more detailed two-fluid model, MSM, were very close. It was concluded from this work that thermodynamic non-equilibrium is insignificant in long pipes except for the early stages of rarefaction wave propagation.

In the light of the above findings, it is decided to use the HEM assumption in this work. This means that the following derivations will not contain two separate momentum conservation equations for each phase of a two-phase mixture and therefore no special treatment is required to obtain clearly defined characteristics.

2.3.3 Minor losses and constant cross-section area of pipe

Since the aim of this study is the rupture modelling of long, straight pipelines, minor losses due to bends and obstacles will be neglected in the derivation of the conservation equations of fluid flow. This assumption is reasonable since these losses are likely to be small compared with the distributed frictional losses in long pipelines. The effect of these minor losses on the fluid transients is investigated by Otwell et. al. (1985).

As regards the assumption of constant cross-section area of pipe, most workers have generally assumed that the cross-section area of the pipe is not a function of the axial distance or varies slowly (Flatt, 1985, 1986; Picard and Bishnoi, 1988,1989; Chen, 1993). In some special cases such as in cooling ducts etc. where the cross-section area varies appreciably with distance, this effect has been incorporated into the basic equations. However, in some studies on compressible flow, including those by Zielke (1968) and Flatt (1989), the equations are based on a variable change in cross-section area.

2.3.4 Horizontal pipeline with no elevation

The pipeline is assumed to be straight with no elevated sections, therefore the gravity term is neglected in the equations.

2.3.5 Negligible fluid structure interaction

The classical water-hammer theory only predicts the extreme loading on a system as long as it is rigidly anchored. When a piping system has certain degrees of freedom severe deviation from the classical theory may occur due to motion of the system. Pressure waves exert forces which cause a compliant system to move. As a result of the motion, pressure waves are formed, a phenomenon known as fluid structure interaction.

Fluid structure interaction is essentially a dynamic phenomenon, the interaction being caused by dynamic forces which act conversely on fluid and pipe. The forces in such

a piping system are classified in two groups namely distributed forces and local forces. Typical examples of distributed forces are fluid pressure and friction. In the case of fluid pressure, rapid pressure fluctuations cause a pipe to expand or contract thereby creating axial stress waves in the pipe wall. The stress waves in return generate pressure fluctuations in the enclosed fluid, resulting in a coupling known as Poisson coupling.

Similarly, friction force is responsible for friction coupling. In most practical systems, frictional coupling is weak. Local forces act on specific points in a system, such as elbows, tees or valves and cause axial and lateral motions which generate pressure waves in the fluid resulting in an interaction called junction coupling. Junction coupling is generally dominant compared with Poisson and Friction couplings. Lawooij and Tijsselling (1990) conducted a study of fluid structure interaction in compliant piping systems. They concluded that the most significant coupling mechanisms are Poisson and Junction coupling. A simple guideline which states when interaction is important is formulated in terms of three time scales i.e., the time in which the pressure is built up, the eigen-periods of the structure and the time scale of the water-hammer waves. They also concluded that Poisson coupling is important for the fluid when significant modes of interaction are dominated by stiffness.

To consider the motion of the pipe, three main displacements are distinguished namely axial displacement, lateral displacement and rotation. Therefore in general, the dynamics of a pipe system are influenced by four wave families, i.e. axial, flexural and torsional waves in the pipe wall and pressure waves in the fluid. These co-exist during transience and have different degrees of influence on the transient behaviour. Fluid structure interaction in compliant piping systems is modelled by extended water-hammer theory for the fluid and by beam theory for the pipes. In buried pipelines, the lateral restraint is usually sufficient to ensure that the overall behaviour is dominated by axial effects. Hence most analyses of fluid structure interaction have focused on the propagation of axial waves i.e. pressure waves propagating along the walls of the pipe. In suspended pipelines however, few lateral restraints exist and account should be taken of flexural and torsional waves.

In a study on fluid structure interaction in flexible curved pipes, Stittgen and Zielke (1990) concluded that the influence of structural motion on the internal pressure is smaller than the time dependent internal pressure but can still be of influence in particular cases. They also concluded that pressure waves in flexible pipes are quite dependent on visco-elastic wall properties.

Rachid and Stuchenbruck (1990) stated that the mechanical properties of the material, the temperature and the degree of stiffness of the supports, have a significant influence on the response of the system. Stiffer pipe materials i.e. those with mechanical damping will experience higher pressures than more compliant pipe systems. They also found that Poisson effects can induce significant piping motion especially in long pipe reaches and cause high frequency peaks for pressure and stress in visco-elastic pipes, e.g. up to 25% above the rigid pipe model. However, mechanical damping of the pipe material tends to degrade the solid wave front quite quickly. In most cases, high frequencies generated by the fluid structure interaction mechanism are virtually eliminated before the first fluid cycle.

In practice the value of the sonic velocity in the fluid in a pipe is influenced by the elasticity of the confining walls and the compressibility of the fluid. As the elasticity of the wall materials increases, the effective value of sonic velocity decreases. This effect is commonly neglected for typical high-pressure gas pipelines. However, some workers including Wood et. al. (1966), Zielke (1968), Hirose (1971) and Beauchemin and Marche (1992) have all taken into consideration the effect of pipe elasticity. This has resulted in an additional term in the continuity equation. In the Beauchemin-Marche model, no simplification was made on the basic equations and in addition the effect of variable cross-section area was included.

In the study by Tiley (1989), the effects of fluid structure interaction were not considered in an effort to maintain simplicity of the model. The same approach is adopted in this study. It is felt that for long straight pipes that are rigidly anchored as considered in this work, fluid structure interaction will not be as significant as frictional and two-phase equilibria effects. It is also assumed that the pipe is inelastic,

i.e. elasticity of the pipe walls is negligible compared with the compressibility of the fluid.

2.3.6 Conservation of Mass

If pipeline rupture occurs at t = 0, then the flow variables can be summarised in Figure 2.3.1 below:

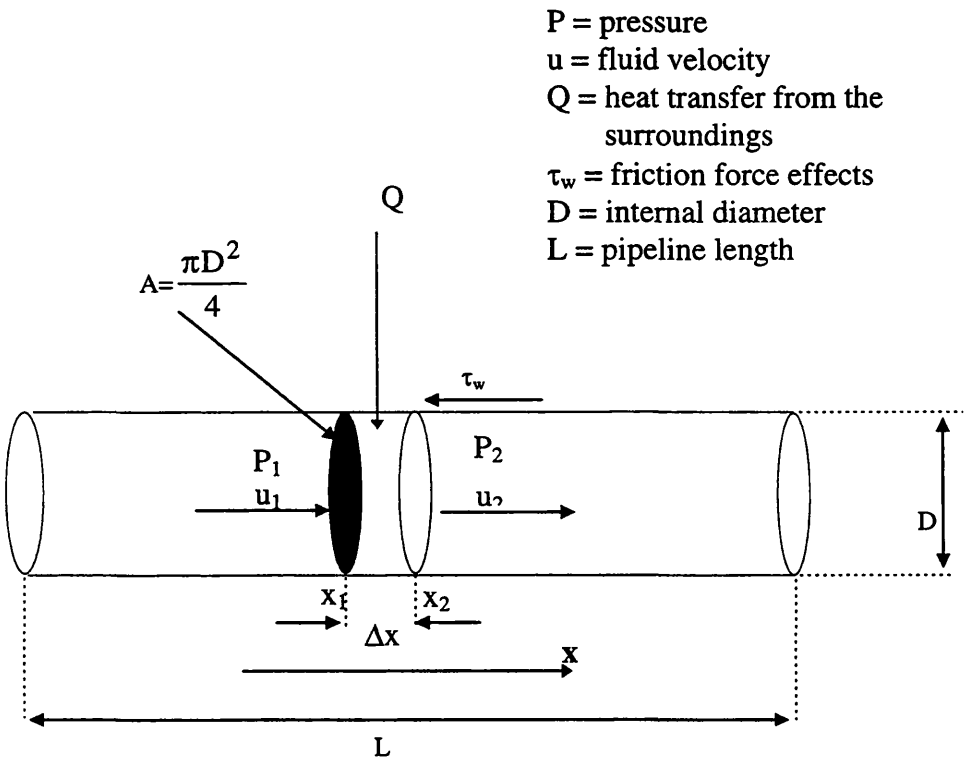

Figure 2.3.1: Control Volume

Let x represent the distance along the pipeline and let $\rho(x, t)$ be the density of the fluid at point x and time t. The total mass of fluid per unit cross-sectional area in any given section from x_1 to x_2, say, is given by the integral of the density,

$$\text{mass in } [x_1,\ x_2] \text{ at time } t\ = \int_{x_1}^{x_2} \rho(x,t)dx \qquad (2.3.1)$$

If we assume that the pipe is impermeable and that mass is neither created nor destroyed, then the mass in this one section can change only because of fluid flowing across the end points x_1 or x_2.

Let u(x, t) be the velocity of the fluid at the point x at time t. Then the rate of flow, or flux of fluid past this point is given by,

$$\text{mass flux at } (x,\ t)\ =\ \rho(x,t)u(x,t) \qquad (2.3.2)$$

Therefore the rate of change of the mass state variable across the control volume given by the spatial domain $[x_1, x_2]$ is given by,

$$\frac{\partial}{\partial t}\int_{x_1}^{x_2} \rho(x,t)dx = \rho(x_1,t)u(x_1,t) - \rho(x_2,t)u(x_2,t) \qquad (2.3.3)$$

This is one integral form of the conservation law. Another form is obtained by integrating this in time from time t_1 to t_2, giving an expression for the mass in $[x_1, x_2]$ at time $t_2 > t_1$ in terms of the mass at time t_1 and the total (integrated) flux at each boundary during this time period,

$$\int_{x_1}^{x_2} \rho(x,t_2)dx = \int_{x_1}^{x_2} \rho(x,t_1)dx + \int_{t_1}^{t_2} \rho(x_1,t)u(x_1,t)dt - \int_{t_1}^{t_2} \rho(x_2,t)u(x_2,t)dt \qquad (2.3.4)$$

To derive the differential form of the conservation law, we assume that ρ(x, t) and u(x,t) are differentiable functions. Then using,

$$\rho(x,t_2)-\rho(x,t_1)=\int_{t_1}^{t_2}\frac{\partial}{\partial t}\rho(x,t)dt \qquad (2.3.5)$$

and,

$$\rho(x_2,t)u(x_2,t)-\rho(x_1,t)u(x_1,t)=\int_{x_1}^{x_2}\frac{\partial}{\partial x}\{\rho(x,t)u(x,t)\}dx \qquad (2.3.6)$$

Substituting equations 2.3.6 and 2.3.5 into equation 2.3.4 allows one to write,

$$\int_{t_1}^{t_2}\int_{x_1}^{x_2}\left\{\frac{\partial}{\partial t}\rho(x,t)+\frac{\partial}{\partial x}(\rho(x,t)u(x,t))\right\}dxdt=0 \qquad (2.3.7)$$

Since this must hold for any section $[x_1, x_2]$ and over any time interval $[t_1, t_2]$, it can be concluded that in fact the integrand in equation 2.3.7 must be identically zero, i.e.,

$$\frac{\partial}{\partial t}\rho+\frac{\partial}{\partial x}(\rho u)=0 \qquad (2.3.8)$$

This is the desired differential form of the conservation law for the conservation of mass.

For flows where two phases are present and the homogeneous equilibrium flow assumption is made, the two phases move at the same velocity and a mass balance for the overall mixture composition, y, in differential form can be written as,

$$\frac{\partial}{\partial t}(y_i)+\frac{\partial}{\partial x}(uy_i)=0 \quad i=1,.....,N-1 \qquad (2.3.9)$$

where

$$y_i=\frac{\alpha\rho_g y_{gi}+(1-\alpha)y_{li}\rho_l}{\rho} \qquad (2.3.10)$$

where the subscript i refers to the i'th component of an N component mixture, α is the volume fraction of the vapour phase, and the subscripts l and g refer to the liquid and gas phase respectively.

Equation 2.3.9 shows that the mixture composition is purely convected by the flow and depends only on the initial fluid composition profile along the pipeline.

2.3.7 Conservation of Momentum

The derivation for the conservation of momentum is slightly different to that of mass. Momentum is a vector quantity and in order to determine all the terms in the momentum conservation equations it is necessary to define the sources influencing the variation of momentum. It is known from Newton's laws, that the forces for the variation of momentum in a physical system are the forces acting on it (Welty et. al., 1984). These forces consist of the external volume forces $\sum F_e$ and the internal forces $\sum F_i$. The latter are dependent on the nature of the fluid considered, and result from the assumptions made about the properties of the internal deformations within the fluid and their relation to the internal stresses.

The internal forces acting on the fluid volume in the pipeline within the spatial domain $[x_1, x_2]$ is given by,

$$\sum F_i = AP(x_1,t) - AP(x_2,t) + A\tau(x_2,t) - A\tau(x_1,t) \qquad (2.3.11)$$

where τ denotes the viscous shear stresses within the fluid and is a tensor quantity. These stresses give rise to fluxes that depend on the spatial gradient of the state variable. In one dimension only, this can be expressed as,

$$\tau_{xx} = \mu\left[2\frac{\partial u}{\partial x} - \frac{2}{3}\frac{\partial u}{\partial x}\right] \qquad (2.3.12)$$

where μ is the dynamic viscosity of the fluid

The external volume forces are the forces that would render the flow non-isentropic. In the assumption of isentropic flow, this term can be expected to change only because of flow of fluid across the end points x_1 and x_2. However for non-isentropic

flows which would be the real case scenario, this is not true. There is likely to be some destruction of momentum within this interval and this loss or sink is denoted as a source term. The source term in non-isentropic homogeneous equilibrium flows can be attributed to wall friction only. Other hydrodynamic effects such as interfacial drag force, mass transfer effect force are not relevant for the homogeneous flow assumption and are therefore ignored with respect to any additional terms in the momentum equation.

The external force term is therefore,

$$\sum F_e = \frac{\rho u|u|}{2}\frac{4f_w}{D}dxA \qquad (2.3.13)$$

where f_w is the fanning friction coefficient. The modulus of velocity is introduced to account for change of direction of flows.

The total momentum of fluid in any given volume of fluid as in that from x_1 to x_2 can be given by the following relation for a constant cross-sectional area conduit,

$$\text{momentum at time t} = A\int_{x_1}^{x_2}\rho(x,t)u(x,t)dx \qquad (2.3.14)$$

where A is the cross-sectional area of the pipeline (assumed to be constant).

The rate of flow of momentum or momentum flux at a point x at time t can be written as,

$$\text{momentum flux at } (x,t) = \rho(x,t)u^2(x,t)A \qquad (2.3.15)$$

The rate of change of momentum within a control volume bounded by the spatial domain $[x_1, x_2]$ will be the sum of the net momentum fluxes through the volume plus any internal and external forces acting on the volume. This can therefore be written as,

$$\frac{\partial}{\partial t}A\int_{x_1}^{x_2}\rho(x,t)u(x,t)dx=\rho(x_1,t)u^2(x_1,t)A-\rho(x_2,t)u^2(x_2,t)A$$

$$+AP(x_1,t)-AP(x_2,t)+A\tau(x_2,t)$$

$$-A\tau(x_1,t)+\frac{\rho u|u|}{2}\frac{4f_w}{D}dxA \qquad (2.3.16)$$

Dividing all sides by A, another form of this equation is obtained by integrating equation 2.3.16 in time from t_1 to t_2 in order to get an expression for the momentum in $[x_1,x_2]$ at time $t_2 > t_1$.

$$\int_{x_1}^{x_2}\rho(x,t_2)u(x,t_2)dx=\int_{x_1}^{x_2}\rho(x,t_1)u(x,t_1)dx+$$

$$\int_{t_1}^{t_2}\left\{\rho(x_1,t)u^2(x_1,t)-\rho(x_2,t)u^2(x_2,t)\right\}dt+$$

$$\int_{t_1}^{t_2}\left\{P(x_1,t)-P(x_2,t)\right\}dt+$$

$$\int_{t_1}^{t_2}\left\{\tau(x_2,t)-\tau(x_1,t)\right\}dt+\int_{t_1}^{t_2}\int_{x_1}^{x_2}\left(\frac{\rho u|u|}{2}\frac{4f_w}{D}\right)dxdt \qquad (2.3.17)$$

The following correlations can also be written for momentum,

$$\rho(x,t_2)u(x,t_2)-\rho(x,t_1)u(x,t_1)=\int_{t_1}^{t_2}\frac{\partial}{\partial t}\rho(x,t)u(x,t)dt \qquad (2.3.18)$$

$$\rho(x_2,t)u^2(x_2,t)-\rho(x_1,t)u^2(x_1,t)=\int_{x_1}^{x_2}\frac{\partial}{\partial x}\left[\rho u^2(x,t)\right]dx \qquad (2.3.19)$$

$$\left(P(x_2,t)-P(x_1,t)\right)=\int_{x_1}^{x_2}\frac{\partial}{\partial x}P(x,t)dx \qquad (2.3.20)$$

$$\left(\tau(x_2,t)-\tau(x_1,t)\right)=\int_{x_1}^{x_2}\frac{\partial}{\partial x}\tau(x,t)dx \qquad (2.3.21)$$

Substituting the relations 2.3.18 - 2.3.21 into equation 2.3.17 and simplifying, we obtain,

$$\int_{t_1}^{t_2}\int_{x_1}^{x_2}\left\{\frac{\partial}{\partial t}\rho(x,t)u(x,t)+\frac{\partial}{\partial x}\left[\rho u^2(x,t)+P-\tau\right]+\beta\right\}dxdt=0 \qquad (2.3.22)$$

where β can be written as,

$$\beta=-2\frac{f_w}{D}\rho u|u| \qquad (2.3.23)$$

As in the case for the conservation of mass, it can be concluded that in fact the integrand in equation 2.3.22 must be identically zero since it must hold for any section $[x_1, x_2]$ and over any time $[t_1, t_2]$,

$$\frac{\partial}{\partial t}(\rho u)+\frac{\partial}{\partial x}(\rho u^2+P-\tau)=-\beta \qquad (2.3.24)$$

Equation 2.3.24 is the differential Navier-Stokes form of the momentum equation and is applicable for all flows in all situations.

2.3.8 Conservation of energy

From thermodynamic analysis of fluid continua it is known that the energy content of a system is measured by its internal energy per unit mass, e. This internal energy is a state variable of a system and hence its variation during a thermodynamic transformation depends only on the final and initial states.

The total energy to be considered in a fluid when deriving the conservation equation is the sum of its internal and kinetic energy per unit mass. Therefore the total energy per unit mass can be given by,

$$E=e+\frac{u^2}{2} \qquad (2.3.25)$$

A third term, gz, that takes account of the potential energy gained by different pipe elevations is ignored because the pipe is assumed to run on the same horizontal axis.

The total energy of the fluid contained in the volume bounded by $[x_1, x_2]$ can be given by,

$$\text{energy in } [x_1, x_2] \text{ at time t } = \int_{x_1}^{x_2} \rho(x,t)E(x,t)A\,dx \qquad (2.3.26)$$

The first law of thermodynamics states that the sources for the variation of the total energy are the work of the forces acting on the system plus the heat transmitted to this system.

Considering the general form of the conservation law for the quantity E, then the rate of flow of energy or energy flux at the point x and time t is given by,

$$\text{convective energy flux at } (x,t) = \rho(x,t)E(x,t)u(x,t)A \qquad (2.3.27)$$

If we consider the general form of the conservation law, then apart from the convective flux of energy there will also be a diffusive flux associated with the internal energy of the fluid,

$$\text{diffusive energy flux at } (x,t) = -k\frac{\partial T}{\partial x}(x,t)A \qquad (2.3.28)$$

where k is the thermal conductivity of the fluid and T is the absolute temperature.

With regard to the sources of energy variations in a fluid system, a distinction has to be made between the surface and the volume sources. The surface sources are the result of the work done on the fluid by the internal shear stresses acting on the surface of the volume considering that there are no surface heat sources and can be written at a point as,

$$\text{surface sources of energy at } (x,t) = -P(x,t)u(x,t)A + \tau(x,t)u(x,t)A \qquad (2.3.29)$$

The volume sources are the sum of the work of the volume forces and any other heat sources other than conduction. This heat source would include any transfer of convective heat from the surroundings. In terms of the volume of fluid in $[x_1, x_2]$ the rate of heat transfer to the fluid from the surroundings can be given by,

$$Q_h = \frac{4}{D}U_h(T_\infty - T)Adx \qquad (2.3.30)$$

where U_h is the overall heat transfer coefficient and the subscript ∞ denotes the conditions external to the pipeline.

The rate of change of total energy in $[x_1, x_2]$ can be given by equating the rate form of equation 2.3.26 to the difference in fluxes at x_1 and x_2 and any source terms as explained above,

$$\frac{\partial}{\partial t}\int_{x_1}^{x_2}(\rho E)(x,t)A\,dx = A\{(\rho Eu)(x_1,t)-(\rho Eu)(x_2,t)\}$$
$$+A\left\{\left(k\frac{\partial T}{\partial x}\right)(x_1,t)-\left(k\frac{\partial T}{\partial x}\right)(x_2,t)\right\}$$
$$+A\{(Pu)(x_1,t)-(Pu)(x_2,t)\}+$$
$$+A\{(\tau u)(x_2,t)-(\tau u)(x_1,t)\}$$
$$+Q_h+W_h \qquad (2.3.31)$$

As in the conservation of momentum equation, another form of the above expression can be obtained by integrating in time from t_1 to t_2, where $t_2 > t_1$,

$$A\int_{x_1}^{x_2}(\rho E)(x,t_2)dx = A\int_{x_1}^{x_2}(\rho E)(x,t_1)dx+\int_{t_1}^{t_2}A\{(\rho Eu)(x_1,t)-(\rho Eu)(x_2,t)\}dt$$
$$+\int_{t_1}^{t_2}A\left\{\left(k\frac{\partial T}{\partial x}\right)(x_1,t)-\left(k\frac{\partial T}{\partial x}\right)(x_2,t)\right\}dt$$
$$+\int_{t_1}^{t_2}A\{(Pu)(x_1,t)-Pu(x_2,t)\}dt$$
$$+\int_{t_1}^{t_2}A\{(\tau u)(x_2,t)-(\tau u)(x_1,t)\}dt+\int_{t_1}^{t_2}(Q_h+W_h)dt \qquad (2.3.32)$$

Expressing the arguments of the integrals on the right hand side using the following generic manipulation,

$$M(x_2,t)-M(x_1,t)=\int_{x_1}^{x_2}\frac{\partial}{\partial x}M(x,t)dx \qquad (2.3.33)$$

we obtain from equation 2.3.32 after some mathematical manipulation,

$$\int_{t_1}^{t_2}\int_{x_1}^{x_2}\left\{\frac{\partial}{\partial t}(\rho E)(x,t)+\frac{\partial}{\partial x}\left[\begin{matrix}(\rho Eu)(x,t)+(Pu)(x,t)\\-\left(k\frac{\partial T}{\partial x}\right)(x,t)-(\tau u)(x,t)\end{matrix}\right]-q_h-w_f\right\}dxdt=0 \qquad (2.3.34)$$

where w_f is the work per unit volume of the external volume forces (shaft work and viscous drag effects), and q_h is the heat transfer per unit volume.

The differential form of the above equation yields the Navier-Stokes form of the conservation of energy ,

$$\frac{\partial}{\partial t}\rho E+\frac{\partial}{\partial x}\left[\rho Eu+Pu-k\frac{\partial T}{\partial x}-\tau u\right]=q_h+w_f \qquad (2.3.35)$$

where the heat transfer per unit volume can be written,

$$q_h=\frac{4}{D}U_h(T_\infty-T) \qquad (2.3.36)$$

The equations that have been derived up to now are the complete set of conservation laws. Expressed together they can be written as,

$$\frac{\partial}{\partial t}\begin{vmatrix}\rho\\\rho u\\\rho E\end{vmatrix}+\frac{\partial}{\partial x}\begin{vmatrix}\rho u\\\rho u.u+P-\tau\\\rho uE+Pu-\tau.u-k\frac{\partial T}{\partial x}\end{vmatrix}=\begin{vmatrix}0\\\beta\\q_h+w_f\end{vmatrix} \qquad (2.3.37)$$

These are the Navier-Stokes equations of motion. These include the dissipative flux terms that depend on the second derivative of velocity (in the case of internal viscous stress in the momentum and energy equations) and the second derivative of the temperature (for heat conduction in the energy equation). Numerically the presence of these dissipative fluxes causes problems because the equations become parabolic rather than hyperbolic. This typically causes severe time step restrictions.

2.3.9 Euler Equations

The system of Navier-Stokes equations, supplemented by empirical laws for the dependence of viscosity and thermal conductivity with other flow variables and by a constitutive law defining the nature of the fluid, completely describes all flow phenomena. For laminar flows no additional information is required and we can consider that any experiment in the laminar flow regime can be accurately modelled by computation. However the flow situation that arises in a pipeline as a result of FBR is highly turbulent and this leads to a form of numerical instability characterised by the presence of statistical fluctuations to all flow quantities. These fluctuations can be considered as superimposed on mean or averaged values and can attain, in many situations the order of 10% (Hirsch, 1995) of the mean values, although certain flow regions such as separated zones, can attain much higher levels of turbulent fluctuations.

Clearly, the numerical description of the turbulent fluctuations is a formidable task which puts very high demands on computer resources (Chapman, 1979; Kutler, 1983). Since this level is currently extremely computationally expensive, the highest level of approximation which could be considered is the Reynolds averaged Navier-Stokes equations supplemented by some models for the Reynolds stresses or fluctuation momentum flux. These models can range from the simple eddy viscosity or mixing length models to transport equations for the turbulent kinetic energy and dissipation rates, the so-called k-ε model, or to still more complicated models directly computing the Reynolds stresses.

The next level of approximation can be introduced for flows with a small amount of separation or back-flow and with a predominant mainstream direction at high

Reynolds numbers. This allows the viscous and turbulent diffusion terms in the mainstream direction to have a negligible effect on flow behaviour. This is the thin shear layer approximation (Pulliam and Steger, 1978; Steger, 1978).

Another level of approximation that is frequently considered is the boundary layer approximation. Prandtl recognised that at high Reynolds numbers the viscous regions remain of limited extension along the surfaces of solid bodies immersed in or limiting the flow. Hence when the viscous regions remain close to the body surfaces (that is, in the absence of separation) the calculation of the pressure field may be separated from that of the viscous velocity field. A detailed discussion of the boundary layer equations can be found in Batchelor (1970), Schlichting (1971), and Cebeci and Bradshaw (1984).

For flows with no separation and thin viscous layers, that is at high Reynolds numbers, a separation of the viscous and inviscid parts of the flow can be introduced, whereby the pressure field is de-coupled from the viscous effects, showing that the influence of the viscous and turbulent shear stresses is confined to small regions close to the walls and that outside these layers the flow behaves as inviscid. This analysis showed that many of the flow properties can accurately be described by the inviscid flow approximation (for example, determination of the pressure distributions), and that a simplified boundary layer approximation allows for the determination of the viscous effects. The calculation of the inviscid and the boundary layer parts of the flow can be performed interactively, taking into account the influence of the boundary layers on the inviscid flow.

Recently a series of approaches in this direction have been developed, i.e. the viscid-inviscid interaction methods, whereby attempts are made to model separated regions in an approximate way while keeping the advantages with regard to the reduced computational effort of the boundary layer approximations (Le Balleur, 1983). When this influence or interaction is neglected we enter the field of the inviscid approximations, which allows generally a good approximation of the pressure field and hence of lift coefficient for non-separated flows.

For very high Reynold's number flows, the inviscid-viscid flow assumption would be relevant. The viscous terms in the Navier-Stokes equations can be described by

momentum interactions or exchanges at the fluid-fluid and fluid-wall interface. The momentum interactions are expressed in terms of drag forces. The generalised drag force at the fluid-fluid interface is usually modelled as a linear combination of three forces: steady viscous drag, transient viscous drag or the Basset force and transient non-viscous drag such as the virtual mass force. At the fluid-wall interface, the viscous drag force can also be modelled as a linear combination of unsteady and steady wall drag or friction.

Chen (1993) in his marginal stability model (MSM) used essentially an inviscid flow model where the viscous effects mentioned previously are considered as constitutive relations and show as source terms in the conservation equations. However the unsteady components of each of the viscous drag effects are ignored except for the effect of transient non-viscous drag force.

The unsteady viscous drag is ignored on the basis that its effect decreases rapidly for bubbles of size larger than 10^{-4} m and for large Reynolds number flows. It is shown that for low Reynolds numbers, which will exist at the closed end of a ruptured pipe, the unsteady viscous drag appears as a time integral in both Stokes or creeping flow (Basset, 1961) and is very difficult to incorporate and solve as all the history of the flow must be stored.

The unsteady wall friction is also usually modelled as a time integral in single phase flow (Zielke, 1968). It is ignored by Chen on the basis that its effect is negligible with the progression of time and with the onset of turbulent flow. The transient non-viscous drag force is incorporated in the MSM model by deriving an inertial coupling constant.

The steady state components of the constitutive hydrodynamic relations are predominantly dependent on the phase slip or relative velocity (u_g - u_l), where u_g is the velocity of the gas phase and u_l is the velocity of the liquid phase. The only exception is the wall friction relation which is a function of fluid velocity. Due to the implicit dependence of many of the hydrodynamic relations on the relative velocity, the MSM model solves two momentum conservation equations, one for each phase.

Chen also developed a META-HEM model which can ignore all the fluid-fluid interface relations because the relative velocity is zero. The only viscous effect terms

which remain are the wall friction terms. In spite of this, as mentioned before, META-HEM gives good agreement for transient flow through long pipes (length ≥ 100m).

Subsequent to FBR of a pipeline, a highly turbulent flow situation will arise and it will essentially be dominated by convective effects. This means that in the bulk regions of flow, the inviscid flow assumption is close to reality with the viscous effects only occurring at the wall so that an inviscid-viscid model is appropriate. This approach is adopted in this study. Therefore, the dissipative fluxes relating to the viscous and heat conducting terms are ignored in the momentum and energy equations respectively and as a result, the Navier-Stokes equations can now be written as,

$$\frac{\partial}{\partial t}\begin{vmatrix}\rho\\ \rho u\\ \rho E\end{vmatrix}+\frac{\partial}{\partial x}\begin{vmatrix}\rho u\\ \rho u.u+P\\ \rho uE+Pu\end{vmatrix}=\begin{vmatrix}0\\ \beta\\ q_h\end{vmatrix} \qquad (2.3.38)$$

or in terms of an absolute frame of reference, for the conservative variables V, defined by,

$$\frac{\partial}{\partial t}V+\frac{\partial}{\partial x}F(V)+G=0 \qquad (2.3.39)$$

The above system of equations are essentially the Euler equations of conservation with the viscous effects at the fluid-wall interface appearing as source terms of wall friction and heat transfer. Although heat conduction effects are neglected, the heat sources term q_h cannot be neglected as there is bound to be heat transfer from the surroundings. Neglecting the heat transfer term would render the model adiabatic.

This approximation introduces a drastic change in the mathematical formulation with respect to all the previous models containing viscous terms, since the system of partial differential equations describing the inviscid flow model reduces from second order to first order. This is of significance, since it determines the numerical and physical approach to the computation of these flows. Also, the number of allowable boundary conditions is modified by passing from second-order viscous equations to the first-order inviscid system.

The vectors of variables formed by density, momentum and total energy, obeying the conservation form of the equations, are the conservative variables. The conservation form of the equations is essential in order to compute correctly the propagation speed and the intensity of discontinuities such as shock waves and contact surfaces that can occur in inviscid flows (LeVeque, 1990).

When FBR occurs, the high pressure fluid within the pipeline is suddenly exposed to a low pressure fluid existing externally. The sudden discontinuity in fluid properties at the point of rupture leads to the creation of centred compression and expansion waves. A centred compression wave is a shock wave and propagates into the low pressure external region whereas a centred expansion wave propagates into the high pressure region, internally through the pipeline creating an 'expansion fan' (Hirsch, 1990; Zucrow and Hoffman, 1976).

The expansion fan region does not give rise to shock wave like discontinuities in the conservative variables and the Euler equations for this scenario can therefore be expressed in terms of more 'direct' variables, i.e. in non-conservative mode. It is important to realise that the mathematical modelling of any flows with shock waves or contact surface discontinuities has to be done in conservative variable form.

The direct variables are density, velocity and pressure. In the expansion fan, they sustain a continuous variation with time. These variables will generally be imposed by the physical boundary conditions and are called the primitive variables. In addition, as the system of Euler equations are hyperbolic in time, quantities that propagate along characteristics can be defined and the system of equations can be transformed to the characteristic form. This procedure is described in Chapter 3, but first the Euler equations have to be expressed in primitive variable form.

2.4 THE IDEAL GAS MODEL

It has been shown that for regions of flow where expansion waves propagate, no special shock wave treatment of the Euler equations according to the Rankine-Hugoniot jump relations are needed (Hirsch, 1995). Shocks are solutions of the Rankine-Hugoniot relations with non-zero mass flow through the discontinuity. Consequently, pressure and normal velocity undergo discontinuous variations, while the tangential velocity remains continuous.

The absence of shock wave propagation within the pipeline after rupture permits the manipulation of the conservative form of the Euler equations, i.e. equation 2.3.38, into primitive variable form.

The mass conservation equation can be written as,

$$\frac{\partial \rho}{\partial t} + \rho \frac{\partial u}{\partial x} + u \frac{\partial \rho}{\partial x} = 0 \qquad (2.4.1)$$

The momentum conservation equation can be written as,

$$u \frac{\partial \rho}{\partial t} + 2\rho u \frac{\partial u}{\partial x} + u^2 \frac{\partial \rho}{\partial x} + \frac{\partial P}{\partial x} = \beta \qquad (2.4.2)$$

Multiplying the mass conservation equation by u, and subtracting it from equation 2.4.2 gives the following form of the Euler momentum conservation equation,

$$\rho \frac{\partial u}{\partial t} + \rho u \frac{\partial u}{\partial x} + \frac{\partial P}{\partial x} = \beta \qquad (2.4.3)$$

Expanding the energy conservation component of equation 2.3.38,

$$E\left(\frac{\partial \rho}{\partial t} + \frac{\partial}{\partial x}(\rho u)\right) + \rho \frac{\partial E}{\partial t} + \rho u \frac{\partial E}{\partial x} + u \frac{\partial P}{\partial x} + P \frac{\partial u}{\partial x} = q_h \qquad (2.4.4)$$

Multiplying the mass conservation equation by E, and subtracting from equation 2.4.4 yields,

$$\rho\frac{\partial E}{\partial t}+\rho u\frac{\partial E}{\partial x}+u\frac{\partial P}{\partial x}+P\frac{\partial u}{\partial x}=q_h \qquad (2.4.5)$$

Replacing the total energy, E by its component parts, we obtain another version of the energy conservation equation,

$$\rho\frac{\partial}{\partial t}\left(e+\frac{u^2}{2}\right)+\rho u\frac{\partial}{\partial x}\left(e+\frac{u^2}{2}\right)+u\frac{\partial P}{\partial x}+P\frac{\partial u}{\partial x}=q_h \qquad (2.4.6)$$

where e is the internal energy per unit mass.

For an ideal gas,

$$e=C_vT \qquad (2.4.7)$$

Substitution of equation 2.4.7 into 2.4.6 gives,

$$\rho\frac{\partial}{\partial t}(C_vT)+\rho u\frac{\partial}{\partial x}(C_vT)+\rho u\frac{\partial u}{\partial t}+\rho u^2\frac{\partial u}{\partial x}+u\frac{\partial P}{\partial x}+P\frac{\partial u}{\partial x}=q_h \qquad (2.4.8)$$

Since for an ideal gas,

$$C_vT=C_v\frac{P}{R\rho}=\frac{1}{\gamma-1}\frac{P}{\rho} \qquad (2.4.9)$$

where γ is the ratio of specific heats (C_p / C_v) and is always a constant for an ideal gas. Substituting equation 2.4.9 into equation 2.4.8, the resulting equation is,

$$\frac{1}{(\gamma-1)}\frac{\partial P}{\partial t}-\frac{P}{(\gamma-1)\rho}\frac{\partial \rho}{\partial t}+\frac{u}{(\gamma-1)}\frac{\partial P}{\partial x}-\frac{Pu}{(\gamma-1)\rho}\frac{\partial \rho}{\partial x}+\rho u\frac{\partial u}{\partial t}+\rho u^2\frac{\partial u}{\partial x}+u\frac{\partial P}{\partial x}+P\frac{\partial u}{\partial x}=q_h \qquad (2.4.10)$$

Multiplying the momentum conservation equation (equation 2.4.3) by u and subtracting from equation 2.4.10 gives ,

$$\frac{1}{(\gamma-1)}\left(\frac{\partial P}{\partial t}+u\frac{\partial P}{\partial x}\right)-\frac{P}{(\gamma-1)\rho}\left(\frac{\partial \rho}{\partial t}+u\frac{\partial \rho}{\partial x}\right)+P\frac{\partial u}{\partial x}+u\beta=q_h \qquad (2.4.11)$$

From the equation of continuity,

$$\frac{\partial u}{\partial x}=\frac{1}{\rho}\left(-\frac{\partial \rho}{\partial t}-u\frac{\partial \rho}{\partial x}\right) \tag{2.4.12}$$

Substituting equation 2.4.12 into 2.4.11,

$$\frac{1}{(\gamma-1)}\left(\frac{\partial P}{\partial t}+u\frac{\partial P}{\partial x}\right)-\frac{P}{\rho}\left(\frac{\partial \rho}{\partial t}+u\frac{\partial \rho}{\partial x}\right)\left(\frac{1}{(\gamma-1)}+1\right)+u\beta=q_h \tag{2.4.13}$$

Rearranging and then multiplying through by (γ-1) we obtain,

$$\left(\frac{\partial P}{\partial t}+u\frac{\partial P}{\partial x}\right)-\frac{\gamma P}{\rho}\left(\frac{\partial \rho}{\partial t}+u\frac{\partial \rho}{\partial x}\right)=(q_h-u\beta)(\gamma-1) \tag{2.4.14}$$

For an ideal gas the acoustic velocity is given by,

$$a^2=\gamma RT=\gamma\frac{P}{\rho} \tag{2.4.15}$$

Therefore the energy equation for an ideal gas is given by,

$$\left(\frac{\partial P}{\partial t}+u\frac{\partial P}{\partial x}\right)-a^2\left(\frac{\partial \rho}{\partial t}+u\frac{\partial \rho}{\partial x}\right)=(\gamma-1)(q_h-u\beta) \tag{2.4.16}$$

Therefore the equations solved in the ideal gas model are,

$$\begin{aligned}
&\rho_t+\rho u_x+u\rho_x=0\\
&\rho u_t+\rho u u_x+P_x=\beta\\
&P_t+uP_x-a^2(\rho_t+u\rho_x)=(\gamma-1)(q_h-u\beta)=\psi\\
&P=\rho RT
\end{aligned} \tag{2.4.17}$$

2.5 THERMODYNAMICS OF VAPOUR/LIQUID MIXTURE AND THE 2-PHASE FLOW MODEL

FBR results in both a drop in pressure and temperature at the ruptured end. This invariably leads to the formation of two-phase flows. In order to establish the number of phases at each x-t co-ordinate and perform the necessary mass balances, a two phase pressure/temperature flash calculation needs to be performed. This necessitates the need for accurate vapour-liquid equilibria predictions. The Peng-Robinson equation of state (EOS) is deemed suitable for such a task.

Phase equilibrium calculations based on the Peng-Robinson EOS are performed using a procedure proposed by Michelsen (1982, 1987). This equation is used primarily because of its suitability in handling multi-component hydrocarbon mixtures, but also because of the need to make a meaningful comparison between models. The Peng-Robinson EOS is used widely in other models such as those developed by Chen (1993) and Philbin and Govan (1993).

For a given fluid composition at a certain pressure and temperature, the Michelsen procedure performs a stability test to ascertain the number of phases present. The initial guess is of single phase flow only. If the stability test fails for this, then two phases are present, and the phase compositions along with phase compressibility factors and phase mole fractions are calculated. The stability tests require no user-provided initial estimates of number of phases present at equilibrium or of the equilibrium factors. The tests are all based on the tangent plane criterion of Gibbs, and for unstable systems they also provide the composition of a new phase which can be split off to decrease the Gibbs energy of the mixture (Michelsen, 1982, 1987). The above procedure is followed regardless of type of flash calculation performed, i.e isothermal, isentropic or isenthalpic.

In terms of the fluid dynamics of a real fluid system, the mass and momentum conservation equations that have already been derived are just as valid as for an ideal gas due to the fact that no assumptions are made in their respective derivation processes regarding the nature of the fluid.

The energy equation however needs to be re-derived for a two-phase fluid.

2.5.1 Deriving the energy equation for a non-ideal homogeneous fluid

The Euler conservation equation for energy is given by,

$$\frac{\partial}{\partial t}(\rho E)+\frac{\partial}{\partial x}(\rho u E+Pu)=q_h \tag{2.5.1}$$

The total energy, E can be expressed as,

$$E=e+\frac{u^2}{2}=h+\frac{u^2}{2}-\frac{P}{\rho} \tag{2.5.2}$$

where h is the specific enthalpy.

Substituting equation 2.5.2 into equation 2.5.1 we obtain,

$$\frac{\partial}{\partial t}\left[\rho\left(h+\frac{u^2}{2}\right)-P\right]+\frac{\partial}{\partial x}\left(\rho u\left(h+\frac{u^2}{2}\right)\right)=q_h \tag{2.5.3}$$

Introducing the total enthalpy, H,

$$H=h+\frac{u^2}{2} \tag{2.5.4}$$

and substituting into equation 2.5.3,

$$\frac{\partial}{\partial t}\left[(H\rho-P)\right]+\frac{\partial}{\partial x}\left[\rho u H\right]=q_h$$

$$H\frac{\partial \rho}{\partial t}+\rho\frac{\partial H}{\partial t}-\frac{\partial P}{\partial t}+\rho u\frac{\partial H}{\partial x}+H\rho\frac{\partial u}{\partial x}+Hu\frac{\partial \rho}{\partial x}=q_h \tag{2.5.5}$$

$$\rho\frac{DH}{Dt}+H\frac{D\rho}{Dt}-\frac{\partial P}{\partial t}+H\rho\frac{\partial u}{\partial x}=q_h$$

Subtracting the continuity equation from equation 2.5.5,

$$\rho\frac{DH}{Dt}-\frac{\partial P}{\partial t}-q_h=0 \qquad (2.5.6)$$

Expanding equation 2.5.6,

$$\rho\frac{\partial H}{\partial t}+\rho u\frac{\partial H}{\partial x}-\frac{\partial P}{\partial t}-q_h=0$$

$$\rho\frac{\partial}{\partial t}\left[h+\frac{u^2}{2}\right]+\rho u\frac{\partial}{\partial x}\left[h+\frac{u^2}{2}\right]-\frac{\partial P}{\partial t}-q_h=0 \qquad (2.5.7)$$

$$\rho\frac{\partial h}{\partial t}+\rho u\frac{\partial u}{\partial t}+\rho u\frac{\partial h}{\partial x}+\rho u^2\frac{\partial u}{\partial x}-\frac{\partial P}{\partial t}-q_h=0$$

Re-expressing equation 2.5.7 we have,

$$\rho\frac{Dh}{Dt}+u\left[\rho\frac{\partial u}{\partial t}+\rho u\frac{\partial u}{\partial x}\right]-\frac{\partial P}{\partial t}-q_h=0 \qquad (2.5.8)$$

Substituting for the momentum equation into equation 2.5.8,

$$\rho\frac{Dh}{Dt}-u\frac{\partial P}{\partial x}+u\beta-\frac{\partial P}{\partial t}-q_h=0$$

$$\rho\frac{Dh}{Dt}-\frac{DP}{Dt}-(q_h-u\beta)=0 \qquad (2.5.9)$$

For any fluid the following thermodynamic relationship holds,

$$dh = Tds + \upsilon dP \qquad (2.5.10)$$

where, s is the specific entropy and υ is the specific volume.

Expressing equation 2.5.10 in substantial derivative form,

$$\frac{Dh}{Dt}=T\frac{Ds}{Dt}+\frac{1}{\rho}\frac{DP}{Dt} \qquad (2.5.11)$$

Substituting equation 2.5.11 into equation 2.5.9,

$$\rho\left[T\frac{Ds}{Dt}+\frac{1}{\rho}\frac{DP}{Dt}\right]-\frac{DP}{Dt}-(q_h-u\beta)=0$$

(2.5.12)

$$\rho T\frac{Ds}{Dt}-(q_h-u\beta)=0$$

The fluid pressure, P, can be expressed as a function of density and entropy, i.e. P = f(ρ,s). Expressed in partial differential form,

$$dP=\left(\frac{\partial P}{\partial \rho}\right)_s d\rho+\left(\frac{\partial P}{\partial s}\right)_\rho ds \qquad (2.5.13)$$

where,

$$\left(\frac{\partial P}{\partial s}\right)_\rho=\varphi \qquad (2.5.14)$$

and

$$\left(\frac{\partial P}{\partial \rho}\right)_s=a^2 \text{ (speed of sound)} \qquad (2.5.15)$$

Equation 2.5.13 can be expressed in substantial derivative form,

$$\frac{DP}{Dt}=a^2\frac{D\rho}{Dt}+\varphi\frac{Ds}{Dt} \qquad (2.5.16)$$

Substituting for Ds/Dt from equation 2.5.16 into equation 2.5.12 and re-arranging, the following expression is derived,

$$\frac{DP}{Dt}-a^2\frac{D\rho}{Dt}-\varphi\left[\frac{q-u\beta}{\rho T}\right]=0 \qquad (2.5.17)$$

If

$$\varphi\left[\frac{q-u\beta}{\rho T}\right]=\psi \qquad (2.5.18)$$

then equation 2.5.17 can be expressed as,

$$\frac{DP}{Dt} - a^2 \frac{D\rho}{Dt} - \psi = 0 \qquad (2.5.19)$$

Thus an energy equation for any fluid is obtained with a form similar to that for the ideal gas model.

The above energy equation together with the continuity and momentum equations are just as valid for a non-ideal multi-phase, multi-component fluid as it is for a perfect gas, providing the following assumptions are always upheld:

- homogeneous flow where the multi-phase mixture moves at the same velocity
- thermodynamic and phase equilibrium is maintained at each x-t increment.

The speed of sound, a and the term, φ in the above equations can be calculated from closure relations derived from the equation of state. This is discussed in the following sections.

2.5.2 The Peng-Robinson Equation of State

The Peng-Robinson equation of state can be written as,

$$P = \frac{RT}{v-b} - \frac{a(T)}{v(v+b)+b(v-b)} \qquad (2.5.20)$$

where,

$$b = 0.07780\frac{RT_c}{P_c} \qquad (2.5.21)$$

$$a(T) = a(T_c)\alpha(T_r,\omega) \qquad (2.5.22)$$

$$a(T_c) = 0.45724\frac{R^2T_c^2}{P_c} \qquad (2.5.23)$$

$$\alpha(T_r,\omega) = \left[1+m\left(1-T_r^{0.5}\right)\right]^2 \qquad (2.5.24)$$

$$m = 0.377464 + 1.54226\omega - 0.26992\omega^2 \qquad (2.5.25)$$

The subscript c denotes properties at critical conditions, r denotes reduced properties, ω is the acentric factor, v is the specific molar volume (m^3/mol).

Mixing Rules

$$b = \sum_i y_i b_i \quad i = 1, n_c \tag{2.5.26}$$

$$a = \sum_i \sum_j y_i y_j a_{ij} \quad i, j = 1, n_c \tag{2.5.27}$$

$$a_{ij} = \left(1 - \delta_{ij}\right) a_i^{0.5} a_j^{0.5} \tag{2.5.28}$$

δ is the binary interaction parameter and y denotes mole fraction.

2.5.3 Closure relations for the HEM model

The cubic equations of state such as Peng-Robinson (Peng and Robinson, 1976) or SRK (Soave, 1972) lend themselves to relatively easy manipulation. The advantages and disadvantages of using a cubic equation of state are well known (Reid et. al., 1986). From a computation point of view, they are more efficient to use than other equations of state such as the corresponding states (Chen, 1993).

In the homogeneous equilibrium model a pseudo-fluid density based on liquid and gas densities needs to be calculated. The equation of state is solved for the compressibility factors from which the density of a two phase mixture can be calculated according to the equation,

$$\rho = \frac{\rho_g \rho_l}{\rho_g (1 - \chi) + \rho_l \chi} \tag{2.5.29}$$

where the subscripts g and l denote gas and liquid phase respectively. The term χ refers to the fluid quality and is the mass of vapour per unit mass of bulk fluid. The

values of the respective phase densities can be calculated according to the following equations,

$$\rho_g = \frac{PM_g}{Z_g RT} \tag{2.5.30}$$

$$\rho_l = \frac{PM_l}{Z_l RT} \tag{2.5.31}$$

The values of a and φ are determined either analytically or numerically depending on whether a single or two-phase mixture is present.

2.5.3.1 Calculation for a single phase

If the fluid consists of a single phase, as determined by Michelsen's flash calculation, then the values of a and φ are determined analytically using the following equations (Picard and Bishnoi, 1988),

$$a^2 = \frac{\gamma}{k\rho} \tag{2.5.32}$$

and

$$\varphi = \frac{\rho\beta T a^2}{C_p} \tag{2.5.33}$$

where γ is the ratio of specific heats, k is the isothermal coefficient of volumetric expansion, β is the isobaric coefficient of volumetric expansion and C_p is the specific heat capacity at constant pressure.

γ is the ratio of specific heats given by,

$$\gamma = \frac{C_p}{C_v} \tag{2.5.34}$$

The heat capacity at constant volume for any fluid is defined as,

$$C_v - C_v^0 = \left[\frac{\partial\left(e - e^0\right)}{\partial T}\right]_v \tag{2.5.35}$$

where e is the specific internal energy and e^0 is the ideal mixture specific internal energy given by,

$$e^0 = \sum_i y_i e_i^0 \quad i = 1, n \text{ (no. of components)} \tag{2.5.36}$$

where y_i is the mole fraction of component i.

To determine the real fluid internal energy, we first write the fundamental property relation for a fluid of any composition (Smith and Van Ness, 1991),

$$de = Tds - Pdv \tag{2.5.37}$$

where e, s and v are either molar or mass specific internal energy, entropy and volume respectively.

Dividing through by dv at constant T,

$$\left(\frac{de}{dv}\right)_T = T\left(\frac{ds}{dv}\right)_T - P \tag{2.5.38}$$

From the Maxwell's equations,

$$\left(\frac{ds}{dv}\right)_T = \left(\frac{\partial P}{\partial T}\right)_v \tag{2.5.39}$$

Rewriting equation 2.5.38,

$$\left(\frac{\partial e}{\partial v}\right)_T = T\left(\frac{\partial P}{\partial T}\right)_v - P \tag{2.5.40}$$

$$\int_{e^0}^{e} de = e - e^0 = \int_{\infty}^{v}\left[T\left(\frac{\partial P}{\partial T}\right)_v - P\right]dv$$

where for an ideal gas mixture the compressibility factor Z approaches unity, the pressure approaches zero and the specific volume will be infinity.

Rewriting equation 2.5.35 in terms of equation 2.5.40,

$$C_v - C_v^0 = -\int_v^\infty \frac{\partial}{\partial T}\left[\left(T\left(\frac{\partial P}{\partial T}\right)_v - P\right)dv\right] = \tag{2.5.41}$$

$$-\int_v^\infty \left[\left(\frac{\partial P}{\partial T}\right)_v dv + T\left(\frac{\partial^2 P}{\partial T^2}\right)_v dv + T\left(\frac{\partial P}{\partial T}\right)_v \left(\frac{\partial (dv)}{\partial T}\right)_v - \left(\frac{\partial P}{\partial T}\right)_v dv - P\left(\frac{\partial (dv)}{\partial T}\right)_v\right]$$

For constant v the differentials involving dv will equal zero and so equation 2.5.41 can be written as,

$$C_v - C_v^0 = -\int_v^\infty T\left(\frac{\partial^2 P}{\partial T^2}\right)_v dv \tag{2.5.42}$$

Performing the necessary differentiation from the Peng-Robinson equation of state,

$$\left(\frac{\partial P}{\partial T}\right)_v = \frac{R}{v-b} - \frac{a'(T)}{v(v+b)+b(v-b)}$$

$$\left(\frac{\partial^2 P}{\partial T^2}\right)_v = -\frac{a''(T)}{v(v+b)+b(v-b)} \tag{2.5.43}$$

where the terms a`(T) and a``(T) refer respectively to single and double differentials of a(T) with respect to temperature, T.

Therefore equation 2.5.42 can be written as,

$$C_v - C_v^o = a''(T)T \int_v^\infty \frac{dv}{v(v+b)+b(v-b)} \tag{2.5.44}$$

Dividing the integral term into partial fractions we obtain,

$$C_v - C_v^o = a''(T)T \int_v^\infty \left[\frac{1}{\sqrt{8}b\left(v-\left(\frac{\sqrt{8}}{2}-1\right)b\right)} - \frac{1}{\sqrt{8}b\left(v+\left(\frac{\sqrt{8}}{2}+1\right)b\right)} \right] dv \tag{2.5.45}$$

Performing the integration we obtain,

$$C_v - C_v^o = \frac{a''(T)T}{\sqrt{8}\,b}\left[\ln\left|v-\left(\frac{\sqrt{8}}{2}-1\right)b\right| - \ln\left|v+\left(\frac{\sqrt{8}}{2}+1\right)b\right| \right]_v^\infty \tag{2.5.46}$$

$$= -\frac{a''(T)}{\sqrt{8}\,b} T \ln \left| \frac{v-\left(\frac{\sqrt{8}}{2}-1\right)b}{v+\left(\frac{\sqrt{8}}{2}+1\right)b} \right|$$

The term a``(T) can be calculated from equation 2.5.22,

$$a(T) = a(T_c)\left[1+m\left(1-\left(\frac{T}{T_c}\right)^{0.5}\right)\right]^2$$

$$a'(T) = a(T_c)2\left[1+m\left(1-\left(\frac{T}{T_c}\right)^{0.5}\right)\right]\left(-0.5m\left(\frac{1}{T_c}\right)^{0.5}T^{-0.5}\right)$$

$$a''(T) = 2a(T_c)\left\{\begin{array}{l}\left[1+m\left(1-\left(\frac{T}{T_c}\right)^{0.5}\right)\right]\left(0.25m\left(\frac{1}{T_c}\right)^{0.5}T^{-1.5}\right)\\ +\left(-0.5m\left(\frac{1}{T_c}\right)^{0.5}T^{-0.5}\right)^2\end{array}\right\} \qquad (2.5.47)$$

The ideal gas specific heat capacity at constant volume is temperature dependant only, and is given by,

$$C_v^o = \sum_i y_i C_{vi}^o = \sum_i y_i\left(C_{pi}^o - R\right), \quad i = 1, n_c \qquad (2.5.48)$$

Therefore using equations 2.5.46 to 2.5.48, the real fluid specific heat capacity at constant volume can be calculated.

The heat capacity at constant pressure is defined as,

$$C_p - C_p^0 = \left[\frac{\partial\left(h-h^0\right)}{\partial T}\right]_P \qquad (2.5.49)$$

where h is the specific enthalpy of the real fluid and h^0 is the specific enthalpy of an ideal mixture, and is given by,

$$h^0 = \sum_i y_i h_i^0 \quad i = 1, n \text{ (no. of components)} \qquad (2.5.50)$$

In order to derive an expression for the specific enthalpy term in equation 2.5.49, the following fundamental property relation needs to be manipulated,

$$dh = de + d(Pv) \tag{2.5.51}$$

For the residual enthalpy term, equation 2.5.51 can be written as,

$$\int_{h^0}^{h} dh = \int_{e^0}^{e} de + \int_{Pv_{ideal}}^{Pv} d(Pv) \tag{2.5.52}$$

i.e.

$$h - h^0 = e - e^0 + Pv - RT \tag{2.5.53}$$

Substituting for the residual internal energy term from equation 2.5.40,

$$h - h^0 = Pv - RT - \int_{v}^{\infty} \left[T\left(\frac{\partial P}{\partial T}\right)_v - P \right] dv \tag{2.5.54}$$

Solving the integral part of equation 2.5.54 separately,

$$\int_{v}^{\infty} \left[T\left(\frac{\partial P}{\partial T}\right)_v - P \right] dv = \int_{v}^{\infty} \left[\frac{RT}{(v-b)} - \frac{a'(T)T}{v(v+b)+b(v-b)} - P \right] dv \tag{2.5.55}$$

Substituting for RT/(v-b) - P from the equation of state (equation 2.5.20),

$$\int_{v}^{\infty} \left[\frac{a(T)}{v(v+b)+b(v-b)} - \frac{a'(T)T}{v(v+b)+b(v-b)} \right] dv = a(T) - a'(T)T \int_{v}^{\infty} \frac{dv}{v(v+b)+b(v-b)} \tag{2.5.56}$$

Breaking the integral up into partial fractions and solving the resulting integrals, the following expression is derived,

$$\frac{a(T)-a'(T)T}{\sqrt{8}\,b}\int_{v}^{\infty}\left[\frac{1}{\left(v-\left(\frac{\sqrt{8}}{2}-1\right)b\right)}-\frac{1}{\left(v+\left(\frac{\sqrt{8}}{2}+1\right)b\right)}\right]dv =$$

$$-\frac{a(T)-a'(T)T}{\sqrt{8}\,b}\ln\left|\frac{v-\left(\frac{\sqrt{8}}{2}-1\right)b}{v+\left(\frac{\sqrt{8}}{2}+1\right)b}\right| \qquad (2.5.57)$$

Therefore, the specific enthalpy term can be expressed from equation 2.5.54 in residual property form as,

$$h-h^0 = Pv-RT+\left[\frac{a(T)-a'(T)T}{\sqrt{8}\,b}\left(\ln\left|\frac{v-\left(\frac{\sqrt{8}}{2}-1\right)b}{v+\left(\frac{\sqrt{8}}{2}+1\right)b}\right|\right)\right] \qquad (2.5.58)$$

Substituting for h - h^0 from equation 2.5.58 into the equation for the specific heat capacity at constant pressure, equation 2.5.49,

$$C_P-C_P^0 = P\left(\frac{\partial v}{\partial T}\right)_P-R+\frac{\partial}{\partial T}\left[\frac{a(T)-a'(T)T}{\sqrt{8}\,b}\ln\left|\frac{v-\left(\frac{\sqrt{8}}{2}-1\right)b}{v+\left(\frac{\sqrt{8}}{2}+1\right)b}\right|\right]_P \qquad (2.5.59)$$

Expanding the large differential term separately, we obtain,

$$\frac{\partial}{\partial T}\left[\frac{a(T)-a'(T)T}{\sqrt{8}\,b}\ln\left|\frac{v-\left(\frac{\sqrt{8}}{2}-1\right)b}{v+\left(\frac{\sqrt{8}}{2}+1\right)b}\right|\right]_p =$$

$$\frac{a(T)-a'(T)T}{\sqrt{8}\,b}\left(\frac{\partial v}{\partial T}\right)_P\left(\frac{v+\left(\frac{\sqrt{8}}{2}+1\right)b-v+\left(\frac{\sqrt{8}}{2}-1\right)b}{\left(v-\left(\frac{\sqrt{8}}{2}-1\right)b\right)\left(v+\left(\frac{\sqrt{8}}{2}+1\right)b\right)}\right)$$

$$+\frac{(a'(T)-a'(T)-a''(T)T)}{\sqrt{8}\,b}\ln\left|\frac{v-\left(\frac{\sqrt{8}}{2}-1\right)b}{v+\left(\frac{\sqrt{8}}{2}+1\right)b}\right| =$$

$$\frac{a(T)-a'(T)T}{\left(v-\left(\frac{\sqrt{8}}{2}-1\right)b\right)\left(v+\left(\frac{\sqrt{8}}{2}+1\right)b\right)}\left(\frac{\partial v}{\partial T}\right)_P-\frac{a''(T)T}{\sqrt{8}\,b}\ln\left|\frac{v-\left(\frac{\sqrt{8}}{2}-1\right)b}{v+\left(\frac{\sqrt{8}}{2}+1\right)b}\right| \quad (2.5.60)$$

Substituting equation 2.5.60 into equation 2.5.59 we obtain,

$$C_P-C_P^0=\left(\frac{\partial v}{\partial T}\right)_P\left[P+\frac{a(T)}{v(v+b)+b(v-b)}-\frac{a'(T)T}{v(v+b)+b(v-b)}\right]-R \quad (2.5.61)$$

$$-\frac{a''(T)T}{\sqrt{8}\,b}\ln\left|\frac{v-\left(\frac{\sqrt{8}}{2}-1\right)b}{v+\left(\frac{\sqrt{8}}{2}+1\right)b}\right|$$

Substituting from the Peng-Robinson equation of state, equation 2.5.20, we obtain,

$$C_P - C_P^0 = T\left(\frac{\partial v}{\partial T}\right)_P\left[\frac{R}{(v-b)} - \frac{a'(T)}{v(v+b)+b(v-b)}\right] - R$$

$$-\frac{a''(T)T}{\sqrt{8}\,b}\ln\left|\frac{v-\left(\frac{\sqrt{8}}{2}-1\right)b}{v+\left(\frac{\sqrt{8}}{2}+1\right)b}\right| \qquad (2.5.62)$$

Substituting equation 2.5.43 for $(\partial P/\partial T)_v$ into the above,

$$C_P - C_P^0 = T\left(\frac{\partial v}{\partial T}\right)_P\left(\frac{\partial P}{\partial T}\right)_v - R - \frac{a''(T)T}{\sqrt{8}\,b}\ln\left|\frac{v-\left(\frac{\sqrt{8}}{2}-1\right)b}{v+\left(\frac{\sqrt{8}}{2}+1\right)b}\right| \qquad (2.5.63)$$

Using the chain rule for PVT relations,

$$\left(\frac{\partial v}{\partial T}\right)_P\left(\frac{\partial P}{\partial v}\right)_T\left(\frac{\partial T}{\partial P}\right)_v = -1 \qquad (2.5.64)$$

Rewriting,

$$\left(\frac{\partial v}{\partial T}\right)_P = \frac{-1}{\left(\frac{\partial P}{\partial v}\right)_T\left(\frac{\partial T}{\partial P}\right)_v} = \frac{-\left(\frac{\partial P}{\partial T}\right)_v}{\left(\frac{\partial P}{\partial v}\right)_T} \qquad (2.5.65)$$

Substituting equation 2.5.65 into equation 2.5.63,

$$C_p - C_p^o = -R - \frac{T\left(\frac{\partial P}{\partial T}\right)_v^2}{\left(\frac{\partial P}{\partial v}\right)_T} - \frac{a''(T)T}{\sqrt{8}\,b}\ln\left|\frac{v-\left(\frac{\sqrt{8}}{2}-1\right)b}{v+\left(\frac{\sqrt{8}}{2}+1\right)b}\right| \qquad (2.5.66)$$

Calculating the differential terms on the right hand side of equation 2.5.66 separately,

$$\left(\frac{\partial P}{\partial v}\right)_T = \frac{-RT}{(v-b)^2} + \frac{(2v+2b)a(T)}{[v(v+b)+b(v-b)]^2} \tag{2.5.67}$$

$$\left(\frac{\partial P}{\partial T}\right)_v^2 = \left[\frac{R}{v-b} - \frac{a'(T)}{v(v+b)+b(v-b)}\right]^2 =$$

$$= \frac{R^2}{(v-b)^2} - \frac{2R}{(v-b)}\frac{a'(T)}{(v(v+b)+b(v-b))} + \frac{a'(T)^2}{[v(v+b)+b(v-b)]^2} =$$

$$= \frac{R^2[v(v+b)+b(v-b)]^2 - 2Ra'(T)(v-b)[v(v+b)+b(v-b)] + a'(T)^2(v-b)^2}{(v-b)^2[v(v+b)+b(v-b)]^2} \tag{2.5.68}$$

Substituting equations 2.5.68 and 2.5.67 into equation 2.5.66 and performing some algebraic manipulations lead to the following expression for the isobaric specific heat capacity,

$$C_p - C_p^o = -R - \frac{T\left[R\left(v^2+bv\right)-(Rb-a'(T))(v-b)\right]^2}{2a(T)(v+b)(v-b)^2 - RT(v(v+b)+b(v-b))^2} \tag{2.5.69}$$

$$-\frac{a''(T)T}{\sqrt{8}\,b}\ln\left|\frac{v-\left(\frac{\sqrt{8}}{2}-1\right)b}{v+\left(\frac{\sqrt{8}}{2}+1\right)b}\right|$$

The ideal gas isobaric specific heat capacity can be written as,

$$C_p^o = \sum_i y_i C_{pi}^o \quad i = 1, n_c \tag{2.5.70}$$

Referring back to the equation for the speed of sound, equation 2.5.32, k is the isothermal coefficient of volumetric expansion and can be defined as,

where v is the specific volume of the fluid.

The term β in equation 2.5.33 refers to the isobaric coefficient of volumetric expansion and can be written as,

$$\beta = \frac{1}{\upsilon}\left(\frac{\partial \upsilon}{\partial T}\right)_P \qquad (2.5.72)$$

The above terms k and β, can also be obtained from the Peng-Robinson equation of state.

For k, substituting the inverse of equation 2.5.67 into equation 2.5.71,

$$k = -\frac{1}{v}\left(\frac{\partial v}{\partial P}\right)_T = -\left[\frac{-\left[v(v+b)(v-b)+b(v-b)^2\right]^2}{2av(v+b)(v-b)^2 - RTv\left[v(v+b)+b(v-b)\right]^2}\right] \qquad (2.5.73)$$

For β, equation 2.5.65 can be substituted into equation 2.5.72 to give the following expression,

$$\beta = \frac{1}{v}\frac{\left(\frac{\partial P}{\partial T}\right)_v}{\left(\frac{\partial P}{\partial v}\right)_T} \qquad (2.5.74)$$

Substituting for the differentials $(\partial P/\partial T)_v$ and $(\partial P/\partial v)_T$ from equations 2.5.43 and 2.5.67 respectively, into equation 2.5.74, we obtain an expression for β ,

$$\beta = \frac{(v-b)\left(v(v+b)+b(v-b)\right)\left[R\left(v(v+b)+b(v-b)\right)-a'(T)(v-b)\right]}{2va(T)(v+b)(v-b)^2 - RTv\left[v(v+b)+b(v-b)\right]^2} \qquad (2.5.75)$$

2.5.3.2 Two Phase Flow

For two-phase flows, the analytical determination of γ and C_p becomes complex. It is more convenient to evaluate the parameters, a and φ numerically. This is done at a given temperature and pressure. The sound velocity can be expressed as,

$$a^2 = \frac{\Delta P}{\rho(T,P) - \rho(T^*, P - \Delta P)} \tag{2.5.76}$$

Since, by definition the sound velocity is given by the change in pressure per unit change in density at constant entropy, the superscript * indicates that the temperature, T is the parameter that is changed until the isentropic condition is satisfied. Therefore the following condition must apply,

$$s(T,P) = s(T^*, P - \Delta P) \tag{2.5.77}$$

To solve for T^*, a Newton-Raphson iteration can be done where the objective function is written as,

$$\varpi^{(n)} = s(T,P) - s(T^{*(n)}, P - \Delta P) \tag{2.5.78}$$

The superscript (n) denotes the iteration level.

For the entropy term, an expression for the residual entropy is needed. A starting point for this is the Maxwell relation,

$$\left(\frac{\partial s}{\partial v}\right)_T = \left(\frac{\partial P}{\partial T}\right)_v \tag{2.5.79}$$

Rearranging,

$$ds = \left(\frac{\partial P}{\partial T}\right)_v dv \tag{2.5.80}$$

Introducing the ideal gas specific volume at the system temperature and pressure,

$$v^{ig} = \frac{RT}{P} \tag{2.5.81}$$

Now integrating equation 2.5.80 for an ideal gas over an ideal gas specific volume range,

$$s^{o} - s^{(\infty)} = \int_{\infty}^{v^{ig}} \left(\frac{\partial P}{\partial T}\right)_{v^{ig}} dv = \int_{\infty}^{v^{ig}} \frac{R}{v} dv \tag{2.5.82}$$

where $s^{(\infty)}$ is the ideal gas entropy at P=0 and s^{o} is the ideal gas entropy at a given temperature and pressure.

Integrating equation 2.5.80 over a whole range of volumes,

$$s^{(\infty)} - s = -\int_{\infty}^{v} \left(\frac{\partial P}{\partial T}\right)_{v} dv \tag{2.5.83}$$

The residual entropy can therefore be given by the summation of equations 2.5.82 and 2.5.83 together with the following,

$$0 = \int_{\infty}^{v} \frac{R}{v} dv - \int_{\infty}^{v} \frac{R}{v} dv \tag{2.5.84}$$

so that,

$$s^o - s = \int_{\infty}^{v^{ig}} \frac{R}{v}dv - \int_{\infty}^{v} \frac{R}{v}dv - \int_{\infty}^{v} \left(\frac{\partial P}{\partial T}\right)_v dv + \int_{\infty}^{v} \frac{R}{v}dv$$

$$= \int_{v}^{v^{ig}} \frac{R}{v}dv + \int_{\infty}^{v} \left[\frac{R}{v} - \left(\frac{\partial P}{\partial T}\right)_v\right]dv \qquad (2.5.85)$$

Re-arranging the above,

$$s - s^o = -R\ln\left|\frac{v^{ig}}{v}\right| - \int_{\infty}^{v} \left[\frac{R}{v} - \left(\frac{\partial P}{\partial T}\right)_v\right]dv$$

$$= -R\ln\left|\frac{RT}{Pv}\right| - \int_{v}^{\infty} \left[\left(\frac{\partial P}{\partial T}\right)_v - \frac{R}{v}\right]dv = R\ln Z - \int_{v}^{\infty} \left[\left(\frac{\partial P}{\partial T}\right)_v - \frac{R}{v}\right]dv \qquad (2.5.86)$$

Often ideal gas entropy values are given at a reference temperature and pressure, so to calculate the ideal gas entropy at the system temperature and pressure (Smith et. al., 1996),

$$s^o = s^o_* + \int_{T_*}^{T} C_P^{id}\frac{dT}{T} - R\ln\left|\frac{P}{P_*}\right| = s^o_* + C_P^{id}\ln\left|\frac{T}{T_*}\right| - R\ln\left|\frac{P}{P_*}\right| \qquad (2.5.87)$$

where the subscript * refers to conditions at the reference point.

Expanding equation 2.5.86 by substituting from equation 2.5.43 for $(\partial P/\partial T)_v$,

$$s - s^o = R\ln Z - \int_v^\infty \left[\frac{R}{v-b} - \frac{a'(T)}{v(v+b)+b(v-b)} - \frac{R}{v}\right]dv \tag{2.5.88}$$

$$= R\ln Z - R\int_v^\infty \left[\frac{1}{(v-b)} - \frac{1}{v}\right]dv + a'(T)\int_v^\infty \frac{dv}{v(v+b)+b(v-b)}$$

Separating the above into partial fractions and performing the integration,

$$s - s^o = R\ln Z + R\ln\left|\frac{v-b}{v}\right| - \frac{a'(T)}{\sqrt{8}\,b}\ln\left|\frac{v-\left(\frac{\sqrt{8}}{2}-1\right)b}{v+\left(\frac{\sqrt{8}}{2}+1\right)b}\right| \tag{2.5.89}$$

The ideal gas mixture entropy can be calculated from the equation,

$$s^o = \sum_i y_i s_i^o - R\sum_i y_i \ln(y_i) \quad i = 1, n_c \tag{2.5.90}$$

The above procedure for calculation of entropy from the equation of state can be followed for either gas or liquid phase. The bulk entropy of the two-phase mixture is then obtained by,

$$s = (1-\chi)s_l + \chi s_g \tag{2.5.91}$$

where χ is the mass fraction of vapour in the mixture as is also used in the calculation of bulk density (equation 2.5.29).

The only parameter left that needs accounting for is φ. The numerical expression for the parameter can be obtained from equation 2.5.14,

$$\varphi = \left(\frac{\Delta P}{\Delta s}\right)_{\rho} = \frac{\Delta P}{s(T,P) - s\left(T^{*}, P - \Delta P\right)} \tag{2.5.92}$$

However, considering the fundamental property relation,

$$d\varphi = Tds - Pd\left(\frac{1}{\rho}\right) = Tds + \frac{P}{\rho^{2}} d\rho \tag{2.5.93}$$

From this the following partial differential relation can be written,

$$\left(\frac{\partial T}{\partial \rho}\right)_{s} = \left(\frac{\partial\left(P/\rho^{2}\right)}{\partial s}\right)_{\rho} \tag{2.5.94}$$

Therefore another expression for φ can be,

$$\varphi = \left(\frac{\Delta P}{\Delta s}\right)_{\rho} = \rho^{2}\left(\frac{\Delta T}{\Delta \rho}\right)_{s} \tag{2.5.95}$$

Hence by performing an isentropic flash calculation as given by equation 2.5.76, the above can be solved numerically.

2.6 CONCLUDING REMARKS

In this chapter, various assumptions regarding flow in a pipeline following FBR are made in the derivation of the Euler equations. Using ideal gas thermodynamic relations, a simple model based on four equations of mass, momentum and energy conservation together with the ideal gas equation of state is derived.

With regards to real fluid flow, the use of the homogeneous equilibrium assumption has been shown to be valid for flow in long pipelines (Chen, 1993) and is also adopted in the present model. By making this assumption, a single momentum equation is sufficient for both phases and likewise with respect to the energy equation for the assumption of thermodynamic equilibrium between the two phases. As a result, the equations obtained for a real fluid are similar to those obtained for an ideal gas, but the use of real fluid thermodynamic relations in the derivation of the energy equation means that the present mathematical model is able to deal with any type of fluid regardless of its state.

The use of the derived thermodynamic relations require prior knowledge of the state of the mixture. This is provided by the Michelsen stability criterion.

CHAPTER 3: NUMERICAL METHODS FOR THE SOLUTION OF HYPERBOLIC SYSTEMS OF EQUATIONS

3.1 INTRODUCTION

As shown in the previous chapter, full-bore rupture (FBR) of high pressure gas pipeline is inherently an unsteady flow phenomenon leading to rapid de-pressurisation at the broken end. Even though this may lead to formation of condensate as both pressure and temperature drop dramatically, comparison with field data (Chen et. al., 1993; Picard and Bishnoi, 1989) for long pipelines indicates that the homogeneous equilibrium model where the two phases are assumed to move at the same velocity at thermal equilibrium is applicable.

The partial differential equations pertaining to conservation of mass, momentum and energy together with an equation of state (EOS) constitute a system of equations that are essentially Euler equations with stiff source terms due to the friction term in the momentum equation and the heat transfer term in the energy equation.

The Euler equations constitute the most complete description of inviscid, non-heat conducting flows and hence, is the highest level of approximation for non-viscous fluids. Obviously the inviscid flow models are not applicable on a universal basis, but the importance of their accurate numerical simulation resides in the dominating convective character of the Navier-Stokes equations at high Reynolds numbers. Therefore most numerical methods developed for the Euler equations are also valid for the Navier-Stokes equations. It is only at very low Reynolds numbers, when the flow is diffusion dominated, that specific methods for the Navier-Stokes equations have to be defined.

Solution of the Euler equations can be traced as far back as the first order schemes of Courant et. al. (1952) and Lax and Friedrichs (Lax, 1954). Many techniques used today for the time-dependent Euler equations are based on pioneering work by Lax

and Wendroff (Lax, 1957; Lax and Wendroff, 1960, 1964). The second order accurate Lax-Wendroff method has led to a whole family of variants for application to non-linear systems, characterised by their common property of being space centred, reducing to the three-point central schemes in one dimension, explicit in time and derived from a combined space and time discretisation.

A variety of high-resolution numerical methods have been developed over the past several decades that resolve discontinuities and rapidly changing flows sharply and yet produce at least second-order accuracy in smooth flows. Understanding of the different numerical methods available and appropriate implementation of a scheme for the resolution of a particular problem requires not only a thorough grasp of the physical nature of the flow being considered, but also a good foundation in the mathematical theory of hyperbolic conservation laws.

In the following sections, a brief introduction to the nature of hyperbolic equations is put forward. It is shown how the Euler equations, derived on the basis of the inviscid bulk fluid flow assumption in chapter 2, can be classified as hyperbolic. Subsequently, all available approaches to the numerical resolution of the Euler equations are presented. This is then followed by a review of the methods used by various authors to model the problem of FBR.

3.2 HYPERBOLIC EQUATIONS

Partial differential equations are said to be hyperbolic if they admit sharp discontinuities such as shock waves in their solution, discontinuities that can form even from smooth initial data. These are mathematical idealisations of the steep gradients that can occur in smooth solutions to the full Navier-Stokes equations, where rapid changes are present over very thin zones (relative to the spatial grid that must be modelled). Often the width of these viscous shock layers are much smaller than the distance between grid points on a reasonable computational grid, in which case modelling the structure within these layers is impossible and hence a good approximation to the macroscopic behaviour has to be used.

Computationally the solution of these hyperbolic equations has many advantages. Explicit methods rather than implicit methods can typically be used, resulting in a substantial reduction in computation time required, although this does depend on the nature of the transient that is being modelled. This is explored further later in the chapter.

In Chapter 2, the Euler equations of flow for a compressible fluid were derived. The equation is repeated here for reference,

$$\frac{\partial}{\partial t}V+\frac{\partial}{\partial x}F(V)+G=0 \qquad (2.3.39)$$

Since in the case of high pressure pipeline rupture problems, the disturbance within the pipeline is an expansion wave as opposed to a shock wave, equation 2.3.39 was expressed in primitive variable form to yield a set of quasi-linear, first order one-dimensional equations of the form,

$$AV_t+BV_x+G=0 \qquad (3.2.1)$$

where

$$V = \begin{pmatrix} \rho \\ u \\ P \end{pmatrix} \tag{3.2.2}$$

$$A = \begin{pmatrix} 1 & 0 & 0 \\ 0 & \rho & 0 \\ -a^2 & 0 & 1 \end{pmatrix} \tag{3.2.3}$$

$$B = \begin{pmatrix} u & \rho & 0 \\ 0 & \rho u & 1 \\ -a^2 u & 0 & u \end{pmatrix} \tag{3.2.4}$$

$$G = \begin{pmatrix} 0 \\ -\beta \\ -\psi \end{pmatrix} \tag{3.2.5}$$

A system of quasi-linear partial differential equations of the first order can be called hyperbolic if its homogeneous part admits wave-like solutions. In order to demonstrate this, equation 2.3.39 needs to be expressed in the following form,

$$V_t + B_1 V_x + G_1 = 0 \tag{3.2.6}$$

Dividing the momentum equation (see equation 2.4.3) by density, ρ, we have,

$$u_t + u u_x + \frac{1}{\rho} P_x = \frac{\beta}{\rho} \tag{3.2.7}$$

and by substituting for the mass conservation equation into the present form of the energy conservation equation (equation 2.5.19), we have,

$$P_t + u P_x + a^2 \rho u_x = \psi \tag{3.2.8}$$

Therefore the matrices B_1 and G_1 can be written as,

$$B_1 = \begin{pmatrix} u & \rho & 0 \\ 0 & u & \frac{1}{\rho} \\ 0 & \rho a^2 & u \end{pmatrix} \tag{3.2.9}$$

and,

$$G_1 = \begin{pmatrix} 0 \\ -\frac{\beta}{\rho} \\ -\psi \end{pmatrix} \tag{3.2.10}$$

The condition for hyperbolicity is expressed by the existence of simple wave-like solutions of the form,

$$V = \hat{V}e^{IS(\vec{x},t)} = \hat{V}e^{I(\vec{k}.\vec{x}-\omega t)}, \qquad I = \sqrt{-1} \tag{3.2.11}$$

The function,

$$S(\vec{x},t) = \vec{k},\vec{x} - \omega t \tag{3.2.12}$$

represents the phase of the wave propagating in the direction $\vec{k}$, with a pulsation ω (for an observer moving with the group velocity of the wave packet).

Wave-like solutions will exist if the eigenvalues of the matrix,

$$\tilde{K} = \tilde{\tilde{B}}_1.\vec{k} \tag{3.2.13}$$

for arbitrary $\vec{k}$, are real with linear independence of the corresponding left eigenvectors $\vec{L}$.

If $\lambda_{(j)}$ denotes a non-trivial solution eigenvalue of the matrix $\tilde{K}$, then this eigenvalue is obtained (by definition) from,

$$\det\left|\tilde{\tilde{B}}_1.\vec{k} - \lambda.\vec{k}\right| = 0 \tag{3.2.14}$$

The vector $\vec{k}$ is one dimensional and hence,

$$\vec{k} = k\vec{l}_x \tag{3.2.15}$$

Since the magnitude of this vector is arbitrary, one can take k = 1, and the eigenvalue equation (3.2.9) becomes,

$$\det\left|\tilde{B}_1 - \lambda\right| = 0 \tag{3.2.16}$$

and,

$$\det\left|\tilde{B}_1 - \lambda\right| = \det\begin{vmatrix} u-\lambda & \rho & 0 \\ 0 & u-\lambda & \frac{1}{\rho} \\ 0 & \rho a^2 & u-\lambda \end{vmatrix}$$

$$(u-\lambda)\left\{(u-\lambda)^2 - a^2\right\} = 0 \tag{3.2.17}$$

Equation 3.2.17 has three real solutions or eigenvalues,

$$\begin{aligned} \lambda_1 &= u \\ \lambda_2 &= u + a \\ \lambda_3 &= u - a \end{aligned} \tag{3.2.18}$$

Associated with these three eigenvalues will be a set of independent left and right eigenvectors so that,

$$B_1 = R\Lambda R^{-1} \tag{3.2.19}$$

where,

$$\Lambda = \begin{pmatrix} \lambda_1 & 0 & 0 \\ 0 & \lambda_2 & 0 \\ 0 & 0 & \lambda_3 \end{pmatrix} \tag{3.2.20}$$

is a diagonal matrix of eigenvalues and R is the matrix of right eigenvectors,

$$R = \left[r_1\right| \ \ r_2\left| \ \ r_3\right|] \tag{3.2.21}$$

The eigenvectors can obtained by considering that,

$$B_1 r_p = \lambda_p r_p \qquad p = 1,2,3 \tag{3.2.22}$$

The phase velocity, $\vec{a}$ of the propagating wave is defined by the usual wave relations,

$$\vec{a} = \frac{\omega}{k}$$

$$\vec{a} = \lambda \frac{\vec{k}}{k^2} = \frac{d\vec{x}}{dt} \tag{3.2.23}$$

in the direction of $\vec{k}$, that is normal to the constant wave phase surface $S(\vec{x},t)$ = constant.

Therefore the three equations of mass, momentum and energy conservation that make up the Euler equations have been shown to have three real eigenvalues. It is this property that makes these equations hyperbolic. This implies that a hyperbolic set of equations will be associated with propagating waves and that the behaviour and properties of the physical system described by these equations will be dominated by wave-like phenomena. In fact the speed of propagation of these waves, known as Mach lines, is given by the eigenvalues (u+a) and (u-a) corresponding to right running and left running characteristics respectively. The pathline characteristic is given by λ_1. These characteristics can handle any type of discontinuity in fluid flow such as a shock wave, contact surface or expansion fan.

3.3 FINITE DIFFERENCE THEORY

This section contains a brief overview of the fundamental theory necessary for the proper discretisation of partial differential equations (PDE's) and ordinary differential equations (ODE's). Many elementary texts are available on this subject, e.g. (Iserles, 1996, Morton and Mayers, 1994, Richtmyer and Morton, 1967).

In essence, there are two numerical techniques for the solution of partial differential equations; implicit and explicit methods. The explicit method is one that yields an explicit expression for each value at time t_{n+1} in terms of nearby values at time t_n. An implicit method couples together values at different grid points at time t_{n+1} and hence an algebraic system of equations must be solved in each time step in order to advance the solution.

3.3.1 Explicit Methods

Explicit finite difference methods integrate the basic partial difference equations by considering the changes in the dependent variables (P, u and ρ in our case) along the directions of the independent variables (x and t).

Considering finite difference grids with mesh spacing $h = \Delta x = \Delta y = \Delta z$ in all spatial directions and $k = \Delta t$ in the time step, subscript indices can be taken to indicate the spatial grid point while the superscript indicates the temporal step, therefore $V_i^n = V(x_i,t_n)$, i.e. the quantity V at space step x_i and time step t_n.

With a finite difference method, the derivatives appearing in the differential equation are discretised so that a system of algebraic relations between (approximate) values at all the grid points are obtained. The solution of this finite set of differential equations for discrete grid point values can then be performed on a computer.

As a means of illustration of different finite difference methods, equation 3.2.6 is used without the source terms for discretisation, i.e.,

$$V_t + AV_x = 0 \qquad (3.3.1)$$

There are many different ways to discretise the derivatives, leading to different finite difference methods. As one example, using one-sided approximations to both V_t and V_x gives,

$$\frac{V_i^{n+1} - V_i^n}{k} + A\left(\frac{V_i^n - V_{i-1}^n}{h}\right) = 0 \qquad (3.3.2)$$

or,

$$\frac{V_i^{n+1} - V_i^n}{k} + A\left(\frac{V_{i+1}^n - V_i^n}{h}\right) = 0 \qquad (3.3.3)$$

Choosing which scheme is more suitable to describe the flow under consideration depends on the velocity u. If u>0 then the fluid flows from left to right and equation 3.3.2 should be used since it updates V_i^n based on the value V_{i-1}^n to the left (in the upstream or upwind direction). Likewise, if u<0 then equation 3.3.3 is better. These methods are called the first order upwind methods. Rewriting them, an explicit formula for V_i^{n+1} in terms of data at the previous time step can be obtained,

$$V_i^{n+1} = V_i^n - \frac{k}{h}A\left(V_i^n - V_{i-1}^n\right) \qquad (3.3.4)$$

To achieve second order accuracy, centred approximations to the derivatives can be used,

$$\frac{V_i^{n+1} - V_i^{n-1}}{2k} + A\left(\frac{V_{i+1}^n - V_{i-1}^n}{2h}\right) = 0 \qquad (3.3.5)$$

which then gives the leapfrog method (Heath and Blunt, 1969),

$$V_i^{n+1} = V_i^{n-1} - \frac{k}{h}A\left(V_{i+1}^n - V_{i-1}^n\right) \qquad (3.3.6)$$

Another approach is based on the Taylor series expansion,

$$V(x,t+k) = V(x,t) + kV_t(x,t) + \frac{1}{2}k^2V_{tt}(x,t) + \ldots\ldots \qquad (3.3.7)$$

From equation 3.3.1, we can say that $V_t = -AV_x$ and so,

$$V_{tt} = -AV_{xt} = -AV_{tx} = A^2V_{xx} \qquad (3.3.8)$$

Substituting the above into equation 3.3.7,

$$V(x,t+k) = V(x,t) - AkV_x(x,t) + \frac{1}{2}k^2A^2V_{xx}(x,t) + \ldots\ldots \qquad (3.3.9)$$

The Lax-Wendroff method then results from retaining only the first three terms of equation 3.3.9 and using centred difference approximations for the derivatives so that,

$$V_i^{n+1} = V_i^n - \frac{k}{2h}A\left(V_{i+1}^n - V_{i-1}^n\right) + \frac{k^2}{2h^2}A^2\left(V_{i+1}^n - 2V_i^n + V_{i-1}^n\right) \qquad (3.3.10)$$

Also possible is a scheme known as predictor-corrector whereby the solution point variables are calculated using standard explicit finite difference theory, but the results are then averaged with the initial conditions to recalculate the solution variables. The MacCormack method (MacCormack, 1969) is an example of one such scheme;

Predictor Step,

$$\overline{V}_i = V_i^n - \frac{k}{h}A\left(V_{i+1}^n - V_i^n\right) \qquad (3.3.11)$$

Corrector Step,

$$V_i^{n+1} = \frac{1}{2}\left[\overline{V}_i + V_i^n\right] - \frac{k}{2h}A\left(\overline{V}_i - \overline{V}_{i-1}\right) \qquad (3.3.12)$$

For systems in which shock waves form, an explicit finite difference method can be used provided that a smoothing parameter or artificial dissipation may be employed to control the considerable overshoot and oscillation that shock waves introduce to a higher than first order solution (Hirsch, 1995; Wylie and Streeter, 1993). This can be empirical and therefore does not lend itself to a universal predictive model.

Another disadvantage of these methods is that boundary conditions, especially the choking condition found in pipeline rupture problems are not solved intrinsically. In

the case of two-phase flow modelling, the flow calculations become coupled with the flash calculations at the ruptured end and an iteration loop is necessary to find the new time-step flow variables as well as the sonic velocity or sonic characteristics (Chen, 1993). The method then becomes rather like an implicit method.

Some finite difference methods such as the Leap-frog method have an additional problem in that they become unstable if the source terms are non-zero (Heath and Blunt, 1969). This is a major drawback for the non-isentropic transient fluid flow model in this study.

For conservation laws arising from physical principles, it is often important to ensure that the numerical methods also convey the appropriate quantities, such as mass, momentum and energy. This is particularly the case when the solution involves shock waves where there is a discontinuity across the shock wave. Resolution of this discontinuity is not a trivial task and even second order methods such as the Lax-Wendroff method (Lax, 1957; Lax and Wendroff, 1960, 1964) resolves this phenomenon with a certain amount of numerical oscillation depending on the size of the discontinuity.

For conservation laws it is thus often preferable to use finite volume methods rather than a finite difference method. In the former, the discrete value V_i^n is viewed as an approximation to the average value of V over a grid cell rather than as an approximation to a point-wise value of V. The cell average is simply the integral of V over the cell divided by its area, so that conservation can be maintained by updating this value based on fluxes through the cell edges. This procedure is discussed in further detail in section 3.4. Although the derivation of such methods can be quite different from finite difference methods, the end formulas may well be identical.

The main issues that should be addressed when developing finite difference methods are outlined below.

3.3.2 Convergence and global order of accuracy

Greater accuracy and hence better approximation to the true solution should be expected if greater refinement of the numerical grid is implemented. The difference

between the true and computed solution is called the global error and the method is convergent if this goes to zero as the mesh is refined. The method has global order r if the global error is $O(h^r + k^r)$ as h, k $\rightarrow$0. In analysing a method it is generally impossible to get an expression for the global error directly since the system of equations to be solved grows without bound in size as the grid is refined.

3.3.3 Consistency and the local truncation error

The local truncation error is a measure of how well the differential equations model the difference equation locally. This is defined by inserting the true solution into the difference equations at a single arbitrary point in space-time. The true solution is generally not known, but if it is a smooth function then the Taylor series can be expanded and the differential equation can be used to determine an expansion for the local truncation error, which shows the local order of the method. If the local truncation error vanishes like $O(h^r + k^r)$ then the method is locally r'th order accurate. If the method is at all reasonable then we expect the local truncation error to at least go to zero as the mesh is refined, in which case the method is called consistent.

3.3.4 Stability

It is hoped that a method which is locally r'th order accurate will also give a global error that is r'th order, and in particular will be convergent. But this is far from obvious and may not hold. The problem lies in the fact that as refinement of the grid progresses, an increasing number of values need to be computed to solve the discrete system, and unless the discretisation is stable in some way then this process may not be convergent even though the method may be consistent. For convergence both consistency and stability are therefore required.

For partial differential equations such as the Euler equations of flow through a pipeline, there is typically some restriction on the relation between the time step k and the spatial grid size, h. Both the Lax-Wendroff method (equation 3.3.10) and the leapfrog method (equation 3.3.6) are stable only if $|\lambda k/h| \leq 1$ for all eigenvalues λ of the matrix A. This is motivated by the discussion of the CFL condition in section

3.3.5 below. The upwind method is stable only if $0 \leq \lambda k/h \leq 1$ and, in particular, can only be used if $\lambda > 0$ for all eigenvalues of A. By contrast, the method with one-sided differences in the other direction is stable only if $-1 \leq \lambda k/h \leq 0$ for all λ (LeVeque, 1990).

3.3.5 The CFL Condition

The CFL condition is named after Courant, Friedrichs and Lewy who wrote a fundamental paper in 1928 that was essentially the first paper on the stability and convergence of finite difference methods for partial differential equations.

To understand this general condition it is necessary to discuss the domain of dependence of a time-dependant partial differential equation. For the equation 3.3.1, the solution $V(x_i, t_n)$ at some fixed point (x_i, t_n) depends on the initial data $V^0(x) = V(x,0)$ at only a single point. Therefore,

$$V(x_i, t_n) = V(x_i - \lambda t_n) \qquad (3.3.13)$$

The domain of dependence of the point (x_i , t_n) is the point $x_i - ut_n$ so that,

$$D(x_i, t_n) = \{x_i - \lambda t_n\} \qquad (3.3.14)$$

where D is the domain of dependence. If the data V^0 at this point is modified then the solution $V(x_i, t_n)$ will change, however alteration to data at any other point will have no bearing on the solution at this point.

For non-linear systems of equations as with linear systems, the wave propagation speeds are given by the eigenvalues of A (linear) or f'(V) (non-linear), i.e. λ_1, λ_2, through to λ_m for m eigenvalues). If these eigenvalues are distinct then it can be shown that the solution $V(x_i, t_n)$ depends on the data at the m distinct points $x_i - \lambda_1 t_n$, through to $x_i - \lambda_m t_n$.

A finite difference method also has a domain of dependence. On a particular fixed grid, the domain of dependence of a grid point (x_i , t_n) will be the set of grid points x_i at the initial time $t = 0$ with the property that the data V_i^0 at x_i has an effect on the

solution V_i^n. For example, with the Lax-Wendroff method (equation 3.3.10) or with any other three point method, the value of V_i^n depends on the values V_{i-1}^{n-1}, V_i^{n-1} and V_{i+1}^{n-1}. These values depend in turn on V_{i-2}^{n-2} through to V_{i+2}^{n-2}. Tracing back to the initial time domain we obtain a triangular array of grid points as seen in figure 3.3.4 and it can be seen that V_i^n depends on the initial data at the points x_{i-n}, through to x_{i+n}.

If the grid is refined further by a factor of 2, (both k and h are reduced by this factor), focusing on the same time interval ($t_4 - t_0 = t_2 - t_0$) but keeping the ratio k/h constant, then the value of (x_i , t_n) now corresponds to V_{2i}^{2n} on the finer grid. This value depends on twice as many values of the initial data, but these values all lie within the same interval and are merely twice as dense.

If the grid is further refined with k/h ≡ r fixed, then clearly the numerical domain of dependence of the point (x_i , t_n) will fall in the interval [$x_i - t_n/r$, $x_i + t_n/r$]. As the grid is further refined, it is hoped that the computed solution (x_i , t_n) will converge to the true solution $V(x_i , t_n) = V^0(x_i - \lambda t_n)$. This can only be possible if

$$x_i - \frac{t_n}{r} \le x_i - \lambda t_n \le x_i + \frac{t_n}{r} \qquad (3.3.15)$$

Otherwise, the true solution will depend only on a value $V^0(x_i - \lambda t_n)$ that is never seen by the numerical method regardless of the fineness of the grid. The data at this point could be changed in order to change the true solution without having any effect on the numerical solution. This however cannot be convergent for general initial data.

The condition given by equation 3.3.15 can be translated into the more well known form of the CFL stability criterion for any explicit finite difference scheme,

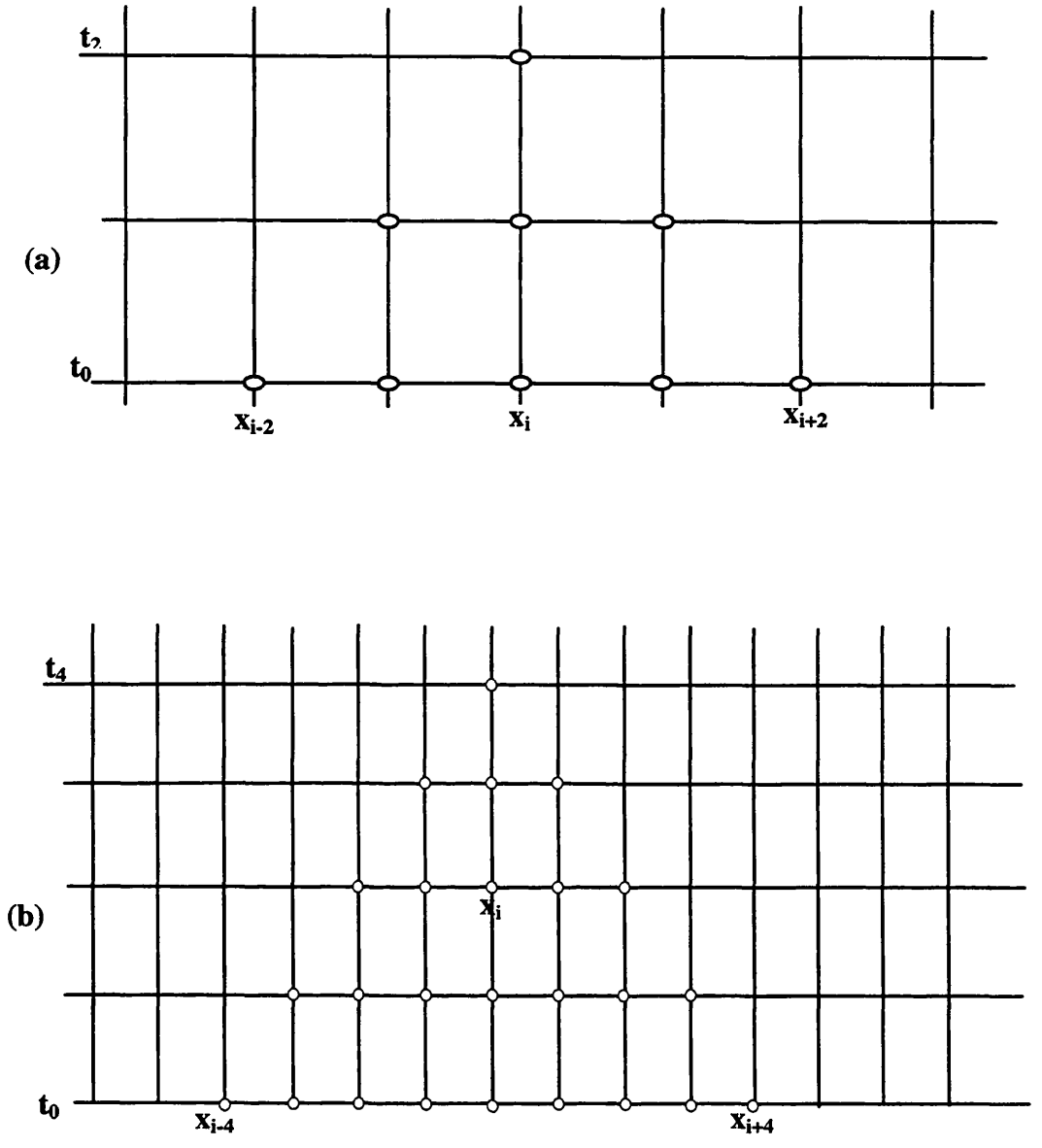

Figure 3.3.4: (a) Numerical domain of dependence of a grid point when using a three point explicit method. (b) On a finer grid

$$|\lambda|r \leq 1$$

or (3.3.16)

$$\left|\lambda\frac{k}{h}\right| \leq 1$$

It is essential that the maximum wave speed at each time domain is chosen when calculating the time step to ensure complete stability over the whole time domain.

It is important to appreciate that in general the CFL condition is only a necessary criterion. If it is violated then certainly the method cannot be convergent. If it is satisfied, then the method might be convergent, but a proper consistency and stability analysis is required to prove this, and to determine the proper stability restriction on k and h.

For an ideal gas, the stability criterion has been shown to give good results, but in cases of two-phase flow when large discontinuities in speed of sound as a result of condensation may occur, satisfaction of the CFL stability criterion as given by equation 3.3.16 might not lead to accurate results (see chapter 5). Care needs to be exercised in choosing a correct time step that gives accurate and stable results.

Implicit methods satisfy the CFL condition for any time step k. In this case, the numerical domain of dependence is the entire real line because the tri-diagonal linear system couples together all points in such a manner that the solution at each point depends on the data at all points. Implicit methods will be further discussed in section 3.3.8.

3.3.6 One-step and multi-step methods

For time-dependent problems, typically time-marching procedures are used in which the solution at all points $x \in \Omega$ at one time t_n are used to compute the solution at the next time $t_{n+1} = t_n + k$. Such a method is called a one-step or a two-level method. A multi-step method can also be tried for greater accuracy because the solution at time t_{n+1} can be based on several previous time steps. However this method requires high

storage requirements from a computer and for cases such as two-phase flow modelling when the complicated flash calculations are being performed continuously, this method becomes too inefficient. Besides standard high-resolution methods are all one-step and hence this method is chosen for this work.

3.3.7 Stiffness

For time dependent problems the idea of stiffness is fundamental as it often dictates the type of numerical method used. Roughly speaking, a problem is said to be stiff if there are a variety of different time scales in the solution and some phenomenon on a relatively slow time scale is being modelled in a situation where the faster processes simply maintain local equilibrium but all visible variations are on a slower scale. It would then be preferable to take a time step that is reasonable relative to the active time scales, and much smaller time steps necessary for modelling activity on the faster time scale would not need to be used. Since these time scales may easily vary by a factor of a million or more for practical problems, this is a major consideration in the efficiency of the method. Unless a method designed for stiff problems is implemented, it would be necessary to take very small time steps appropriate for the fastest time scales in order to maintain stability. Methods for stiff problems are necessarily implicit in time.

Stiffness causes numerical difficulties because any finite difference method is constantly introducing errors. The local truncation error acts as a perturbation to the system that moves the computed solution away from the true solution. The true solution is very robust and the solution is almost completely insensitive to errors made in the past. The stability of the true solution is of help as long as the numerical method is also stable.

The difficulty arises from the fact that many numerical methods, including all explicit methods, are unstable (in the sense of absolute stability) unless the time step is small relative to the time scale of the rapid transient. The time step for a stiff problem is much smaller than that of the smooth solution that is being computed. Although the true solution is smooth and it seems that a reasonably large time step

would be appropriate, the numerical method must always deal with the rapid transients introduced in every time step and may need a very small time step to do so in a stable manner.

Hyperbolic equations are usually not stiff. The time step, k for an explicit method is typically limited by the CFL condition as discussed before in section 3.3.5. For a non-linear system of equations the maximum wave speed should be chosen in determining the stable time step. Provided some disturbance of interest is propagating at this maximum speed, then this is generally the right size time step to use in order that the temporal resolution is consistent with the spatial resolution. In this case, there is no need to use an implicit method.

Stiffness can also occur when the equations of gas dynamics such as the Euler equations are coupled together with source terms that model radiative transfer or chemical reactions that may have much faster time scales than the fluid dynamics.

In our case however, the source terms present in the Euler equations are those representing frictional force effects and heat transfer. The heat transfer term is based on the temperature gradient between the fluid temperature and the external ambient temperature which is assumed to be constant over the length of the pipe.

The frictional force term is flow dependent and therefore the time scale for this phenomenon is the same as that for the flow and hence does not lead to any stiffness. In fact its magnitude is directly linked to the nature of turbulence of flow at each node where it is calculated (see chapter 5).

The heat transfer term is quasi steady state and since the parameter that controls its nodal variation is temperature, has no spatial or temporal derivative terms in the flow equations. This therefore has no effect in terms of stiffness with respect to the solution procedure.

3.3.8 Implicit Methods

Implicit finite difference methods have the advantage over explicit methods in being unconditionally stable. This implies that the maximum practical time step is limited by the rate of change of the variables imposed at the boundary conditions rather than by a limitation required by a stability criterion. However, Wylie and Streeter (1993) say that in order to achieve reasonable accuracy for most transient pipeline problems, the time step-distance interval relationship specified by the Courant condition is, in fact, a requirement.

Considering again equation 3.3.1 a fully implicit method can be written as,

$$\frac{V_i^{n+1} - V_i^n}{k} + A\frac{V_{i+1}^{n+1} - V_{i-1}^{n+1}}{2h} = 0 \qquad (3.3.17)$$

This method is a backward difference method as opposed to a forward difference scheme (explicit finite difference methods).

A variation of this scheme is the Crank-Nicolson method (Forsythe and Wasow, 1960) which is a central difference scheme of high order accuracy. The Crank-Nicolson approximation to equation 3.3.1 would be,

$$\frac{V_i^{n+1} - V_i^n}{k} + A\frac{\left(V_{i+1}^{n+1} - V_{i-1}^{n+1}\right) + \left(V_{i+1}^{n} - V_{i-1}^{n}\right)}{4h} = 0 \qquad (3.3.18)$$

This solution is however prone to oscillate about the true solution for sudden changes in forcing function. Guy (1967), and Heath and Blunt (1969) used the Crank-Nicolson method to solve the conservation of mass and the conservation of momentum equations for slow transients in isothermal gas flow. Both sets of researchers neglected the elevation term ($\rho g \sin\theta$), and the differential of the kinetic energy with distance ($\partial(\rho u^2)/\partial x$) in the momentum equation.

Wylie et al. (1971) used a centred difference method to solve for isothermal gas transients in a network. In this method the partial derivatives are calculated for sections of the pipeline rather than node points. This method can be written as,

$$\frac{\left(V_{i+1}^{n+1}-V_{i+1}^{n}\right)+\left(V_{i}^{n+1}-V_{i}^{n}\right)}{k}+$$

$$\frac{A\left\{\left(V_{i+1}^{n+1}-V_{i}^{n+1}\right)+\left(V_{i+1}^{n}-V_{i}^{n}\right)\right\}}{h}=0 \qquad (3.3.19)$$

Although this method requires a large amount of computer storage to handle the coefficient matrix and leads to lengthy execution times, these major disadvantages can be overcome in one dimension by using Gaussian elimination techniques.

A further development of this method incorporating upstream weighting was used by Taylor (1978) and is given by,

$$\frac{\theta\left(V_{i+1}^{n+1}-V_{i+1}^{n}\right)+(1-\theta)\left(V_{i}^{n+1}-V_{i}^{n}\right)}{k}$$

$$+\frac{\phi A\left(V_{i+1}^{n+1}-V_{i}^{n+1}\right)+(1-\phi)A\left(V_{i+1}^{n}-V_{i}^{n}\right)}{h}=0 \qquad (3.3.20)$$

where θ and ϕ are the weighting factors,

$$0\le\theta\le 1,\quad 0\le\phi\le 1 \qquad (3.3.21)$$

The implicit finite difference methods described above are the most commonly used for fluid transient analysis, although there are others such as the explicit-implicit methods (Padmanabhan et. al., 1978) employed to solve for pressure transients in bubbly two-phase mixtures or the three time level implicit scheme discussed by Osiadacz (1983). Chen (1993) also developed an implicit-explicit scheme based on Hamilton's variation principle (Rund, 1966; Bedford, 1985; Salmon, 1988) to model blowdown of pipes.

The major disadvantage of using an implicit finite difference method is that they require the solution of a set of non-linear simultaneous equations at each time step. For a complex system of pipe network the matrix becomes quite large. Other disadvantages of these methods of solution are that they can yield unsatisfactory

results for sharp transients, in fact implicit methods have always been used to model slow transients when they are much more efficient than explicit methods.

Explicit methods are generally preferable if they can be used with the time step that seems reasonable for the problem, which depends on how fine the spatial grid and how smooth the solution are. For many problems however, an explicit method turns out to be unstable unless the time step is orders of magnitude smaller than what seems reasonable based on accuracy considerations. If the solution is varying smoothly then we expect variations in time to be on roughly the same scale as variations in space and so we would typically like to take a time step $k \approx h$. This is possible with an implicit method whereas the explicit method would require taking a time step, k smaller than this by a factor of h.

3.4 FINITE VOLUME METHODS

In the previous section the basic theory for finite difference methods for linear hyperbolic problems was reviewed. These methods will now be re-interpreted as finite volume methods, a viewpoint that is important in properly extending these methods to non-linear conservation laws.

For flows that have shock wave propagation this method is fundamental for achieving high resolution across the shock wave. For the specific problem of FBR of high pressure gas pipelines there is no actual shock wave propagation within the pipeline (the shock waves will actually propagate away from the rupture plane into the surrounding atmosphere). Instead, using the terminology of the shock tube or Riemann problem (Liepmann and Roshko, 1957; Zucrow and Hoffman, 1976) there is an expansion fan region that propagates into the high pressure gas within the pipeline.

Hence there is no severe discontinuity of flow variables to worry about and the finite volume method is not essential for high accuracy. However the finite volume method has the advantage of being all encompassing in that it can intrinsically handle all types of transient flow situations. Upto now finite volume methods have only been used for transient isothermal fluid flow (Zhou and Adewumi, 1996; Adewumi et. al., 1996). A brief introduction is given here.

In finite difference method the value of the conservation variable V_i^n is used as an approximation to the single value V at point (x_i, t_n). In the finite volume method the variable V_i^n is viewed as approximating the average value of V over an interval of length $h = \Delta x$, where over the physical spatial domain [a,b] with N intervals, $h = (b-a)/N$. Therefore $x_i = a + (i-1)h$. The value V_i^n will approximate the average value over the i'th interval at time t_n,

$$V_i^n \approx \frac{1}{h}\int_{x_i}^{x_{i+1}} v(x_i, t_n)dx \equiv \int_{C_i} v(x, t_n)dx \qquad (3.4.1)$$

where $C_i = [x_i, x_{i+1}]$.

If v(x, t) is a smooth function then the integral in equation 3.4.1 agrees with the value of v at the midpoint of the interval to $O(h^2)$. By working with cell averages, however, it is easier to use important properties of the conservation laws in deriving numerical methods. In particular, we can ensure that the numerical method is conservative in a way that mimics the true solution, and this is extremely important in accurately calculating shock waves. This is because $h\sum_{i=1}^{N} V_i^n$ approximates the integral of v over the entire interval [a, b], and if a method that is in conservation form is used for its calculation, then this discrete sum will change only due to fluxes at the boundaries x = a and x = b. The total mass within the computational domain will be preserved, or at least will vary correctly provided the boundary conditions are properly imposed.

Taking equation 3.3.1 and introducing the concept of a flux function,

$$V_t + AV_x = 0$$
$$V_t + F_x = 0 \qquad (3.4.2)$$

where,

$$F_x = AV_x = f(V_x) \qquad (3.4.3)$$

In finite difference form, equation 3.4.2 can be expressed as,

$$V_i^{n+1} = V_i^n - \frac{k}{h}\left(F_{i+1}^n - F_i^n\right) \qquad (3.4.4)$$

where F_i^n is some approximation to the average flux along $x = x_i$,

$$F_i^n \approx \frac{1}{k}\int_{t_n}^{t_{n+1}} f(V(x_i, t))dt \qquad (3.4.5)$$

A fully discrete method is possible if this average flux can be approximated based on values of V^n.

Since information propagates with finite speed, it is reasonable to first suppose that we can obtain F_i^n based only on the values V_{i-1}^n and V_i^n, the cell averages on either side of this interface. This allows us to define the numerical flux function by a formula of the type,

$$F_i^n = F\left(V_{i-1}^n, V_i^n\right) \tag{3.4.6}$$

Therefore equation 3.4.4 becomes,

$$V_i^{n+1} = V_i^n - \frac{k}{h}\left[F\left(V_i^n, V_{i+1}^n\right) - F\left(V_{i-1}^n, V_i^n\right)\right] \tag{3.4.7}$$

The specific method obtained depends on how the formula for F is chosen, but in general any method of this type is an explicit method with a three point stencil. Given that a method in conservation form is sought, a first attempt at a definition of the average flux at a point based on data to the left and right of this point, would be the simple average,

$$F\left(V_i^n, V_{i+1}^n\right) = \frac{1}{2}\left(f\left(V_i^n\right) + f\left(V_{i+1}^n\right)\right) \tag{3.4.8}$$

Substituting this into 3.4.7 would give,

$$V_i^{n+1} = V_i^n - \frac{k}{2h}\left[f\left(V_{i+1}^n\right) - f\left(V_{i-1}^n\right)\right] \tag{3.4.9}$$

In general, however, this method turns out to be unconditionally unstable for any value of k/h. In these situations it is better to use the modified flux,

$$F\left(V_i^n, V_{i+1}^n\right) = \frac{1}{2}\left(f\left(V_i^n\right) + f\left(V_{i+1}^n\right)\right) - \frac{h}{2k}\left(V_{i+1}^n - V_i^n\right) \tag{3.4.10}$$

From this definition of flux function, the Lax-Friedrichs method is obtained,

$$V_i^{n+1} = \frac{1}{2}\left[V_{i-1}^n + V_{i+1}^n\right] - \frac{k}{2h}\left[f\left(V_{i+1}^n\right) - f\left(V_{i-1}^n\right)\right] \tag{3.4.11}$$

It is interesting to note that the additional term in equation 3.4.10 is a diffusive flux based on an approximation to $\frac{h^2}{2k}V_x$, and hence this modification amounts to adding some artificial viscosity to the centred flux formula. This makes a finite volume approach particularly attractive to treatment of shock wave flow since no additional smoothing parameter is needed to control overshoot and oscillation as is the case with higher order explicit finite difference schemes. Implementation of an effective finite volume approach requires an appropriate method to define the numerical flux function. Many techniques exist to do this and come under the general heading of flux-difference splitting schemes.

3.4.1 Flux Difference Splitting Schemes

The basic principle of flux splitting is that the numerical flux function can be split and discretised directionally according to the sign of the associated propagation speeds. Hence the eigenvalue solutions to the hyperbolic equations are important since the flux functions are split along them and hence different types of flow are naturally accounted for. For example if there is a transonic region, the negative characteristic (λ = u-a) eigenvalue will change sign from being negative when subsonic since u is less than, a, to being positive when supersonic since u is greater than, a.

The flux-vector splitting methods were pioneered by Steger and Warming (1981). Van Leer (1977) developed a flux vector splitting with an implicit relaxation algorithm, which is efficient, simple and capable of capturing the sharp shock waves.

The simplicity of this method, however, came at a price of reduced accuracy for viscous flows due to the large dissipation. Higher-Order Polynomial Expansion (HOPE) scheme of Liou and Steffen (1993) and the Low-Diffusion Flux-Vector Splitting Scheme of Van Leer were aimed at building up a pure flux-vector splitting scheme with vanishing mass diffusion. They did achieve the required split mass but instability and non-monotonicity of the schemes are not acceptable for practical calculations.

Efforts have also been made to improve the original Van Leer scheme by using some techniques borrowed from the flux-difference splitting schemes first suggested by Hanel and then extended by Van Leer. The Van Leer-Hanel (1990) Scheme uses the net mass flux and the one side velocity, and the total enthalpy for the transverse momentum and energy equations. A successful and more promising scheme was suggested by Liou and Steffen, the Advection Upstream Splitting Method (AUSM). They introduced an advective Mach number by combining split Mach number contributions from the original Van Leer's mass splitting. In a variety of calculations, this scheme was reported to be as accurate and convergent as the Roe flux-difference splitting scheme (Roe, 1981), which was considered to be the most accurate.

One of the more recent works in this area is that of Zha and Bilgen (1993, 1996). A new flux vector splitting scheme, using the velocity component normal to the volume interface as the characteristic speed, and yielding a vanishing individual mass flux at the stagnation point has been developed. Flux-difference schemes can correctly capture shock waves and provide criteria to discriminate the correct information carried by propagating waves. The difference in flux between two adjacent node points is split into terms that will affect the flow evolution at points either side of the section under investigation. It is assumed that uniform flow occurs at each node point and over the cell extending one and a half grid intervals each side of the node point.

A discontinuity generally separates two neighbouring cells in the middle of the interval, and the evolution in time of this discontinuity provides the criteria for splitting the flux difference over an interval into terms associated with waves that propagate up and down the pipe. The above procedure is known as the Roe method (Roe, 1981). This method was extended by Pandolfi (1985, 1989) to hyperbolic equations. The Roe method was used frequently since it can take care of both steady shocks and contact discontinuities.

In an attempt to extend the upwind idea to global methods such as spectral or pseudo-spectral methods, Huang and Sloan (1993) developed a new upwind pseudo-spectral method for solution of linear singular perturbation problems without turning points. Glaister (1994) presented a flux difference splitting; numerical scheme for the solution of the Euler equations of compressible flow of a gas in a single spatial co-

ordinate. The scheme uses the Riemann solver for the Euler equations for a duct of variable cross-section and using the arithmetic mean (in contrast to the usual square root averaging of Roe's Riemann solver) for computational efficiency.

Flux-difference splitting methods can correctly capture shock waves and provide criteria to discriminate the correct information carried by propagating waves. Good results have been obtained for flux-difference splitting methods, but required numerical experimentation. Flux-difference splitting methods are unconditionally stable and solution at boundaries create no difficulties.

3.5 FINITE ELEMENT METHOD

Solving an engineering problem by the finite-element approach involves the following steps:

(a) Formulation of governing equations and boundary conditions

(b) Division of the analysis region into finite elements

(c) Selection of interpolation functions

(d) Determination of element properties

(e) Assembling of global equations

(f) Solution of global equations

(g) Verification and validation of solution

The finite-element method consists primarily of replacing a set of differential equations in terms of unknown variables with an equivalent but approximate set of algebraic equations where each of the unknown variables is evaluated at a nodal point. Several different approaches may be used in the evaluation of these algebraic equations, and finite-element methods are often classified according to the method used. In order to arrive at a proper method for a particular problem, it may be necessary to examine several methods. The three most common methods of formulation of the equations in finite difference form are direct, variational and residual.

Division of the solution region into elements can take the form of either one-, two or three-dimensional elements of varying shapes. There is usually not a single correct way of dividing a particular region to obtain a solution. Decisions on how to divide up the solution region into elements is based on engineering judgement and there are no definitive guidelines available. Depending on the positioning of nodes in the element and whether the sides of the element are straight or curved, finite elements are generally classified as simplex or higher order elements. Regardless of the geometrical shape, finite elements are categorised as either Lagrangian or Hermite elements.

In contrast to the Lagrange family of elements, the Hermite category includes derivatives of the variables as well as values defined at the nodes. The theoretical basis of the finite-element methods has been covered extensively by Allaire (1985). Finite-element methods have not been extensively used for gas transients.

Until recent years, only two methods namely the Galerkin Method, employed by Rachford and Dupont (1974), and more recently by Osiadacz and Yedroudj (1989) and Kiuchi (1987), and the moving finite-element method, have been used for transient fluid flow analysis. Bisgaard et. al. (1987) developed a weighted residual finite-element method which uses the Galerkin finite-element method to discretise the equation.

Finite-element methods have some advantages over finite-difference methods. The former can be used to solve virtually any engineering problem for which a differential equation can be written. They have a higher accuracy because cubic hermite splines which should give errors of $O(h^4)$ could be used.

However, this accuracy cannot always be usefully realised due to the geographical nature of networks. Finite element methods are most useful for two and three-dimensional problems. Variational methods are easy to extend to two and three-dimensional problems. Residual methods can be applied to any problem for which a governing boundary value problem can be applied. For the case of residual methods, once techniques are learnt, the details are relatively straightforward.

The major disadvantage of finite-element methods is that they are somewhat complex, with complexity being proportional to the complexity of the differential equations for that particular problem. Direct methods are difficult to apply to two and three-dimensional problems. Variational methods lack a functional form for certain classes of problems, for example those dealing with the flow of viscous fluids. In addition, it is difficult to define variational methods for some problems. The procedure for finite element solution is rather lengthy and not widely used in gas network simulation. When the solution possesses discontinuities, higher-order methods may not always give more accurate solutions.

The Galerkin method requires a lengthy execution time. It is formulated to treat slow transients. Computer resources required are small and it has some significant theoretical advantages. In using the moving finite-element method, care is needed in treatment of boundary conditions.

3.6 METHOD OF LINES

In this method, a system of partial differential equations is transformed into a system of ordinary differential equations by discretising the equations in the spatial domain and leaving the time domain continuous. The number of ordinary differential equations is equal to the number of partial differential equations multiplied by the number of grid points used. The resulting set of ordinary differential equations can then be integrated with an appropriate ordinary differential equation solver.

The spatial derivatives are replaced by difference quotients. Since for the numerical solution of the generated system of ordinary differential equations the time variable is in fact discretised too, we finally obtain a full finite-difference system.

Many of the known finite-difference methods can be thought of as being generated in this way. The boundary within which the method is applied is taken to be a rectangular grid. Boundaries of more general shapes can be reduced to this form by suitable co-ordinate transformations. Boundary conditions are prescribed on all or some sides of the grid rectangle. For applications in transient gas flow analysis, a parabolic form of the partial differential equations is used, for which the boundary conditions are only needed on three sides.

Ames (1977), Holt (1984) and Osiadacz (1987) gave a theoretical analysis of this method. In Holt's description, the method is based on a second-order partial differential equation of elliptic or mixed type whereas Osiadacz uses a parabolic partial differential equation. Osiadacz further discusses the application of this method to solve a system of partial differential equations describing the unsteady flow of gas in pipes and problems associated with its use, when dealing with rapidly varying signals and means of avoiding and overcoming them. It has been found that the procedure is satisfactory only where transients are gradual and continuous. There has been some recent studies where this method has been used practically to analyse unsteady flow of gas in pipelines.

Sophisticated packages based on the method of lines exist for numerical solution of ordinary differential equations. The method of lines is empirical and extremely

simple. Higher-order methods can be used (Hirsch, 1995) for the integration of time, for example fourth-order Runge-Kutta or multi-step predictor-corrector methods, which is approximate for parabolic problems. Numerical time-domain solutions using the method of lines can be compared directly with corresponding method of characteristics solutions. The main advantage of the method of lines is that it offers the possibility of utilising highly developed software for ordinary differential equations. The method of lines is only suitable for numerical solution of partial differential equations of elliptic, mixed-elliptic and parabolic type. It is usually but not exclusively applied to parabolic problems.

3.7 METHOD OF CHARACTERISTICS

The method of characteristics is the natural numerical method for quasi-linear hyperbolic systems with two independent variables. It is essentially an explicit finite difference scheme with a sufficiently different approach to warrant separate treatment. It is based on the principle of the propagation of characteristic waves and is therefore well suited to handling fast transient flow where each disturbance is captured along the propagating Mach lines which are used in the formulation of the final form of the finite difference equations. The choking condition is handled easily by the fact that the left-running sonic characteristic, denoted by the eigenvalue (u-a) is equal to or greater than zero.

By an appropriate choice of co-ordinates, the characteristic lines as discussed in section 3.2.1 can be defined such that the system of partial differential equations is converted into a system of ordinary differential equations (compatibility equations) that may be solved by standard, single step finite-difference methods for ordinary differential equations. The basic rationale underlying the use of characteristics is that by an appropriate choice of co-ordinates, the original system of hyperbolic equations can be replaced by a system whose co-ordinates are the characteristics. The use of this method becomes particularly simple when applied to two equations in two dependent variables as is often the case when the isothermal flow assumption is made (see for example Wylie and Streeter, 1993).

When the characteristic co-ordinates are used in this way, the method is known as the natural method of characteristics or the characteristic grid method (CG) (Wylie and Streeter, 1993). This method has been extended to the three characteristic model necessary to describe non-isothermal transient fluid flow by Chen et. al (1993) and is referred to as the Wave Tracing method.

In all these characteristic grid methods, the position of the new solution point is not specified a priori, but is determined from the intersection of left and right running characteristics with origins located at known solution points or initial data. Hence a free floating grid is developed in the xt plane as shown in Fig. 3.3.1. This method of

characteristics is particularly accurate since the solution progresses naturally along the characteristic lines. However, when more than two characteristic lines are present, i.e. when an energy equation is solved in addition to the mass and momentum conservation equations, a pathline (λ = u) is present in addition to the two Mach lines (λ = u+a; λ = u-a) and this introduces some interpolation to locate the pathline intersection between known initial points.

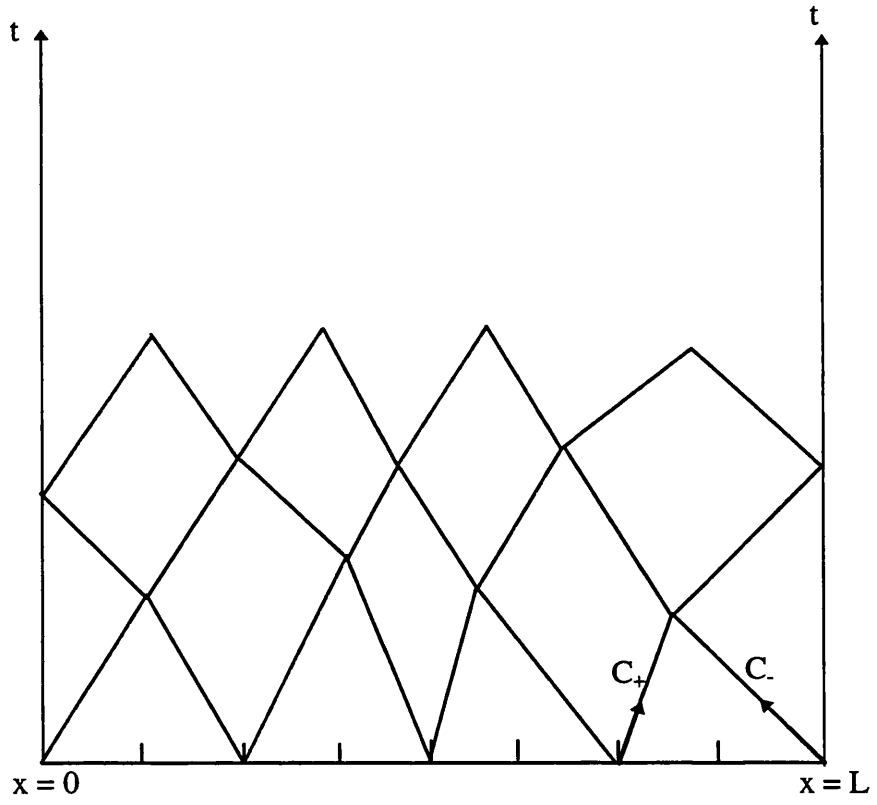

Fig. 3.3.1 Characteristic Grid

Another method that can be used for numerical discretisation of the Euler equations is the inverse marching method or the mesh method of characteristics called the method of specified time intervals (ST) (see Figure 4.4.1 in Chapter 4). In this

method, the location of the solution points in the space-time grid is specified a priori and the characteristic curves are extended backwards in time to intersect a time line on which initial-data points are known from a previous solution. This necessitates interpolation to locate the intersection of all three characteristic curves and as a result can lead to a greater loss of accuracy than the CG method.

The advantages and disadvantages of the ST and CG methods are summarised below:

- Although accurate results are obtained at grid intersection points in the characteristic grid method, results are not directly available at a particular instant along the pipe nor at a particular section as a function of time. Some interpolation scheme is needed to extract this information. The method of specified time intervals is capable of providing results where needed; however it can suffer from inaccuracy introduced by interpolations at each time step, and the greater the interpolation the larger the error. (Wiggert and Sundquist, 1977; Vardy, 1977)
- No control is possible in maintaining the position of grid intersection points in the *xt* plane in the characteristic grid method. Intersection points may move outside the region of the pipeline and thus lose physical significance. To overcome the problem of distortion of the grid under extreme conditions in the CG method, a procedure can be used to straighten the grid by an adjustment to it after a certain number of time steps (Tullis et. al. 1976; Wylie and Streeter, 1976). It involves a double interpolation scheme in the region of the *xt* plane in which data are already computed. Once regular spacing is re-established, the CG method can be continued over another time span. The number of times this type of interpolation is needed is dependent on the severity of the variation in wavespeed. The numerical damping introduced with this interpolation is not nearly as significant as that introduced in the ST method of characteristics.
- The ST method is subject to the constraints of the CFL condition which lengthens computation time. The CG method is free of any such restriction.
- The user has no direct control on the time of input variables at boundaries, whereas boundary conditions may be introduced at predefined times in the ST approach. This feature makes the ST method very attractive when modelling more complex systems such as valves in line, compressors or pipeline networks.

☞ Equal length reaches may be selected and maintained along the pipeline in the ST method.

The method of characteristics has many advantages compared with other numerical methods of solution. Discontinuities in the initial value may propagate along the characteristics, making it easy to handle. Large time steps are possible in the natural method, since they are not restricted by a stability criterion. The boundary conditions are also properly posed. The method of characteristics is relatively accurate, but requires understanding of how it operates, particularly in choosing a suitable time step. The method can be readily adapted to solve for three dependent variables required for the analysis of non-isothermal transient fluid flow. Discontinuous initial data do not lead to solution with overshoot and details are not smeared in the CG method. Exact solution is possible in the constant coefficient case with two dependent variables, regardless of eventual discontinuities in the initial data, in the case of the natural method.

In choosing a numerical scheme for the resolution of the Euler equations governing flow following FBR, the first decision that needs to be taken is whether to choose an implicit or explicit scheme. The need to solve a set of time dependent partial differential equations where time step limitations have to be introduced for reasons of accuracy, even for implicit schemes, means that an explicit scheme had to be chosen.

From the variety the explicit schemes that have been discussed, the MOC is chosen as the numerical scheme for the solution of the Euler equations on the basis that it has been proven to be an accurate tool in the solution of hyperbolic equations and is relatively simple to program. Since the CG method does not permit modelling of valves in line at different locations and with different closure times, the ST method is chosen.

A detailed description of the MOC as used in this work in given in Chapter 4.

3.8 REVIEW OF LITERATURE ON PIPELINE RUPTURE

The majority of the techniques for modelling pipeline rupture and blowdown are based on the MOC. The rest are either based on various finite-element or finite-difference schemes. The following is a review of these methods.

Sens et al (1970) used an explicit finite-difference method for the numerical solution of partial differential equations to simulate transient flow in a gas pipeline a few seconds after rupture.

Lyczkowski et al (1978) investigated several explicit finite-difference numerical schemes for solution of homogeneous equations of change for one-dimensional fluid flow and heat transfer. The Alternating Gradient Method (AGM), which is based on the two-step Lax-Wendroff procedure, was found to be the most successful.

Numerical tests performed using AGM for the blowdown of an ideal gas in an ideal shock tube gave good predictions when compared to analytical results. Also good agreement was obtained between numerical predictions and experimental data for the blowdown of a steam-water mixture.

Comparison of the AGM with the two-step Lax-Wendroff method for the shock tube indicated that the AGM is more accurate than the Lax-Wendroff scheme, probably due to greater numerical damping in the AGM.

Although the AGM is restricted by a time-step limitation which is slightly smaller than the standard Courant condition for a given time-step and mesh size, it is at least as accurate as Implicit schemes. Since only two cycles per time step are needed, the AGM is faster than a fully implicit scheme. In addition, the AGM is simple to programme.

In the study by the Alberta Petroleum Industry, Government Environmental Committee (1978) to evaluate and improve hydrogen sulphide isopleth predictions, the following techniques were reviewed: two dispersion models, the IN'IERA Environmental Consultants Ltd. (INTERA) model and the Energy Resource Conservation Board (ERCB) model; and two blowdown models, the INTERCOMP Resource Development and Engineering (INTERCOMP) model and a simplified

blowdown model. Common blowdown curves generated by the INTERCOMP "TRANSFLOW" blowdown model were used in both the ERCB and INTERA atmospheric dispersion calculations. The INTERCOMP "TRANSFLOW" model uses the basic mass, momentum, and energy balances in a numerical simulator to calculate the time curve defining the rate of gas blowdown from the pipeline. Among other things, the model has the capability of including valve closure time, frictional effects and gas flow rate in the line before rupture in the calculations. No further details of the models are given in the report.

Knox et. al. (1980), reported on a project to assess the basic source characteristic assumptions relevant to modelling of sour gas pipeline ruptures and well blowouts. A 3.2 kilometres long, 168 millimetre diameter pipeline was ruptured 32 times under varied conditions. A 7.1 kilometres long, 323 millimetre diameter pipeline was also ruptured and results were photographically recorded. The experimental rupturing technique, transient release rate and sensitivity to source configuration were evaluated. Parameters investigated included overburden, wind speed, release angle, fracture length, rupture mode and line pressure. Computer input parameters which needed verification are plume rise, volume dilution and rate of release. The study was based on three computer release rate models which existed [Alberta Petroleum Industry, Government Environmental Committee (1978)] and which have been described in the previous paragraph. It was confirmed that all the three computer release rate models adequately predict the transient release of gas from a ruptured pipeline.

Cronje et. al. (1980) described a procedure to solve the equations for single-phase, one-dimensional, unsteady, compressible, frictional flow with heat transfer. The procedure is based on Hartree's hybrid method for solving the governing hyperbolic partial differential equations. In this numerical method, a rectangular grid is superimposed on the characteristic mesh in the time-distance plane. The values of the variables at points lying on the characteristics at time t are calculated by linear interpolation from their known values prevailing at the rectangular grid points at the same time, t. The governing equations are integrated along their characteristics over a time step δt in time, to obtain the new values of these variables at the grid points at

time t + δt, and the process is repeated until the required time interval is covered. The method was applied to shock tube data that simulate a gas pipeline rupture. It was shown that the effect of friction is considerably more important than the effect of heat transfer. For large elapse times, the effect of friction is significant and the numerical model predicted well the available experimental values at these times. However, the numerical model agreed with experimental data at higher pressure ratios, at short elapse times and near the rupture plane.

Jones and Gough (1981) reported on a theoretical model for analysing high-pressure natural gas decompression behaviour. The method was incorporated in a computer programme called DECAY and was tested with a series of experimental data. Jones and Gough (1981) also reported that other organisations such as Exxon Production Research and the University of Calgary, were involved in studies on high-pressure gas decompression behaviour and that they had developed similar models to that of British Gas.

Fannelop and Ryhming (1982) studied the sudden release of gas from long pipelines. A straight forward solution based on the time-honoured concept of integral methods in boundary-layer theory was used. Spatial profiles of pressure and flow rate were assumed which satisfy the boundary conditions. They define different time regimes, each requiring a different method of solution. The inviscid regime is often of very short duration, probably much shorter than the time required for a full break to occur. It is followed by a viscous expansion process in which wave and dissipation processes are both important and in which the pressure at the break approaches the ambient value. The combined inviscid and viscous expansion phase were categorised as the early time regime. The time regime when the pressure decreases monotonically towards the open end, such as in the case of a break at the low-pressure end was referred to as the late time regime. The intermediate time regime is defined as the time which lasts from t = 25 seconds to the time when the pressure peak has moved to the other (closed) end. Simple solutions were developed for flow cases of prime interest. Validity and accuracy of the methods were checked using two procedures, namely variations of profile families and mathematical analysis of the partial

differential equations based on an iterative approach carried out to second order. The integral method is shown to have adequate accuracy for engineering studies.

Van Deen and Reintsema (1983), developed a computer model for high-pressure gas transmission lines based on the method of characteristics and compared it with experimental data from the Gasunie transmission system. A leak was simulated by the fast opening of a valve connecting the pipeline to a nearby parallel pipeline at a lower pressure. Pressure responses at a point 10km downstream of the leak were investigated. Lack of agreement in the magnitude of the reflected pressure waves was observed and attributed to imperfect modelling of the boundary conditions. It was also observed that changes in the numerical values of the resistance factor of the pipeline have only a slight influence on the value of the result.

Flatt (1985-1989), studied the use of the method of characteristics for analysis of unsteady compressible flow in long pipelines following a rupture. In his model the simplifying assumptions of isothermal and low Mach number, often applied in the case of unsteady compressible flow in pipelines, were not used. To achieve higher accuracy, higher-order polynomials and an assumption of correspondingly curved characteristic lines were also used. The algorithms used were limited to shock free flows. An accuracy criterion showed that higher numerical accuracy may be obtained if the number of grid points was sufficiently large and if a special modified form of the boundary conditions at the broken section was used. The major difficulty encountered was due to the singularity which resulted from the combined effects of friction and choking (Ma = 1), occurring at the broken end. The results confirmed conclusions established earlier that viscous flows with large values of 4fL/d (order of magnitude of 1000) behave very differently from flows without friction. In particular, the mass flow escaping through the broken section, and the pressure there, fall to much smaller values. On the other hand, at some distance from the broken section the pressure stays at high values much longer than in the case without friction. The study concluded that the method of characteristics is more suited to problems with relatively low values of the parameter fL/d. Cases with important frictional effects

are advised to be carefully checked regarding the accuracy of the results, and require many more grid points than cases without friction.

Bisgaard et. al. (1987), reported on a finite-element method developed for transient compressible flow in pipelines. A weighted residual method with a one-dimensional straight line element with two nodes was combined with an implicit Euler method and applied to the basic equations without making any simplifications. Higher-order polynomials were used as interpolating functions, since derivatives must be specified at the nodes in addition to the variable itself. The Galerkin finite-element method was used to discretise the equations. Gauss quadrature was used for the integration, where the order of the Gauss quadrature was adjusted to the order of the polynomial. A fully implicit Euler integration method was used for time integration after a third-order Runga-Kutta method had failed the stability criterion. The method was used to describe blowout and to determine the performance of a leak detection system. The first derivative of density and the first and second derivatives of velocity were included since small leaks are more easily recognised from derivatives of specified variables than from the variables themselves. A comparison was made between full-scale measurements carried out on a 77.33 kilometres gas transmission line from Neustadt through Sorzen to Unterfohring, in Germany, and corresponding finite element calculations. In the rupture simulation, the fluid was assumed to behave like an ideal gas with constant specific heat flowing through a convergent nozzle and calculations were carried out with 21 elements and a time step length of 0.5 seconds. It is claimed that results from the computer model had successfully been compared with process data from a full-scale pipeline. However, this was not shown in the paper for the case of a pipe rupture. It therefore remains doubtful as to whether the method could accurately and efficiently be used for the analysis of pipe rupture problems.

Lang and Fannelop (1987) reported on a method for efficient computation of the pipeline break problem. This involved the reduction of the partial differential equations to a set of ordinary differential equations by means of procedures in the family of the method of weighted residuals. The reduced equations were integrated by standard numerical techniques. The finite-element method, the spectral Galerkin

method and the spectral collocation method were all used and results compared. It was demonstrated that stable, accurate and efficient solutions to the pipeline break problem could be obtained by the method of weighted residuals. Although the approximate functions used with the spectral collocation method would appear to be suited primarily for elliptic problems, it was possible to apply them to the hyperbolic equations by modifying one of the coefficients. Good results were obtained, and it was recommended that the computer time required by this method could be further reduced without loss of accuracy when the number of polynomials in the approximate solutions is reduced successively during the course of the calculation, as the gradients of pressure and velocity become smaller. It was concluded that the best results in terms of stability, accuracy and computing time were obtained with the collocation method.

Cheng and Bowyer (1987) presented a general quasi-one-dimensional unsteady compressible fluid flow code, which adopted the Eulerian approach and used the artificial viscosity method for finite-difference numerical integration of the governing equations. The numerical method a generalised two-step explicit Lax-Wendroff finite-difference scheme that includes an adjustable implicit artificial viscosity term. Two sample computations were used to demonstrate the code capability. In the first case, the fluid transient imposed on a system undergoing a pipe rupture was studied for different combinations of the effects of elbows and restrictors. A steam vessel was considered to be the reservoir with a pressure of 1000 psi (69bar) and a temperature of 550°F (288°C). A flow restrictor (with a throat whose cross-sectional area is 36% of the duct flow area) was located aft (2.5m) downstream of the second elbow. In the second case, transients caused by a sudden pipe rupture at the left side of a three-duct system were predicted.

Picard and Bishnoi (1988 and 1989) used their three models namely the Perfect-gas Isentropic Decompression (PID) model Real-fluid Isentropic Decompression (RID) model and Real-fluid Non-isentropic Decompression (AND) model to investigate the importance of real-fluid behaviour in the modelling of high pressure gas pipeline ruptures. All these models are based on the method of characteristics.

Botros et. al. (1989) discussed some computational models and solution methods for gas pipeline blowdown and assessed the significance of the various assumptions involved. Two physical models namely a volume model where a pipe is considered as a volume with stagnation conditions inside; and a pipe model where a pipeline section is considered as a pipe with velocity increasing towards the exit were considered. The pertinent equations for each model were solved analytically and numerically. The volume model was represented by a set of quasi-linear ordinary differential equations which were solved by a variable order backward differentiation formula method (Gear's method). The pipe model is governed by a set of non-linear first-order parabolic partial differential equations which were solved by a first-order Euler implicit finite-difference scheme. It was concluded that the accuracy of results obtained from the various models and solution methods depends greatly on the ratio fL/d of the pipe section under blowdown and the stack relative size with respect to the main pipe size. Generally as fL/d increases predictions using all models tend to become inaccurate. For relatively low fL/d values all models provide reasonable predictions and therefore the simple analytical volume calculations can be used effectively.

Thorley and Tiley (1987) used the method of characteristics for pressure transients in a ruptured gas pipeline with friction and thermal effects included. A real gas equation of state (Berthelot equation) was used and the "small terms" in the basic equations were neglected. A reducing grid size was used in the vicinity of the break to enable rarefaction waves to be modelled following a rupture. The friction term was represented by a second-order approximation. The values at an initial condition at the base of the characteristic were found by interpolating between known grid points. Hence by solving these equations, a first-order approximation was obtained for the predicted pressure, temperature and flow velocity. Since the required stability and accuracy was not achieved using the first-order approximation, this solution was used as an initial estimate in a second-order procedure. Although the exact procedure of this second order model is dependent on the type of grid point being examined, in principle, new values for the variable at the initial condition were found using quadratic interpolation. The coefficients in the characteristic equations were then

calculated using these values. The coefficients were averaged with the previous initial condition coefficients, and the results were substituted back into the characteristic equations. By this method, new values for the predicted pressure, temperature and flow velocity were obtained. Results were obtained by performing a number of computer simulations for a set of data and comparing the results with shock tube and full-size pipeline experimental data. Problems were encountered with numerical stability and accuracy of results. For certain grid size and initial conditions, the solution became unstable at random points along the pipeline. It was concluded that although this type of instability could be controlled to an extent by varying the grid size and break boundary conditions, the problem may be totally alleviated by using an alternative numerical method for solving the theoretical equations.

Lang (1991) reported on the computation of gas flow in pipelines following a rupture using a spectral method. The governing partial differential equations were converted into a scheme suitable for solution by a computer by a two step procedure. In the first step, the collocation version of the spectral method was used to calculate the space derivatives. The remaining ordinary differential equations were then integrated by standard numerical techniques in the second step. Accurate results were obtained for short computing times with only a few collocation points.

Kunsch et. al. (1991) reported on a study of the flow characteristics close to a shut-down valve for an offshore gas pipeline, and over the length of the segment between the valve and a rupture. Integration of the partial differential equations was performed with the two-step MacCormack method. A fine mesh size was imposed at the boundaries where the gradients can be large. Treatment of boundary conditions, especially those relative to the valve, based on concepts from the method of characteristics, proved to be adequate. The calculations showed a better accuracy than previously used models.

In another publication, Kunsch et. al.(1995) concluded that a precise knowledge of the coefficient of friction and other losses coefficients is not necessary. They demonstrated that the mass flow rates are insensitive to the exact geometric shape and contraction ratio of the break, resulting from an accidental rupture. They also

compared their model results with those obtained by Flatt (1985b). They admitted that the results from Flatt's model (which was based on the method of characteristics) were probably more accurate than their's, for the inertia dominated early time regime. They observed that the ideal gas assumption overestimated [Flatt (1993-94)] the mass flow rate. Flatt (1985b) observed the opposite effect, when the perfect gas assumption was used.

Chen et. al. (1992) presented a model for simulation of blowdown or rapid depressurisation following a full-bore rupture of pipelines containing perfect gases. The equations of gas dynamics were solved by the method of characteristics using four different algorithms namely the hybrid method, the hybrid method with multi-grid system, wave-tracing and multiple wave-tracing methods. The multiple wave-tracing method was found to be the most efficient and accurate method among the other methods for simulating long gas line rupture problems. This method was used to simulate the blowdown of the sub-sea pipeline between the Piper Alpha and MCP-01 offshore platforms and the result was compared with measurements made during the night of the tragedy on the Piper Alpha platform. The results were found to be in moderate agreement, the discrepancy being due to real fluid behaviour. It was concluded that although the perfect gas blowdown model is not capable of modelling real fluid behaviour, its simplicity and speed combined with the multiple wave-tracing method should provide a quick yet reasonably accurate evaluation of gas dynamics for risk assessment to a gas transmission line.

Chen et. al. (1993) also developed a simplified finite-difference method to solve transient two-phase pipe flow problems. In this method, the flow channel is discretised using staggered meshes where the flow velocity is defined at the cell edge and all other variables defined at cell centre. Following the guidelines of the Fourier stability analysis, the scheme treats the momentum convection term explicitly and the flow velocity is expressed in terms of pressure. The density in the mass conservation equation is further eliminated using a locally linearised equation of state so that the discretised conservation laws can be reduced to two difference equations in terms of mixture enthalpy and pressure only. The only assumption made is that there is thermodynamic equilibrium between the two phases. The method has several

advantages. Since the velocities in the momentum calculations are de-coupled from other state variables, the extension of this method to other two-phase flow models is very straight forward The size of time step for the integration is not limited by a Courant number restriction The choice of mixture enthalpy and pressure permits the method to make the transition between single-phase and two-phase without difficulty. Extension to a multi-component system with concentration stratification effects is possible, but is shown to be insignificant for long pipelines. Results of the model were presented by way of example for the blowdown of a 100m long pressurised LPG pipeline using a homogeneous two-phase flow model.

Olorunmaiye and Imide (1993) presented a mathematical model based on unsteady isothermal flow theory and solved by the method of characteristics. It was reported that the model predicted results for natural gas pipeline rupture problems consistent with predictions of other workers. The accuracy of the numerical scheme when using linear characteristics with quadratic interpolation was found to be adequate. It was found that the curvature of the characteristics is not as pronounced in isothermal flow as it is in adiabatic flow and therefore it is not necessary to include the effect of curvature of the characteristics in the computation of unsteady isothermal flows. It was concluded that the model is useful in analysing other unsteady flows associated with pipeline operation, such as controlled venting to the atmosphere prior to shutdown or repair, and sudden changes in pressure at either end of the pipeline. The waves generated in these operations cannot be as strong as waves associated with pipeline rupture.

Gasunie of the Netherlands have developed a PC-model for gas out flow for complex pipeline networks with different elements and different out flow scenarios all in one model. It can model line-break, venting and leakage. It can handle elements like valves, vessels, restrictions and elements defining different boundary conditions, which can represent e.g. the behaviour of a compressor. The basic relations are solved using an implicit finite-difference scheme. A graphical user interface makes inputting of the network very easy. In developing the model, emphasis was put on user-friendliness, robustness and the ability to model complex networks. The accuracy of the model is estimated at 5 to 20%, which is considered by Gasunie to be sufficient for hazard analysis purposes.

The Southwest Research Institute (SwRI) [Morrow (1996)] has conducted a study, to simulate venting of natural gas pipelines, for the Gas Research Institute. The computer model which was reported by Olorunmaiye and Imide (1993) was used. One of the aspects which were considered was whether a leak detection system could distinguish between a signal caused by a pipeline leak and other transient signals caused by normal operation, such as compressor start-up and shutdown and deliveries of gas through branched lines. Initially, the computed transient results overestimated the gas outflow and pressure drop. In order to match the computed results to experimental data, the throat area of the relief valve was reduced below its physical size. This empirical adjustment, which is called "exit loss factor", resulted in a fairly well agreement between computed and measured pressures.

3.9 CONCLUDING REMARKS

In this chapter, a variety of numerical methods available to solve the Euler equations for one-dimensional homogeneous flow in thermodynamic equilibrium are presented. As a result of the present review, the method of characteristics based on the specified time (ST) interval grid is chosen for the following reasons:

- discontinuities in the initial value may propagate along the characteristics, making it easy to handle
- no additional smoothing parameter is needed to control overshoot and oscillation as is the case with second or higher order explicit finite difference schemes
- the boundary conditions are properly posed
- boundary conditions may be introduced at predefined times in the ST grid approach. This feature makes the ST method useful in modelling the dynamic effects of ESDV closure at various locations within the pipeline by choosing an appropriate grid spacing.

In the following chapter, the MOC based on the ST grid scheme is applied with a modification to the calculation procedure that considerably quickens CPU times and renders it considerably more efficient when compared to the classical method for an ideal gas mixture. This gain in computer run time allows its further development with regards to modelling two-phase flows as presented in Chapter 5.

CHAPTER 4: APPLICATION OF THE MOC FOR FBR SIMULATION AND MODELLING OF ESDV OR SSIV RESPONSE: IDEAL GAS

4.1 INTRODUCTION

This chapter describes the development of a methodology based on the MOC for the solution of the conservation equations derived in chapter 2 in conjunction with an ideal gas. This includes:

- transformation of the partial differential equations, derived in Chapter 2, to particular total differential equations called the compatibility equations,
- solution of the compatibility equations based on a modification to the classical ST method and using the Euler predictor-corrector technique (Zucrow and Hoffman, 1976) to enhance accuracy of the numerical analysis. This technique utilises first order finite difference discretisation of the compatibility equations for the predictor step followed by a second order discretisation for the corrector step.

Various procedures with the primary objective of reducing the CPU run times without compromising accuracy in order to produce an optimised model are also discussed. These include the application of a nested grid system as well as the use of curved characteristics.

Accuracy of the simulation is assessed by comparing output data with measurements taken during the Piper Alpha tragedy, and by making comparisons with results obtained by the models of Chen et. al (1992).

Some workers such as Flatt (1985), as well as Olorunmaiye and Imide (1993) respectively make the assumptions of adiabatic and isothermal flow following FBR. The deficiencies of these approaches with respect to accurate prediction over long depressurisation times, and the influence of fire on the rate of heat transfer to the fluid are also highlighted.

The optimised model is then used to simulate the dynamic response of emergency shutdown of both ball and check valves subsequent to FBR. The principal aim is to

demonstrate the importance of predicting the rapid variations in the fluid dynamics within the pipeline during FBR and their influence on the appropriate choice of ESDV or SSIV. Of particular interest are the evaluations of lost inventory and resulting pressure surges as a function of valve proximity to the rupture plane and its response time. Pipelines containing gases whose behaviour may be approximated as ideal are considered here.

The appropriate valve dynamic simulations for high pressure pipelines containing two-phase mixtures are presented in Chapter 5.

4.2 CHARACTERISTIC AND COMPATIBILITY EQUATIONS

In Chapter 2, the Euler equations for unsteady ideal gas fluid flow were derived in the following final form,

$$\rho_t + \rho u_x + u\rho_x = 0$$

$$\rho u_t + \rho u u_x + P_x = \beta$$

$$P_t + uP_x - a^2(\rho_t + u\rho_x) = (\gamma - 1)(q_h - u\beta) = \psi \qquad (2.4.16)$$

$$P = \rho RT$$

$\beta = -2\frac{f_w}{D}\rho u|u|$ where f is the fanning friction factor at the wall

The first step in any method of characteristics solution is to convert the basic partial differential equations of flow into ordinary differential equations. The two most common methods of achieving this are the matrix transformation method, such as the one used by Tiley (1989), and that of multiplying the basic equations by an unknown parameter and subsequent summation. The latter method is used by Lister (1960), Wylie and Streeter (1978) for isothermal flow and by Zucrow and Hoffman (1977) for non-isothermal flow. The method used by Zucrow and Hoffman (1977) is adapted in this study because of its simplicity and mathematical rigour.

Multiplying the mass, momentum and energy conservation equations by σ_1, σ_2 and σ_3 respectively, and then summing,

$$\sigma_1\rho_t + \sigma_1 u\rho_x + \sigma_1\rho u_x + \sigma_2\rho u_t + \sigma_2\rho u u_x + \sigma_2 P_x - \sigma_2\beta + \qquad (4.2.1)$$

$$\sigma_3 P_t + \sigma_3 u P_x - \sigma_3 a^2\rho_t - \sigma_3 a^2 u\rho_x - \sigma_3\psi = 0$$

Factorising equation 4.2.1,

$$(\sigma_1\rho+\sigma_2\rho u)\left(u_x+\frac{\sigma_2\rho}{\sigma_1\rho+\sigma_2\rho u}u_t\right)+(\sigma_2+u\sigma_3)\left(P_x+\frac{\sigma_3}{\sigma_2+u\sigma_3}P_t\right)$$

$$+(\sigma_1 u-\sigma_3 a^2 u)\left(\rho_x+\frac{\sigma_1-\sigma_3 a^2}{\sigma_1 u-\sigma_3 a^2 u}\rho_t\right)-\sigma_2\beta-\sigma_3\psi=0 \qquad (4.2.2)$$

If u(x,t), P(x,t) and ρ(x,t) are assumed to be continuous functions, then

$$\frac{du}{dx}=\frac{\partial u}{\partial x}+\frac{\partial u}{\partial t}\frac{dt}{dx}=u_x+\lambda u_t$$

$$\frac{dP}{dx}=\frac{\partial P}{\partial x}+\frac{\partial P}{\partial t}\frac{dt}{dx}=P_x+\lambda P_t \qquad (4.2.3)$$

$$\frac{d\rho}{dx}=\frac{d\rho}{dx}+\frac{d\rho}{dt}\frac{dt}{dx}=\rho_x+\lambda\rho_t$$

$$\text{where } \lambda=\left(\frac{dt}{dx}\right) \qquad (4.2.4)$$

Comparing equations 4.2.2 and 4.2.3 we see that the slopes of the characteristic curves, dt/dx = λ, are the coefficients of the derivatives u_t, P_t, and ρ_t. Hence,

$$\lambda=\frac{\sigma_2}{\sigma_1+\sigma_2 u}=\frac{\sigma_3}{\sigma_2+u\sigma_3}=\frac{\sigma_1-\sigma_3 a^2}{\sigma_1 u-\sigma_3 a^2 u} \qquad (4.2.5)$$

Rearranging equation 4.2.3 and expressing in terms of P_x, u_x and ρ_x,

$$P_x=\frac{dP}{dx}-\lambda P_t$$

$$u_x=\frac{du}{dx}-\lambda u_t \qquad (4.2.6)$$

$$\rho_x=\frac{d\rho}{dx}-\lambda\rho_t$$

Substituting into equation 4.2.2, we obtain,

$$(\sigma_1\rho + \sigma_2\rho u)du + (\sigma_2 + u\sigma_3)dP$$

$$+(\sigma_1 u - \sigma_3 a^2 u)d\rho - (\sigma_2\beta + \sigma_3\psi)dx = 0 \qquad (4.2.7)$$

The above equation is the compatibility equation which is valid along the characteristic curves that can be determined from equation 4.2.5

σ_1, σ_2 and σ_3 can be determined from equation 4.2.5 by multiplying out all sides and equating, whereby,

$$\sigma_1(\lambda) + \sigma_2(\lambda u - 1) + \sigma_3(0) = 0 \qquad (4.2.8)$$

$$\sigma_1(0) + \sigma_2(\lambda) + \sigma_3(\lambda u - 1) = 0 \qquad (4.2.9)$$

$$\sigma_1(\lambda u - 1) + \sigma_2(0) + \sigma_3 a^2(1 - \lambda u) = 0 \qquad (4.2.10)$$

For equations 4.2.8 to 4.2.10 to have a solution other than the trivial solution, i.e. $\sigma_1 = \sigma_2 = \sigma_3 = 0$, the determinant of the coefficient matrix for these equations must vanish, i.e.

$$\begin{vmatrix} \lambda & (\lambda u - 1) & 0 \\ 0 & \lambda & (\lambda u - 1) \\ (\lambda u - 1) & 0 & -a^2(\lambda u - 1) \end{vmatrix} = 0 \qquad (4.2.11)$$

Expanding the above determinant along the first column,

$$\lambda \begin{vmatrix} \lambda & (\lambda u - 1) \\ 0 & -a^2(\lambda u - 1) \end{vmatrix} + (\lambda u - 1) \begin{vmatrix} (\lambda u - 1) & 0 \\ \lambda & (\lambda u - 1) \end{vmatrix} =$$

$$\lambda\left(-a^2\lambda(\lambda u - 1)\right) + (\lambda u - 1)\left((\lambda u - 1)^2\right) = 0 \qquad (4.2.12)$$

Further simplifying equation 4.2.12, we obtain,

$$(\lambda u - 1)\left[(\lambda u - 1)^2 - a^2\lambda^2\right] = 0 \qquad (4.2.13)$$

Equation 4.2.13 has three roots, the first being,

$$\lambda u - 1 = 0$$

$$\lambda_0 = \left(\frac{dt}{dx}\right)_0 = \frac{1}{u} \tag{4.2.14}$$

This is the equation of the pathline of the fluid particles, and the subscript 0 is employed to denote the pathline. The other two roots can be given by,

$$(\lambda u - 1)^2 = a^2\lambda^2$$

$$\lambda u - 1 = \pm a\lambda \tag{4.2.15}$$

$$\lambda_\pm = \left(\frac{dt}{dx}\right)_\pm = \frac{1}{u \pm a}$$

The three roots obtained are the same three real and distinct eigenvalues which prove the hyperbolicity of the equations as discussed in section 3.2.

The solutions for σ_1, σ_2 and σ_3 can now be obtained for each root. Substituting the pathline root, $\lambda = 1/u$, into equations 4.2.8 to 4.2.10,

$$\sigma_1\lambda = 0 \Rightarrow \sigma_1 = 0$$

$$\sigma_2\lambda = 0 \Rightarrow \sigma_2 = 0 \tag{4.2.16}$$

$$-\sigma_3 a^2(\lambda u - 1) = 0 \Rightarrow \sigma_3 = \text{arbitrary}$$

Substituting the above result into equation 4.2.7,

$$u\sigma_3 dP - a^2 u\sigma_3 d\rho - \sigma_3\psi dx = 0 \tag{4.2.17}$$

Dividing both sides by $u\sigma_3$ we obtain,

$$dP - a^2 d\rho = \frac{\psi}{u}dx = \psi dt \tag{4.2.18}$$

This is the pathline compatibility equation along the characteristic curve.

Along the other two characteristics $\lambda u-1=\pm\lambda a$, equations 4.2.8 to 4.2.10 become,

$$\sigma_1 = -\sigma_2 \frac{\lambda u - 1}{\lambda} \tag{4.2.19}$$

$$\sigma_2 = -\sigma_3 \frac{\lambda u - 1}{\lambda} \tag{4.2.20}$$

$$\sigma_3 = \frac{\sigma_1}{a^2} \Rightarrow \sigma_1 = a^2\sigma_3 \tag{4.2.21}$$

Substituting for σ_2 from equation 4.2.20 into equation 4.2.19,

$$\sigma_1 = --\sigma_3 \frac{(\lambda u - 1)^2}{\lambda^2} = \sigma_3 \frac{a^2\lambda^2}{\lambda^2} = \sigma_3 a^2 \tag{4.2.22}$$

Therefore there are only two independent relationships between σ_1, σ_2 and σ_3 and so one of them (say σ_3) has an arbitrary value. Substituting the results of equations 4.2.21 and 4.2.22 into the general compatibility equation 4.2.7,

$$\rho\sigma_3\left(a^2 - \frac{u(\lambda u - 1)}{\lambda}\right)du + \sigma_3\left(u - \frac{\lambda u - 1}{\lambda}\right)dP + u\sigma_3\left(a^2 - a^2\right)d\rho - \sigma_3 \frac{\lambda u - 1}{\lambda}\beta dx - \sigma_3\psi dx = 0 \tag{4.2.23}$$

Dividing through by σ_3 and substituting for $\lambda u-1=\pm\lambda a$,

$$\rho\left(a^2 \pm au\right)du + (u \pm a)dP \pm a\beta dx + (k-1)u\beta dx = 0$$

$$\Rightarrow \pm a\rho(u \pm a)du + (u \pm a)dP \pm a\beta dx - \psi dx = 0 \tag{4.2.24}$$

Dividing through by $(u\pm a)$,

$$dP_{\pm} \pm \rho a du_{\pm} = \pm a\beta \frac{dx}{(u \pm a)} + \psi \frac{dx}{(u \pm a)} \tag{4.2.25}$$

From equation 4.2.15,

$$dt = \frac{dx}{(u \pm a)} \tag{4.2.26}$$

Substituting this into equation 4.2.25 we obtain the set of compatibility equations for information propagated along C_+ and C_- characteristic lines,

$$dP_{\pm} \pm \rho a du_{\pm} = (\psi \pm a\beta) dt_{\pm} \tag{4.2.27}$$

The upper subscript + attached to the differentials dP, du, and dt and the upper sign + in the coefficient ρa correspond to the C_+ characteristic, whereas the lower subscript - and the lower sign - correspond to the C_- characteristic.

The compatibility equations are,

$$d_0P - a^2 d_0\rho = \psi d_0 t \text{ along } \frac{d_0 t}{d_0 x} = \frac{1}{u}$$

$$d_+P + \rho a d_+u = [\psi + a\beta]\beta d_+t \text{ along } \frac{d_+t}{d_+x} = \frac{1}{(u+a)} \tag{4.2.28}$$

$$d\_P - \rho a d\_u = [\psi - a\beta]\beta d\_t \text{ along } \frac{d\_t}{d\_x} = \frac{1}{(u-a)}$$

Equation 4.2.13 are the Mach lines of unsteady flow, being analogous to the Mach lines in a steady flow. These lines together with the path lines define the characteristic curves of solution to the Euler conservation equations.

The C_+ and C_- characteristics, corresponding to the + and - signs respectively in equation 4.2.13, lie on either side of the pathline, but are asymmetrical with respect to C_0. The negative or left-running characteristic provides a sure indication of the type of flow present as shown in Figure 4.2.1 below:

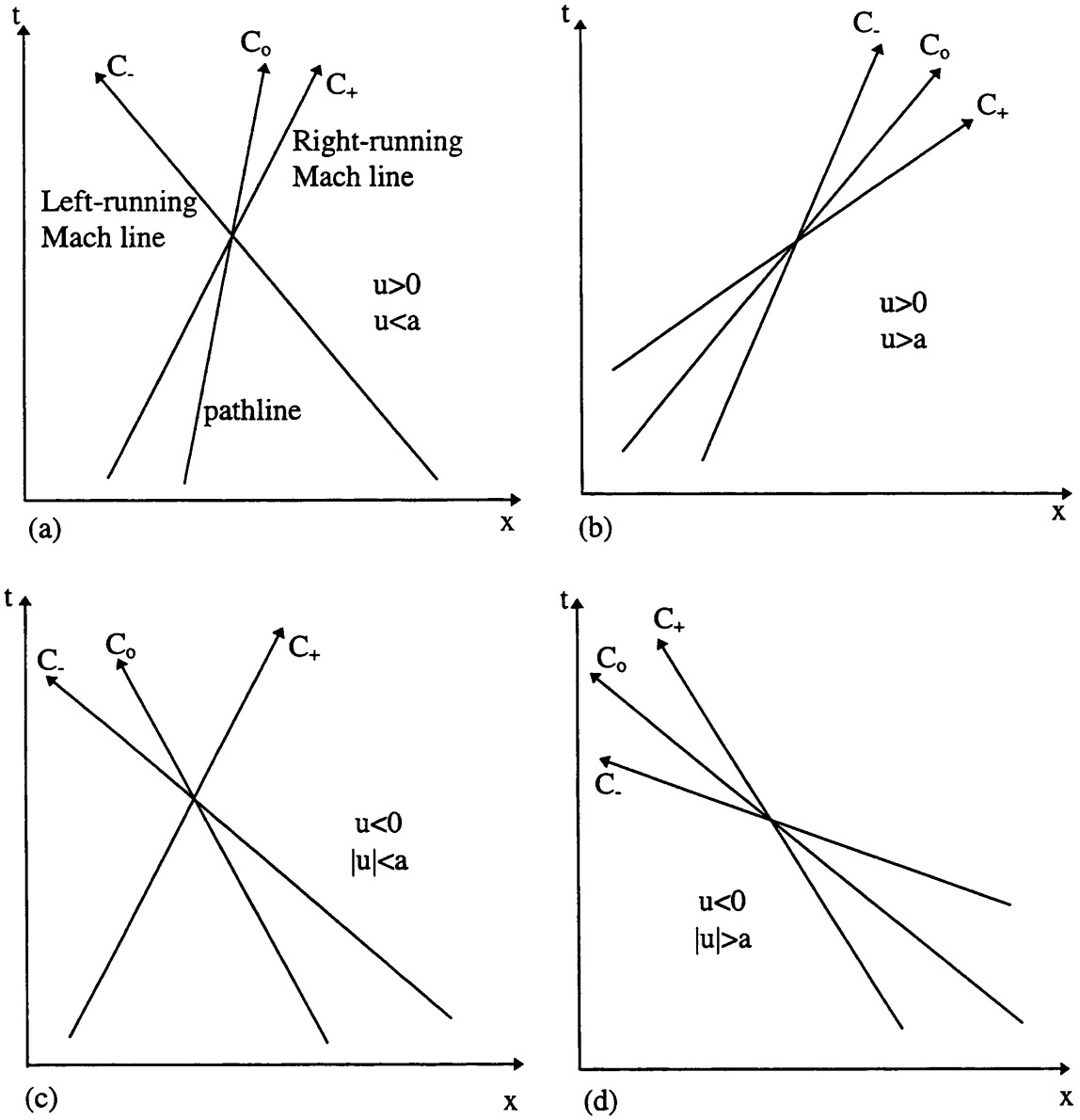

Figure 4.2.1: Characteristics for unsteady one-dimensional flow.

a) Subsonic flow from left to right

b) Supersonic flow from left to right

c) Subsonic flow from right to left

d) Supersonic flow from right to left

4.3 FINITE DIFFERENCE APPROXIMATIONS FOR A METHOD OF CHARACTERISTICS SOLUTION

The common practice in the method of characteristics solution is to use first-order and linear approximations to calculate values at the next time level.

The first order or linear finite difference approximation is expressed by the formula:

$$\int_{x_2}^{x_1} f(x)dx \approx f(x_0)(x_1 - x_0) \qquad (4.3.1)$$

The characteristic equations shown by equations 4.2.14 and 4.2.15 can be represented in the space time domain as in Figure 4.3.1

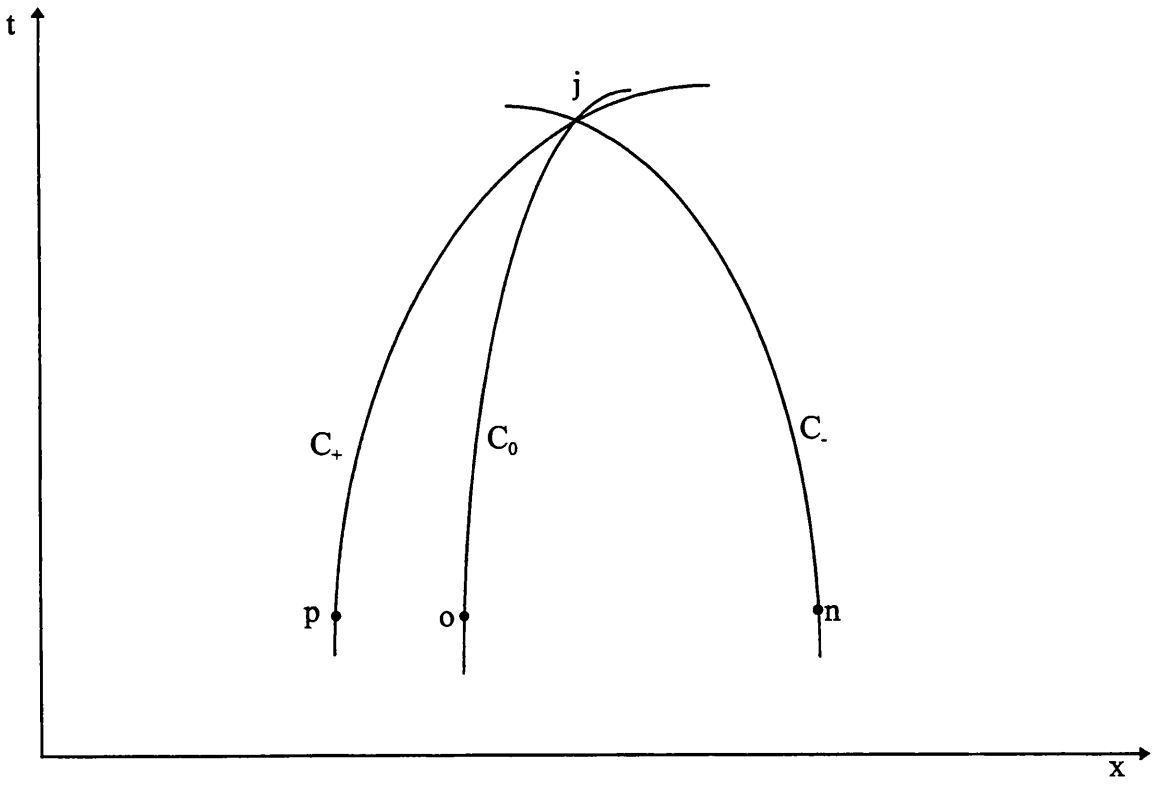

Figure 4.3.1: Characteristic curves in x-t space

From Figure 4.3.1 the linear approximation to the set of equations given by equation 4.2.28 can be given for,

Pathline characteristic;

$$x_j - x_o = (\lambda_0)_o (t_j - t_o) \tag{4.3.2}$$

Pathline compatibility;

$$P_j - P_o - (a^2)_o (\rho_j - \rho_o) = \psi_o (t_j - t_o) \tag{4.3.3}$$

Positive Mach line or right running characteristic;

$$x_j - x_p = (\lambda_+)_p (t_j - t_p) \tag{4.3.4}$$

Positive Mach line compatibility,

$$P_j - P_p + (\rho a)_p (u_j - u_p) = (\psi + a\beta)_p (t_j - t_p) \tag{4.3.5}$$

Negative Mach line or left running characteristic;

$$x_j - x_n = (\lambda_-)_n (t_j - t_n) \tag{4.3.6}$$

Negative Mach line compatibility,

$$P_j - P_n - (\rho a)_n (u_j - u_n) = (\psi - a\beta)_n (t_j - t_n) \tag{4.3.7}$$

The subscripts to the various properties in equations 4.3.2 to 4.3.7 denote the location for calculation of their magnitude.

The second order approximation to equation 4.2.28 can be given for,

Pathline characteristic;

$$x_j - x_o = \frac{1}{2}\left((\lambda_0)_o + (\lambda_0)_p\right)(t_j - t_o) \tag{4.3.8}$$

Pathline compatibility;

$$P_j - P_o - \frac{1}{2}\left(\left(a^2\right)_o + \left(a^2\right)_j\right)\left(\rho_j - \rho_o\right) = \frac{1}{2}\left(\psi_o + \psi_j\right)\left(t_j - t_o\right) \tag{4.3.9}$$

Positive Mach line or right running characteristic;

$$x_j - x_p = \frac{1}{2}\left(\left(\lambda_+\right)_p + \left(\lambda_+\right)_j\right)\left(t_j - t_p\right) \tag{4.3.10}$$

Positive Mach line compatibility,

$$P_j - P_p + \frac{1}{2}\left(\left(\rho a\right)_p + \left(\rho a\right)_j\right)\left(u_j - u_p\right)$$

$$= \frac{1}{2}\left(\left(\psi + a\beta\right)_p + \left(\psi + a\beta\right)_j\right)\left(t_j - t_p\right) \tag{4.3.11}$$

Negative Mach line or left running characteristic;

$$x_j - x_n = \frac{1}{2}\left(\left(\lambda_-\right)_n + \left(\lambda_-\right)_j\right)\left(t_j - t_n\right) \tag{4.3.12}$$

Negative Mach line compatibility,

$$P_j - P_n - \frac{1}{2}\left(\left(\rho a\right)_n + \left(\rho a\right)_j\right)\left(u_j - u_n\right)$$

$$= \frac{1}{2}\left(\left(\psi - a\beta\right)_n + \left(\psi - a\beta\right)_j\right)\left(t_j - t_n\right) \tag{4.3.13}$$

The common practice in the method of characteristics solution is to use first-order and linear approximations to calculate values at the next time level based on convergence of some iteration criteria. The second order scheme is initiated after the first-order solution has been reached. This can however be expensive computationally and rather cumbersome (Tiley, 1989). Some workers have done just one calculation using the first order approximation to obtain an initial guess of flow variables at the solution point followed by a second order approximation (Kimambo, 1996). Adopting this procedure makes the solution more like the Euler Predictor-Corrector method (Zucrow and Hoffman, 1976).

The Euler predictor-corrector technique employs as a first predictor step the same equation as an explicit first order sequence as given by equations 4.3.2 to 4.3.7. This first estimate is then enhanced by the corrector step where equations of the same form as in the second order approximation are used, i.e. equations 4.3.8 to 4.3.13.

There are several ways of using either the set of equations 4.3.2 to 4.3.7 or the set 4.3.8 to 4.3.13 to obtain an approximate numerical solution to the original set of partial differential equations. The two most common that have been implemented have already been discussed in Chapter 3, namely the characteristic grid (CG) method and the method of specified time intervals (ST). It was decided to use the ST method so that valves-in line could be modelled.

4.4 THE METHOD OF SPECIFIED TIME INTERVALS

In the method of specified time intervals, the solution is sought at pre-determined points in the space-time domain (Wylie and Streeter, Lister, Zucrow and Hoffman al.). This method of solution has many names including the inverse marching method, the mesh method, and the hybrid method of characteristics.

4.4.1 The First Order Solution

In the first order approximation, the characteristic curves are assumed to be straight lines. The flow field is discretised by using a rectangular grid in space and time according to the inverse marching method. Figure 4.4.1 shows the grid scheme.

The Courant-Friedrich-Lewy criterion (Zucrow and Hoffman, 1976) that has to be satisfied in order to ensure numerical stability is:

$$\Delta t \leq \frac{\Delta x}{\left(|u + a|_{max}\right)} \tag{4.4.1}$$

There are two open end scenarios that need to be considered. One is the case of choked flow at the ruptured end which will be sustained until the pressure at this point drops down to the external pressure. Choking is characterised by a Mach number of 1. The second case occurs when the external pressure is reached and the choking condition no longer holds (i.e. the outflow is subsonic at this point). The calculation procedure for the end point will therefore differ according to the pressure at the ruptured end. The interior point and the intact end boundary point calculations are not affected by this condition.

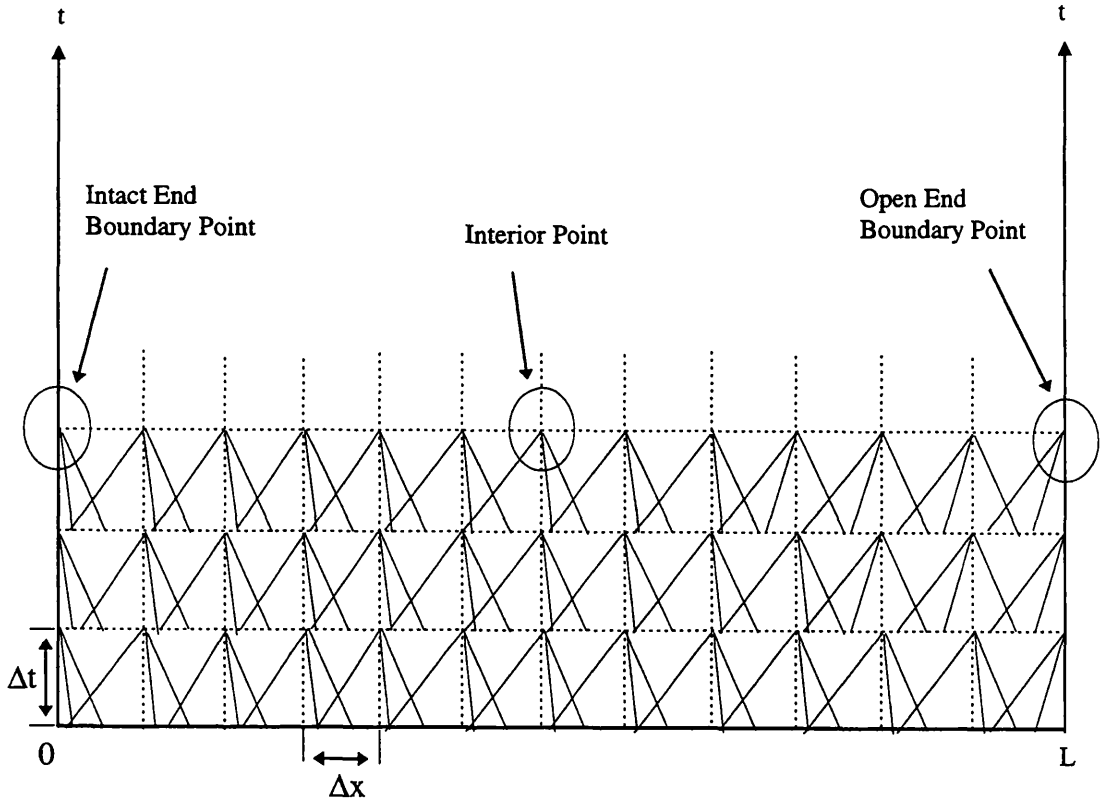

Figure 4.4.1: The Method of Specified Time Intervals

4.4.1.1 The Interior Point Calculation

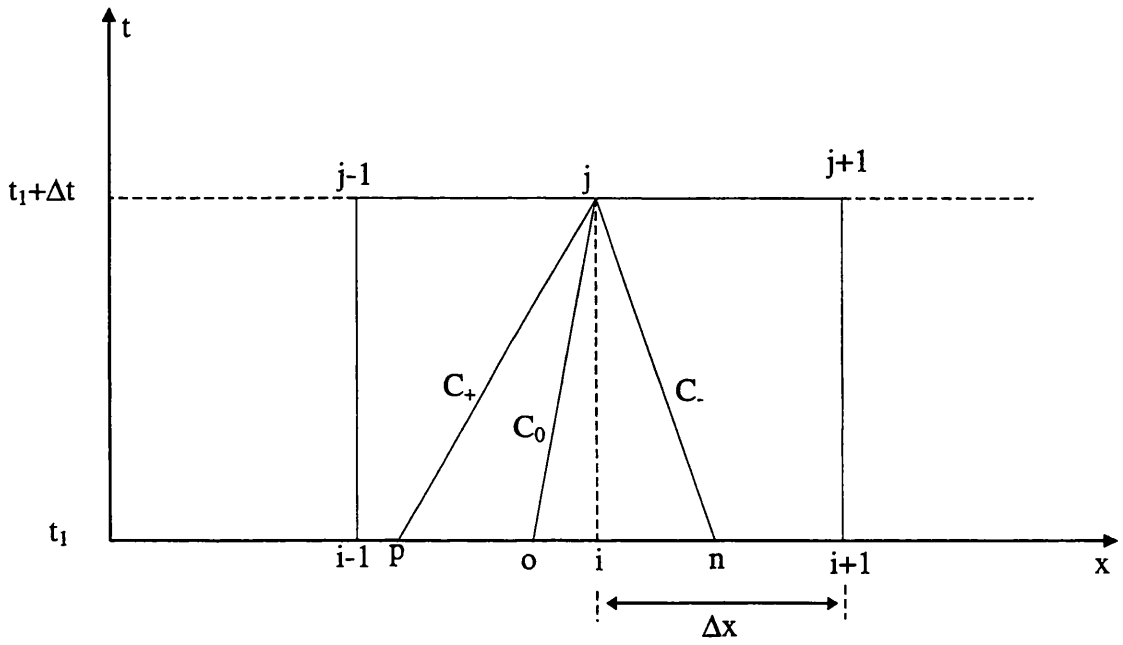

Figure 4.4.2: **Grid Scheme for an interior point**

In order to work out the conditions at the solution point j-1, the initial conditions at points p,o and n need to be calculated. Recalling the slopes of the characteristic lines,

$$\frac{d_o t}{d_o x} = \frac{1}{u} \qquad \frac{d_+ t}{d_+ x} = \frac{1}{u+a} \qquad \frac{d_- t}{d_- x} = \frac{1}{u-a} \tag{4.4.2}$$

The usual method to solve for the interior point is to first compute the positions of the initial points p,o and n. This is done by making the initial approximation that,

$u_o=u_{i-1}$, $u_p=u_{i-2}$, $u_n=u_i$ so that the characteristic slopes as given by equation 4.4.2 can be written as:

$$\lambda_o = \frac{1}{u_o} = \frac{1}{u_i} = \frac{\Delta t}{x_i - x_o} \Rightarrow x_o = x_i - \Delta t u_i \tag{4.4.3}$$

$$\lambda_+ = \frac{1}{u_p + a_p} = \frac{1}{u_{i-1} + a_{i-1}} = \frac{\Delta t}{x_i - x_p} \Rightarrow x_p = x_i - \Delta t\left(u_{i-1} + a_{i-1}\right) \tag{4.4.4}$$

$$\lambda_- = \frac{1}{u_n - a_n} = \frac{1}{u_{i+1} - a_{i+1}} = \frac{\Delta t}{x_i - x_n} \Rightarrow x_n = x_i - \Delta t\left(u_{i+1} - a_{i+1}\right) \tag{4.4.5}$$

Once the positions of the points p,o and n are known, the variables at these points can be calculated by linear interpolation along the spatial axis, between points i-1, i, and i+1. Therefore,

$$Z_p = Z_{i-1} + \frac{Z_i - Z_{i-1}}{x_i - x_{i-1}}\left(x_p - x_{i-1}\right) \tag{4.4.6}$$

$$Z_n = Z_i + \frac{Z_{i+1} - Z_i}{x_{i+1} - x_i}\left(x_n - x_i\right) \tag{4.4.7}$$

$$Z_o = \begin{cases} Z_{i-1} + \dfrac{Z_i - Z_{i-1}}{x_i - x_{i-1}}\left(x_o - x_{i-1}\right) & \text{if } \lambda_o > 0 \\ Z_i + \dfrac{Z_{i+1} - Z_i}{x_{i+1} - x_i}\left(x_o - x_i\right) & \text{if} \lambda_o < 0 \end{cases} \tag{4.4.8}$$

where: Z = u, P, ρ, and a.

The above yields tentative values for the location and flow properties at points p,o and n. These values can be improved by repeating the above steps iteratively, each time using the most recent values as calculated from the interpolation equations. Once a specified tolerance for the values at x_p, x_n, and x_o have been satisfied, the solution point (j) flow variables can be calculated from the compatibility equations 4.3.3, 4.3.5 and 4.3.7 for the predictor step followed by equations 4.3.9, 4.311, and 4.3.13 for the corrector step.

Thus the solution point flow variables are evaluated, first using the initial estimate to get tentative solutions and then repeated using the average values of u, p, ρ, and a along each characteristic. This procedure is repeated until another convergence tolerance is satisfied for the solution point, j.

This is the established procedure for the method of specified time intervals.

A new modification to this method is hereby proposed whereby the location of the initial points is immediately found without the need for any iteration.

For the predictor step,

$$\frac{d_o t}{d_o x} = \frac{1}{u_o} = \frac{\Delta t}{x_i - x_o} \Rightarrow x_o = x_i - \Delta t u_0 \tag{4.4.9}$$

$$\frac{d_+ t}{d_+ x} = \frac{1}{u_p + a_p} = \frac{\Delta t}{x_i - x_p} \Rightarrow x_p = x_i - \Delta t\left(u_p + a_p\right) \tag{4.4.10}$$

$$\frac{d_- t}{d_- x} = \frac{1}{u_n - a_n} = \frac{\Delta t}{x_i - x_n} \Rightarrow x_n = x_i - \Delta t\left(u_n - a_n\right) \tag{4.4.11}$$

In equations 4.4.9 to 4.4.11, expressions for the velocity and speed of sound can be obtained from the first order interpolation formulas. These expressions can then be substituted back into the above characteristic equations, 4.4.9 to 4.4.11 to give,

For u_p,

$$\begin{aligned} u_p &= u_{i-1} + \frac{u_i - u_{i-1}}{x_i - x_{i-1}}\left[x_i - x_{i-1} - \Delta t\left(u_p + a_p\right)\right] \\ &= u_i - \frac{u_i - u_{i-1}}{x_i - x_{i-1}}\Delta t\left(u_p + a_p\right) \end{aligned} \tag{4.4.12}$$

Rearranging the above, we can write,

$$u_p\left(1 + \frac{u_i - u_{i-1}}{x_i - x_{i-1}}\Delta t\right) + \frac{u_i - u_{i-1}}{x_i - x_{i-1}}\Delta t a_p = u_i \tag{4.4.13}$$

Carrying out the same manipulation for a_p, we obtain,

$$a_p\left(1+\frac{a_i-a_{i-1}}{x_i-x_{i-1}}\Delta t\right)+\frac{a_i-a_{i-1}}{x_i-x_{i-1}}\Delta tu_p=a_i \qquad (4.4.14)$$

Equations 4.4.13 and 4.4.14 can be solved simultaneously for u_p and a_p.

Similarly a 2×2 system of equations can be set up for u_n and a_n based on the same mathematical manipulation to yield,

$$u_n\left(1+\frac{u_{i+1}-u_i}{x_{i+1}-x_i}\Delta t\right)-\frac{u_{i+1}-u_i}{x_{i+1}-x_i}\Delta ta_n=u_i \qquad (4.4.15)$$

$$a_n\left(1+\frac{a_{i+1}-a_i}{x_{i+1}-x_i}\Delta t\right)-\frac{a_{i+1}-a_i}{x_{i+1}-x_i}\Delta tu_n=a_i \qquad (4.4.16)$$

For u_o, the solution depends on whether the slope of the pathline characteristic is positive or negative. The nature of the sign determines which way the fluid is flowing, if it is positive the flow is travelling towards the ruptured end, if negative it is travelling towards the intact end.

If $\lambda_o > 0$ then,

$$u_o=u_{i-1}+\frac{u_i-u_{i-1}}{x_i-x_{i-1}}\left(x_i-\Delta tu_o-x_{i-1}\right)$$

$$=u_{i-1}+u_i-u_{i-1}-\frac{u_i-u_{i-1}}{x_i-x_{i-1}}\Delta tu_o \qquad (4.4.17)$$

$$=u_i-\frac{u_i-u_{i-1}}{x_i-x_{i-1}}\Delta tu_o$$

Rearranging we can write,

$$u_o=\frac{u_i}{\left(1+\frac{u_i-u_{i-1}}{x_i-x_{i-1}}\Delta t\right)} \qquad (4.4.18)$$

If $\lambda_o < 0$, a similar equation for u_o can be derived,

$$u_o = \frac{u_i}{\left(1+\frac{u_{i+1}-u_i}{x_{i+1}-x_i}\Delta t\right)} \tag{4.4.19}$$

The locations of x_p, x_n, and x_o can now be calculated directly from equations 4.4.9 to 4.4.11 by substituting the calculated values for u_p, a_p, u_n, a_n, and u_o from the above equations.

The values of P at the three initial points are then calculated using the interpolation equations, 4.4.6 to 4.4.8. The density, ρ, and temperature T can then be calculated from the following relations for an ideal gas,

$$T = \frac{a^2}{\gamma R} \tag{4.4.20}$$

$$\rho = \frac{P}{RT} \tag{4.4.21}$$

All the initial point flow variables are now available to compute the flow conditions at the solution point j.

From equations 4.3.5 and 4.3.7, we obtain

$$P_j = K_1 - (\rho a)_p (u_j - u_p) + P_p \tag{4.4.22}$$

$$P_j = K_2 + (\rho a)_n (u_j - u_n) + P_n \tag{4.4.23}$$

where

$$K_1 = (\psi + a\beta)_p \Delta t \tag{4.4.24}$$

and,

$$K_2 = (\psi - a\beta)_n \Delta t \tag{4.4.25}$$

Solving the above two equations simultaneously for u_j we can write,

$$u_j = \frac{K_1 - K_2 + (\rho a)_p u_p + (\rho a)_n u_n + P_p + P_n}{(\rho a)_n + (\rho a)_p} \tag{4.4.26}$$

Once the velocity is known, the pressure at the solution point, P_j can be calculated by direct substitution for u_j into either equations 4.4.22 or 4.4.23.

The density at the solution point can now be obtained from the pathline compatibility, i.e. equation 4.3.3,

$$\rho_j = \frac{(P_j - P_o) + a_o^2 \rho_0 - \psi_o \Delta t}{a_o^2} \tag{4.4.27}$$

Once the pressure and density are known, the temperature can easily be calculated from equation 4.4.21. In the ideal gas model, the ratio of specific heats, γ, is a constant for a given fluid and hence the speed of sound can subsequently be calculated from equation 4.4.20.

The above steps are the predictor steps. For the corrector steps, these solution point parameters are now re-evaluated using the average values of u, p, ρ, and, a along each characteristic.

The procedure for the implementation of the corrector steps based on average values is summarised below,

For calculation of u_o;

$$\frac{d_o t}{d_o x} = \frac{1}{\left(\frac{u_o + u_j^r}{2}\right)} = \frac{\Delta t}{x_i - x_o} \Rightarrow x_o = x_i - \frac{\Delta t}{2}\left(u_o + u_j^r\right) \tag{4.4.28}$$

If $\lambda_o > 0$ then,

$$u_o = u_{i-1} + \frac{u_i - u_{i-1}}{x_i - x_{i-1}}\left(x_i - \frac{\Delta t}{2}\left(u_o + u_j^r\right) - x_{i-1}\right)$$

$$u_o\left(1 + \frac{u_i - u_{i-1}}{x_i - x_{i-1}}\frac{\Delta t}{2}\right) = u_i - \frac{u_i - u_{i-1}}{x_i - x_{i-1}}\frac{\Delta t}{2}u_j^r \qquad (4.4.29)$$

$$u_o = \frac{u_i - \frac{u_i - u_{i-1}}{x_i - x_{i-1}}\frac{\Delta t}{2}u_j^r}{\left(1 + \frac{u_i - u_{i-1}}{x_i - x_{i-1}}\frac{\Delta t}{2}\right)}$$

where the subscript j together with superscript r refer to the solution condition at the previous iteration step, r.

For calculation of u_p and a_p,

$$\frac{d_+ t}{d_+ x} = \frac{1}{\frac{1}{2}\left(u_p + u_j^r\right) + \frac{1}{2}\left(a_p + a_j^r\right)} = \frac{\Delta t}{x_i - x_p}$$

$$\Rightarrow x_p = x_i - \frac{\Delta t}{2}\left(u_p + a_p + u_j^r + a_j^r\right) \qquad (4.4.30)$$

u_p from linear interpolation,

$$u_p = u_{i-1} + \frac{u_i - u_{i-1}}{x_i - x_{i-1}}\left[x_i - x_{i-1} - \frac{\Delta t}{2}\left(u_p + a_p + u_j^r + a_j^r\right)\right]$$

$$= u_i - \frac{u_i - u_{i-1}}{x_i - x_{i-1}}\frac{\Delta t}{2}\left(u_p + a_p + u_j^r + a_j^r\right) \qquad (4.4.31)$$

Rearranging for the unknowns, u_p and a_p,

$$u_p\left(1 + \frac{u_i - u_{i-1}}{x_i - x_{i-1}}\frac{\Delta t}{2}\right) + \frac{u_i - u_{i-1}}{x_i - x_{i-1}}\frac{\Delta t}{2}a_p = u_i - \frac{u_i - u_{i-1}}{x_i - x_{i-1}}\frac{\Delta t}{2}\left(u_j^r + a_j^r\right) \qquad (4.4.32)$$

Performing the same manipulation for a_p, we obtain,

$$a_p = a_{i-1} + \frac{a_i - a_{i-1}}{x_i - x_{i-1}}\left[x_i - x_{i-1} - \frac{\Delta t}{2}\left(u_p + a_p + u_j^r + a_j^r\right)\right]$$

$$= a_i - \frac{a_i - a_{i-1}}{x_i - x_{i-1}}\frac{\Delta t}{2}\left(u_p + a_p + u_j^r + a_j^r\right) \tag{4.4.33}$$

$$a_p\left(1 + \frac{a_i - a_{i-1}}{x_i - x_{i-1}}\frac{\Delta t}{2}\right) + \frac{a_i - a_{i-1}}{x_i - x_{i-1}}\frac{\Delta t}{2}u_p = a_i - \frac{a_i - a_{i-1}}{x_i - x_{i-1}}\frac{\Delta t}{2}\left(u_j^r + a_j^r\right) \tag{4.4.34}$$

As for the predictor step, equations 4.4.32 and 4.4.34 can be solved simultaneously for u_p and a_p.

Similarly a 2×2 system of equations can be set up for u_n and a_n in the corrector step,

$$\frac{d\_t}{d\_x} = \frac{1}{\frac{1}{2}\left(u_n + u_j^r\right) - \frac{1}{2}\left(a_n + a_j^r\right)} = \frac{\Delta t}{x_i - x_n}$$

$$\Rightarrow x_n = x_i - \frac{\Delta t}{2}\left(\left(u_n - a_n\right) + \left(u_j^r - a_j^r\right)\right) \tag{4.4.35}$$

$$u_n = u_i + \frac{u_{i+1} - u_i}{x_{i+1} - x_i}\left[x_i - x_i - \frac{\Delta t}{2}\left(u_n - a_n + u_j^r - a_j^r\right)\right]$$

$$= u_i - \frac{u_{i+1} - u_i}{x_{i+1} - x_i}\frac{\Delta t}{2}\left(u_n - a_n + u_j^r - a_j^r\right) \tag{4.4.36}$$

$$u_n\left(1 + \frac{u_{i+1} - u_i}{x_{i+1} - x_i}\frac{\Delta t}{2}\right) - \frac{u_{i+1} - u_i}{x_{i+1} - x_i}\frac{\Delta t}{2}a_n = u_i - \frac{u_{i+1} - u_i}{x_{i+1} - x_i}\frac{\Delta t}{2}\left(u_j^r - a_j^r\right) \tag{4.4.37}$$

$$a_n\left(1 + \frac{a_{i+1} - a_i}{x_{i+1} - x_i}\Delta t\right) - \frac{a_{i+1} - a_i}{x_{i+1} - x_i}\frac{\Delta t}{2}u_n = a_i - \frac{a_{i+1} - a_i}{x_{i+1} - x_i}\frac{\Delta t}{2}\left(u_j^r - a_j^r\right) \tag{4.4.38}$$

The locations of x_p, x_n, and x_o can now be calculated directly from equations 4.4.28, 4.4.30 and 4.4.35 by performing the relevant substitutions. The dependent flow variables at the solution point can now be calculated at the next r+1 iteration step;

$$P_j^{r+1} = K_1 - \frac{1}{2}\left[(\rho a)_p + (\rho a)_j^r\right]\left(u_j^{r+1} - u_p\right) + P_p \tag{4.4.39}$$

$$P_j^{r+1} = K_2 + \frac{1}{2}\left[(\rho a)_n + (\rho a)_j^r\right]\left(u_j^{r+1} - u_n\right) + P_n \tag{4.4.40}$$

where K_1 is given by,

$$K_1 = \frac{1}{2}\left[(\Psi + a\beta)_p + (\Psi + a\beta)_j^r\right]\Delta t \tag{4.4.41}$$

and K_2 by,

$$K_2 = \frac{1}{2}\left[(\Psi - a\beta)_n + (\Psi - a\beta)_j^r\right]\Delta t \tag{4.4.42}$$

Solving the equations 4.4.39 and 4.4.40 simultaneously for u_j we can write,

$$u_j^{r+1} = \frac{K_1 - K_2 + \frac{1}{2}\left[(\rho a)_p + (\rho a)_j^r\right]u_p + \frac{1}{2}\left[(\rho a)_n + (\rho a)_j^r\right]u_n + P_p - P_n}{\frac{1}{2}\left[(\rho a)_p + (\rho a)_j^r\right] + \frac{1}{2}\left[(\rho a)_n + (\rho a)_j^r\right]} \tag{4.4.43}$$

Once u_j^{r+1} is calculated, P_j^{r+1} can be calculated from either equation 4.4.39 or equation 4.4.40. The density is given by,

$$\rho_j^{r+1} = \frac{\left(P_j^{r+1} - P_o\right) + \frac{1}{2}\left(a_o^2 + a_j^{r2}\right)\rho_0 - \psi_o \Delta t}{\frac{1}{2}\left(a_o^2 + a_j^{r2}\right)} \tag{4.4.44}$$

The speed of sound and temperature are calculated according to relations 4.4.20 and 4.4.21.

The above calculation procedure is repeated until a certain tolerance is satisfied for the three dependent variables, i.e. P, u, and ρ. The advantage of this process is that only one iteration calculation is involved since the location of the initial points p, o and n are computed directly without any iteration and results in considerable savings in calculation time without any loss of global accuracy (see section 4.6).

4.4.1.2 The Intact End Point Calculation

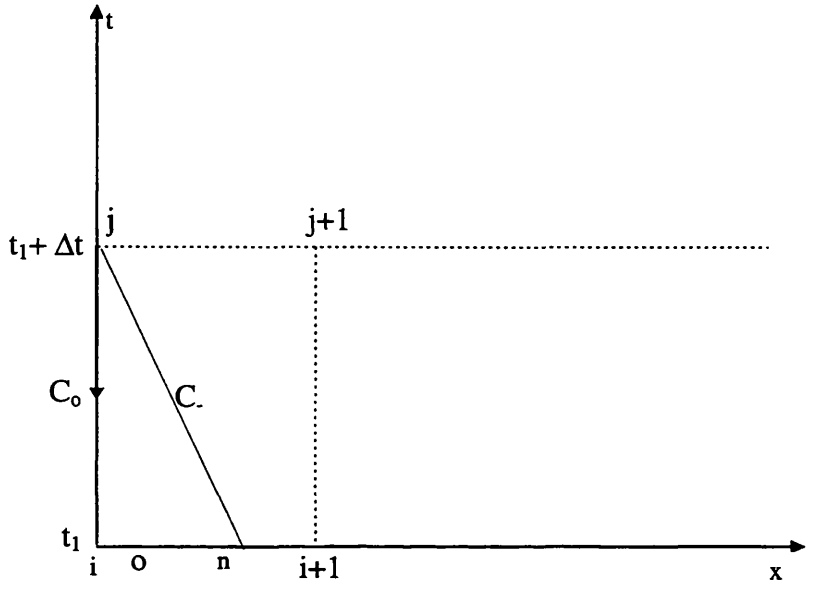

Figure 4.4.3: Grid Scheme for an intact end point

In this case, the positive characteristic λ_+ is non-existent, the pathline characteristic λ_o (C_o) is infinity, and the solution point velocity u_j is zero. The flow conditions at the initial points n and o are worked out as for the interior point. Just the predictor steps are presented here. The corrector steps are then applied as in section 4.4.1.1.

The relevant compatibility equations are,

$$P_j - P_o - a_o^2(\rho_j - \rho_o) = (k-1)(q-u\beta)_o \Delta t = \Psi_o \Delta t \qquad (4.4.45)$$

$$P_j - P_n - (\rho a)_n (0 - u_n) = \left[(k-1)(q-u\beta)_n - (a\beta)_n\right]\Delta t = \left[\Psi - a\beta\right]_n \Delta t \qquad (4.4.46)$$

Equation 4.4.46 can be rearranged to give an expression for P_j.

$$P_j = P_n - (\rho a)_n u_n + [\Psi - a\beta]_n \Delta t \qquad (4.4.47)$$

Thus the solution point density is given by,

$$\rho_j = \frac{P_j - P_o - \Psi_o \Delta t + a_o^2 \rho_o}{a_o^2} \qquad (4.4.48)$$

The temperature and speed of sound are calculated from the ideal gas equations 4.4.20 and 4.4.21 respectively.

4.4.1.3 The Ruptured End Point Calculation

There are two time domains for discharge at the rupture point. The first to occur is the choked flow time domain whose duration depends on how quickly the pressure at this point drops down to the external pressure. When choked, the flow at this point is sonic and no further disturbance can propagate upstream. Once the external pressure is reached, the second time domain is initiated and in this period the outflow is subsonic.

As for the interior point calculation, at each node, both predictor and corrector steps are performed in the calculation procedure. Just the predictor steps are presented here. The corrector steps are then applied as in section 4.4.1.1.

For sonic flow,

$$Ma = \frac{u}{a} = 1 \qquad (4.4.49)$$

Therefore at the solution point, we can take $u_j = a_j$.

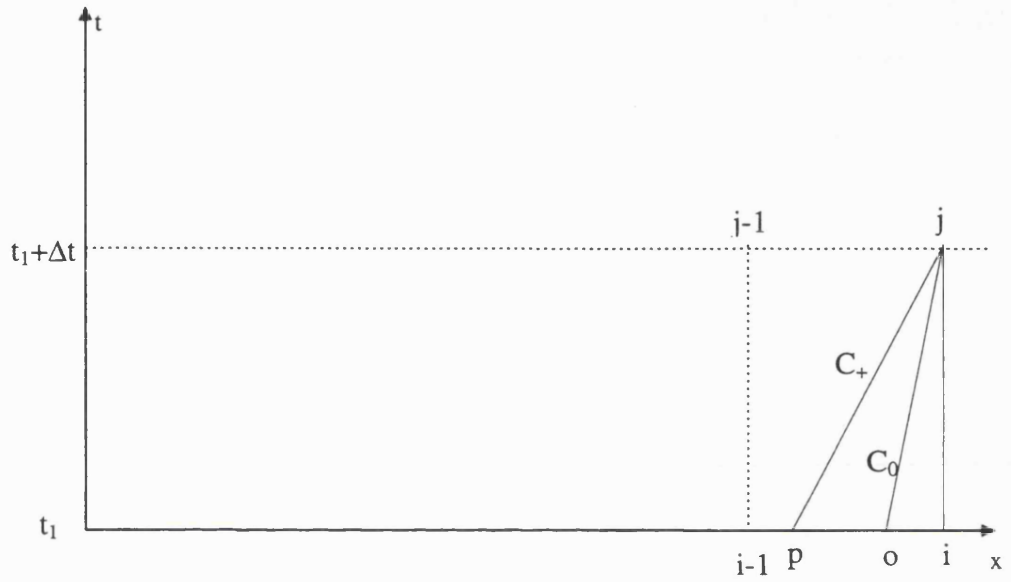

Figure 4.4.4: Grid Scheme for the ruptured end point

From equation 4.4.49 and the ideal gas expressions given by equations 4.4.20 and 4.4.21 we obtain,

$$a_j^2 = u_j^2 = k\frac{P_j}{\rho_j} \Rightarrow P_j = \rho_j \frac{u_j^2}{k} \qquad (4.4.50)$$

Once the flow conditions at the initial points, p and o are established according to the procedure shown for the interior point, the other flow conditions at the solution point can be calculated.

The relevant compatibility equations are:

$$P_j - P_o - a_o^2(\rho_j - \rho_o) = (k-1)(q-u\beta)_o \Delta t = \Psi_o \Delta t \quad (4.4.51)$$

$$P_j - P_p + (\rho a)_p (u_j - u_p) = \left[(k-1)(q-u\beta)_p + (a\beta)_p\right]\Delta t = \left[\Psi + a\beta\right]_p \Delta t \quad (4.4.52)$$

Rearranging equation 4.4.51 and 4.4.52,

$$P_j - a_o^2 \rho_j = P_o - a_o^2 \rho_o + \Psi_o \Delta t = A_1 \quad (4.4.53)$$

$$P_j + (\rho a)_p u_j = P_p + (\rho a)_p u_p + \left[\Psi + a\beta\right]_p \Delta t = A_2 \quad (4.4.54)$$

Substituting for P_j from equation 4.4.50 into the above two equations,

$$\frac{\rho_j u_j^2}{k} - a_o^2 \rho_j - A_1 = 0 \quad (4.4.55)$$

$$\frac{\rho_j u_j^2}{k} + (\rho a)_p u_j - A_2 = 0 \quad (4.4.56)$$

The system of 2×2 equations above are solved simultaneously for u_j and ρ_j. P_j is then obtained from either 4.4.53 or 4.4.54. The above process is repeated iteratively using the corrector steps until a convergence tolerance is satisfied for u_j and ρ_j.

In the case of subsonic flow, the solution point pressure P_j equals the external pressure P_{ext}.

The velocity at the solution point can therefore be calculated by rearranging equation 4.4.54.

$$u_j = \frac{A_2 - P_{ext}}{(\rho a)_p} \quad (4.4.57)$$

The density at the solution point can be calculated from equation 4.4.53,

$$\rho_j = \frac{P_{ext} - A_1}{a_o^2} \quad (4.4.58)$$

The temperature and speed of sound are calculated as usual from equations 4.4.21 and 4.4.20 respectively.

4.4.2 The Second Order Solution

The first order approximation does not account for the curvature of the characteristics in regions where fluid properties change dramatically in a non linear manner. This is usually the case for two-phase mixtures or condensible gases when the first order approximation can lead to a significant global error.

Flatt (1985) proposed a singly-iterative second order method of characteristics which accounts for the curvature of the characteristics by considering them as arcs of parabolas. The advantage of this approach over the classical ST method is that only a single iteration is needed for the solution point properties. The previous time line properties are calculated directly from solution of quadratic interpolation formulas for spatial discretisation.

4.4.2.1 Interior Point Solution

The characteristic line can be considered to be curved by making the approximation that it is a section of a parabola with a horizontal axis as shown in Figure 4.4.5. This approximation permits use of a well-known geometric property, i.e., the tangents to points j and p meet halfway along the time axis at point q, so that

$$t_q = \frac{1}{2}\left(t_p + t_j\right) = t_p + \frac{\Delta t}{2} = t_j - \frac{\Delta t}{2} \qquad (4.4.59)$$

The interior point grid for a second order solution is given below,

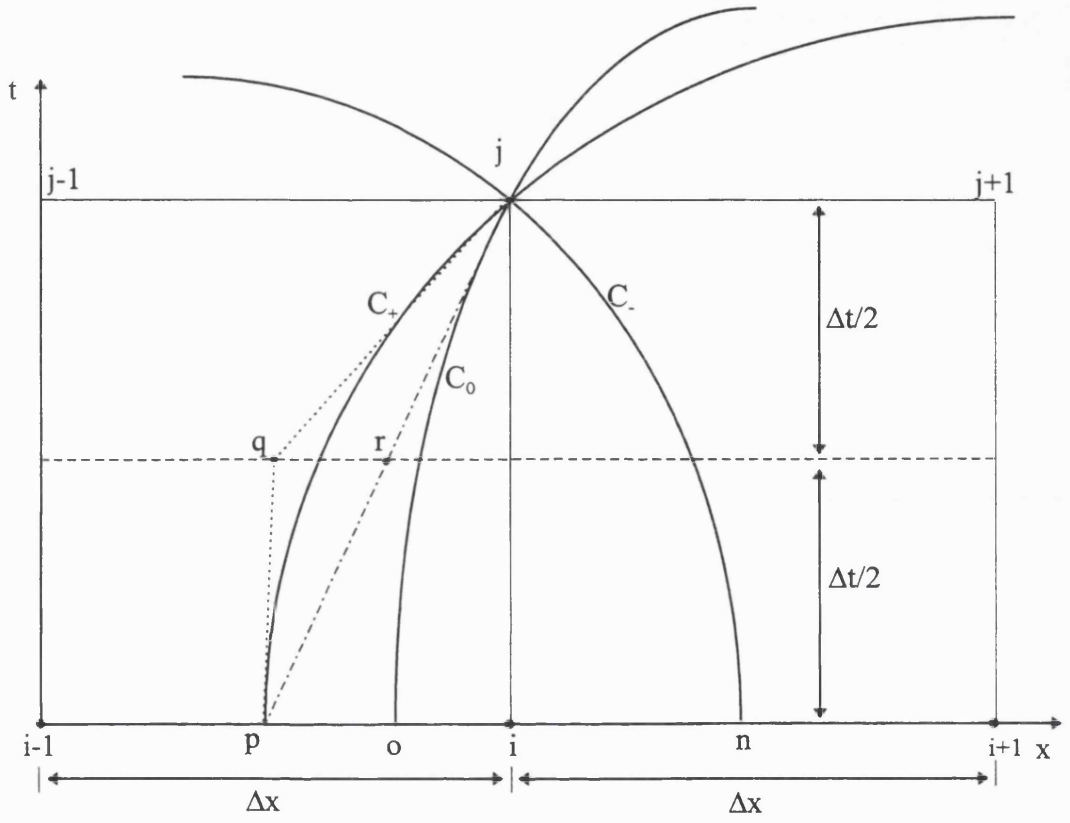

Figure 4.4.5 Curved characteristics in the ST MOC method

Introducing the parameter, L, so that at any point along the pathline characteristic,

$$L = \frac{1}{\lambda} = u \tag{4.4.60}$$

Along the positive characteristic,

$$L_{(+)} = \frac{1}{\lambda_+} = u + a \tag{4.4.61}$$

Along the negative characteristic,

$$L_{(-)} = \frac{1}{\lambda_-} = u - a \tag{4.4.62}$$

Considering only the positive Mach line characteristic, the slope of the tangent at the node point j can be written as,

$$\frac{\frac{\Delta t}{2}}{x_j - x_q} = \frac{1}{L_{j(+)}}$$

$$x_q = x_j - \frac{\Delta t}{2} L_{j(+)} \tag{4.4.63}$$

Similarly for the tangent at, p on the same positive characteristic,

$$\frac{\frac{\Delta t}{2}}{x_q - x_p} = \frac{1}{L_{p(+)}}$$

$$x_q = x_p + \frac{\Delta t}{2} L_{p(+)} \tag{4.4.64}$$

Equation 4.4.63 to 4.4.64 and eliminating x_q,

$$x_p = x_j - \frac{\Delta t}{2}\left(L_{p(+)} + L_{j(+)}\right) \tag{4.4.65}$$

$L_{p(+)}$ falls on the same time line as points i-1 and i where conditions are known, so interpolation is needed to evaluate conditions at point p(+). To maintain a coherent second order scheme, a quadratic interpolation is needed based on the three point stencil, i-1, i, and i+1.

$$L_{p+} = C_1\left(x_p - x_i\right)^2 + C_2\left(x_p - x_i\right) + L_{i+} \tag{4.4.66}$$

where

$$C_1 = \frac{L_{i-1(+)} - 2L_{i(+)} + L_{i+1(+)}}{2(\Delta x)^2} \tag{4.4.67}$$

and

$$C_2 = \frac{L_{1+1(+)} - L_{i-1(+)}}{2\Delta x} \tag{4.4.68}$$

From equation 4.4.61,

$$L_{p(+)} = \left(x_j - x_p\right)\frac{2}{\Delta t} - L_{j(+)} = -\left(x_p - x_i\right)\frac{2}{\Delta t} - L_{j(+)} \tag{4.4.69}$$

Equating equation 4.4.69 to equation 4.4.66

$$C_1X^2 + \left(C_2 + \frac{2}{\Delta t}\right)X + L_{i(+)} + L_{j(+)} = 0$$

$$C_1X^2 + 2C_3X + C_4 = 0 \tag{4.4.70}$$

where

$$X = \left(x_p - x_i\right) \tag{4.4.71}$$

$$C_3 = \left(\frac{C_2}{2} + \frac{1}{\Delta t}\right) \tag{4.4.72}$$

$$C_4 = L_{i(+)} + L_{j(+)} \tag{4.4.73}$$

The solution to the quadratic equation 4.4.66 can be expressed in the special form,

$$X = x_p - x_i = -\frac{C_4}{C_3 \pm \sqrt{C_3^2 - C_1 C_4}} \qquad (4.4.74)$$

Expressing the solution in this form has been shown to give better numerical results (Flatt, 1985) than the conventional form if the coefficient C_1 becomes very small.

Considering equation 4.4.70 for $C_1 = 0$, the physically correct solution of equation 4.4.74 will be the one with the upper sign if $C_3>0$, or lower sign if $C_3<0$. Both cases can be expressed in the single form,

$$X = x_p - x_i = -\frac{C_4}{C_3\left[1+\sqrt{\left(1-\frac{C_1 C_4}{C_3^2}\right)}\right]} \qquad (4.4.75)$$

Using the above technique, the positions of the points of intersection of pathline, positive Mach line and negative Mach line can be determined without the need for any iteration. The conditions at these points are then calculated using quadratic interpolation formulas as shown by equation 4.4.66.

The conditions at the solution point are obtained by solving the relevant compatibility equations using a second order finite difference scheme as proposed in section 4.3. The calculations are continued until convergence is reached for the dependent variables at the solution point in the same way as outlined for the first order solution, see section 4.4.1.

4.4.2.2 Ruptured End Point Solution

To deal with the curved characteristics in the boundary cell, the concept of a ghost cell is introduced. The addition of an extra "ghost" cell adjacent to the boundary cell permits quadratic interpolation for points, p and o in figure 4.4.6. The conditions at the node i+1 are the same as at node i, i.e.

$$Z_{i+1} = Z_i \qquad (4.4.76)$$

where

Z = P,u,ρ,T,a.

The rest of the calculations are exactly the same as for the interior point, section 4.4.2.1.

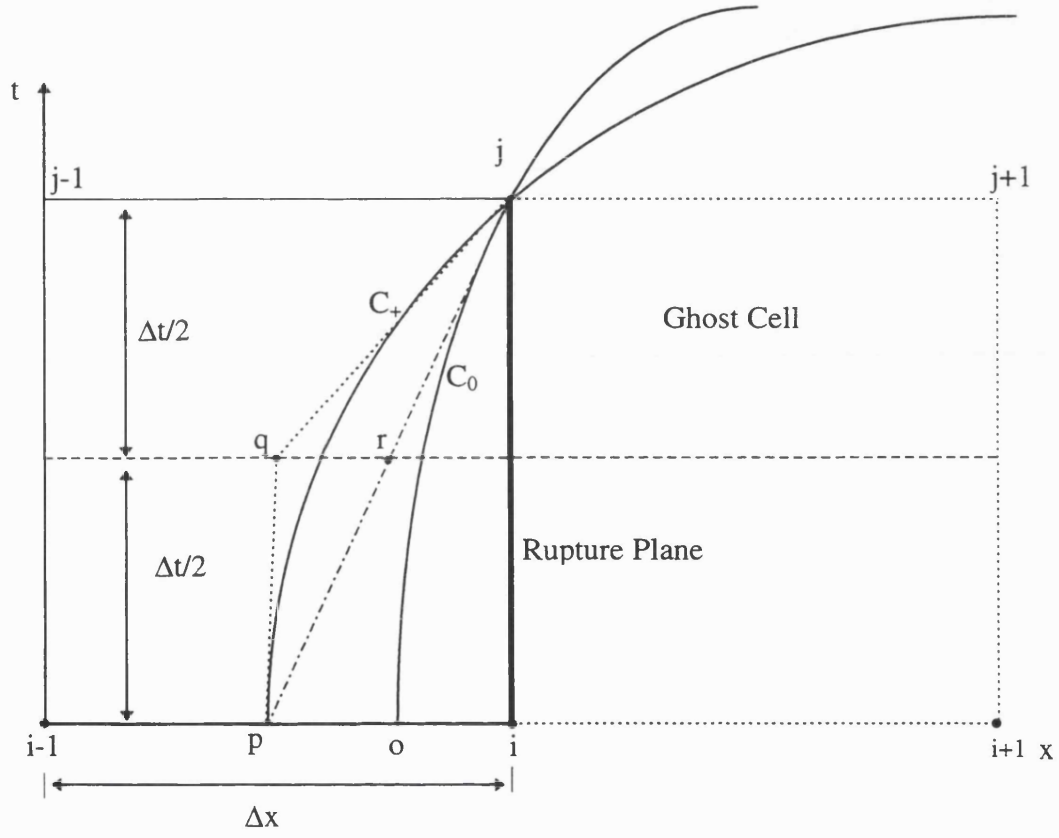

Figure 4.4.6 Boundary cell layout for second order scheme

4.5 THE INITIAL CONDITION

4.5.1 Steady State

Most often, the initial condition for a transient problem is steady state. Compatibility between the specified initial condition and the unsteady equations throughout the system is highly desirable. Inasmuch as steady state is a special case of unsteady flow it should be possible to utilise an unsteady simulation code to determine a balanced steady-state solution. There are obvious advantages to this procedure since only a single code for the transient analysis would be needed along with the corresponding data set. However, in most systems, convergence to steady state from arbitrary initial conditions is very slow, requiring many iterations (Fox, 1975; Vardy and Chen, 1983; Shimada, 1988).

Following FBR of long gas transmission lines, unsteady state flow stops only when the pipe is fully evacuated. The massive bulk of contained inventory coupled with the choking condition at the rupture plane considerably lengthens the convergence time to steady state.

The flow in the pipeline prior to rupture can be taken to be isothermal steady state. This can be justified by the fact that flow is slow (Flatt, 1986) and since the pipeline is very long, there is ample opportunity for heat transfer to maintain isothermal conditions. Typically flow velocities in pipelines vary from 10 to 25 m/s and therefore for pipeline lengths of greater than 100 kilometres, a residence time of hours per particle is to be expected.

The equations for steady state isothermal flow of a compressible fluid can be derived from the same set of conservation equations that are used for the unsteady state analysis (see 2.4.16 in sec. 4.2). For steady state, all the partial derivatives with respect to time, t, are set to zero, thus resulting in ordinary differential equations with respect to x. The resulting steady state equations are:

Continuity equation:

$$\rho\frac{du}{dx}+u\frac{d\rho}{dx}=0 \qquad (4.5.1)$$

Momentum equation:

$$\frac{dP}{dx}+\rho u\frac{du}{dx}-\beta=0 \qquad (4.5.2)$$

Energy equation:

$$u\frac{dP}{dx}-a^2u\frac{d\rho}{dx}-\psi=0 \qquad (4.5.3)$$

From the continuity equation, equation 4.5.1, we can write,

$$d\rho=-\rho\frac{du}{u} \qquad (4.5.4)$$

and from the momentum equation, equation 4.5.2, we get,

$$dP=-\rho udu+\beta dx \qquad (4.5.5)$$

Differentiating the ideal gas equation of state with respect to ρ, we get,

$$d\rho=\frac{dP}{RT} \qquad (4.5.6)$$

Equating equations 4.5.4 to 4.5.6, the following equation is obtained,

$$\frac{dP}{RT}=-\rho\frac{du}{u} \qquad (4.5.7)$$

$$du=-\frac{u}{\rho RT}dP$$

Substituting for du from equation 4.5.7 into equation 4.5.5 yields,

$$dP = \frac{u^2}{RT} dP + \beta dx$$

$$dP = \frac{\beta dx}{\left[1 - \frac{u^2}{RT}\right]} \tag{4.5.8}$$

Therefore, the solution procedure using finite difference equations based on fluid properties at the previous grid point are as follows,

First calculate the pressure drop across the space step, Δx,

$$\Delta P = \frac{\beta}{\left[1 - \frac{u^2}{RT}\right]} \Delta x$$

$$P_i = P_{i-1} + \frac{\beta_{i-1}}{\left[1 - \frac{u^2}{RT}\right]_{i-1}} \Delta x \tag{4.5.9}$$

where i denotes the grid point where the fluid conditions are being calculated and the subscript i-1 denotes fluid conditions at the previous grid point.

Next calculate the change in velocity as a result of this pressure drop,

$$\Delta u = -\frac{u}{\rho RT} \Delta P$$

$$u_i = u_{i-1}\left(1 - \frac{\Delta P}{(\rho RT)_{i-1}}\right) \tag{4.5.10}$$

Finally the change in density can be calculated once the change in velocity is known,

$$\Delta\rho = -\frac{\rho}{u}\Delta u$$

$$\rho_i = \rho_{i-1}\left(1 - \frac{\Delta u}{u_{i-1}}\right) \tag{4.5.11}$$

The temperature T remains constant throughout and therefore the energy equation is redundant.

The speed of sound for an ideal gas is given by,

$$a_i = \sqrt{(\gamma RT)} \tag{4.5.12}$$

where γ is the ratio of specific heats and for a given ideal gas is always constant regardless of both temperature and pressure.

4.5.2 Pipeline Rupture at t = 0

In terms of a graphical representation of the system, the pipeline runs along the x-axis from x=0 to x=L, however the flow at normal steady-state conditions travels from right to left and hence the velocity, u, has a negative magnitude. Once rupture occurs (at t=0), choking over the entire cross-section of the pipe at the rupture point (assumed to be at x=L) takes place. This sudden disturbance to the steady-state system results in the creation of a pressure or expansion wave which quickly travels from x=L to the left of the pipe. In so doing it effectively carries information of the conditions that existed at x=L along the pipeline.

To the right of the expansion wave there will be a large pressure drop from the pressure peak at the expansion wave front to the open end rupture point where the pressure is continuously decreasing with time, albeit slowly, to atmospheric pressure. To the left of the expansion wave, flow will continue unperturbed by the changes that are occurring on the other side of the expansion wave. In fact, the flow in this region can be approximated by the isothermal steady state equation.

Taking frictional effects into consideration, the pressure gradient $(dP/dx)_t$ is positive in the isothermal flow region that is as yet undisturbed by the expansion wave.

Therefore in the initial time domain, there will be a pressure peak somewhere in between x=0 and x=L. It moves slowly from right to left until it reaches $x=0^5$. Its location is always close to the point of flow reversal where u=0.

The conservation equations are solved numerically because they are highly non-linear, and finding an analytical solution is made difficult by the existence of a singularity at the ruptured end (Flatt, 1986). At the time of rupture, choked flow conditions occur at x=L and therefore the Mach Number, Ma=1. The conservation equations can be simplified and then solved to give a linear system of equations for pressure, temperature, Mach number, and velocity in terms of x. These partial derivatives all tend to infinity as Ma tends to 1.

This singularity problem is overcome by assuming that at t=0:

1. there is isentropic expansion flow over the first Δx mesh
2. the location of the pressure peak at the expansion wave front occurs at a distance of one Δx from the rupture point. The flow conditions at this point will be that which existed at x=L at t<0
3. all points in the flow field on subsequent grid points to the left of the pressure peak can be approximated by steady state isothermal flow conditions.

The assumption of isentropic expansion flow over the first Δx leads to the use of the 'Riemann variables' (Hirsch, 1995) in calculating the conditions at x=L.

For the special case of isentropic flow, the flow is adiabatic and reversible. Therefore,

$$q_h = 0$$

$$\beta = 0 \qquad (4.5.13)$$

$$\psi = 0$$

The compatibility equations for unsteady isentropic flow are therefore,

pathline compatibility,

$$dP - a^2 d\rho = 0 \tag{4.5.14}$$

positive Mach line compatibility,

$$dP + \rho a du = 0 \tag{4.5.15}$$

negative Mach line compatibility,

$$dP - \rho a du = 0 \tag{4.5.16}$$

Introducing the Riemann variable, w, so that,

$$\frac{dw}{dt} = \frac{\partial w}{\partial t} + \frac{dx}{dt}\frac{\partial w}{\partial x} = \frac{\partial w}{\partial t} + \lambda \frac{\partial w}{\partial x} \tag{4.5.17}$$

where λ is the characteristic slope

With reference to equations 4.5.14 to 4.5.16 the Riemann variables are,

$$\delta w_1 = \delta\rho - \frac{1}{a^2}\delta P \qquad \text{along } \frac{dx}{dt} = u$$

$$\delta w_2 = \delta u + \frac{1}{\rho a}\delta P = \delta u + a\frac{\delta\rho}{\rho} \qquad \text{along } \frac{dx}{dt} = u + a \tag{4.5.18}$$

$$\delta w_3 = \delta u - \frac{1}{\rho a}\delta P = \delta u - a\frac{\delta\rho}{\rho} \qquad \text{along } \frac{dx}{dt} = u - a$$

Expressing equations 4.5.18 in the form of equation 4.5.17, and using equations 4.5.14 to 4.5.16 to perform the partial differentials with respect to x and t, the following result is obtained,

$$\frac{dw_1}{dt} = \frac{dw_2}{dt} = \frac{dw_3}{dt} = 0 \tag{4.5.19}$$

Equation 4.5.19 shows that the variable, w is a constant for isentropic flow and is termed as a Riemann invariant.

The Riemann invariants, C_+ or C_- can be integrated to give,

$$w_2 = u + \int a(\rho)\frac{d\rho}{\rho}$$

$$w_3 = u - \int a(\rho)\frac{d\rho}{\rho} \qquad (4.5.20)$$

Using the isentropic relations,

$$P = k\rho^{\gamma} \qquad (4.5.21)$$

and

$$a^2 = k\gamma\rho^{\gamma-1} \qquad (4.5.22)$$

where k is a constant.

From equation 4.5.21,

$$\frac{dP}{d\rho} = k\gamma\rho^{\gamma-1} = a^2$$

$$\therefore a = (k\gamma)^{\frac{1}{2}}\rho^{\frac{\gamma-1}{2}} \qquad (4.5.23)$$

From equation 4.5.22,

$$\frac{da}{d\rho} = (k\gamma)^{\frac{1}{2}}\frac{\gamma-1}{2}\rho^{\frac{\gamma-3}{2}}$$

$$\frac{d\rho}{\rho} = \frac{da}{(k\gamma)^{\frac{1}{2}}\frac{\gamma-1}{2}\rho^{\frac{\gamma-1}{2}}} \qquad (4.5.24)$$

Substituting for $d\rho/\rho$ from equation 4.5.24, and for 'a' from equation 4.5.23 into equation 4.5.20, the Riemann invariant along λ_+ becomes,

$$w_2 = u + \frac{2}{\gamma - 1}a \tag{4.5.25}$$

and along λ_-,

$$w_2 = u - \frac{2}{\gamma - 1}a \tag{4.5.26}$$

Therefore for any point in an isentropic flow field, w_2 and w_3 which represent the propagation of pressure waves along their respective characteristics are always constant. This principle can be used to obtain the conditions at the rupture plane.

Denoting conditions at the rupture plane by the subscript, rp and conditions at the next grid point by the subscript in, and using the Riemann invariant along λ_+,

$$u_{rp} + \frac{2}{\gamma - 1}a_{rp} = u_{in} + \frac{2}{\gamma - 1}a_{in} \tag{4.5.27}$$

u_{in} and a_{in} are known quantities as they are the steady state conditions that existed at the rupture plane prior to FBR.

For FBR of high pressure pipelines, we assume that at the rupture plane, Ma = 1, and so both velocity and speed of sound at that point at t = 0 are given by,

$$u_{rp} = a_{rp} = \frac{\gamma - 1}{\gamma + 1}\left(u_{in} + \frac{2}{\gamma - 1}a_{in}\right) \tag{4.5.28}$$

As a check for a_{rp}, it can also be obtained from equation 4.5.27 once u_{rp} is known.

$$a_{rp} = a_{in} + \frac{\gamma - 1}{2}\left(u_{in} - u_{rp}\right) \tag{4.5.29}$$

Another relation for an ideal gas in an isentropic environment is,

$$TP^{-\frac{(\gamma-1)}{\gamma}} = k \tag{4.5.30}$$

where T is the temperature.

Substituting for T from equation 4.5.12 into equation 4.5.30, and equating conditions at the rupture plane to those at the next grid point (denoted by subscript in),

$$\frac{a_{rp}^2}{\gamma R} P_{rp}^{-\frac{(\gamma-1)}{\gamma}} = \frac{a_{in}^2}{\gamma R} P_{in}^{-\frac{(\gamma-1)}{\gamma}} \tag{4.5.31}$$

Re-arranging the above, an expression for P_{rp} is obtained,

$$P_{rp} = \left(\frac{a_{in}}{a_{rp}}\right)^{\frac{2\gamma}{\gamma-1}} P_{in} \tag{4.5.32}$$

The temperature at the rupture plane at t=0 is obtained from equation 4.5.12 and the density is obtained from the ideal gas equation of state.

Hence all the conditions at the various grid points on the initial time line, t=0 are accounted for. These conditions form the basis for the initiation of the calculation procedure outlined in section 4.4. A summary of the procedure is given below.

4.5.4 Summary of Calculation Procedure

1. Divide the pipeline length into grid points of equal length, Δx.
2. Calculate the maximum Δt permissible for numerical stability using the CFL criterion (equation 4.6.1). In this study a value of $0.9\Delta t$ is used in order to avoid loss of accuracy due to the resulting relatively large values of Δx (see section 4.6).
3. The conditions at the ruptured end at t=0 are calculated using the Riemann variables, thus making the assumption of isentropic flow over the first Δx. The conditions at the other grid points at t=0 are calculated using the isothermal flow equation.
4. Once the solutions are obtained at $t = 0$, the characteristic and compatibility equations are applied at $t > 0$ in equal intervals of $0.9\Delta t$. The pipeline will be completely evacuated when there is equal pressure along the whole length of the pipeline thus giving $u = 0$.

4.6 OPTIMISATION AND VALIDATION OF THE FBR IDEAL GAS MODEL

In this section, the models proposed in sections 4.4.1 and 4.4.2 are optimised in terms of an evaluation of performance with respect to CPU times and accuracy. This is followed by comparisons of the optimised model results with field data, and those from the MWT and HYBRID-MG models developed by Chen et. al. (1992). The importance of taking into account heat transfer effects on FBR simulation are also discussed.

Field data are those obtained on the night of the Piper-Alpha tragedy when FBR of a long gas line between the Piper Alpha and MCP-01 platforms occurred due to excessive fire loading. A FORTRAN based computer programme, called PIPERUP is developed for this purpose.

The prevailing conditions prior to FBR are given below:

Pipeline length, L	54 km
Inner diameter, D	0.4191 m
Initial pressure, P_{in}	117 bar
Initial temperature, T_{in}	283 K
Average molecular weight, MW_{av}	0.0211 kg/mol
Heat capacity ratio, k	1.26
Heat transfer coefficient, U_h	5.0 W/m^2K
Fanning friction factor, f	0.00324
Ambient temperature, T_∞	300 K

Table 4.1: Piper Alpha Input Data

The fluid within the pipeline comprises methane (ca. 73.6 mole%) and ethane (ca. 13.4%). Their behaviour is assumed to be approximated by an ideal gas during the depressurisation process.

4.6.1 The modelling of the fast transient near the ruptured end: Nested grid system

The Courant-Friedrich-Lewy stability criterion has to be satisfied for the required time step, Δt. This is given by

$$\Delta t \leq \frac{\Delta x}{\left(|u + a|_{max}\right)} \qquad (4.6.1)$$

The space step, Δx is dependent on the number of grid points used to discretise the flow field. This is defined as

$$\Delta x = \frac{L}{\text{No. of grid points}} \qquad (4.6.2)$$

where L is the pipe length.

Clearly, greater accuracy is achieved when Δx is small so that interpolation errors are minimised. This however means a greater number of calculations per time step, and in the case of simulation of FBR of a long pipeline, the above will result in a significant increase in CPU time.

Figure 4.6.1 shows the effect of Δx on the predicted variation of discharge rate with time using PIPERUP, within the range of Δt stipulated by equation 4.6.1. Curves A - F show the results obtained for Dx's of 200m, 100m, 54m, 27m, 2.7m, and 1m respectively.

The data have been generated using a first order MOC for the case of the Piper Alpha pipeline FBR. The discretisation is based on a Simple Grid Scheme (SGS) where uniform spacing is used throughout.

As the grid is refined, the solution tends to convergence thus confirming that the MOC is both consistent and stable (see chapter 3 for definitions).

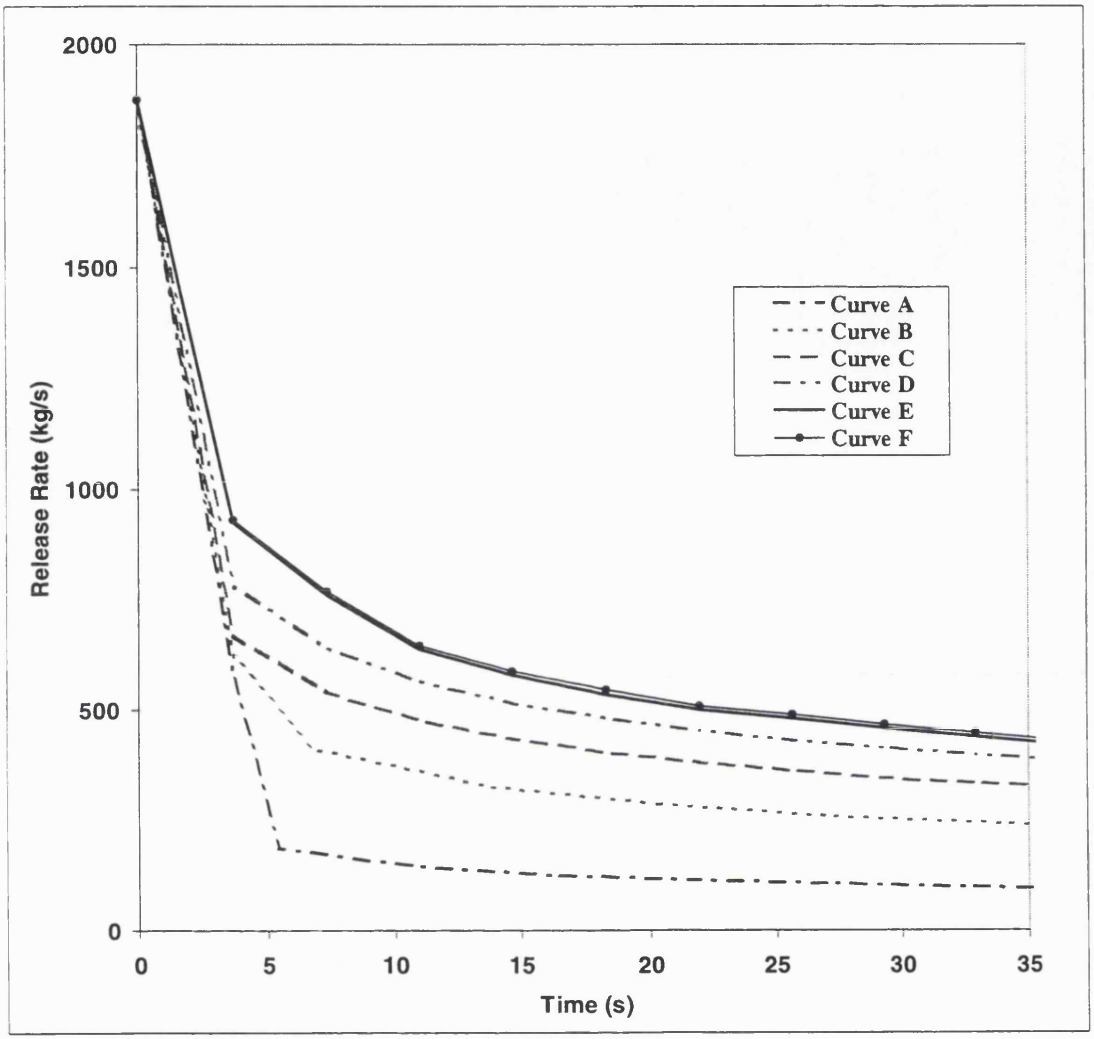

Figure 4.6.1: Variation of release rate with decreasing space-step (PIPERUP)

Curve A: $\Delta x = 200m$
Curve B: $\Delta x = 100m$
Curve C: $\Delta x = 54m$
Curve D: $\Delta x = 27m$
Curve E: $\Delta x = 2.7m$
Curve F: $\Delta x = 1m$

The results obtained using a space step of 1m (Δt = 1.4ms) are taken to be the converged solution of the test problem. For this, space step, the CPU time simulating the first 36.9 seconds of discharge is 333.45 seconds on a 100MHz Pentium computer. For a space step of 2.7m, the corresponding CPU time (Δt = 3.7ms), is only 118.33 seconds: the decrease in time is almost inversely proportional to the increase in space step. However, as can be seen from figure 4.6.1, the differences in predicted release rates are negligible for these two cases.

For a space-step greater than 225 metres, PIPERUP is unable to resolve the 2×2 system of quadratic equations 4.4.13 and 4.4.14 for initial point data at, p in the rupture cell, obtained from interpolation over such a large space step.

The corresponding CPU time for the complete evacuation (20,000s) of the pipeline using the SG method for a space step of 2.7 m is estimated to be 17.5 hrs on the same computer as above.

In order to reduce the CPU time, a nested grid system used by Picard and Bishnoi (1989) and later by Chen et. al. (1992) is implemented. This involves modelling the fast transient near the rupture plane with a grid that is smaller than that for the slow transient which will exist through the rest of the pipeline. Clearly the longer the pipeline, the slower is the transient at the closed end, and therefore a large Δx is sufficient to accurately model the flow conditions in this region. In addition, a large Δx is particularly attractive with regards to lowering CPU times.

In this study, the nested grid scheme is implemented in the following manner:

A chosen number of normal time-space meshes at the pipe exit is divided into 5×5 cells where Δx_2 is the length of each step.

A number of columns of meshes in the first normal time-space mesh at the pipe exit is further divided into 5×5 cells such that the space-step is Δx_1 (see figure 4.6.2).

Figure 4.6.2 shows a schematic representation.

Since the smaller cells are geometrically similar, and contained within the large normal mesh (space-step = Δx_3), a consistent Courant number is maintained all the way through the discharge and numerical instability is avoided. Therefore accuracy

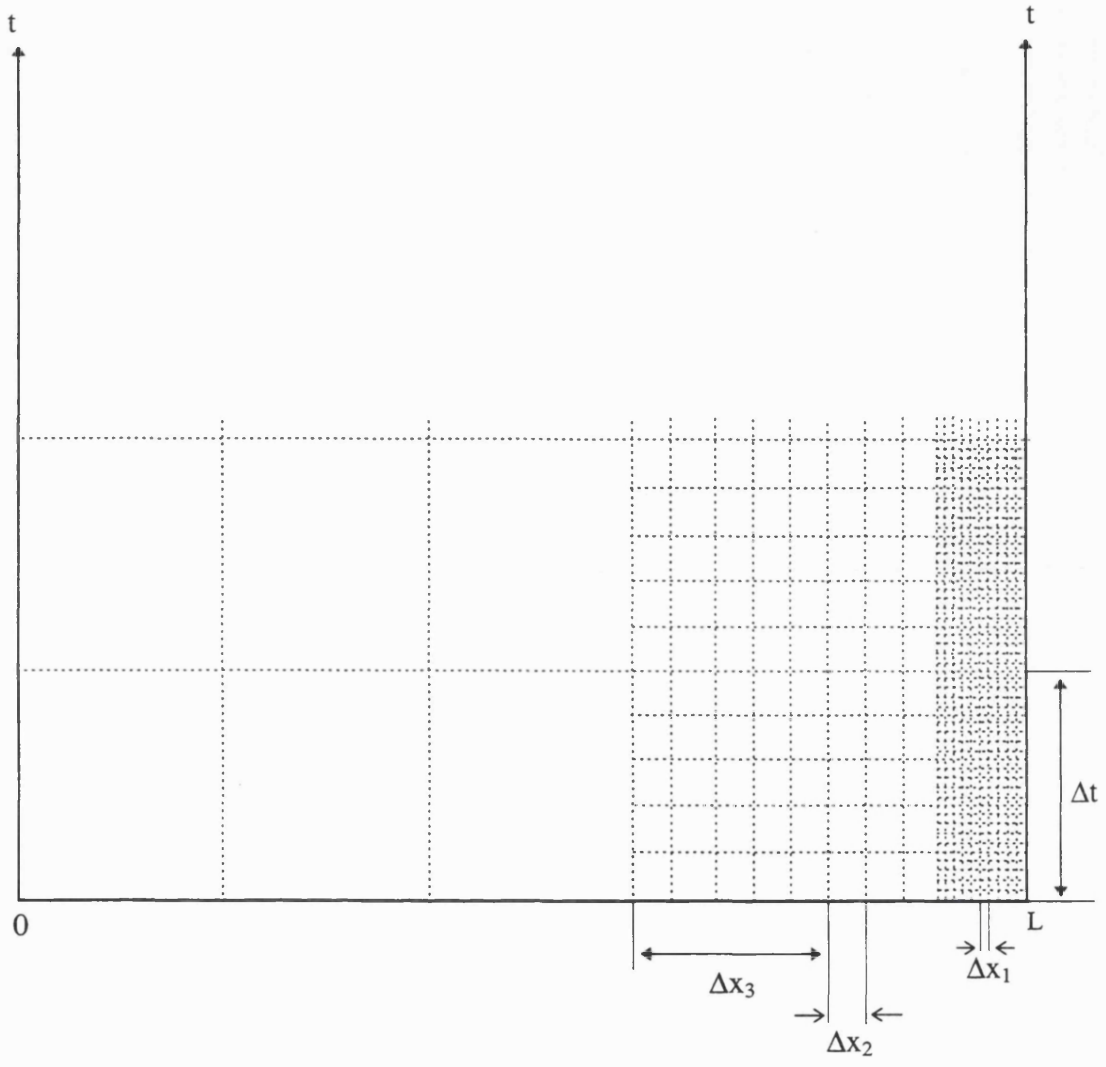

Figure 4.6.2: Multiple Grid System Arrangement

in the fast transient region near the open end is assured, whilst speeding up the rest of the calculations along the coarser grid where Δx_3 is large.

For the purposes of terminology, a single refinement to the simple grid system (just one 5×5 division over the two Δx's next to the rupture plane) will be termed 'Nested Grid Scheme (NGS)', whereas the double refinement (two 5×5 divisions) will be termed as 'Compound Nested Grid Scheme (CNGS)'.

At the junctions of different size meshes, the flow variables at the finer grids are linearly interpolated in time from the values on the coarse grids.

In the case of highly transient two-phase flows, however, a different technique based on direct solution of the compatibility equations is used (see chapter 5). This is primarily because of the non-linear variation of fluid properties along the pipeline.

Figure 4.6.3 shows the release rate data obtained using the various schemes described above. Curve A shows the data using the SGS. Curves B and C on the other hand show the corresponding data using NGS and CNGS respectively. The appropriate choice of Δx for each scheme and the corresponding CPU times using a Hewlett Packard 486 PC are given in the figure legend.

From the data, it is clear that a nested grid scheme for fine resolution near the ruptured end is essential if an underestimation of the release rate, one of the most important factors in risk assessment, is to be avoided.

The difference in results, albeit small, between NGS and CNGS is due to the higher resolution of the fast transient near the pipe exit in the latter case.

In fact, CNGS has a resolution five times greater than NGS at the ruptured end. The SGS model takes the longest because its grid is coarsest near the rupture plane and therefore convergence of the iteration procedure for the solution points takes longer. This is despite the fact that the total number of elements used in this scheme is the least compared to the other schemes used here.

Likewise, convergence in CNGS will be faster than in NGS, but the CPU time is longer because of the fact that more calculations are performed in CNGS than can be

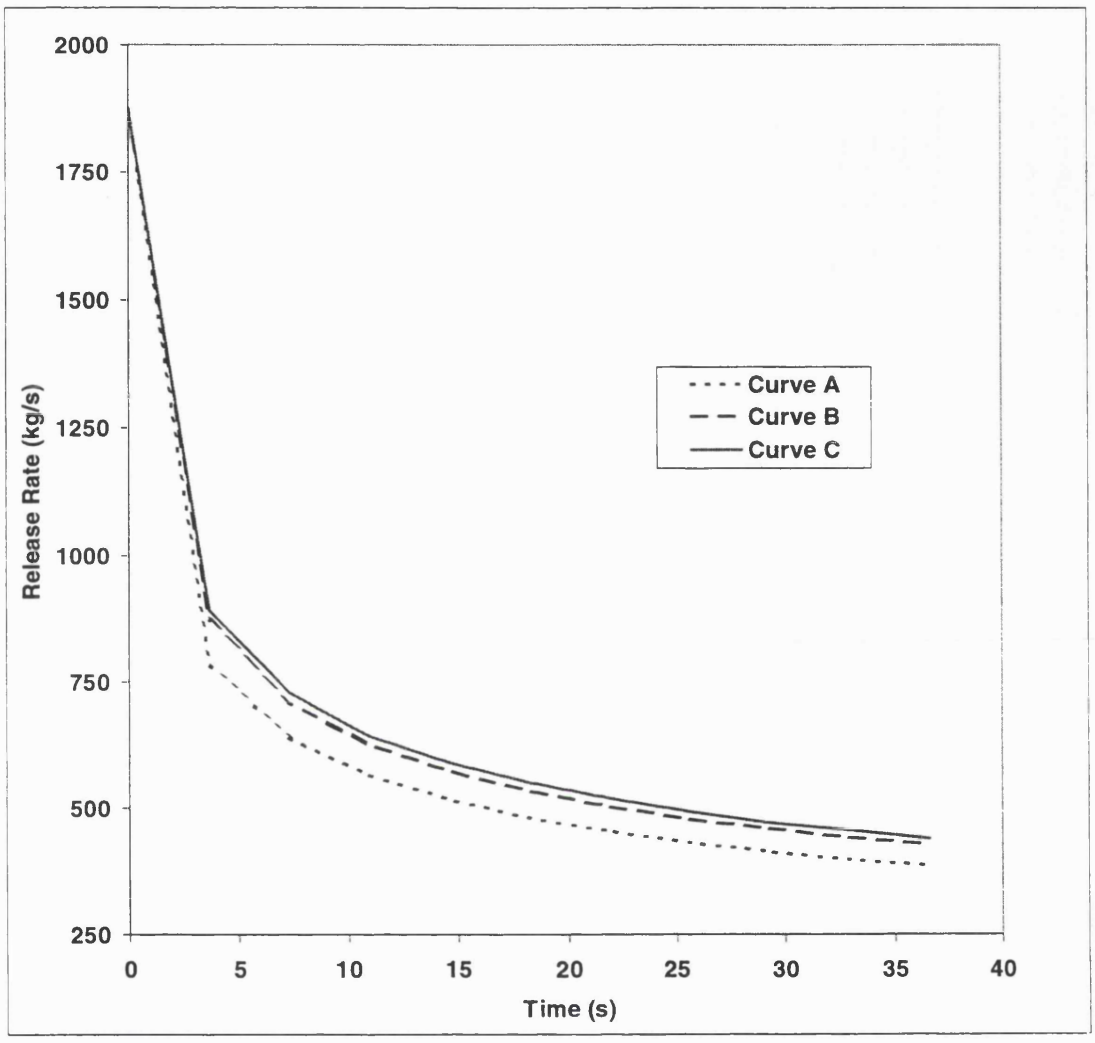

Figure 4.6.3: Comparison of predicted release rate for the various schemes

Curve A: SGS; Δx_3 =27m. Elapsed CPU time = 994s

Curve B: NGS; Δx_3 =27m, Δx_2 =5.4m. Elapsed CPU time = 541s

Curve C: CNGS; Δx_3 =27m, Δx_2 = 5.4m, with Δx_1 = 1.08m. Elapsed CPU time = 755s

compensated for by faster convergence. CNGS has 5 more calculations for each space step and 5 more for each time step than NGS.

To obtain the same resolution as CNGS, SGS would need a space step of 1.08m and the CPU time is estimated to be ca. 25,000 s. Therefore the CNGS model gives the same resolution but is about 33 times faster. This becomes particularly relevant when simulating complete discharge following FBR of long pipelines.

There is little difference in the results between NGS and CNGS presented here because they have been applied to a permanent gas. However, care should be taken when using the same argument to depressurisation of two-phase mixtures or condensible gases where fluid properties are expected to vary markedly along the pipeline .

Henceforth, the CNGS model is chosen to perform validation tests because it gives the best accuracy in a reasonably fast time. Chen et. al. (1992) have published data obtained by two models called Multiple Wave Tracing (MWT) and Hybrid MULTI-GRID (Hybrid-MG). Both employ the compound nested grid scheme as used in this study.

The Hybrid-MG model uses the classical method of specified time intervals whereas the MWT model is a characteristic grid type method (see Chapter 3) where the waves at t=0 are traced forward in time.

Figure 4.6.4 shows a comparison of the predicted release rates over the full period of depressurisation of the Piper to MCP-01 pipeline for the three models mentioned above. Curve A shows the results obtained using CNGS whereas curves B and C show the results for Chen's Hybrid-MG and MWT methods respectively.

It is striking to note that the CPU time for the CNGS (curve A) using the modified method of specified time intervals as used in this study on a Hewlett Packard 486 PC is only 2.4 hours. The corresponding CPU times for HYBRID-MG (curve B) and MWT (curve C) as developed by Chen et. al. are 22.1 hours and 2.9 hours respectively on a SUN SPARC workstation.

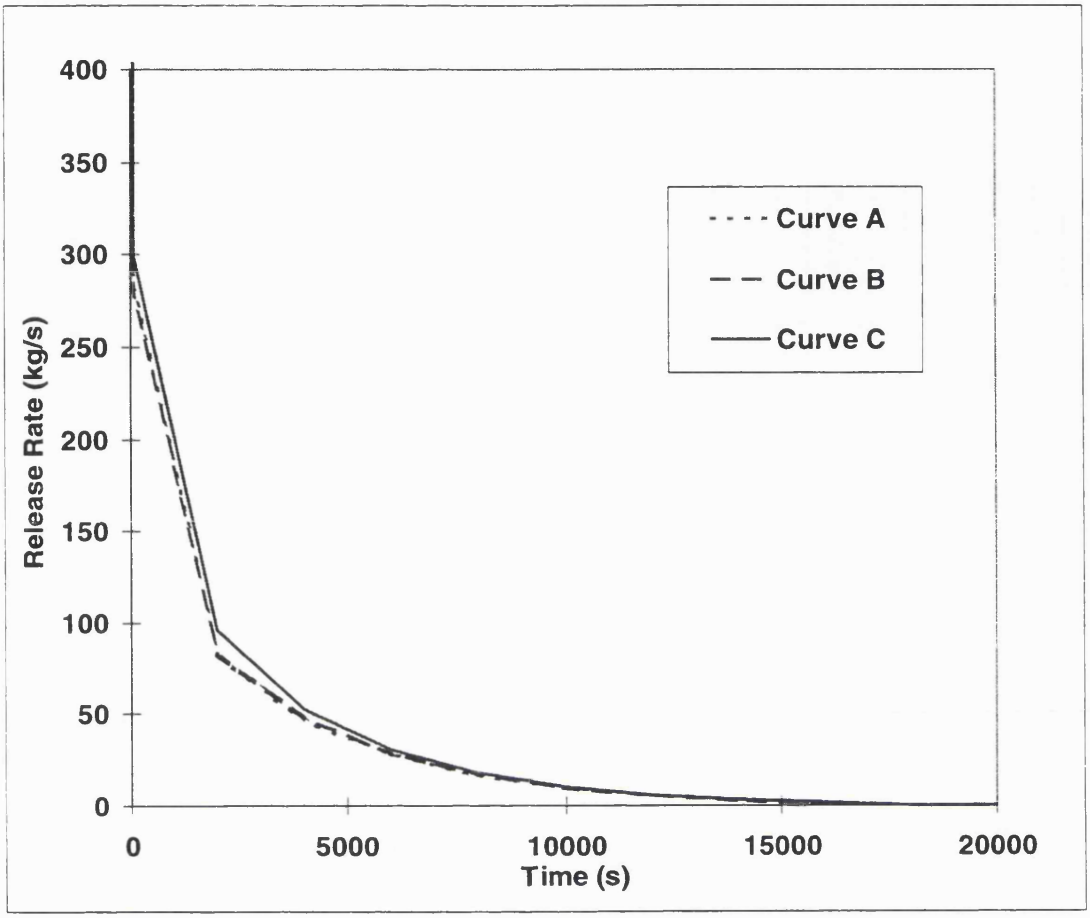

Figure 4.6.4: Comparison of the predicted release rates over the full period of depressurisation of the Piper to MCP-01 pipeline.

Curve A: CNGS; Δx_3 =200m, Δx_2 = 40m, with Δx_1 = 8m; CPU time = 2.4 hrs (Hewlett Packard, 486 PC).

Curve B: Hybrid-MG; Δx_3 =200m, Δx_2 = 40m, with Δx_1 = 8m; CPU time = 22.1 hrs (SUN SPARC workstation).

Curve C: MWT; Δx_3 = 125 m, Δx_2 = 50 m, Δx_1 = 10 m; CPU time = 2.9 hrs (SUN SPARC workstation).

The slight difference in values given in figure 4.6.4 between our modified ST method (Curve A), and Chen et. al.'s MWT (Curve C) can be attributed to the different approaches adopted.

In the former, some smearing of the solution always results because of the need to interpolate to calculate the conditions at the intersection points of Mach lines and path-lines with the initial time line (p,o and n) (see figure 4.4.2). The extent of the smearing diminishes with the magnitude of space-step at and near the rupture point.

For MWT, the only smearing of the exact solution is due to interpolation of the pathline intersection. At very small Δx's near the rupture plane, the results of CNGS for the modified ST method can be expected to approach those from MWT.

Both Hybrid-MG and CNGS for the modified ST method give the same accuracy, but CNGS developed in this study is almost ten times faster. This is due to solving a matrix of interpolation equations simultaneously (see section 4.4.1) which drastically reduces the number of iterations involved.

For the sake of comparison, the CPU time for the same simulation using the CNGS model developed in this study is only 40 minutes on a Pentium PC. (Hewlett Packard 100MhZ Vectra Series 4 Pentium PC).

4.6.2 The effect of curved characteristics

In addition to the errors resulting from linear interpolation of fluid properties, a second source of inaccuracy can be attributed to the approximation of the characteristic curves by straight lines.

Particularly difficult are problems where the nonlinear friction term of the momentum equation has a high fL/D value (f, L and D are the friction factor, the length and the hydraulic diameter of the pipe respectively) and where the Mach number range is high subsonic (Flatt, 1985). For flows where either or both of these phenomena result in curved characteristics, the linear characteristic assumption as made in the first order solution can lead to global errors greater than first order. For

FBR this can also lead to numerical instability for the ruptured end boundary calculation.

Figure 4.6.5 shows predicted release rate data for the first order linear characteristic (Curve A) and the second order curved characteristic (Curve B) models. The corresponding CPU times are given in the figure legend.

As explained earlier, the release rate data is most sensitive to the mode of calculation near the rupture plane, and is therefore chosen here as the parameter by which the effect of incorporating curved characteristics is judged. The methodology for modelling of curved characteristics near the rupture plane was given in section 4.4.2.

The results in figure 4.6.5 show that both first and second order solutions produce very similar results (the curved characteristic solution giving slightly higher estimates for release rate). This is to be expected, since the properties of a permanent gas are expected to vary relatively linearly along the pipeline. The difference in the results is however more significant in the case of two phase mixtures (see section 5.8.1).

The CPU times for both are also very similar with the second order solution taking slightly longer to reach convergence.

4.6.3 Intact End Pressures

During the Piper Alpha FBR, measurements of intact end pressure were recorded (Chen, 1993). These are used for comparison with predictions from the present CNGS using linear characteristics and the MWT models developed by Chen et al., (1992).

Figure 4.6.6 shows such data. Curve A shows the measured data whereas curves B and C show the results of Chen et. al's MWT and our CNGS models respectively.

Both models show excellent agreement with each other but underestimate the intact end pressure. This is due mainly to the assumption of ideal gas. The effect of inclusion of real fluid behaviour including two-phase flow on the above results will be shown later (see chapter 5).

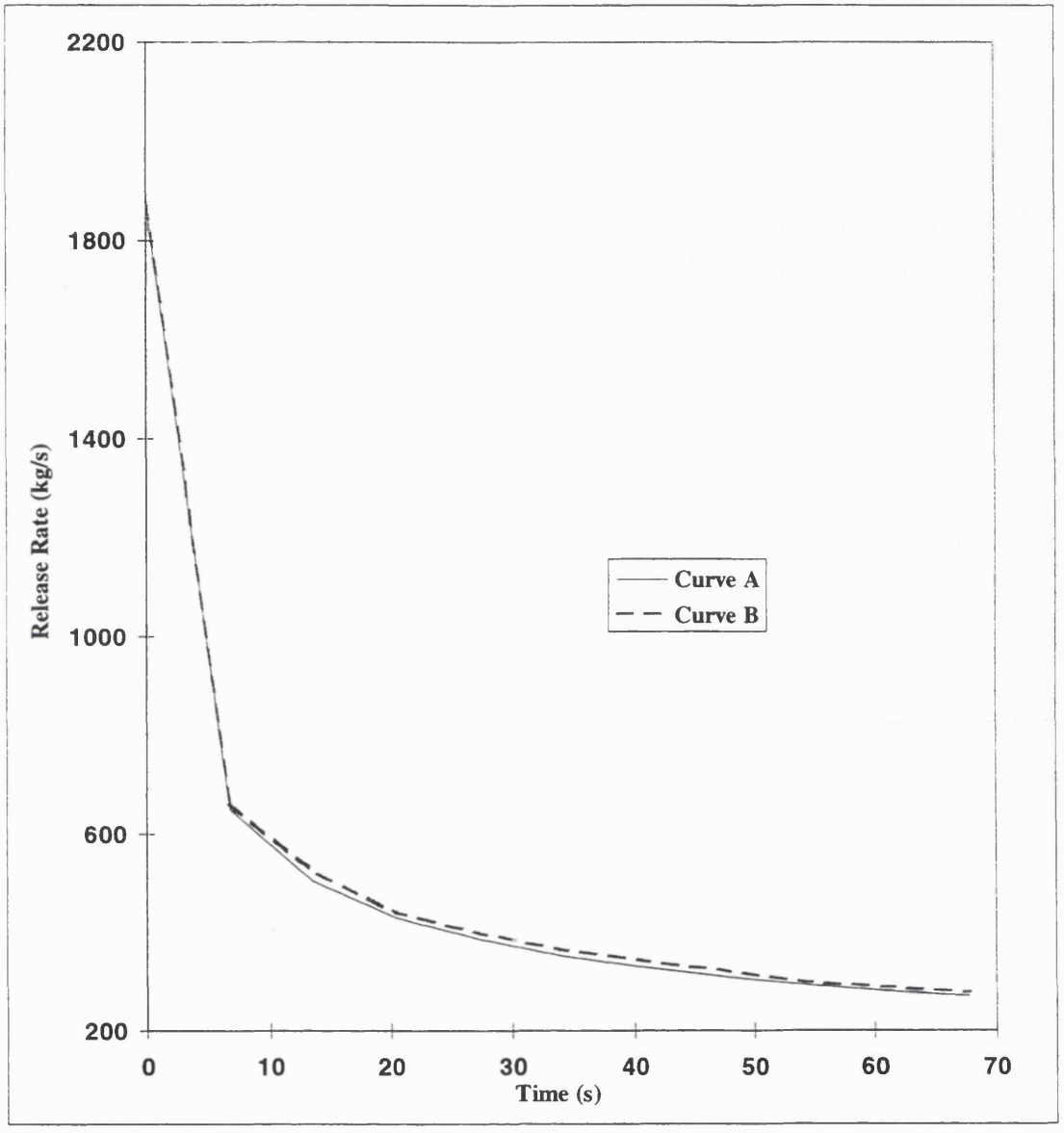

Figure 4.6.5: Predicted release rate versus time profiles for first and second order CNGS.
Curve A; First order solution; CPU time = 9 seconds
Curve B; Second order solution; CPU time = 24 seconds
Δx_3=500m, Δx_2=100m, Δx_1=20m

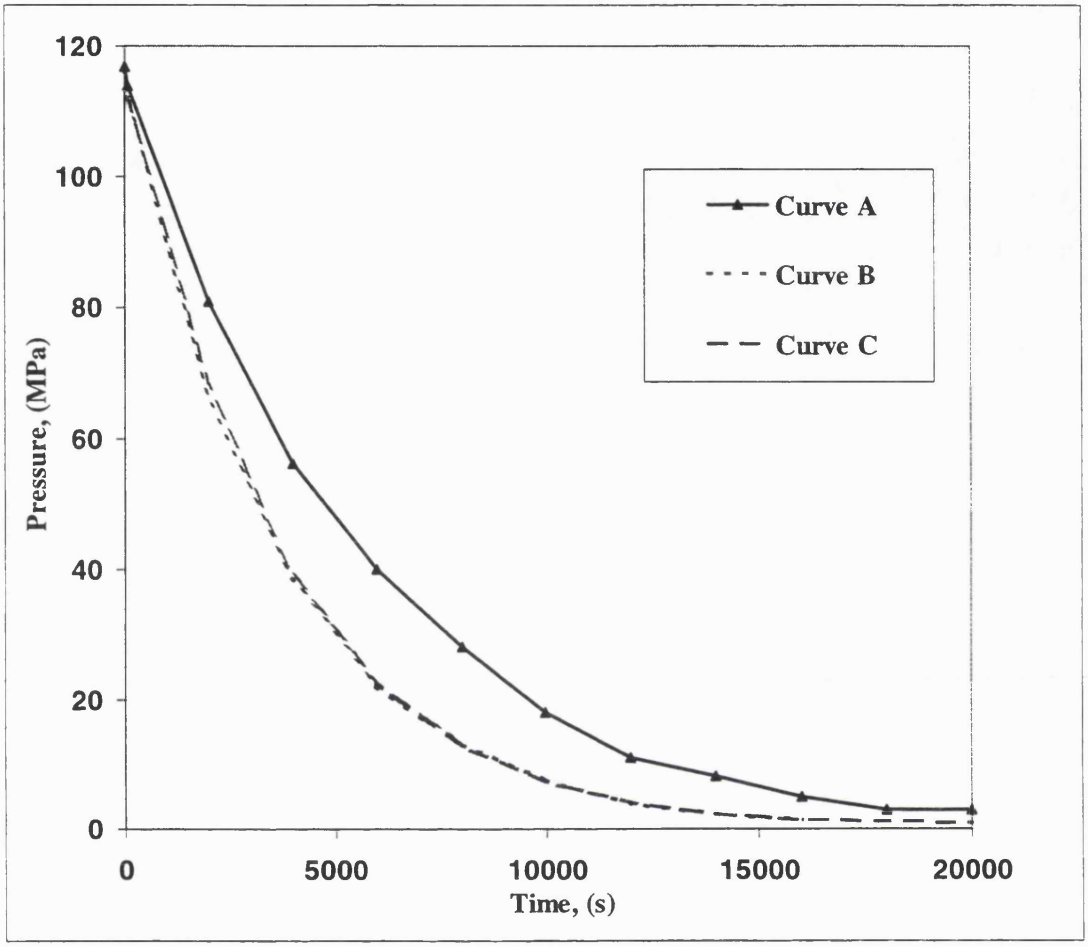

Figure 4.6.6: Comparison of Piper-Alpha intact end pressure predictions

Curve A: Measurement
Curve B: Chen et. al.'s MWT; Δx_3 = 125 m, Δx_2 = 50 m, Δx_1 = 10 m; CPU time = 2.9 hrs (SUN SPARC workstation).
Curve C: CNGS; Δx_3 =200m, Δx_2 = 40m, with Δx_1 = 8m; CPU time = 2.4 hrs (Hewlett Packard, 486 PC).

At the intact end of the pipe, the properties change much less dramatically with time and the global error is linear, i.e. for a constant time-step, a change in space-step will affect a change in intact end pressure in a linear fashion. The results from Chen et. al.'s MWT model are very close to the results from the present CNGS indicating that interpolation errors do not affect accuracy in the intact end region where the transient is much slower than at the ruptured end.

4.6.4 Heat Transfer Effects

As soon as rupture occurs, choking takes place across the entire cross-section of the pipe at the ruptured end. Immediately a pressure peak is set up which travels as an expansion wave towards the intact end. The pressure peak effectively divides the pipeline into two regions, the ruptured end side and the intact end side (Flatt, 1985).

On the ruptured end side, strong expansion due to the massive pressure drop will produce a reversal of flow so that there is an outflow through the ruptured end. In the initial time period, i.e. the first few seconds after rupture, there is such a large change in flow conditions with time so that the flow can be considered to be adiabatic.

Figure 4.6.7 shows plots of the fluid temperature profiles with distance from the ruptured end in the first few seconds after FBR. Curves A - C are the adiabatic temperatures (heat transfer coefficient of zero) at 1.36, 20.4 and 135.9 seconds after rupture respectively. Curves D - F show the corresponding temperatures at the same times by taking heat transfer into account. The heat transfer coefficient is taken to be 5 W/m^2K.

The closeness of the data for adiabatic and non-adiabatic release illustrates the prevalence of adiabatic flow (Flatt, 1985), especially near the broken end. In this region, the gas molecules are accelerated relatively rapidly and at least initially, over a relatively short distance, the adiabatic assumption does not differ much from the non-adiabatic case. However with the progression of time, heat transfer effects will become increasingly important and therefore should be taken into account. The results at 135.9 seconds (c.f. curves C and F) already show that the adiabatic model will underestimate fluid temperatures. The extent of this underestimation increases with time and is expected to affect the release rate data.

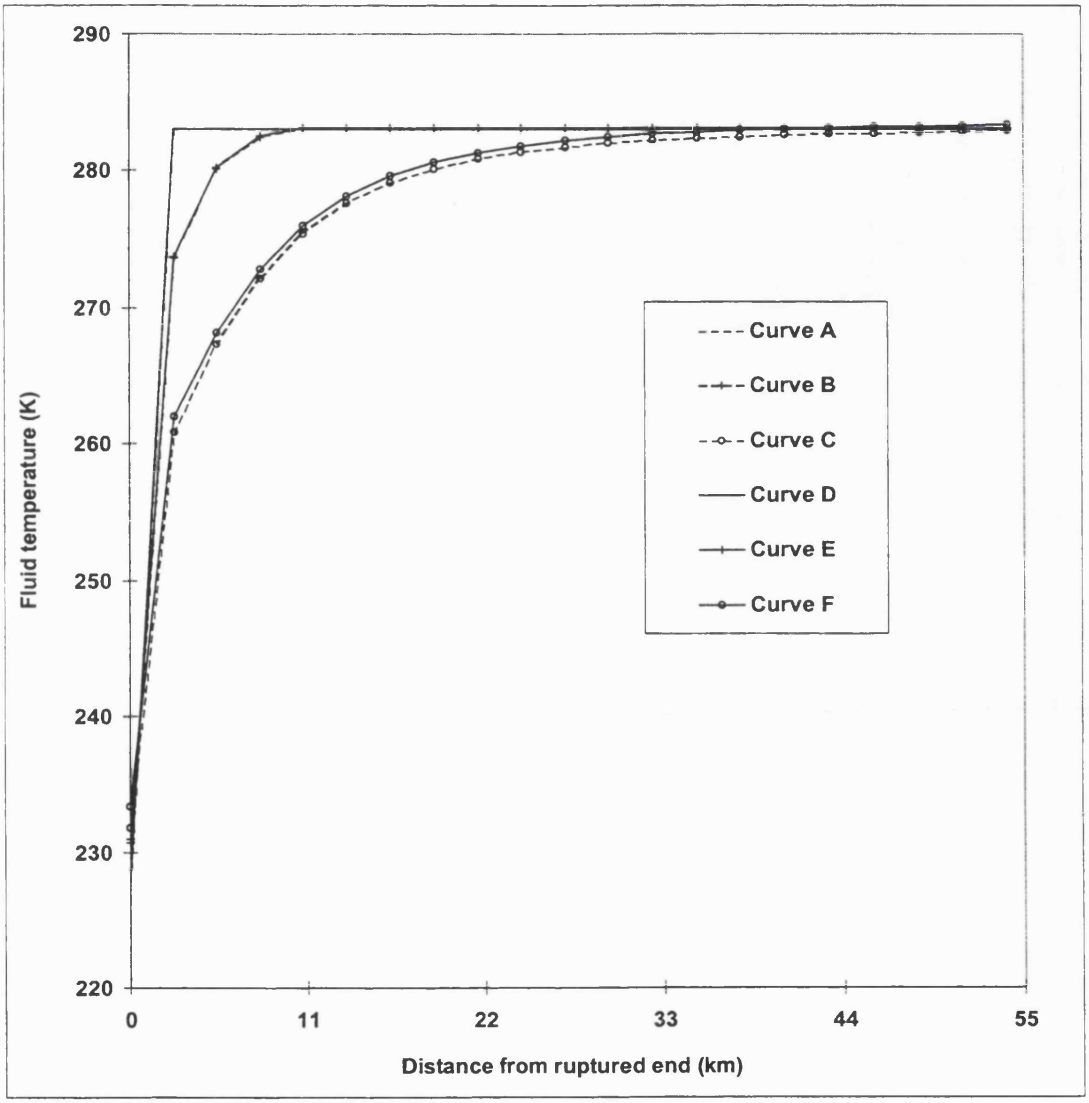

Figure 4.6.7: Comparison of adiabatic and non-adiabatic temperature variations with distance from the ruptured end.

Curve A: Adiabatic model, t = 1.36s
Curve B: Adiabatic model, t = 20.4s
Curve C: Adiabatic model, t = 135.9s
Curve D: Non-adiabatic model, t = 1.36s
Curve E: Non-adiabatic model, t = 20.4s
Curve F: Non-adiabatic model, t = 135.9s

Some workers such as Fannelop and Rhyming (1982), Lang and Fannelop (1987), along with Olorunmaiye and Imide (1993) have assumed isothermal flow in modelling FBR. This simplifies the solution since only two equations have to be solved, thus rendering it faster than any adiabatic or heat transfer models. However such assumptions have been shown to underestimate mass flow rate at the ruptured end by as much as 20% (Olorunmaiye and Imide, 1993). Also an isothermal assumption will not permit accounting for the effect of pipe lagging and changes in external temperature, for example due to fire, on the rate of heat transfer and hence the release rate. Lagging around a pipe has the effect of decreasing the heat transfer coefficient and therefore the fluid temperatures can be expected to be lower in lagged pipes.

Finally, figure 4.6.8 shows the effect of thermal radiation such as that due to a fire on the variation of fluid temperature along the pipeline in the first $\approx$ 140 s following FBR. In this case, the ambient temperature is taken as 1500 K. Curves A - C show the fluid temperature profiles in the case of an external fire at 1.36, 20.4 and 135.9 s following FBR.

The corresponding data at the same times subsequent to FBR, in a no fire situation (ambient temperature = 294 K) are also given (Curves D - F). It is interesting to note that even at such high flowrates as encountered during FBR, a relatively significant rise in the temperature of the fluid may be observed due to fire. This is the case even during the early stages of the discharge process.

As FBR is usually accompanied by a fire, it is therefore important to be aware of its potential effect on release rate data. In the Piper Alpha case examined here, fire is ignored as it is assumed that the pipeline was mainly submerged under water during FBR.

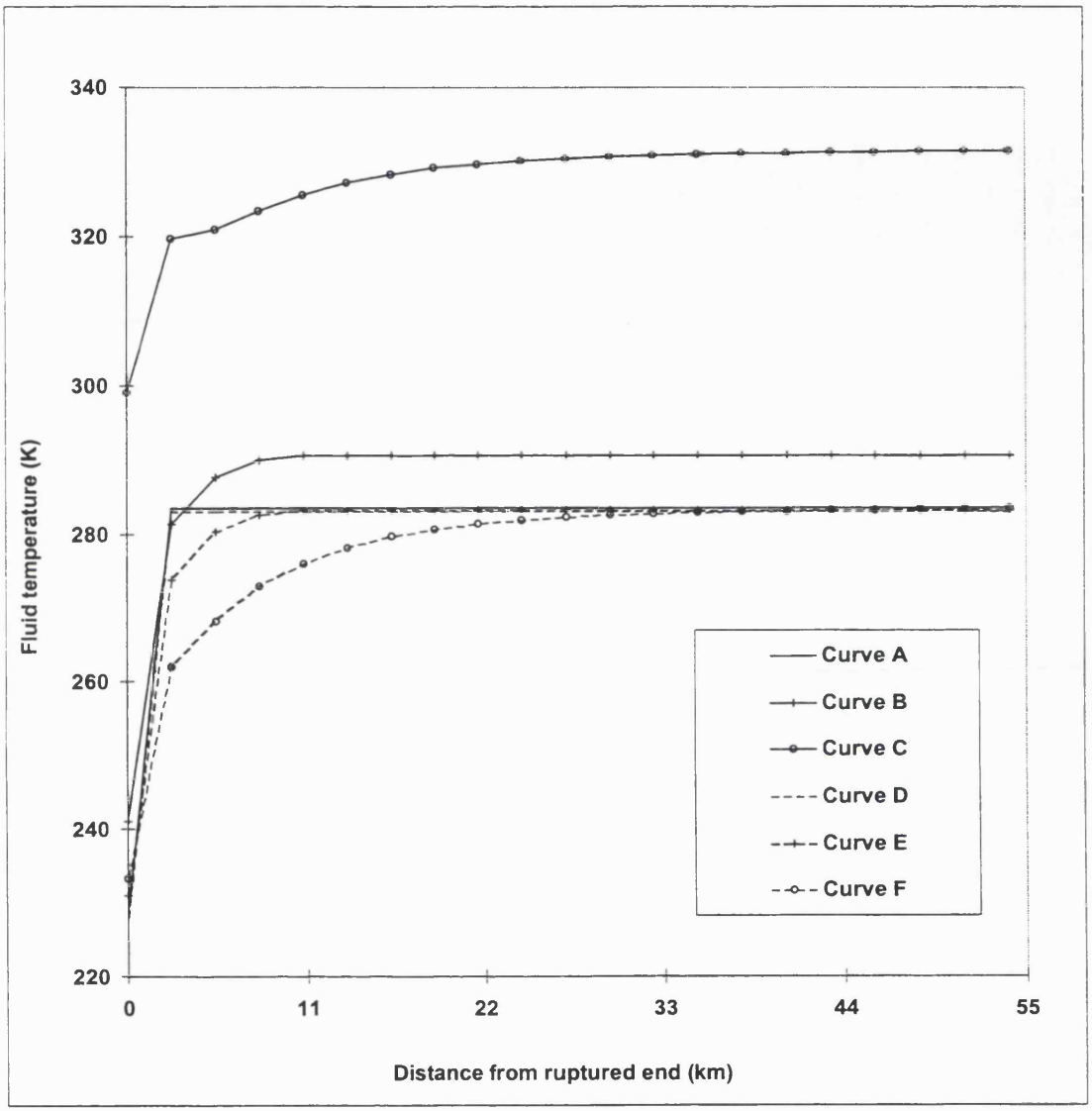

Figure 4.6.8: Effect of external conditions on fluid temperature variation within the pipeline as a function of distance from the rupture plane.

Curve A: External fire, t = 1.36s
Curve B: External fire, t = 20.4s
Curve C: External fire, t = 135.9s
Curve D: No fire, t = 1.36s
Curve E: No fire, t = 20.4s
Curve F: No fire, t = 135.9s

4.7 VALVE CLOSURE MODELLING

The characteristic equations as given by equation 4.4.2 in section 4.4.1 stipulate the way in which information is propagated through a flow field. As such, they play a fundamental role in dictating the ESDV response time. To illustrate this, it is important to appreciate the nature of the process taking place following FBR.

FBR results in a centred expansion wave that propagates along the pipeline away from the rupture plane with the speed of sound. The origin of a centred expansion wave is a singular point where infinite values for flow properties exist at any given time and distance (Zucrow & Hoffman, 1976). The velocity at the front of the wave which is a C_+ characteristic is, a. This wave imparts a drop in pressure which in turn results in a series of expansion waves which propagate into the disturbed fluid with an increasing negative velocity, -u and decreasing speed of sound, a. These waves result in the acceleration of the fluid particles (which have a C_0 characteristic with velocity, u) in the opposite direction and hence result in outflow. Accordingly, the speed of propagation , dx/dt = u + a of each consecutive expansion wave is smaller than that of the preceding wave and hence the waves diverge.

Figure 4.7.1 is a schematic representation of the above phenomenon. The zone near the rupture plane represent domains of rapid changes in flow properties such as pressure and discharge velocity. Indeed this type of behaviour is synonymous with FBR where massive amounts of inventory are released during the first few seconds following rupture. This trend is immediately superseded by a much lower and gradually decreasing discharge rate.

In the case of a check valve, its activation time, t_a is predominantly governed by the time it takes for the first centred expansion wave (C_{+t0} characteristic) to travel from the rupture plane to the location of the valve. At this instance, the velocity, u_r of the gas in the reverse direction is zero and hence the valve will not be exposed to a pressure surge provided it closes instantaneously. The problem arises for larger values of t_c when the flow velocity u_r rapidly increases. The resulting pressure surge which may be significant is estimated from Joukowski's equation (Wylie and Streeter, 1978) which is given by:

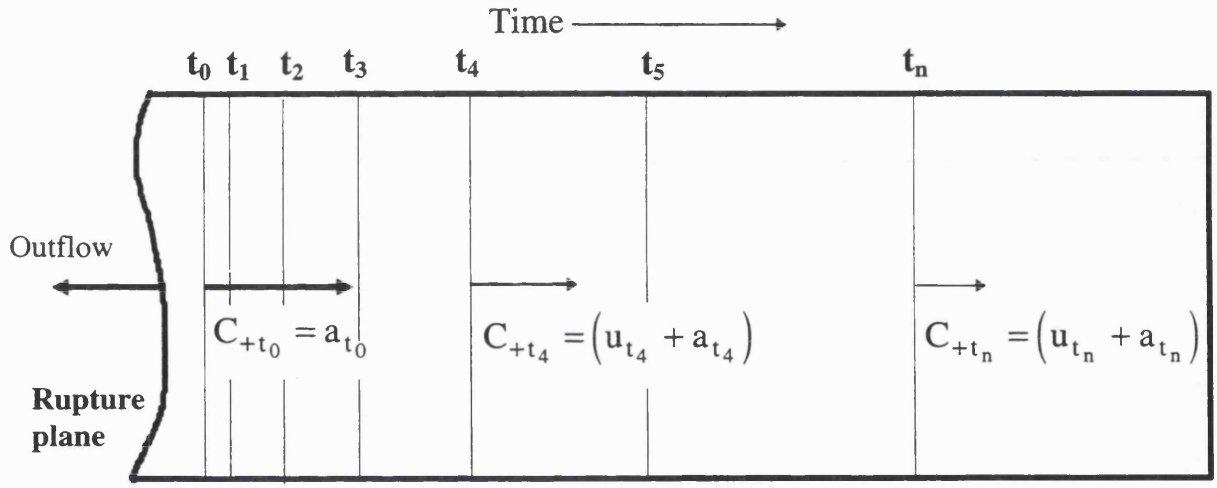

Figure 4.7.1: A schematic representation of expansion wave propagation with time following full bore pipeline rupture.

$$\Delta P = \rho\left(a u_r + u_r^2\right) \qquad (4.7.1)$$

It is then up to the design engineer to decide whether the mechanical integrity of the pipeline may be undermined following exposure to this level of pressure surge. Such a decision clearly requires a prior knowledge of the fluid velocity, u_r.

For a ball valve on the other hand, t_a depends on whether sufficient time has lapsed for the expansion waves to cause a drop in the fluid pressure equal to that for which the valve has been set to trigger.

4.7.1 Check Valve

Check valves, or non-return valves, are placed in pipelines to prevent back flow. Ideally, when the flow reverses at the location of the check valve, it closes instantaneously preventing back flow. More realistically, since the position is controlled by the flow and valve dynamics, closure occurs after some level of back flow is established. This causes an instantaneous stoppage of the reverse flow with a corresponding rise in pressure.

The study of the effects of FBR of a single pipeline can be considered as the study of a single element system. The introduction of valves in line turns a single element system into a multi-element one.

Check valve closure is simply modelled by introducing closed end boundary conditions at the required time and space co-ordinates, relative to the passage of flow reversal and distance from the rupture plane respectively. Here we are assuming a worst case scenario in which the flow of gas is assumed to remain unhindered until complete closure of the valve.

Figure 4.7.2 shows a schematic representation of the appropriate boundary conditions on either side of the valve. i, and j, are the local initial and solution nodes respectively in the space-time grid and p, and n, are the points where the C_+ and C_- characteristic lines intersect the spatial axis between two adjacent nodes. The C_0 characteristic on either side is zero since the flow velocity at that point is zero.

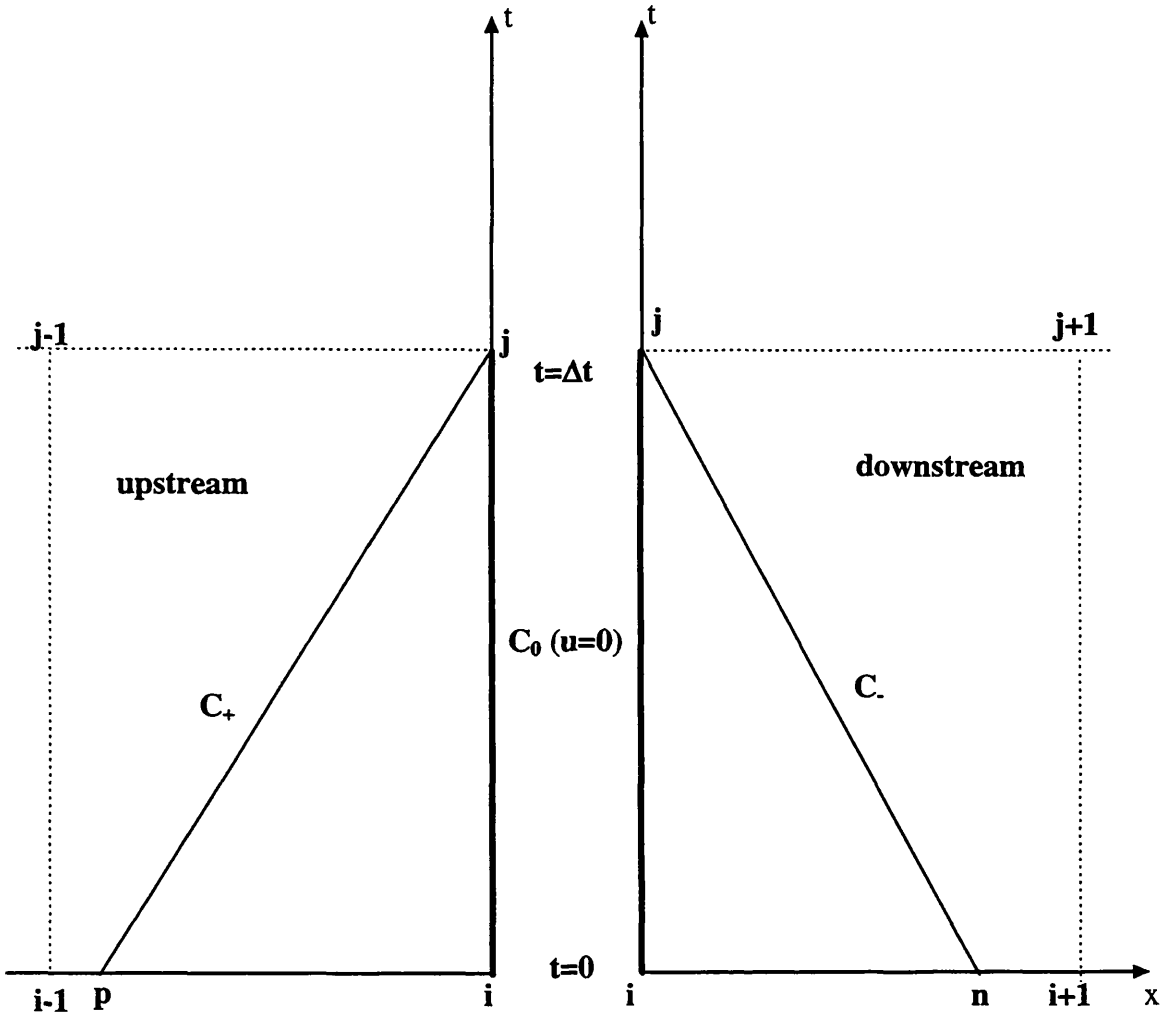

Figure 4.7.2: Grid scheme for the check valve closure.

The solution pressure, P_j is obtained on the downstream side by rearranging the negative compatibility equation and using average values for the discrete parameters for iteration steps greater than 1 as in the predictor corrector method. Hence

$$P_j = P_n - (\overline{\rho a})_{jn} u_n + (\overline{\psi} - \overline{a\beta})_{jn} \Delta t \qquad (4.7.2)$$

whereas on the upstream side, the positive compatibility is used,

$$P_j = P_p + (\overline{\rho a})_{jp} u_p + (\overline{\psi} + \overline{a\beta})_{jp} \Delta t \qquad (4.7.3)$$

The density on either side of the valve can be obtained from the pathline compatibility equation.

4.7.2 Ball Valve

The modelling of the ball valve is more complex due to its relatively complicated 'closure geometry' and slow closure rate. Here, the variations in fluid flow properties must be evaluated as a function of time during valve closure.

The compatibility equations need to be re-arranged to take account of the pressure drop across the closing valve. If conditions on the upstream and down stream sides of the valve are denoted by the subscript j'+ and j'- respectively, then the corresponding characteristics diagram for the conditions on either side of the valve is given in Figure 4.7.3.

The compatibility equations for each of the characteristic lines, C+, C- and C_o are respectively given by:

$$P_{j'+} - P_p + (\overline{\rho a})_{pj'+}(u_j - u_p) = (\overline{\psi} + \overline{a\beta})_{pj'+} \Delta t = K_1 \qquad (4.7.4)$$

$$P_{j'-} - P_n - (\overline{\rho a})_{nj'-}(u_j - u_n) = (\overline{\psi} - \overline{a\beta})_{nj'-} \Delta t = K_2 \qquad (4.7.5)$$

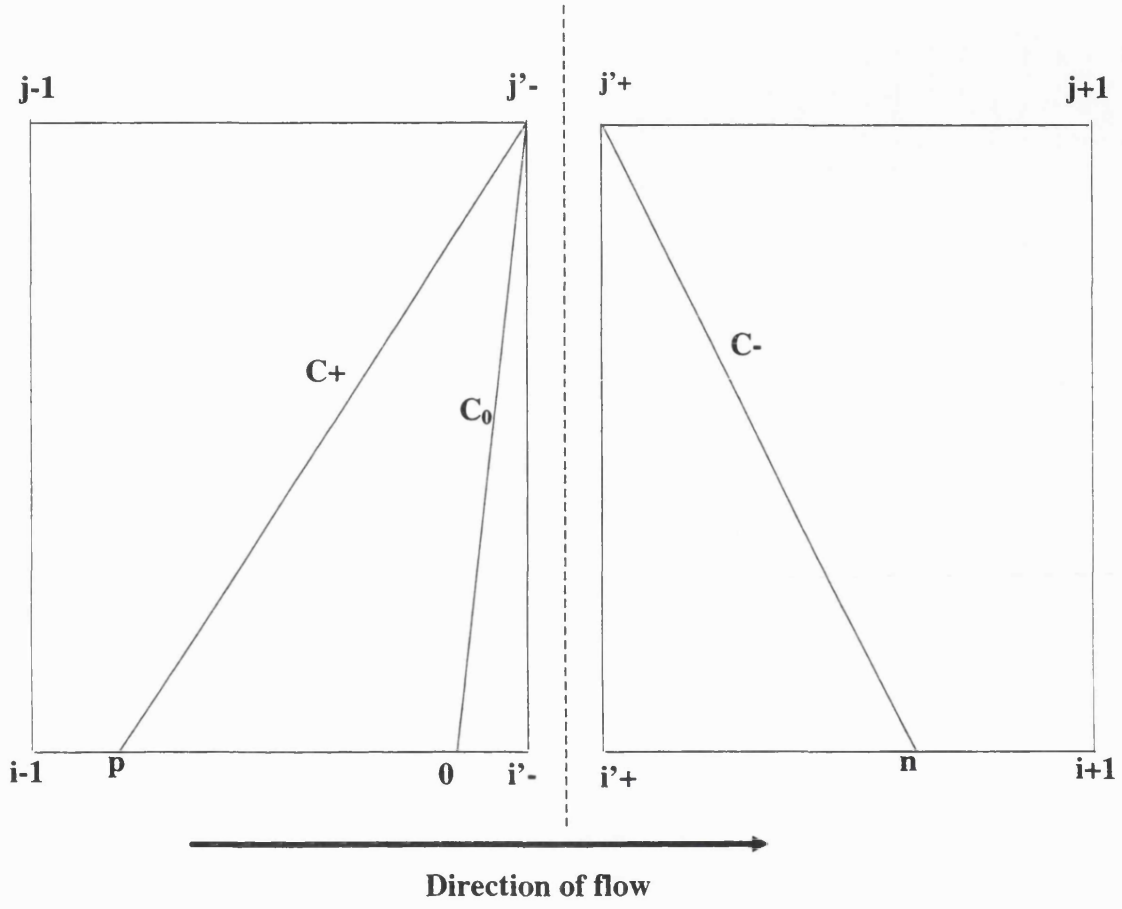

Figure 4.7.3: Grid scheme for the conditions on either side of the closing ball valve.

$$P_{j'+} - P_o - \left(\overline{a^2}\right)_{oj'+}\left(\rho_j - \rho_o\right) = (\overline{\psi})_{oj'+}\Delta t = K_3 \qquad (4.7.6)$$

Equations 4.7.4 to 4.7.6 contain 4 unknowns that change with time, namely P_{j+}, P_{j-}, u_j and ρ_j. The closure relation for the above system of equations can be derived from the valve loss equation (Swaffield and Boldy, 1993; Wylie and Streeter, 1993):

$$Q(t) = C_d(t)A_f(t)\sqrt{\frac{2\Delta P(t)}{\rho(t)}} \qquad (4.7.7)$$

where Q is the volumetric flowrate through the valve at any time, t during closure, C_d is the valve discharge coefficient, and A_f is the valve area open to flow.

Equation 4.7.7 represents the variation of flow rate of a fluid through a closing valve as a function of the pressure drop. It has been derived essentially for an incompressible fluid flow but it may be used in conjunction with a gas pipeline by assuming that the inertial effects of the gas within the boundary of the valve are minimal (Wylie and Streeter, 1993, Wylie, 1997, Boldy, 1997). This can be justified by the time constant for flow through the valve which is very small in relation to that for flow through the pipeline.

For example, the pipeline time constant is given by (Wylie and Streeter, 1993),

$$t_p = \frac{2L}{a} \qquad (4.7.8)$$

where L is the length of the pipeline and a, is the acoustic velocity through the pipe. For a 1 km pipeline containing methane as presented in the case study in section 4.8 the minimum time constant, $t_p = 5$ s.

The time constant for a closing valve (Wylie and Streeter, 1993) is given by,

$$t_v = 2\pi\sqrt{\frac{M}{\Delta P u}} \qquad (4.7.9)$$

M, and u are respectively the mass flowrate and fluid velocity through the valve. ΔP is the pressure drop for a closing valve . For the valve under study, the maximum t_v is

ca. 1×10^{-4}s which is orders of magnitude shorter than the minimum time constant for the pipeline.

The above also provides a justification to using a steady state equation such as equation 4.7.7 in an unsteady flow simulation. When the time constant for any element such as valve, compressor or pump is much smaller than that of the pipeline, steady state equations can always be used, even in highly unsteady flow situations (Wylie and Streeter, 1993, Wylie, 1997).

The valve discharge coefficient is a function of valve type and degree of opening. For the purposes of this thesis we use the following correlation fitted to the data given by Wylie[5] for a ball valve:

$$C_d = A_0 + A_1\varpi + A_2\varpi^2 + A_3\varpi^3 + A_4\varpi^4 \qquad (4.7.10)$$

where A_0 to A_4 are the curve fitting constants (see nomenclature) and ϖ is the percentage area of valve opening.

The valve area open to flow is a function of the speed of closure of the valve. If the valve is moving across at u_v m/s then at time t, the valve will have travelled a distance of $u_v \times t = x$ metres. The distance left to travel by the closing valve will be 2R-x. Figure 4.7.4 illustrates the ball valve closure geometry.

From figure 4.7.4 it is apparent that the area available to flow is twice the area CBD. The area CBD is obtained by subtracting the area of the triangle ABD from the area of the sector subtended by the angle θ, ABCD. ABD is always an isosceles triangle where,

$$R\cos\frac{\theta}{2} = R - \frac{2R - x}{2} \qquad (4.7.11)$$

or,

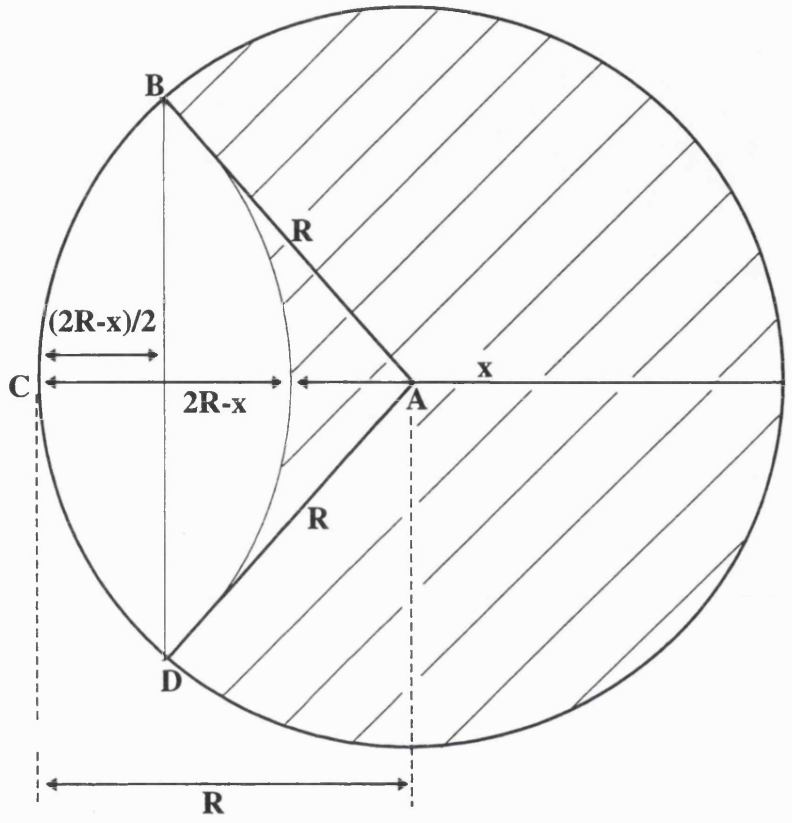

Figure 4.7.4: A schematic representation of ball valve closure geometry. The unshaded area represents the valve flow area, A_f (equation 4.7.15). The shaded area is the area covered by the valve.

$$\theta = 2\cos^{-1}\left[\frac{R-\left(\frac{2R-x}{2}\right)}{R}\right] \tag{4.7.12}$$

Area of segment ABCD is given by,

$$ABCD = \frac{\theta}{360}\pi R^2 = \frac{2\cos^{-1}\left[\frac{R-\frac{2R-x}{2}}{R}\right]}{360}\pi R^2 \tag{4.7.13}$$

The area of the triangle ABD is given by ½ × base × height, i.e.

$$ABD = \left[R-\frac{(2R-x)}{2}\right]\sqrt{R^2-\left[R-\frac{(2R-x)}{2}\right]^2} \tag{4.7.14}$$

Therefore valve area, $A_f = 2(ABCD-ABD)$.

The valve flow area at any given time, t during closure is related to ϖ via

$$A_f(t) = 2\left[\pi R^2\frac{2\cos^{-1}\left(\frac{R-\left(\frac{2R-x(t)}{2}\right)}{R}\right)}{360} - \left(R-\frac{(2R-x(t))}{2}\right)\left(\sqrt{R^2-\left(R-\frac{(2R-x(t))}{2}\right)^2}\right)\right] \tag{4.7.15}$$

where R is the pipeline radius and x, is the distance traversed by valve at time, t as indicated in figure 4.7.4.

The corresponding volumetric flowrate through the valve can be simply expressed in terms of the fluid velocity, u(t) as:

$$Q(t) = u(t)A_f(t) \tag{4.7.16}$$

Substituting for Q(t) from equation 4.7.16 into equation 4.7.7,

$$u(t) = C_d(t)\sqrt{\frac{2\Delta P(t)}{\rho(t)}} \tag{4.7.17}$$

When the valve is just about to shut, the discharge coefficient, C_d, is unity since no constriction of flow has taken place yet. The flow velocity at this moment can be expressed from the valve equation 4.7.7 as,

$$u_0 = \sqrt{\frac{2\Delta P_0}{\rho_0}} \tag{4.7.18}$$

ΔP_0 is the valve fully open pressure loss over the pipe element that contains the valve (P_{i-1} - P_{i+1} ; figure 4.7.3) and u_0 and ρ_0 are the respective fluid velocity and density through the fully open valve.

Taking ratios of flow rate over a given time interval during closure, the pressure loss across the closing valve is:

$$\Delta P(t) = P_{j'+} - P_{j'-} = \frac{\Delta P_0}{u_0^2 C_d^2 \rho_0} u_j^2 \rho_j = K_4 u_j^2 \rho_j \tag{4.7.19}$$

where,

$$K_4 = \frac{\Delta P_0}{u_0^2 C_d^2 \rho_0} \tag{4.7.20}$$

The pressure drop across the valve can also be obtained from the compatibility equations by subtracting equation 4.7.5 from equation 4.7.4,i.e.:

$$P_{j'+} - P_{j'-} = K_1 - K_2 + P_P - P_n - u_j\left((\overline{\rho a})_{pj'+} + (\overline{\rho a})_{nj'-}\right) + (\overline{\rho a})_{pj'+} u_p + (\overline{\rho a})_{nj'-} u_n \tag{4.7.21}$$

Similarly from equations 4.7.5 and 4.7.6:

$$P_{j'+} - P_{j'-} = K_3 - K_2 + P_o - P_n - u_j(\overline{\rho a})_{nj'-} + (\overline{\rho a})_{nj'-} u_n + \left(\overline{a^2}\right)_{oj'+} \rho_j - \left(\overline{a^2}\right)_{oj'+} \rho_o \quad (4.7.22)$$

Equating equations 4.7.21 to 4.7.22 and re-arranging we have:

$$\rho_j = \frac{K_5 - (\overline{\rho a})_{pj'+} u_j}{\left(\overline{a^2}\right)_{oj'+}} \quad (4.7.23)$$

where,

$$K_5 = K_1 - K_3 + P_p - P_o + (\overline{\rho a})_{pj'+} u_p + \left(\overline{a^2}\right)_{oj'+} \rho_o \quad (4.7.24)$$

Substituting for ρ_j from equation 4.7.23 into equation 4.7.19,

$$P_{j'+} - P_{j'-} = K_4 u_j^2 \rho_j = K_4 u_j^2 \left[\frac{K_5 - (\overline{\rho a})_{pj'+} u_j}{\left(\overline{a^2}\right)_{oj'+}} \right] \quad (4.7.25)$$

Equation 4.7.25 gives the pressure drop across the valve in terms of the fluid velocity through it. Therefore by equating it to equation 4.7.21, a cubic equation for the fluid velocity, u_j is obtained:

$$u_j^3 + K_6 u_j^2 + K_7 u_j + K_8 = 0 \quad (4.7.26)$$

where,

$$K_6 = \frac{-K_5}{(\overline{\rho a})_{pj'+}} \quad (4.7.27)$$

$$K_7 = \frac{\left[(\overline{\rho a})_{pj'+} + (\overline{\rho a})_{nj'-} \right] \left(\overline{a^2}\right)_{oj'+}}{(\overline{\rho a})_{pj'+} K_4} \quad (4.7.28)$$

$$K_8 = \left[K_1 - K_2 + P_p - P_n + \left(\overline{\rho a}\right)_{pj'+} u_p + \left(\overline{\rho a}\right)_{nj'-} u_n \right] \frac{\left(\overline{a^2}\right)_{oj'+}}{\left(\overline{\rho a}\right)_{pj'+} K_4} \qquad (4.7.29)$$

Equation 4.7.26 results in three real roots for the fluid velocity, two of which are positive. The solution is taken as that which is less than the maximum choke velocity at the rupture plane.

The remaining dependent variables $P_{j'-}$, $P_{j'+}$, and ρ_j can then be calculated from the three compatibility equations 4.7.4 to 4.7.6.

4.8 CASE STUDY

The particular case examined here relates to a real North Sea pipeline of length and diameter 145km and 0.87m, respectively, containing methane. The initial flow velocity is 10m/s and the line pressure and temperature are 133 bar and 283 K respectively. Under such conditions the inventory is in the gas state and its properties may be approximated as ideal. A constant fanning friction factor, f = 0.0018205 and ratio of specific heats, γ = 1.33 are used. The pipeline is partially insulated with a heat transfer coefficient of 5 W/m^2K.

For the sake of analysis, worst case scenarios are assumed in which rupture occurs during pumping at the high pressure end of the pipeline (at the riser section in the case of offshore platforms). Additionally, the ball valve is assumed to be set to trigger at a 10 bar drop below the normal operating pressure.

The following is a quantitative assessment of hypothetical situations following FBR involving the provision of both check valves and ball valves placed at various distances from the rupture plane.

4.8.1 Fluid Dynamics Data

Figure 4.8.1a shows fluid velocity and pressure profiles at various time intervals spanning the first 50 s following FBR in the absence of ESDVs. Some of the salient features of the data together with their implications are summarised in the following:

i) FBR produces an expansion wave which results in a significant change in fluid pressure and velocity to choke conditions in the immediate vicinity of the rupture plane. However, the conditions downstream of the expansion waves remain much the same as those prior to rupture, oblivious to the rapid changes occurring at the rupture end. This is manifested in the constant pressure and velocity lines shown in the figure.

ii) The sudden loss in pressure results in flow of gas in opposite directions, so that there is an outflow at both ends of the pipeline. The position of flow reversal

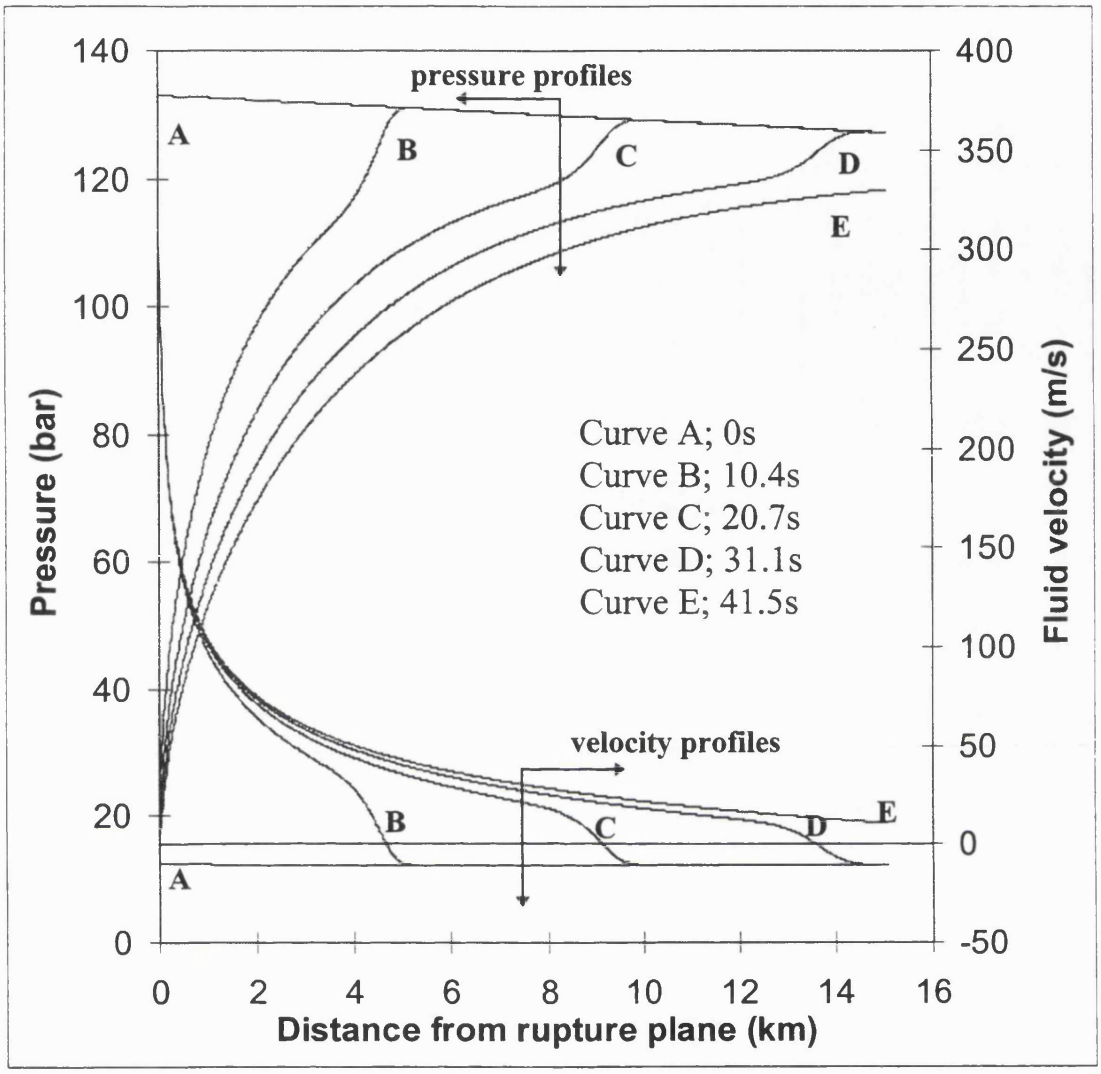

Figure 4.8.1a: Pressure and fluid velocity profiles following FBR.

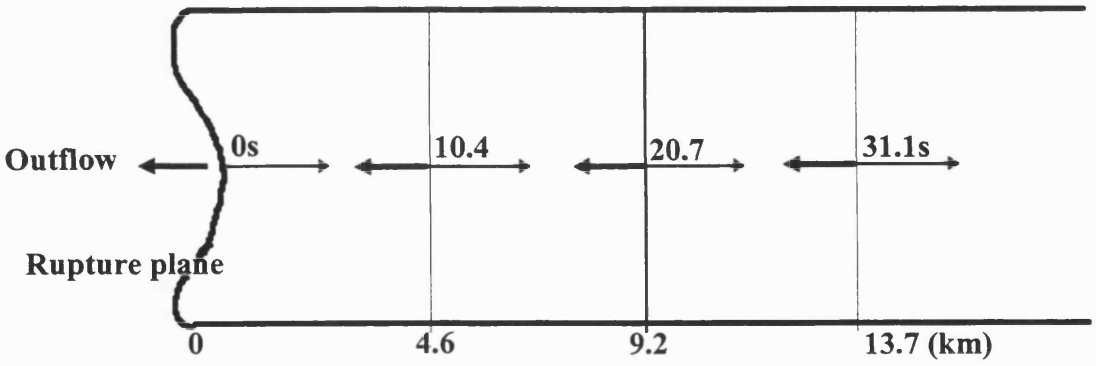

Figure 4.8.1b: Flow reversal location along the pipeline as a function of time following FBR.

corresponds to the points at which the velocity profiles cross the abscissa (positive values denote flow towards the rupture plane in figure 4.8.1a). For clarity, the flow reversal location is also mapped as a function of time and distance along the pipeline in figure 4.8.1b.

iii) At any given time, the flow reversal point lags the pressure peak.

iv) In the case of a check valve, its activation time, t_a is directly dictated by its location relative to the position of the flow reversal. For example from figure 5a, the minimum activation time, t_a for a valve positioned 4.6 km from the rupture plane is 10.4 s. However, for a ball valve located at the same location and set at 10 bara below the working pressure, the corresponding activation time is 11.2 s. This difference in time, although small represents a considerable difference in the amount of inventory released.

4.8.2 Mass release data

Figure 4.8.2 shows the effect of ESDV proximity to the rupture plane on the total amount of inventory release prior to complete pipeline isolation. Curve A represents the data for a check valve whereas curve B represents the corresponding data for a ball valve. Negligible closure time is assumed for the former. The ball valve on the other hand is assumed to close at a rate of 2.54 cm/s. The released inventory has been calculated on the basis of fitting a polynomial to discharge rate versus time data and integrating the resulting equation over the valve response time, t_r. Added to this is the amount that remains in the isolated section of the pipeline following complete valve shut-down and de-pressurisation to the ambient pressure.

From the data it is clear that in terms of limiting the inventory loss, a check valve offers a far better degree of protection as compared to a ball valve when either is placed in close proximity to the rupture plane. This is of course on the basis of the assumption that the check valve closes instantaneously, upon the detection of flow reversal and as such it would not be exposed to a pressure surge. Ironically, experience in the nuclear industry (Lee et. al., 1993) has shown that relatively large values of flow reversal velocity are required to ensure complete valve closure.

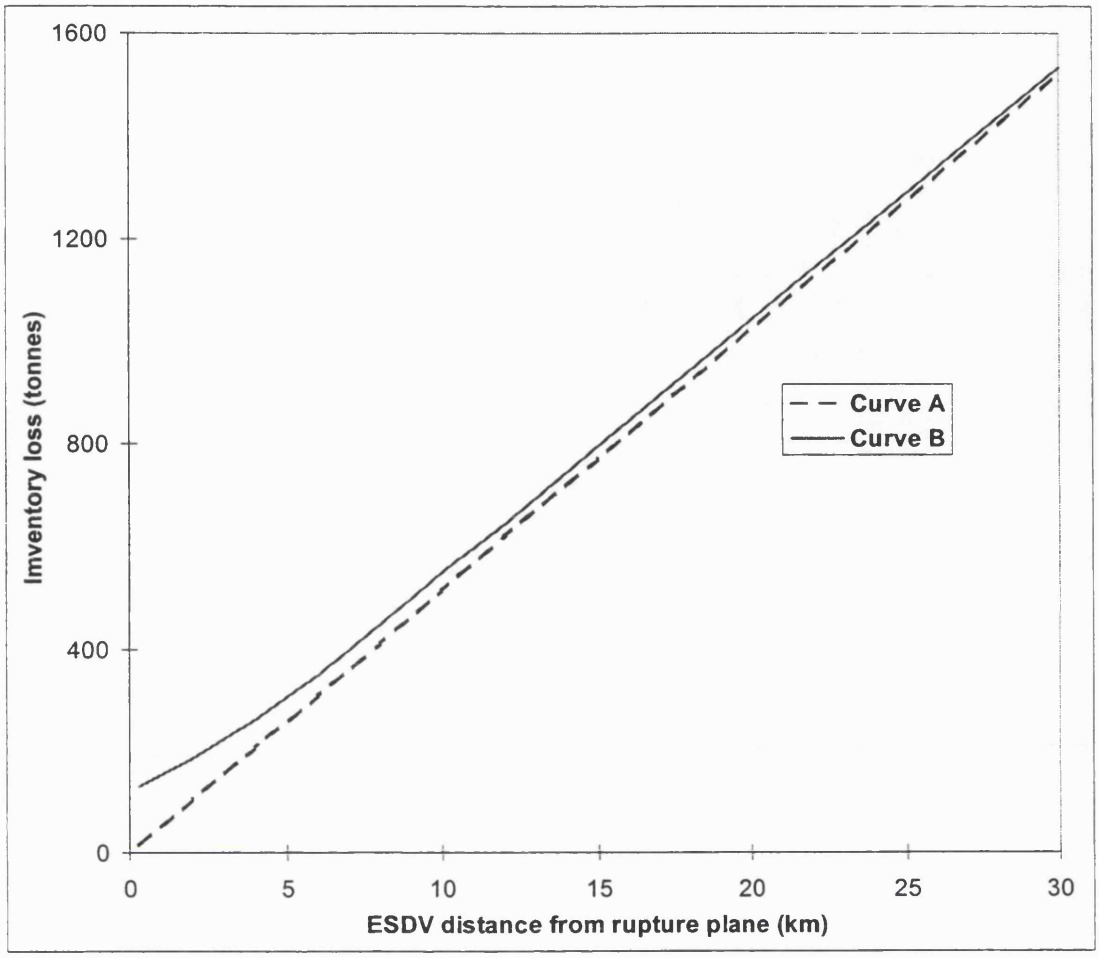

Figure 4.8.2: The variation of inventory loss as a function of ESDV proximity to the rupture plane: curve A; check valve; curve B; ball valve.

At longer distances, the difference in performance between the two valves becomes insignificant.

It is noteworthy that the deceptively simple argument assuming that the total inventory released following valve shut-down is equal to that within the isolable section of the pipeline prior to FBR results in significant underestimates. This is particularly so in the case of ball valves placed in close proximity to the rupture plane. Figure 4.8.3 graphically supports this argument. Curves A and B show the results for a check and ball valve respectively.

The data show the variation of the % underestimate of inventory released as a function of valve proximity to the rupture plane.

4.8.3 Pressure/time history

4.8.3.1 The effect of time delay

Figure 4.8.4 shows various pressure transients created on the upstream side of a check valve positioned 300 m from the rupture plane (just above the sea level in offshore platforms) . Curve A represents the response for valve closing upon sensing flow reversal. Curves B, C and D on the other hand, represent the data for closure at 0.55,1.4, and 6.5 s after the passage of flow reversal. In practice such time delays may represent an intentional damped closure of valve in order to avoid damage due to valve slamming (Thorley, 1989; Koetzier et. al., 1986; Lee et. al., 1993).

The data relate to a short pipeline (10 km) as pressure fluctuations are more pronounced in such cases (see later).

The data in figure 4.8.4 indicate significant pressure oscillations, the amplitude of which directly increases with time delay. Indeed such fluctuations have often been observed in practice primarily in pipelines transporting water and steam in the nuclear industry (Lee et. al., 1993). They arise as a consequence of the reflection of the expansion waves (generated following FBR) from the closed end of the pipeline. As the speed of the reflected wave is equal to the local speed of sound relative to the fluid velocity (left running characteristic) such oscillations are expected to be more frequent in pipelines containing liquids. Experimental data reported in the literature

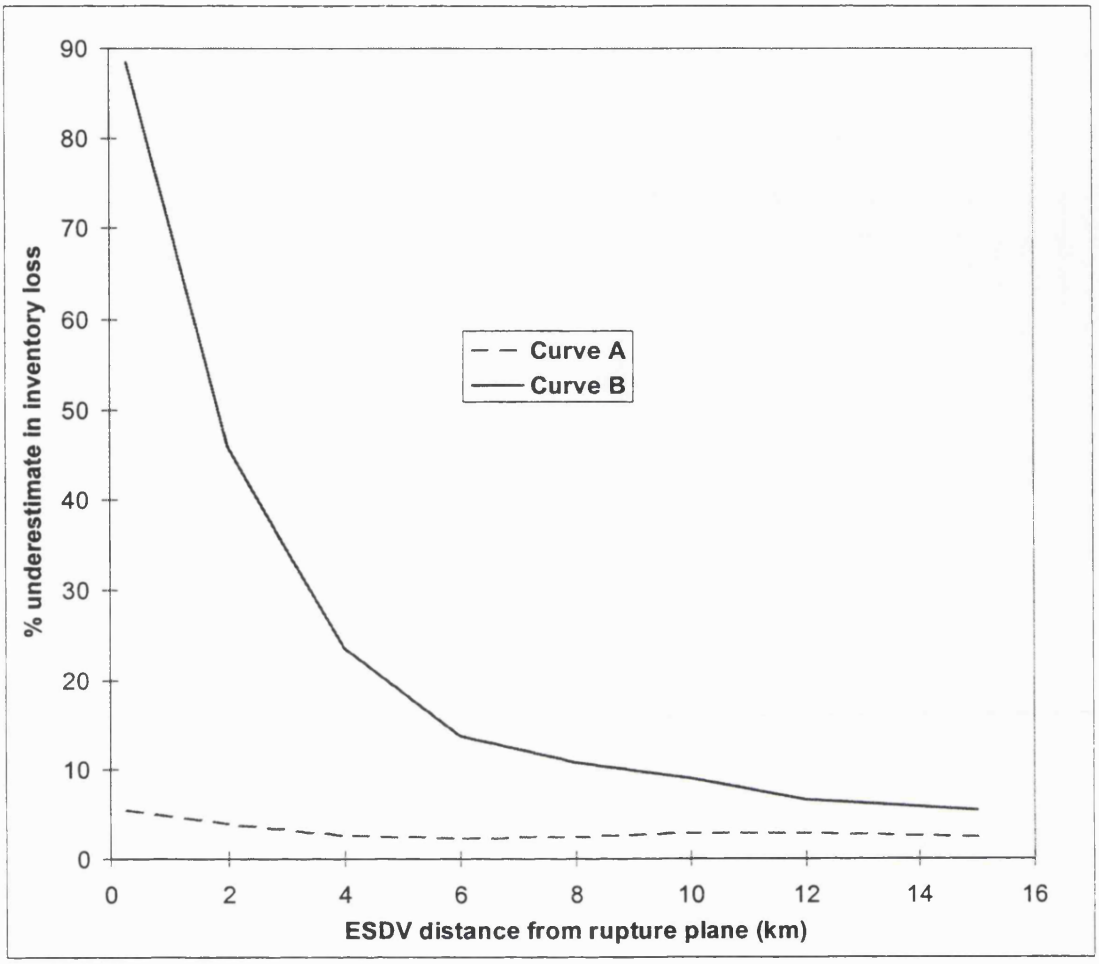

Figure 4.8.3: Percentage underestimate of total inventory loss based on the simple isolation section approximation: curve A; check valve: curve B; ball valve.

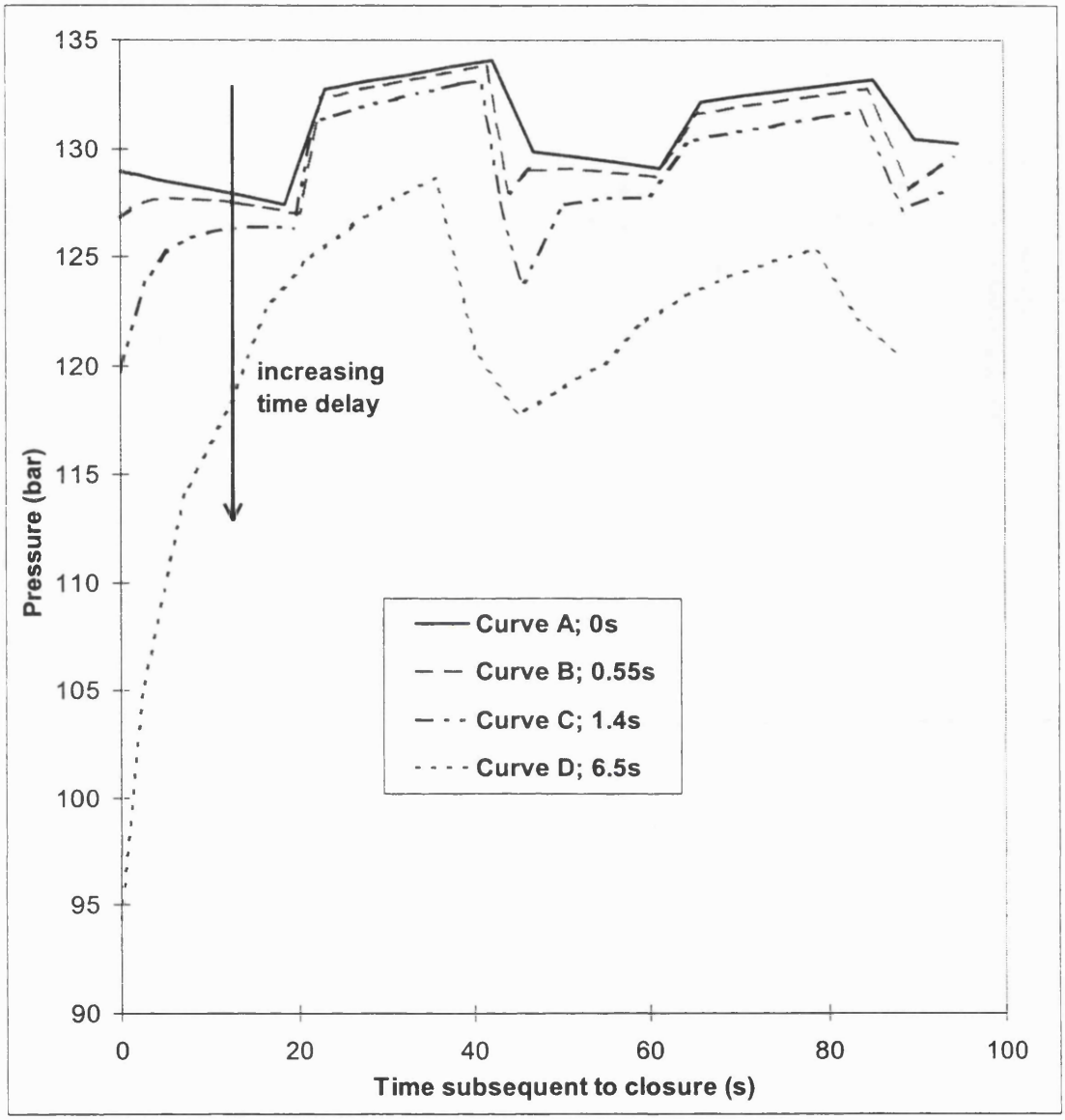

Figure 4.8.4: The effect of time delay on pressure-time history at the upstream side of a check valve placed 300m from rupture plane.

(Hsu and Graham, 1976; Kieffer, 1977; Picard and Bishnoi, 1987) are in support of this view.

Figure 4.8.5 shows the same data as in figure 4.8.4 but for different length pipelines. For the sake of illustration, the check valve is assumed to close 1.7s after the passage of flow reversal. The data indicate that short pipelines are particularly prone to transient pressure oscillations. For example, in the case of a 1 km pipeline, emergency isolation would result in a massive (40 bar) pressure pulse occurring during the first 4s following emergency shut-down. Such dynamic oscillations are clearly undesirable in practice as they can give rise to serious pipeline vibration problems. They are less pronounced in long pipelines because of frictional losses which cause attenuation of the pressure waves.

An additional danger, particularly in the case of pipelines transporting condensible liquids is due to cavitation (Simpson and Bergant, 1996). In such cases, if the drop in fluid pressure is sufficient to reach its vapour pressure, a vaporous cavity is produced which may suddenly collapse in response to a reflected pressure wave. This may cause the check valve to open momentarily thus resulting in further loss of inventory.

Figure 4.8.6, shows the variation of upstream valve pressure during closure, modelled using the appropriate theory described earlier. Curves A and B show the results for a check and ball valve respectively.

The closure rate for the ball valve is 5.3 cm/s which is approximately double the rate used in practice for such diameter pipelines. No fluctuations in pressure can be observed despite such a rapid closure rate. The data for a check valve are also included for comparison.

When choosing the time step, Δt for the ball valve simulation, it is important to bear in mind that the time step for the simulation always has to be appreciably less than the valve closure time if the valve dynamics is of primary interest. The valve closure time in our case is 16.5s, and the time step for the simulation is 2.3×10^{-3}s.

Figure 4.8.7 shows the effect of faster ball valve closure times on the upstream pressure time profile. Curve A shows the closure rate at 5.27 cm/s whereas curves B

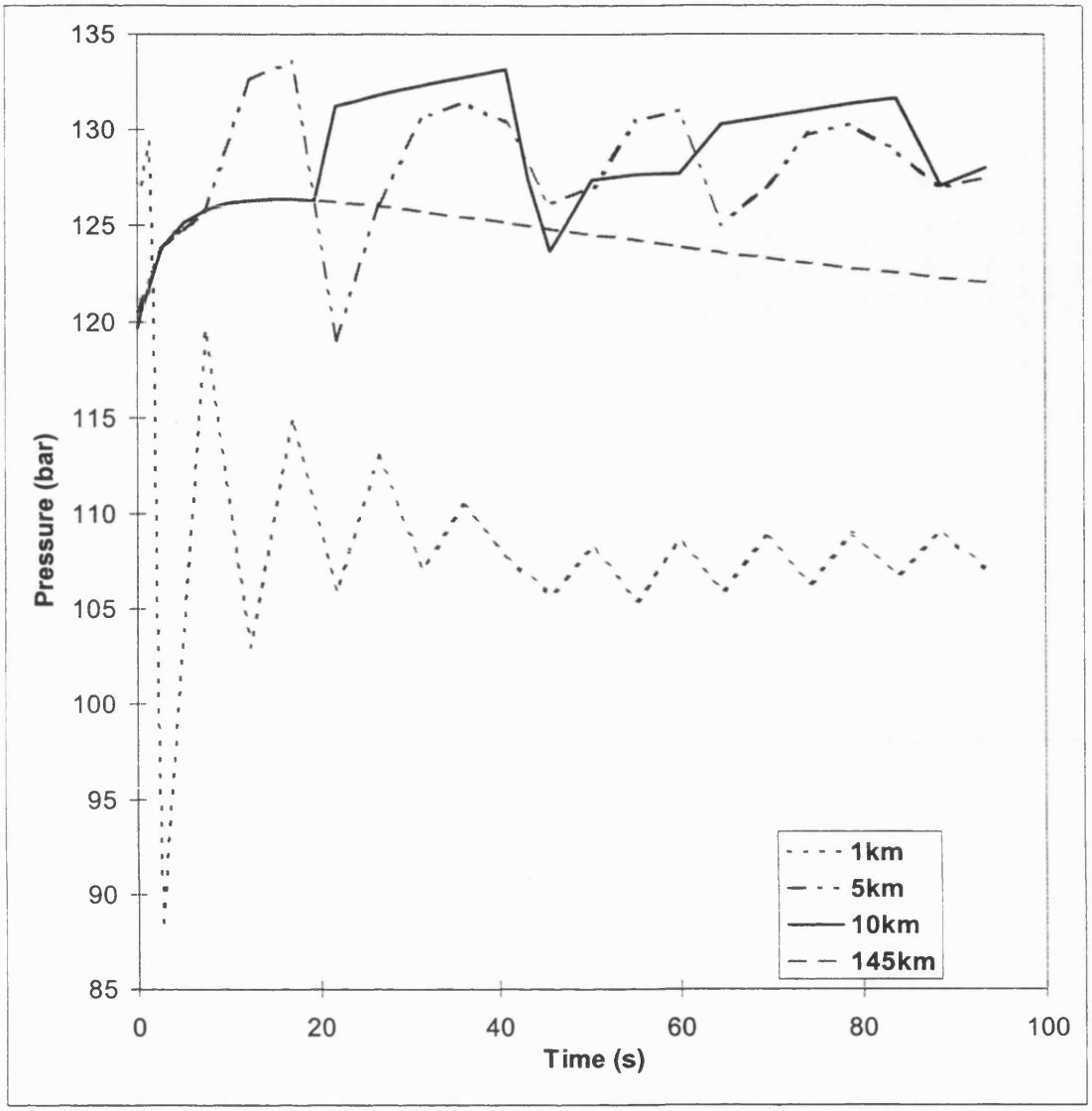

Figure 4.8.5: The effect of pipeline length on the upstream pressure-time history of a check valve, placed 300m from the rupture plane. The valve is assumed to close 1.35 seconds after the passage of flow reversal.

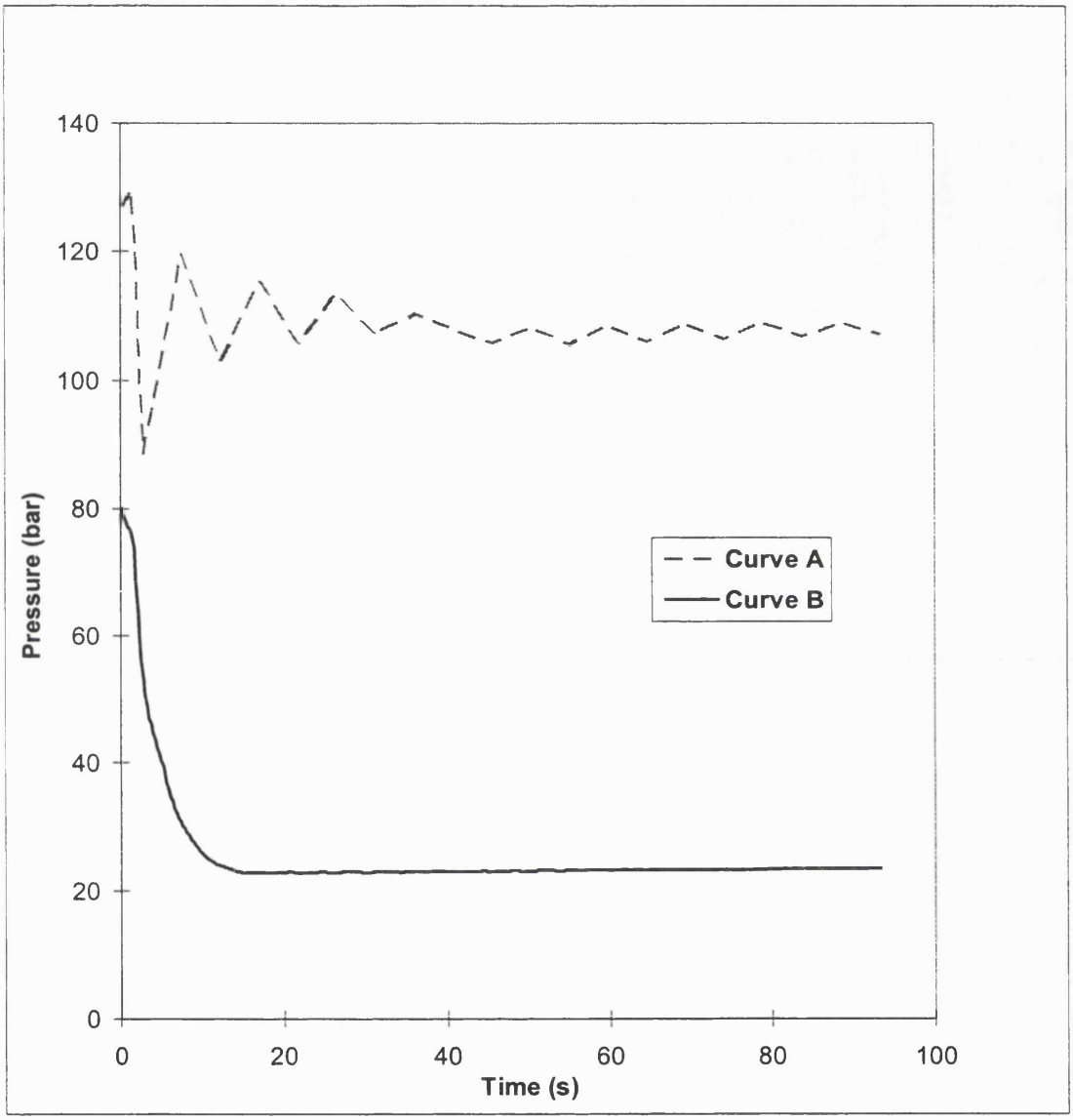

Figure 4.8.6: Upstream valve pressure-time histories: curve A; check valve: curve B - ball valve.

and C show the results for closure at 8.7 and 10 cm/s respectively. As is to be expected the pressure build up is greater, the faster the valve shuts.

4.8.3.2 Pressure surge data

Figure 4.8.8 shows the variation of pressure surge developed at the upstream side of the check valve as a function of the delay in its closure relative to the passage of flow reversal. Each pressure surge has been calculated on the basis of equation 4.7.1 and corresponds to the resulting head caused by bringing of the fluid impinging on the upstream side of the valve to rest.

As expected zero pressure surge is recorded when the valve closes instantaneously, upon the detection of flow reversal. However, only a small delay (ca. 1.1 s) in valve closure results in a significant build up in pressure head reaching a peak of 49 bar (corresponding to ca. 37% increase in line pressure). Interestingly, further increase in time delay actually results in a reduction in pressure head. This is primarily because the drop in the line pressure due to inventory loss has a more marked effect on reducing the pressure head that is developed during the latter stages of discharge.

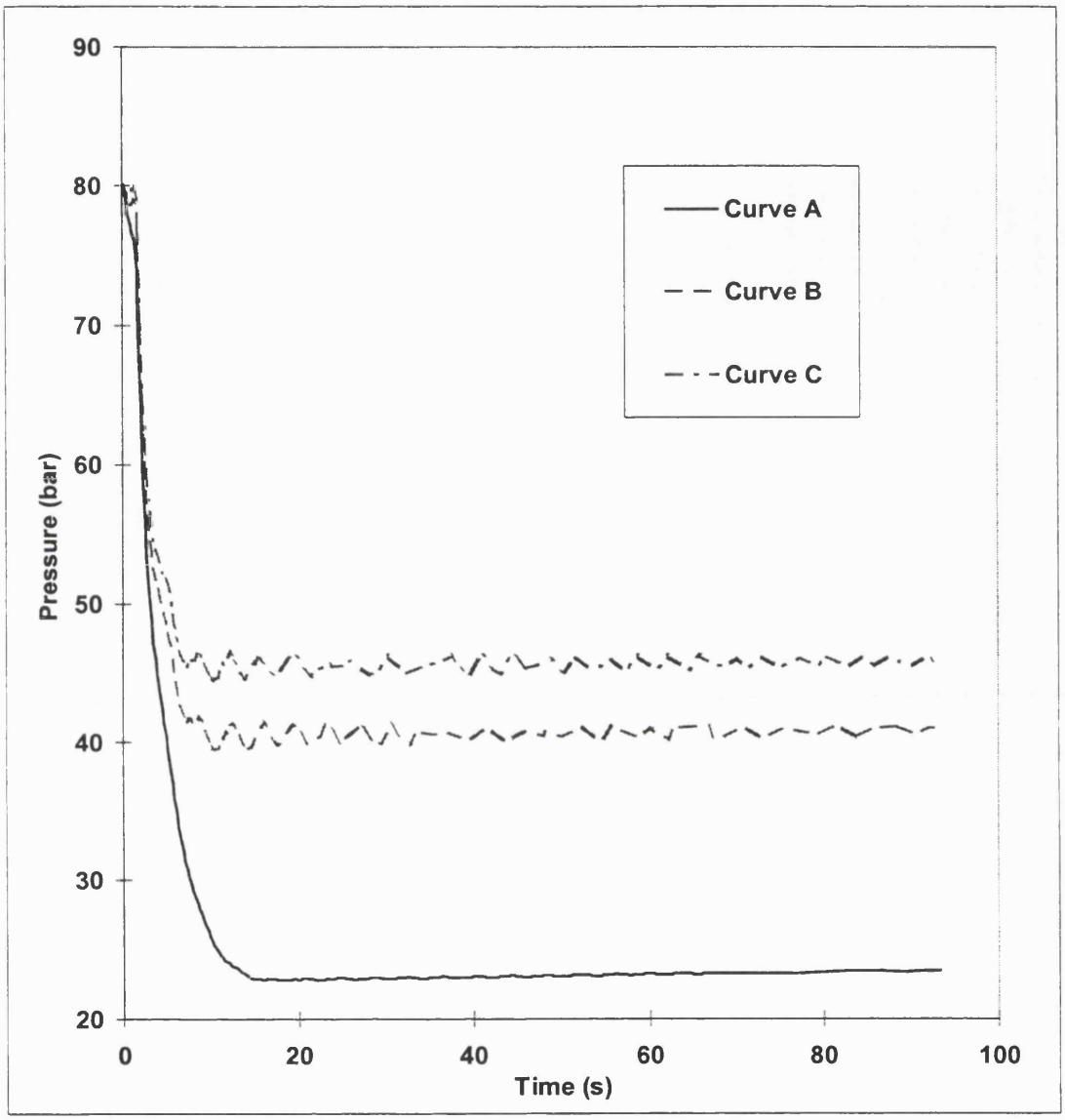

Figure 4.8.7: Upstream ball valve pressure-time histories for different valve closure rates
Curve A: Closure rate = 5.27cm/s
Curve B: Closure rate = 8.7 cm/s
Curve C: Closure rate = 10 cm/s

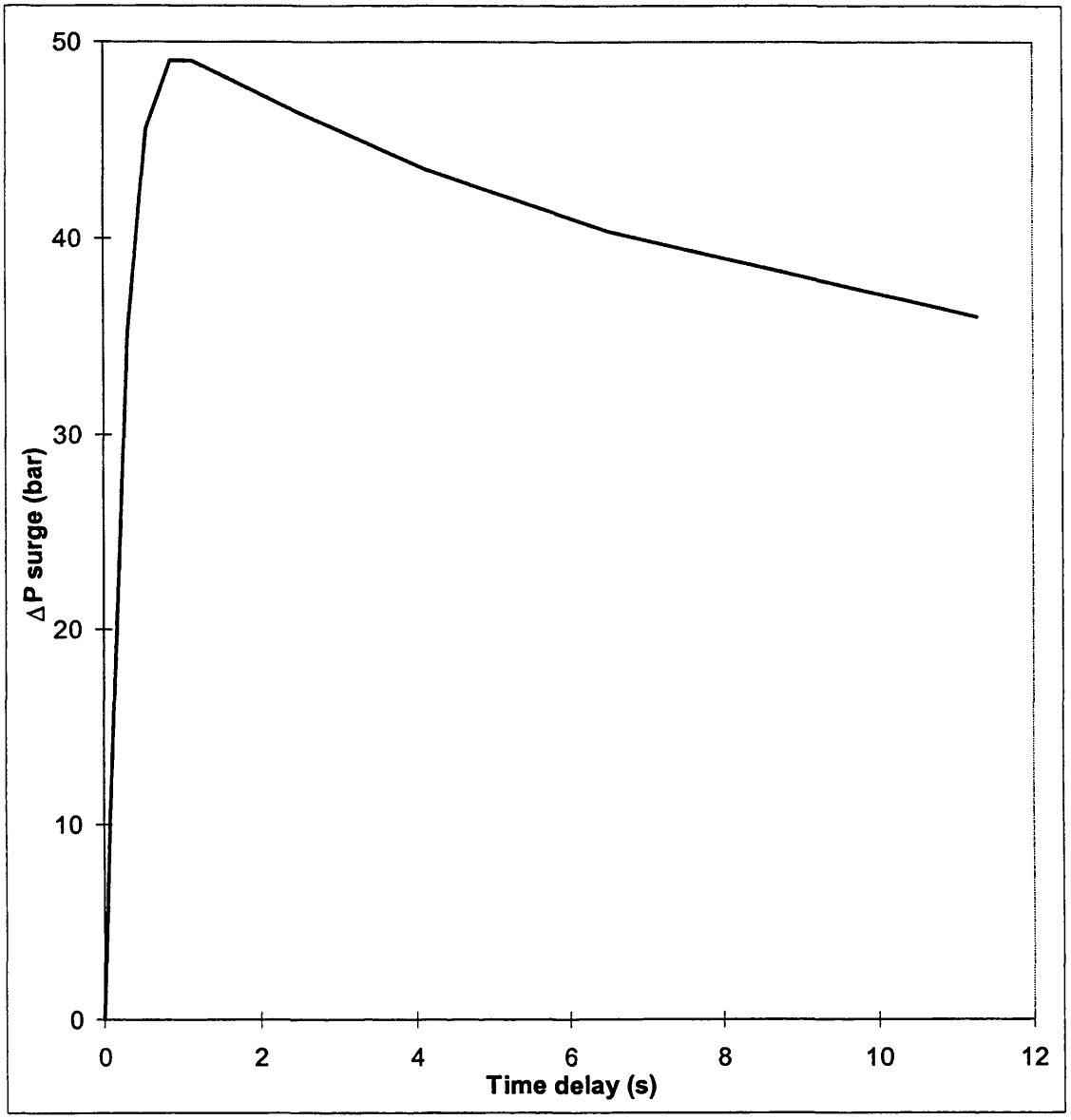

Figure 4.8.8: Variation of surge pressure at the upstream side of a check valve with closure time delay (relative to the passage of flow reversal). The valve is positioned 300 m from the rupture plane.

4.9 CONCLUSIONS

Some of the important conclusions of our findings are:

i. The modification to the classical ST method of characteristics proposed in this chapter gives the same accuracy of results as the classical ST method but for a given run, CPU time for the former is less than a tenth of the latter. This is because in the modified case, no iteration is needed to calculate the locations of the initial points. The validity of this approach is tested by comparison of this model's results (CNGS) with the classical ST approach for the Piper Alpha FBR scenario. Good agreement is also obtained with the Wave Tracing Method, based on a characteristic grid type solution, of Chen et. al. (1993).

ii. The use of a nested grid is essential if underestimation of the release rate is to be avoided and if accuracy in the fast transient region near the rupture plane is not to be compromised.

iii. For a given pipeline, although the number of elements in a nested grid scheme is greater than that for a simple grid scheme, the CPU time for the former is faster due to accelerated convergence near the rupture plane.

iv. In the case of permanent gases, the use of curved characteristics makes little difference to accuracy as compared to the first order linear solution. However the CPU time is significantly longer.

v. The inclusion of heat transfer effects is necessary if the late time regime is to be modelled accurately. The effects of a fire surrounding a pipeline can only be modelled if the model includes heat transfer from the surroundings.

vi. The dynamic response of both check valves and ball valves following FBR depends primarily on their proximity to the rupture plane and the flow reversal propagation speed. As the latter is directly related to the velocity of sound in the fluid medium relative to the escaping fluid,

a) pipelines containing gases are expected to be more susceptible to delayed emergency shut-down compared to those containing liquids. This however should be balanced against the higher pressure surges expected in liquid pipelines.

b) shut-down delay is expected to be longer when rupture occurs during 'normal' flow as compared to that occurring during 'shut-in'. This is because in the former the expansion wave propagation velocity, which directly affects the valve activation time, is decelerated due to the normal flow of gas in the steady state direction.

vii. In the case of a check valve, the amplitude and frequency of upstream pressure fluctuations following emergency shut-down are directly related to,

a) gas flow reversal velocity at the time of valve closure

b) valve proximity to the rupture plane

c) pipeline length

d) fluid compressibility

Pipelines incorporating ball valves are generally not susceptible to pressure surges or oscillations.

viii. No pressure surge is expected in the case of a check valve closing instantaneously upon sensing flow reversal. However, even in the case of a very short delay (ca 2s), a relatively large build-up in the pressure surge to a maximum value can be expected. It then diminishes in magnitude for larger closure delays.

ix. In terms of limiting the amount of released inventory following emergency shut-down, a check valve offers a far better degree of performance as compared to a ball valve when either is placed at close proximity of the rupture plane. At longer distances however, the difference in performance becomes insignificant.

x. A deceptively simple argument that the total amount of inventory released following FBR is equal to that present in the isolable section of the pipeline prior to ESD may give rise to gross underestimates particularly in the case of ball valves placed in close proximity of the rupture plane.

CHAPTER 5: DEVELOPMENT AND VALIDATION OF THE CNGS-HEM MODEL AND ITS APPLICATION IN PREDICTING ESDV OR SSIV RESPONSE

5.1 INTRODUCTION

In this chapter, the CNGS coupled with the Homogeneous Equilibrium Model, (CNGS- HEM) described in chapter 2 is used to derive the relevant characteristic and compatibility equations for simulating FBR of pipelines containing two-phase multi-component hydrocarbon mixtures.

In solving these equations, particular areas of attention, primarily due to the highly non-linear variation of the physical properties of such fluids are:

- use of a flash calculation procedure for accurate prediction of fluid properties such as ρ, a and P at each node, and at each interpolation point during the numerical discretisation
- accurate prediction of the 'wall' friction factor as its is shown that this parameter has an important effect on fluid dynamics
- the calculation for the initial conditions (t=0) at the broken end
- direct use of the method of characteristics to calculate fluid conditions at the boundaries between the coarse and fine grids. Linear interpolation is not deemed to be sufficiently accurate for this purpose
- use of curved characteristics near the rupture plane
- use of smaller than maximum permissible Δt, according to the CFL condition, for accurate simulation of the choking condition, thus avoiding numerical instability.

The above is followed by optimisation and validation of the model by comparison with various field data. The validated model is then used to predict the dynamic response of ESDV or SSIV's following FBR of a pipeline containing a condensable gas mixture and comparisons are made in terms of the general trends observed in chapter 4 for pipelines containing permanent gases.

5.2 CHARACTERISTIC AND COMPATIBILITY EQUATIONS

The conservation equations for a real fluid as derived in Chapter 2 are as follows,

$$\begin{aligned} &\rho_t + \rho u_x + u\rho_x = 0 \\ &\rho u_t + \rho u u_x + P_x = \beta \\ &P_t + uP_x - a^2(\rho_t + u\rho_x) = \varphi\frac{q_h - u\beta}{\rho T} = \psi \end{aligned} \qquad (5.2.1)$$

where q_h is the equation for heat transfer and is discussed in section 5.4, β is the friction force term and is discussed in section 5.3.

The expressions for the speed of sound, a, and the thermodynamic parameter, φ for real multi-component multi-phase fluids have been derived in Chapter 2, and can be written as;

Single phase mixtures,

$$a^2 = \frac{\gamma}{k\rho} \qquad (5.2.2)$$

$$\varphi = \frac{\rho\beta T a^2}{C_p} \qquad (5.2.3)$$

Two-phase mixtures,

$$a^2 = \left(\frac{\Delta P}{\Delta \rho}\right)_s \qquad (5.2.4)$$

$$\varphi = \rho^2\left(\frac{\Delta T}{\Delta \rho}\right)_s \qquad (5.2.5)$$

The conservation equations for a real fluid are very similar in form to those for an ideal gas. The derivation procedure for the characteristic and compatibility equations are exactly the same as for an ideal gas and will therefore not be dealt with in this chapter (see Chapter 4, section 4.2 for details).

The characteristic equations for propagation of the disturbance caused by FBR are given by the same equations as derived in chapter 4; i.e. equation 4.2.14 for the

pathline characteristic and equations 4.2.15 for the left running and right running Mach line characteristics.

The final form of the compatibility equations are also given in Chapter 4; equation 4.2.28.

Discretisation of the above equations is based on the modifications to the classical method of specified time intervals (ST) (see section 4.4.1, chapter 4, for details), but bulk mixture parameters such as density and entropy are calculated by performing a pressure temperature flash. The coupling of the flow equations together with the thermodynamic and phase equilibrium equations form the basis of the CNGS-HEM model. Before the calculation procedure for this model can be presented, the important hydrodynamic constitutive relations relevant to a homogenous flow model, namely wall friction and wall heat transfer need to be addressed. All hydrodynamic constitutive relations pertaining to momentum exchange between two phases are non-existent.

5.3 FRICTIONAL FORCE EFFECTS

In all cases of depressurisation of a pipeline containing non-volatile liquid, volatile liquid or gas, the main contribution to the pressure drop in the pipeline can be attributed to frictional effects at the wall (Richardson and Saville, 1991). The longer the pipeline the greater the significance of frictional pressure drop on the transient flow profiles. Therefore an accurate representation of the friction forces acting on the fluid in the pipeline is of primary importance.

For gas flow in short and medium length pipelines, frictional effects are often small and localised, hence they have normally been considered to be relatively unimportant. However, for long pipelines, such effects can be important.

Frictional effects are, cumulative and become important for long term transients. In long pipes, they can give rise to significant pressure drop and 'line packing' under transient conditions. Modelling of frictional effects may be done either by numerically calculating the friction factor in equation (2.4.16) using known field data or by using experimental correlations. The shear stress at the wall tends to be proportional to the pressure gradient, while the average velocity may be out of phase with the pressure gradient because of the inertia of the main flow.

Assuming that the minor losses are negligible, the frictional force can be expressed by the empirical relation

$$\beta = -2\frac{f_w}{D}\rho u|u| \qquad (5.3.1)$$

As the transients progress, and the high frequency content of the pressure waves dies out, a point is reached where the explicit procedure is no longer suitable. An implicit procedure that allows large time-steps is more appropriate.

Despite the importance of pressure drop in these transient flow situations, and the consequent extensive research into this topic, there is still no satisfactory method for calculating frictional pressure drop, especially for two-phase flows. The most popular methods are often cumbersome, heavily dependent on empirically determined coefficients, and have considerable uncertainty (Thorley and Tiley, 1987). Simpler

forms or firmer theoretical bases for predictive methods can only be achieved with a narrowing of the ranges of applicability.

At the fluid wall interface, the presence of the viscous drag force can be modelled as a linear combination of unsteady and steady wall drag or friction. The significance of each of these effects on the fluid flow is now discussed.

5.3.1 Unsteady Wall Friction

Unsteady wall friction has been known to be important in transient one-dimensional liquid flow, particularly, in affecting pressure propagation in a pipe. It is well known that quasi-steady state wall friction alone under-predicts the attenuation of pressure wave propagation in a pipe (Holmboe and Rouleau, 1967). Zielke (1968) has shown that in transient laminar flow, the shear stress at the pipe wall can be written as a combination of steady state drag and a transient component,

$$\tau_w = \frac{16\mu u}{\rho D} + \frac{8\mu}{\rho D}\int_0^t W(t-t')\frac{\partial u}{\partial t}(t')dt' \qquad (5.3.2)$$

where,

$$\eta = \frac{4\mu t}{\rho D^2}$$

$$W(t) \equiv \overline{W}(\eta)$$

$$\overline{W}(\eta) = \begin{cases} 0.282095\eta^{-0.5} - 1.25 + 1.057855\eta^{0.5} + 0.9375\eta + \\ 0.3967\eta^{1.5} - 0.351563\eta^{2} \quad \text{for } \eta \le 0.02; \\ e^{-26.3744\eta} + e^{-70.8493\eta} + e^{-135.0198\eta} + e^{-218.9216\eta} \\ + e^{-322.5544\eta} \quad \text{for } \eta > 0.02. \end{cases} \qquad (5.3.3)$$

In the above correlation, the transient component is a time integral and its evaluation requires the storage of all previous flow velocity gradient. This requires enormous computer capacity and therefore the calculation process is rather cumbersome.

Hirose (1971) extended the correlation of Zielke into turbulent flow. He developed an empirical weighting function to adapt the method characteristics which is very simple compared to the analytical expression for laminar flow based on Zielke's approach.

This approach was further developed by Trikha (1975) who proposed the following approximation for the time integral,

$$\int_0^{t+\Delta t} W(t-t')\frac{\partial u}{\partial t}(t')dt' = w_1(t+\Delta t) + w_2(t+\Delta t) + w_3(t+\Delta t) \qquad (5.3.4)$$

where,

$$w_i(t+\Delta t) = w_1(t)e^{-n_i\left(4\mu/\rho D^2\right)\Delta t} + m_i e^{-n_i\left(4\mu/\rho D^2\right)(\Delta t/2)}\left[u(t+\Delta t)-u(t)\right]$$

$$n_1 = 26.4, n_2 = 200, n_3 = 8000$$

$$m_1 = 1, m_2 = 8.1, m_3 = 40 \qquad (5.3.5)$$

Equation 5.3.5 enables the calculation of the time integral explicitly in terms of the previous time-step velocity only and is based on the method of characteristics, so it is well suited for use in conjunction with the CNGS-HEM model.

Both Zielke and Trikha's methods give good predictions for the pressure wave attenuation data of Holmboe and Rouleau (1967). These authors concluded in their study that for viscous liquids, the frequency dependent shear term is valid and can accurately predict the distortion and decay of transients in the laminar flow regime. They also showed however that for low viscosity liquids such as water a frictionless solution is just as valid, especially in cases of water hammer. The drawback as far as the use of these correlations for highly turbulent flow as experienced in a pipeline

following FBR, is that they are only applicable in the laminar flow regime. In addition, pipe roughness is not taken into account.

Chen (1993) used Trikha's approximation to Zielke's correlation, equation 5.3.3 to assess the significance of unsteady frictional effects in modelling Edward's and O'Brien's (1970) blowdown experiments of sub-cooled water lines. It is shown that the unsteady wall friction reaches a maximum of 5% of the steady wall friction immediately following rupture, but then decreases rapidly to less than 0.01% of the steady wall friction after 0.001s. Based on this study, Chen concludes that unsteady wall friction is negligible in high pressure blowdown problems.

The effect of transient wall friction in turbulent liquid flow was first studied by Wood and Funk (1970). They showed that unsteady wall friction is a factor of 2.5 larger than steady wall friction at a Reynolds number of 10000, but it diminishes quickly to only 40% of the steady wall friction at Reynolds number of 35000. At higher Reynolds numbers, the effect can be expected to be even smaller, but no further data is presented.

Kagawa et. al. (1983) developed a model which requires less computer storage and computation than Zielke's exact model, yet is more accurate than Trikha's approximation model. Kagawa's weighting function is derived by approximating Zielke's function with a series of first-order lag elements.

By comparing predictions with experimental data, Budny et. al. (1990) concluded that frequency-dependent friction factor for laminar flow based o Zielke's equation can be extended into the transition zone and beyond, at least to a Reynolds number of 11,000 and is capable of predicting the decay over many cycles.

Yigang and Jing-Chao (1990) developed a new approach for simulating frequency-dependent terms both in the frequency and time domain by using the method of non-linear square integral optimum. Because this new method is optimised over a large frequency range and requires fewer terms of the first order lag elements than Kagawa's model, it is computationally efficient and accurate in both frequency and time simulations. The model is appropriate for analysing the frequency and transient responses, pressure surges, and pressure attenuation in hydraulic pipelines. In the

Trikha and Kagawa models, the frequency dependent friction equation in the time domain includes an unknown current flow rate. Therefore an interactive algorithm is needed to calculate the frequency-dependent friction in the MOC, which makes the simulation complex and time consuming. The Yigang-Jing-Chao method does not need any iterations and requires only half of the computation time of Trikha and Kagawa models.

Eichinger and Lein (1992) proposed and investigated two new methods of presenting the unsteady friction term, one method being based on wall shear stress and the other on friction power.

The formula for unsteady friction term based on wall shear stress is solely dependent on the value of the gradient of velocity in the near wall region. In this case, calculation of the velocity profile near the wall is necessary. This is particularly true in turbulent flow because as the Reynolds number increases, so does the gradient near the wall.

On the other hand the formula for the friction term based on the friction power is based on consideration of energy of the incompressible fluid. The difference between the work of the internal and external forces, and of the kinetic energy of a volume element of an incompressible fluid is the friction dissipation per unit of time. Preliminary investigations by Eichinger and Lein (1992) revealed that friction factor based on wall shear stress gave considerably better results.

Vardy et. al. (1993) show that expressions similar to that developed by Zielke for transient laminar friction in pipes, is justified both theoretically and experimentally for transient turbulent friction. They develop the idea of a family of Curves, one for each value of the product of friction factor, pipe diameter and Reynolds number (fDRe). The Zielke expression is shown to be an asymptotic limit of the family of weighting function Curves. However the correlations are only valid for smooth pipes.

From the review carried out in this study, it seems that there is still some uncertainty in the accurate prediction of unsteady friction factor in rough pipes where highly turbulent flows prevail. Moreover from the few studies performed to date (Wood and Funk, 1970; Chen, 1993) the effect of the unsteady component in wall shear stress

calculations seems to diminish in magnitude the greater in turbulence the flow becomes.

In the absence of any theoretically and experimentally justified transient turbulent friction calculation for rough pipes, it has been decided to ignore this component in the model proposed in this study. The effect of this approximation will be evaluated by comparing the results of the simulation with field data (see section 5.9).

The advantage of using a method of characteristics solution for FBR as indeed for any transient flow scenario is that any unsteady state friction factor correlation such as that given from equations 5.3.4-5.3.5 can easily be incorporated. (see for example Zielke, 1968;Trikha, 1975; Brown, 1969; Eichinger & Lein, 1992 ; Vardy et. al., 1995, 1996).

5.2.2 Steady Flow Friction Factor

For the calculation of unsteady flow in pipes, the steady state friction term is usually used, and can produce acceptable results although it is well known that this term does not describe the real physical phenomenon accurately. Perhaps it is reasonable to expect this to be valid for small perturbations around a steady flow condition and some experimental evidence exists to support this. However this would not be expected to be true in the case of large and rapid disturbances.

Flatt (1985) and Van Deen and Reintsema (1983) argue that the friction factor is weakly dependent on Reynolds number, and may be considered as constant at high Re ($> 10^7$) typically encountered during FBR.

Thorley and Tiley (1987) use a constant friction term in the modelling of unsteady transient flow of compressible fluids in relatively short pipelines with a reasonable degree of accuracy.

The effect of utilising either a steady flow friction factor or a flow dependent friction factor on modelling FBR particularly for a long pipeline containing a condensable gas is investigated by comparison with experimental data in section 5.8.1.

5.2.3 Flow Dependent Friction Factor

Friction factor is dependent on the type of flow which may vary from point to point in a pipeline, and in addition on pipe roughness. The traditional way of estimating the friction factor for a Newtonian fluid flowing through a pipe is based on the well known Moody Friction Chart. This however is unsuitable for computer simulations and therefore explicit correlations are sought.

For fully developed turbulence, the 'rough pipe law' (Perry and Green, 1997) which assumes that the friction factor is solely dependent on the pipe roughness and size is used.:

$$\frac{1}{\sqrt{f_w}} = 2A_1 \log\left(\frac{D}{\varepsilon}\right) B_1 \qquad (5.3.6)$$

where f_w is the fanning friction factor, and A_1 and B_1 are constants.

For partially developed turbulence either the smooth pipe law (Perry and Green, 1997) or the Blasius form of the smooth pipe law are used. Here the friction factor is assumed to be only dependent on the fluid properties and pipe size. The smooth pipe law is traditionally expressed as,

$$\frac{1}{\sqrt{f_w}} = 2A_2 \log\left(2\,\mathrm{Re}\sqrt{f_w}\right) B_2 \qquad (5.3.7)$$

The Blasius form of the smooth pipe law is given as,

$$f_w = \frac{A_3}{4}\mathrm{Re}^{B_3} \qquad (5.3.8)$$

where A_2, B_2, A_3 and B_3 are all constants.

The above equation is applicable only over a very limited range of Re. For the transition zone between partially and fully developed turbulence a combination of both the rough and smooth pipe laws is used. The Colebrook equation (Perry and Green, 1997) has been universally adopted for this regime.

The key factor in applying a flow-dependent friction factor is the determination of which flow regime is prevalent at a particular point and time. Typical high-pressure

gas pipeline flows are characterised by their high Reynolds numbers. The key decision to be made for such flows therefore, is whether it can be assumed that fully developed turbulence has been achieved, so that the rough pipe law which is independent of Reynolds number and hence flow may be employed. For partially developed turbulent and transition zone flow however, the friction factor would vary with changes in Reynolds number.

Many expressions exist for calculating friction factor with respect to the transition zone from partially to fully developed turbulent flow. The most accurate to date, based on agreement with experimental data, is the Colebrook equation (Perry and Green, 1997). It presents results within 5% of experimental data, though its major disadvantage is that the solution for the friction factor requires iteration, i.e. it is non-explicit and hence not practical for use in a computer simulation.

An extensive review of nineteen explicit friction factor equations was presented by Zigrang and Sylvester (1985). They classified the equations according to precision, into three categories, namely, simple, intermediate and high precision equations. The equations were compared for precision against the Colebrook equation, in the range $2500 \leq Re \leq 10^7$ and $4\times10^{-5} \leq \varepsilon \leq 0.005$. All the equations in the intermediate and high precision categories were found to give rise to relative errors well within 1% of the Colebrook equation (within 6% of experimental data).

In this study, the Moody (Massey, 1983) approximation to the Colebrook equation is used,

$$f_w = 0.001375\left[1+\left(20000\frac{\varepsilon}{D}+\frac{10^6}{Re}\right)^{\frac{1}{3}}\right] \qquad (5.3.9)$$

which is valid for $Re \geq 2000$.

For $Re \leq 2000$, the following well established laminar flow correlation is employed,

$$f_w = \frac{16}{Re} \qquad (5.3.10)$$

where the Reynolds number is given by,

$$Re = \frac{\rho u D}{\mu} \tag{5.3.11}$$

where μ is the fluid viscosity.

In their review, Zigrang and Sylvester (1985) categories the Moody (Massey, 1983) approximation as an intermediate precision formulation. It is chosen instead of a high precision equation because its relative simplicity means that it involves less CPU time, but difference in accuracy is only a maximum of 1%.

Other friction factor expressions that have been used for transient fluid flow analysis are those of Chen (1979) and Churchill (1977). The convenience of these correlations are that they cover the whole range of Reynolds numbers and pipe roughness, and produce results of almost the same accuracy as those produced by the Colebrooke equation. The Chen equation was used by Bisgaard et. al. (1987) in modelling the transients as a result of rupture of high pressure gas pipeline. It has the advantage of being simpler than the Churchill equation, yet producing the same accuracy of results (Chen, 1979) .

In this study the Chen (1979) equation for friction factor is compared with predictions obtained using the Moody approximation, equation 5.3.9. The Chen correlation is,

$$\frac{1}{\sqrt{f_w}} - 4.0\log\left[\frac{\varepsilon}{3.7065D} - \frac{5.0452}{Re}\log\left(\frac{1}{2.8257}\left(\frac{\varepsilon}{D}\right)^{1.1098} + \frac{5.8506}{Re^{0.8981}}\right)\right] \tag{5.3.12}$$

5.3.4 Friction factor for two-phase homogeneous flow

The friction resulting from the viscous boundary at the wall is similar to the single phase one. It is usually represented by the single phase wall friction multiplied by a two-phase multiplier (Friedel, 1979) or with single phase variables replaced by some two-phase mixture variables (Egely and Saha, 1984). A comparative study of two-phase frictional pressure drops is given by Idsinga et. al. (1979).

For a two-phase mixture, the wall friction is assumed to arise from the liquid phase only, so that f_{wg}, the gas friction part is zero.

When the two-phase multiplier is used, the wall friction pressure drop is written in terms of the liquid friction factor,

$$\beta = -2\phi_{lo}^2 \frac{f_{wl}}{D} \rho u|u| \tag{5.3.11}$$

where f_{wl} is the liquid friction factor and ϕ_{lo}^2 is the two-phase multiplier.

The liquid friction factor can be calculated from any single phase friction factor equation such as equation 5.3.9 or equation 5.3.10.

ϕ_{lo}^2 is given by the following correlation of Friedel (1979),

$$\phi_{lo}^2 = B + \frac{3.24FH}{Fr^{0.045} We^{0.035}}$$

$$B = (1-\chi)^2 + \chi^2 \frac{\rho_l f_{wg}}{\rho_g f_{wl}}$$

$$F = \chi^{0.78}(1-\chi)^{0.224}$$

$$H = \left(\frac{\rho_l}{\rho_g}\right)^{0.91} \left(\frac{\mu_g}{\mu_l}\right)^{0.19} \left(1-\frac{\mu_g}{\mu_l}\right)^{0.7}$$

$$Fr = \frac{G^2}{gD\rho_m^2}$$

$$We = \frac{G^2 D}{\sigma \rho_m} \tag{5.3.12}$$

where χ is the fluid quality, σ is the surface tension, G is the mass flowrate and Fr and We are the Froude and Weber numbers respectively. The subscripts g, l and m refer to gas, liquid and mixture properties respectively.

The other alternative to calculating two-phase momentum loss due to friction is based on replacing single phase properties by mixture properties. It is only suitable for homogeneous flows where both phases move at the same velocity so that,

$$\beta = -2\frac{f_{wm}}{D}\rho_m u|u| \tag{5.3.13}$$

where f_{wm} is the two-phase mixture friction factor and can be determined either by equation 5.3.9 or equation 5.3.10 where the following substitutions are made for flow parameters,

$$Re = Re_m = \frac{\rho_m u D}{\mu_m} \tag{5.3.14}$$

The mixture density can be calculated from equation 2.5.29, see chapter 2.

The mixture viscosity is given by,

$$\frac{1}{\mu_m} = \frac{\chi}{\mu_g} + \frac{(1-\chi)}{\mu_l} \tag{5.3.15}$$

The gas and liquid viscosities are calculated according to the Ely and Hanley scheme for non-polar gaseous mixtures, and the Dymond and Assael scheme for liquid mixtures (Assael et. al., 1996).

The merits of either method with regard to accuracy has been tested by Chen (1993) with relation to the depressurisation of Edwards and O'Briens (1970) blowdown experiments of subcooled water lines. He shows that both methods do not vary significantly in their blowdown predictions.

The advantage of the method whereby the single phase properties are replaced by two-phase mixture properties is that no additional calculation needs to be performed for surface tension. In this study, this method is therefore preferred to the Friedel method.

5.4 WALL HEAT TRANSFER

It was shown in Chapter 4 that the inclusion of a heat transfer term in the conservation equations is important when simulating depressurisation from long pipelines over a long duration. Heat transfer occurs by means of forced convection through the turbulent boundary layer of the gas in the pipe, conduction through the pipe wall, by natural convection outside the pipe, and radiation to the surroundings.

In terms of the effect on fluid dynamics during FBR, heat transfer is expected to have a much smaller impact than frictional forces. For this reason, as an approximation, the external heat transfer at the wall is modelled in the same way as for a permanent gas,

$$q_h = \frac{4}{D} U_h \left(T_\infty - T\right) \qquad (5.4.1)$$

The above equation assumes that the pipe wall thickness is small and that the pipe wall is at the same temperature as the fluid.

The true heat transfer coefficient varies with the flow conditions, e.g. flashing or condensing flow, and necessitates different correlations for different conditions. A constant heat transfer coefficient of 5 W/m^2K and 100 W/m^2K for lagged and non-lagged pipes respectively are used.

5.5 THE INITIAL CONDITION

5.5.1 Steady State Flow

In Chapter 4 the equations for the steady state isothermal flow for an ideal gas were derived. The corresponding equations for a real fluid are presented here. The energy equation is redundant since temperature remains constant. The steady state conservation equations of mass and momentum are exactly the same as for the ideal gas, see equations 4.5.1 and 4.5.2 in section 4.5. However the equation of state for a real fluid will include a compressibility factor, so by differentiating the equation of state with respect to ρ, we get,

$$d\rho = \frac{dP}{ZRT} \tag{5.5.1}$$

Performing the same algebraic manipulation as in section 4.5, the following equations for a real fluid are used to describe isothermal steady state flow:

Pressure drop

$$\Delta P = \frac{\beta}{\left[1 - \frac{u^2}{ZRT}\right]} \Delta x \tag{5.5.2}$$

$$P_i = P_{i-1} + \frac{\beta_{i-1}}{\left[1 - \frac{u^2}{ZRT}\right]_{i-1}} \Delta x$$

Change in velocity as a result of this pressure drop,

$$\Delta u = -\frac{u}{\rho ZRT}\Delta P$$

$$u_i = u_{i-1}\left(1-\frac{\Delta P}{(\rho ZRT)_{i-1}}\right) \tag{5.5.3}$$

The density and speed of sound of the fluid at the required grid point can be obtained by performing a pressure-temperature flash based on the isothermal temperature, and pressure as calculated from equation 5.5.2.

5.5.2 Rupture Plane Calculation at t=0

Two separate procedures are used for determining the rupture plane boundary condition at t=0 depending on the type of fluid present in the pipeline prior to rupture.

For a gas pipeline, the assumption of isentropic expansion as used in Chapter 4 is utilised. In such a case, there is isentropic expansion flow over the first Δx mesh, with the outflow conditions calculated according to Riemann variables.

Taking the Riemann invariant along the positive characteristic, λ_+,

$$w_2 = u + \int a(\rho)\frac{d\rho}{\rho} = u + \int \frac{dP}{\rho a} \tag{5.5.4}$$

When FBR occurs, a decompression process at the initial pressure P_{in} is initiated. If the new pressure after a decompression of ΔP is P, then the local fluid velocity at that point in the decompression process is given by,

$$u = -\int_{P_{in}}^{P} \frac{dP}{\rho a} \tag{5.5.5}$$

The flow properties u, ρ and a are those of the bulk fluid. An analytical solution to the above is not possible for a real gas, unlike an ideal gas. If the pipeline fluid is a non-ideal multi-component dense gas mixture which may form a liquid phase during decompression, then the thermodynamic relationship between ρ, a and P becomes highly non-linear (see Chapter 2 for thermodynamic relationships). Consequently, equation 5.5.5 can only be solved numerically as done by Groves et. al. (1978) and Picard and Bishnoi (1988) in the following manner.

Expressing equation 5.4.5 in finite difference form,

$$u_{r+1} = u_r - \left[\frac{P_{r+1} - P_r}{(\rho a)_r}\right] \tag{5.5.6}$$

where r shows the current level of decompression and r+1 denotes the new level resulting from an incremental decompression step.

In this study the new pressure is taken as,

$$P_{r+1} = 0.95P_r \tag{5.5.7}$$

The calculation procedure for the boundary condition at the rupture plane at t=0 is as follows:

- Starting the decompression process at the initial pressure, P_{in} and temperature, T_{in} calculate the bulk density and speed of sound by performing an isothermal flash, making a note of the initial entropy (kept constant throughout the decompression process)
- calculate the new fluid pressure and velocity using equations 5.5.7 and 5.5.6 respectively. Perform an isentropic pressure-entropy flash based on the initial entropy and the new pressure to obtain new density and speed of sound. Compare the new speed of sound, a_{r+1}, and velocity u_{r+1} . If velocity is less than speed of sound then repeat calculation until $u_{r+1}=a_{r+1}$, when the fluid conditions at the rupture plane are known based on an isentropic decompression.

Thus making the above assumption of isentropic flow over the first Δx, the initial conditions for a multi-component non-ideal gas mixture are calculated.

In the case of FBR of a pipeline containing a volatile liquid such as an LPG mixture (used for validation purposes in this thesis), the initial pressure of the liquid falls almost immediately to the saturation pressure which for this fluid is greater than atmospheric pressure. Hence gas evolution starts immediately and the decompression process during the transition from compressed liquid to saturated liquid can be assumed to be isothermal.

5.6 CALCULATION PROCEDURE FOR CNGS-HEM

5.6.1 Interior point calculation

In this section the calculation procedure for CNGS-HEM at t >0 for an interior point in the discretisation grid is given. The grid structure for numerical discretisation of the compatibility equations is ST (see section 4.4.1), and the CNGS with the same specifications as outlined in chapter 4, section 4.6.1 is used. The solution procedure for the first order method is first outlined followed by that for the second order curved characteristics.

In the ST grid, solution points are forced to coincide with a specific grid pattern. The Mach and pathlines are extended backwards to intersect the previous time level grid line. The location of the points of intersection, p and n, for the positive and negative Mach lines respectively, are located by solving a set of simultaneous equations for u_p, a_p and u_n, a_n using derivations based on linear interpolation and characteristic equations (see section 4.4.1). The location of the pathline intersection is calculated just on the basis of linear interpolation and characteristic equation for u_o.

Once the positions of points p, o, and n are determined, the values of P and T are calculated at each location by linear interpolation. An isothermal pressure-temperature flash is then performed at each location to ascertain the bulk density and φ at all points p, o and n, and for the point o, also the value of the speed of sound. The latter can be calculated in such a manner since there is no prior requirement to calculate the location of point, o unlike points, p and n where linear interpolation is used to estimate the speed of sound. The term ψ is also calculated at each location based on φ determined from a flash calculation.

Once all the flow conditions are known at points p, o and n, then the compatibility equations can be solved for density, pressure and velocity as shown in section 4.4.1. To calculate the temperature at the solution point, an iterative numerical scheme to solve the following equation is employed,

$$\rho_j - \rho\left(T_j^r, P_j\right) = 0 \qquad (5.6.1)$$

where P, ρ and T are pressure, density and temperature respectively. The subscript, j denotes conditions at the solution point, and the superscript, r relates to the unknown temperature.

Solution of equation 5.6.1 becomes a root finding problem where a temperature is sought to match the density obtained from the compatibility equations to that calculated from an isothermal pressure-temperature flash.

This is achieved using the method of Brent (Brent, 1973, Press et. al, 1994). It combines root bracketing, bisection and inverse quadratic interpolation to converge from the neighbourhood of a zero crossing. The bracketing of the root is performed by a routine which, given a function such as equation 5.5.1 and an initial guessed range for the root, expands the range geometrically until a root is bracketed by the returned values (see the ZBRAC routine in Press et. al. 1994). The above combines the robustness of bisection with the speed of a higher-order method when appropriate. Based on our experience of using this technique for FBR simulation, it produces rapid convergence.

Once the temperature is obtained at the solution point, the speed of sound and the parameter φ is found by a flash calculation.

The above steps are repeated until convergence is achieved for the dependent variables, P, ρ and u.

For the second order method, the same procedure is adopted, except for quadratic interpolation equations replacing linear equations. A block diagram indicating the various steps involved in shown in figure 5.6.1.

5.6.2 Rupture Plane Calculation at t>0

The calculation at the ruptured end for a two-phase mixture will be slightly different than that for a permanent gas as detailed in Chapter 4. Since no algebraic relationship exists for the speed of sound of a two phase mixture, simultaneous solution of the positive and pathline compatibility equations is not possible (see section 4.4.1.3).

Calculation procedure

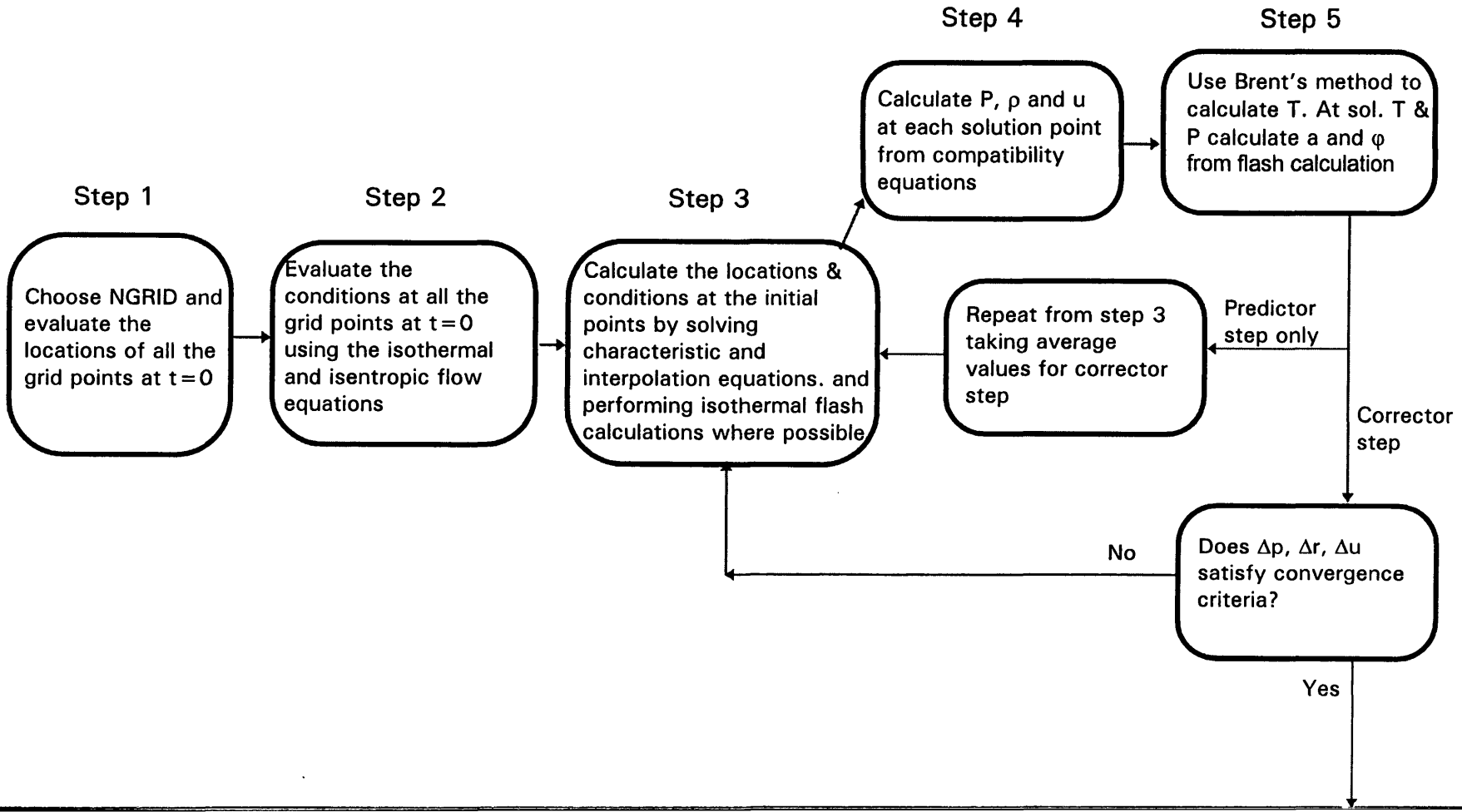

The negative or left running characteristic at the rupture plane will be vertical (the gradient, 1/(u-a) is infinity), and hence perpendicular to the x-axis as shown in figure 5.6.2 below.

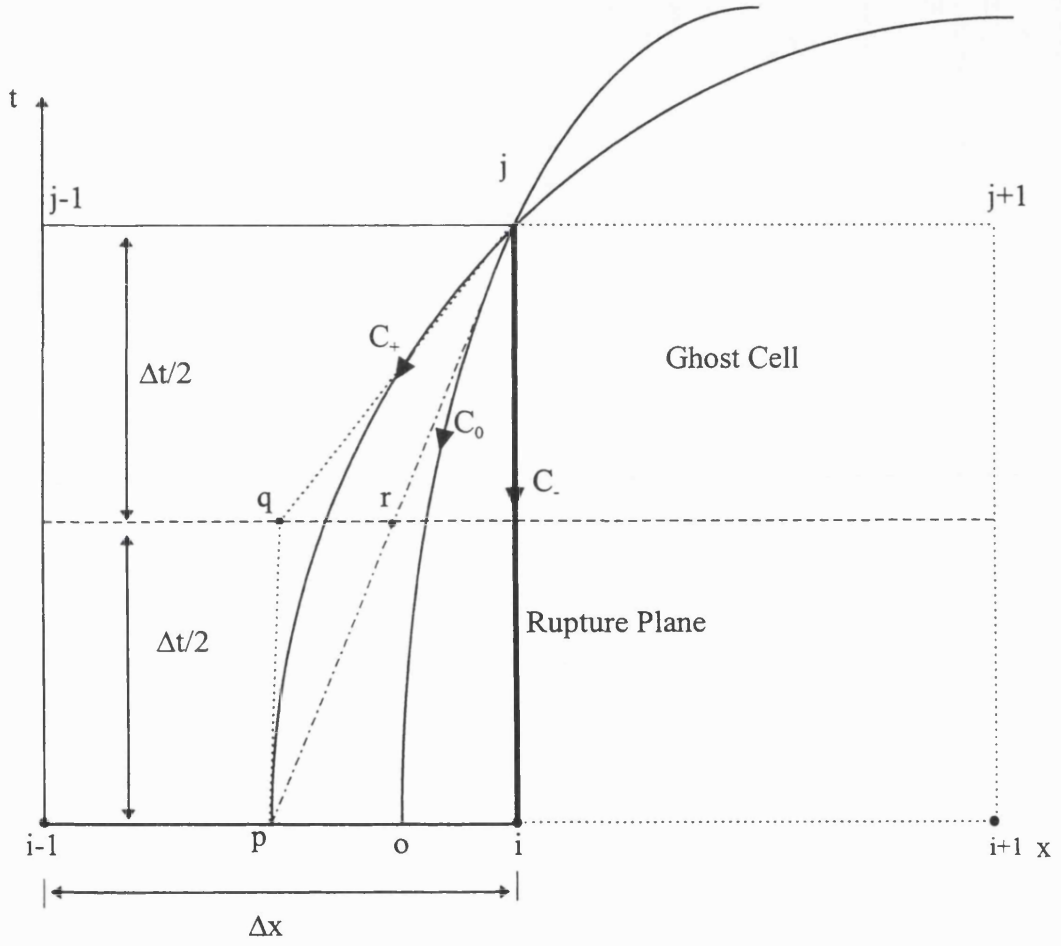

Figure 5.6.2: Three characteristic curves at the rupture plane

Since the negative Mach line is vertical, the conditions at the previous time level, x_i are already known so that the negative compatibility equation becomes,

$$P_j - P_i - \frac{1}{2}\left((\rho a)_i + (\rho a)_j\right)\left(u_j - u_i\right)$$

$$= \frac{1}{2}\left((\psi - a\beta)_i + (\psi - a\beta)_j\right)\left(t_j - t_i\right) \qquad (5.6.2)$$

This compatibility equation can be solved together with the pathline and positive compatibility equations given by equations 4.3.9 and 4.3.11 respectively (see section 4.3). The calculation of bulk density and speed of sound is as discussed in section 5.6.1.

5.6.3 Calculation at the boundary between grids of different size

The introduction of a nested grid system in chapter 4 created boundaries between different size grids. At the junctions, the flow variables at the finer grids are linearly interpolated in time from the values on the coarse grids.

In the case of highly transient two-phase flows, however, a different technique based on direct solution is proposed.

The calculation procedure for the predictor step only is presented here. The corrector step will follow the same procedure as outlined in chapter 4.

The calculation at solution point j+4 in figure 5.6.3 is given as an example.

For the predictor step,

$$\frac{d_o t}{d_o x} = \frac{1}{u_o} = \frac{4\Delta t_1}{x_i - x_o} \Rightarrow x_o = x_i - 4\Delta t_1 u_o \qquad (5.6.3)$$

The characteristic grid at the boundary is illustrated in figure 5.6.3 below:

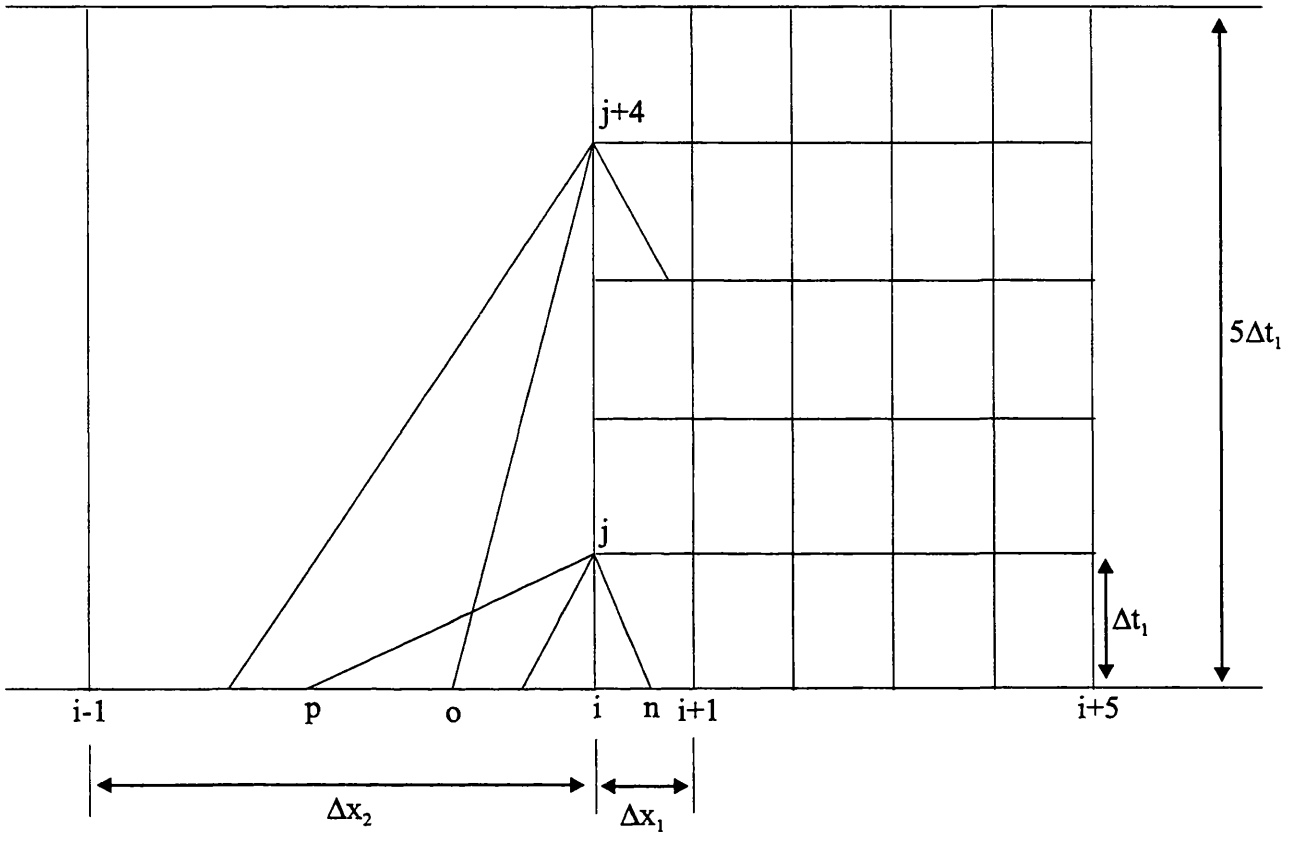

Figure 5.6.3 Boundary between fine and coarse mesh

$$\frac{d_+t}{d_+x} = \frac{1}{u_p + a_p} = \frac{4\Delta t_1}{x_i - x_p} \Rightarrow x_p = x_i - 4\Delta t_1\left(u_p + a_p\right) \qquad (5.6.4)$$

$$\frac{d\_t}{d\_x} = \frac{1}{u_n - a_n} = \frac{\Delta t_1}{x_i - x_n} \Rightarrow x_n = x_i - \Delta t_1\left(u_n - a_n\right) \qquad (5.6.5)$$

Following the same mathematical manipulation as that performed in section 4.4.1, the simultaneous equations obtained for the solution of points u_p and a_p are,

$$u_p\left(1+\frac{u_i-u_{i-1}}{\Delta x_2}4\Delta t_1\right)+\frac{u_i-u_{i-1}}{\Delta x_2}4\Delta t_1 a_p = u_i \tag{5.6.6}$$

$$a_p\left(1+\frac{a_i-a_{i-1}}{\Delta x_2}4\Delta t_1\right)+\frac{a_i-a_{i-1}}{\Delta x_2}4\Delta t_1 u_p = a_i \tag{5.6.7}$$

Similarly a 2×2 system of equations can be set up for u_n and a_n based on the same mathematical manipulation to yield,

$$u_n\left(1+\frac{u_{i+1}-u_i}{\Delta x_1}\Delta t_1\right)-\frac{u_{i+1}-u_i}{\Delta x_1}\Delta t_1 a_n = u_i \tag{5.6.8}$$

$$a_n\left(1+\frac{a_{i+1}-a_i}{\Delta x_1}\Delta t_1\right)-\frac{a_{i+1}-a_i}{\Delta x_1}\Delta t_1 u_n = a_i \tag{5.6.9}$$

The solution for u_o depends on the direction of fluid flow.

If $\lambda_o > 0$ then,

$$u_o = \frac{u_i}{\left(1+\frac{u_i-u_{i-1}}{\Delta x_2}4\Delta t_1\right)} \tag{5.6.10}$$

If $\lambda_o < 0$,

$$u_o = \frac{u_i}{\left(1+\frac{u_{i+1}-u_i}{\Delta x_1}\Delta t_1\right)} \tag{5.6.11}$$

The locations of x_p, x_n, and x_o can now be calculated directly from equations 5.6.3 to 5.6.5 by substituting the calculated values for u_p, a_p, u_n, a_n, and u_o from the above equations.

The values of P and T at the three initial points are then calculated using the interpolation equations, 4.4.6 to 4.4.8. The density, ρ, and speed of sound, a, can then be calculated by performing an isothermal flash.

All the initial point flow variables are now available to compute the flow conditions at the solution point j.

For the positive compatibility,

$$P_j - P_p + (\rho a)_p (u_j - u_p) = (\psi + a\beta)_p 4\Delta t_1 = K_1 \qquad (5.6.12)$$

The negative compatibility,

$$P_j - P_n - (\rho a)_n (u_j - u_n) = (\psi - a\beta)_n \Delta t_1 = K_2 \qquad (5.6.13)$$

The pathline compatibility if $\lambda_o > 0$,

$$P_j - P_o - (a^2)_o (\rho_j - \rho_o) = \psi_o 4\Delta t_1 \qquad (5.6.14)$$

The pathline compatibility if $\lambda_o < 0$,

$$P_j - P_o - (a^2)_o (\rho_j - \rho_o) = \psi_o \Delta t_1 \qquad (5.6.15)$$

Solving equations 5.6.12 and 5.6.13 simultaneously for u_j we can write,

$$u_j = \frac{K_1 - K_2 + (\rho a)_p u_p + (\rho a)_n u_n + P_p - P_n}{(\rho a)_n + (\rho a)_p} \qquad (5.6.16)$$

The above equation has the same form as that for an ideal gas (see equation 4.4.26 in section 4.4.1.1).

The pressure is calculated either from equation 5.6.12 or equation 5.6.13. The density at the solution point can now be obtained from the pathline compatibility, if $\lambda_o > 0$, then,

$$\rho_j = \frac{\left(P_j - P_o\right) + a_o^2 \rho_0 - \psi_o 4\Delta t_1}{a_o^2} \tag{5.6.17}$$

The above steps are the predictor steps. The corrector steps can be repeated according to the procedure outlined in chapter 4.

5.7 REVIEW OF RELEVANT EXPERIMENTAL DATA FOR TWO PHASE FBR SIMULATION

For obvious reasons, the amount of experimental data available relating to FBR is very scarce and the limited data that is reported is mainly confined to short (ca 100m) small diameter (ca. 0.1 m) pipelines containing single component fluids.

Chen et. al (1993) report that even with such short pipelines, except for the early stages of rarefaction wave propagation, sufficient time exists for the discharging fluid to reach thermodynamic equilibrium. Hence, such small scale experiments are expected to adequately represent the changes occurring during FBR of much longer pipelines encountered in practice. The only data which actually relate to the FBR of a long pipeline (> 5 km) are those which were taken during the Piper Alpha tragedy. The following is a review of the experimental work pertinent to FBR.

Foothills Pipeline (Yukon) Ltd. (1981) reported the results of a series of tests at their Northern Alberta Burst Test Facility. A total of six tests were performed. The main purpose of the tests was to examine the effect of gas composition on the fracture behaviour of the pipe. This renders the data unsuitable for validating FBR by the fact that, during experiment, the pipeline fracture propagates along the axial direction covering some considerable lengths. Modelling the rupture condition effectively is thus made difficult in the CNGS-HEM since the rupture boundary is assumed to be fixed.

Jones and Gough (1981) performed a series of tests under the auspices of British Gas using short pipe sections of 120ft (36.6m) length and 4in(0.1016m) diameter containing natural gas, with a bursting disk at one end. However, the very short length and small diameter of pipeline make the data unsuitable for modelling with CNGS-HEM.

Some data for long pipelines have been reported by Sens et. al. (1970). The test involved a 11.8km pipeline of internal diameter 0.1065m. However no details are provided regarding the gas composition and therefore effective validations cannot be performed in our case.

Two sets of data found to be suitable for the modelling of long pipes (≥100m) are those of intact end pressure data obtained from Piper Alpha tragedy, and a series of experiments carried out by Shell and BP on the Isle of Grain (Chen, 1993, Richardson and Saville, 1996).

In the case of the Piper Alpha FBR, the conditions prior to rupture are given in chapter 4, section 4.6. The exact fluid composition is given in the table below:

Component	**mole%**
CH_4	73.6
C_2H_6	13.4
C_3H_8	7.4
i-C_4H_{10}	0.4
n-C_4H_{10}	1.0
i-C_5H_{12}	0.08
n-C_5H_{12}	0.07
n-C_6H14	0.02
N_2	4.03

Table 5.7.1: Composition of mixture in sub-sea line from Piper-Alpha to MCP-01

Another set of data available are the Isle of Grain depressurisation tests. Two parallel pipelines, both extensively instrumented and of length 100m are used. The pipeline diameter is 150mm. Pressure transducers and thermocouples measuring fluid temperature were attached along each line. Inventory and hold-up were also measured using load-cells and neutron back scattering.

The pipelines contain commercial propane or LPG. This usually comprises a mixture of propane and other low molecular weight hydrocarbons, such as butane and ethane.

The exact composition is not given, but Chen (1993) assumes a mixture of 95 mole% propane and 5 mole% butane.

Both the steady and transient tests that take place were initiated by rupture of a disc at the downstream end of the pipeline. A series of tests simulating small bore to full bore rupture were performed. Of the transient full bore tests, tests P40 and P42 are chosen for validation with the present CNGS-HEM model. The relevant conditions are,

Test	**Initial LPG pressure (Bara)**	**Initial LPG temperature (C)**	**Ambient air temperature (C)**
P40	21.6	17.8	19.1
P42	11.3	20.0	18.6

Table 5.6.2: Initial and ambient conditions for LPG tests

5.8 OPTIMISATION OF CNGS-HEM

In this section, the CNGS-HEM model will be optimised in terms of accuracy and CPU time minimisation in conjunction with Piper Alpha data.

The above will involve investigating the influence of various approaches such as the CNGS (chapter 4, section 4.6.1), curved characteristics (second order solution), and the effect of various Δt. As a test for accuracy, an HEM based on a simple grid scheme (SGS-HEM) model as used in chapter 4, is set up to provide a means for comparison.

The effect of the use of curved characteristics in the region of phase transition is also discussed.

5.8.1 Convergence and accuracy of first and second order solutions

To ascertain the most suitable method of solution, a series of tests were performed with SGS-HEM, and first and second order CNGS-HEM to investigate the effects on CPU times and accuracy. All simulations were performed on a DEC Alphaserver 8400 5/440 running at 440MHz.

All thermodynamic information required by the model (including gas-liquid phase behaviour), is provided by the Peng-Robinson equation of state. Real fluid departures from idea gas behaviour are also determined from this equation (see chapter 2).

The introduction of a real fluid equation of state and subsequent calculation of component mass balances at each node in the discretisation grid renders the calculation very slow. For example, performing a sample calculation over 1 Δt using the permanent gas model CNGS with a coarse grid Δx_3 (see figure 4.6.2) of 500 metres takes 0.65 seconds on a 100MHz Pentium PC, whereas the same calculation using CNGS-HEM takes 85.63 seconds. As a means of providing a test for the converged solution, it would be most appropriate to use a Δx of 1m all the way along the pipeline as was the case in chapter 4. However, this is very impractical in terms of the extra computation time for the HEM. As a result, the reference solution to

which comparisons are made is taken to be that provided by the SGS-HEM with a uniform Δx of 10m.

Figure 5.8.1 shows the results of release rate versus time over a depressurisation period of 450 seconds. Curve A shows the results for the 2nd order curved characteristics solution for CNGS-HEM with a coarse grid Δx of 500m. Curve B shows the results for the 2nd order solution with Δx of 250m, Curve C shows the first order solution with Δx of 250m and finally, Curve D shows the results for the SGS-HEM model with a Δx of 10m (reference solution).

The first order CNGS-HEM solution (Curve C) consistently underestimates release rate whereas both second order solutions give better agreement with the SGS-HEM. For the second order solutions, increase in Δx does not lead to a significant loss of accuracy, but savings in CPU times are significant. Based on this test, the 2nd order CNGS-HEM with a grid spacing, Δx_3 of 500m is chosen for the validation tests.

Both second order solutions exhibit a certain amount of oscillation, with the amplitude of oscillation increasing with Δx. Further increase in Δx can be expected to lead to greater oscillation and is therefore not tested. This oscillatory phenomenon in second order solutions is well documented (Hirsch, 1995). The important point to note is that these oscillations, even at a Δx_3 of 500m, are not intense as reported by Picard and Bishnoi (1989).

Although a first order solution is attempted by Picard and Bishnoi (1989) for the modelling of a hypothetical break to a sour gas pipeline, they still report diverging oscillations in pressure and density values with eventual termination of the simulation. The authors claim that these oscillations can be controlled by using a critical grid spacing equivalent to 0.5 nodes per metre of pipeline.

This implies that the application of a grid spacing of greater than 2 metres would give rise to a divergent solution. This trend is clearly not reproduced in our study, either in the first order or the second order solution. A stable solution is obtained in each case as it is evident in figure 5.8.1.

One possible reason for the greater stability of the present model is the use of an isothermal pressure-temperature flash to calculate the bulk mixture density (see

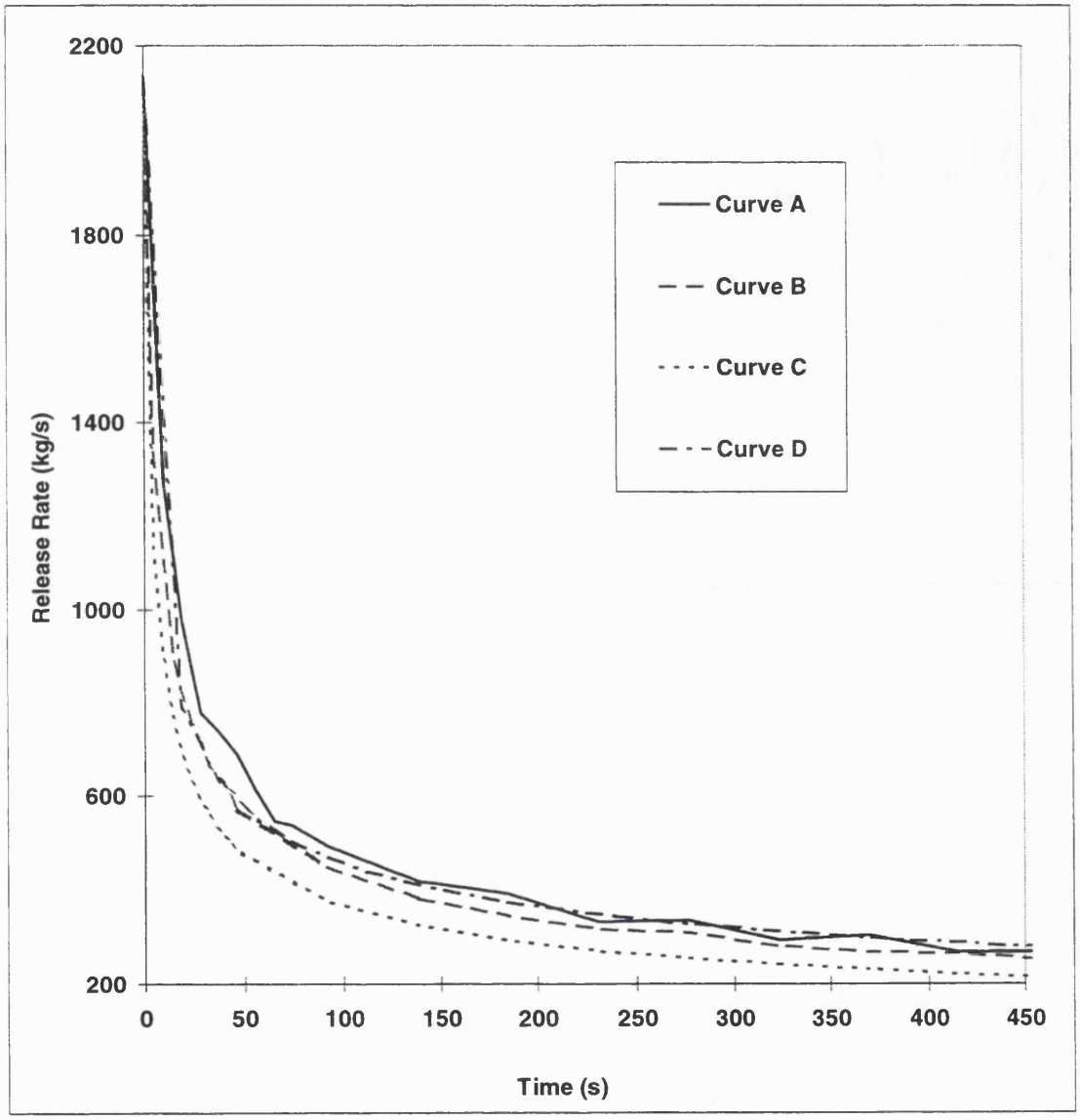

Figure 5.8.1: Release rate profiles for different grid settings
Curve A; 2nd order, Δx = 500m, CPU time = 3.75 hours
Curve B; 2nd order, Δx = 250m, CPU time = 12.2 hours
Curve C; 1st order, Δx = 250m, CPU time = 12.1 hours
Curve D; 1st order simple, Δx = 10m, CPU time = 250hours

One possible reason for the greater stability of the present model is the use of an isothermal pressure-temperature flash to calculate the bulk mixture density (see section 5.4) at the locations p, o and n (see figure 4.4.2) on the previous time level. The linear interpolation technique employed by Picard and Bishnoi (1988, 1989) to calculate mixture density might not necessarily correspond to that obtained by solving the equation of state at the interpolated values of pressure and temperature. The discrepancy is likely to be further exacerbated in the highly transient flow area that exists near the rupture plane.

The argument that second order curved characteristics alleviates this type of numerical instability is not appropriate because both first and second order CNGS-HEM are stable. As a check, a first order CNGS-HEM is run over a longer period (2000s) of depressurisation for the Piper Alpha FBR. No stability problem is encountered. It can be said however that a second order solution that takes into account curved characteristics is likely to give better predictions near the rupture plane (see figure 5.8.1).

Another interesting phenomenon that needs addressing when dealing with a fluid undergoing a phase change during depressurisation is the abrupt change in speed of sound on crossing the gas/liquid phase transition interface. This places an additional restriction, in addition to that given by the CFL criterion, on the choice of Δt.

5.8.2 Effect of Δt on flow predictions

In a study by Picard and Bishnoi (1987) on a numerical procedure for the prediction of the acoustic velocity in two-phase multi-component fluids, a sudden reduction in expansion wave velocity was observed at approximately the calculated dew point. The sudden drop in the speed of sound can be attributed to the fact that as a second phase forms, the compressibility of the fluid decreases abruptly.

Figure 5.8.2 shows a plot of variation of predicted sound velocity for a range of temperatures along various isobars for the Piper Alpha mixture. Curve A shows the

isobar of 80 bar, and Curves B and C show the isobars corresponding to 70 and 60 bar respectively.

The procedure for the calculation of the sound velocity is given in chapter 2 and is the same as that proposed by Picard and Bishnoi (1987).

The sudden drop in speed of sound coincides with the onset of condensation in the mixture. The higher the pressure, the greater the drop in sound velocity. The high speeds of sound are obtained for gas phase flows and the onset of two phase condensate flows causes a sudden reduction in the expansion wave velocity, the magnitude of which will vary depending on mixture. On either side of the sharp transition however, the variations in the speed of sound are relatively linear.

Figure 5.8.3 shows the variation of predicted fluid density for a range of temperatures along various isobars for the Piper Alpha mixture. Curve A shows the isobar of 80 bar, and Curves B and C show the isobars corresponding to 70 and 60 bar respectively; the same ranges over which the phase transition from single phase to two phase takes place.

Unlike the speed of sound predictions, the variation of density does not exhibit a step like change across the phase boundary but the overall behaviour is non-linear.

A boundary between a gas and two-phase can be termed as a condensation boundary whereas that between liquid and two phase can be termed as a boiling boundary. Either boundary may have a velocity faster or slower than the fluid velocity during depressurisation. The basic assumptions in dealing with such interfaces are firstly that a distinct interface exists and secondly that no mixing occurs across any such interface.

The presence of the interface between a single phase and a two-phase mixture poses problems from a computational viewpoint for two reasons.

Firstly, the substantial difference in acoustic velocities between the two different states (depending on the difference in compressibility) means that if the characteristic lines were to cross such an interface, significant refraction would occur as schematically represented in figure 5.8.4 for a left travelling interface.

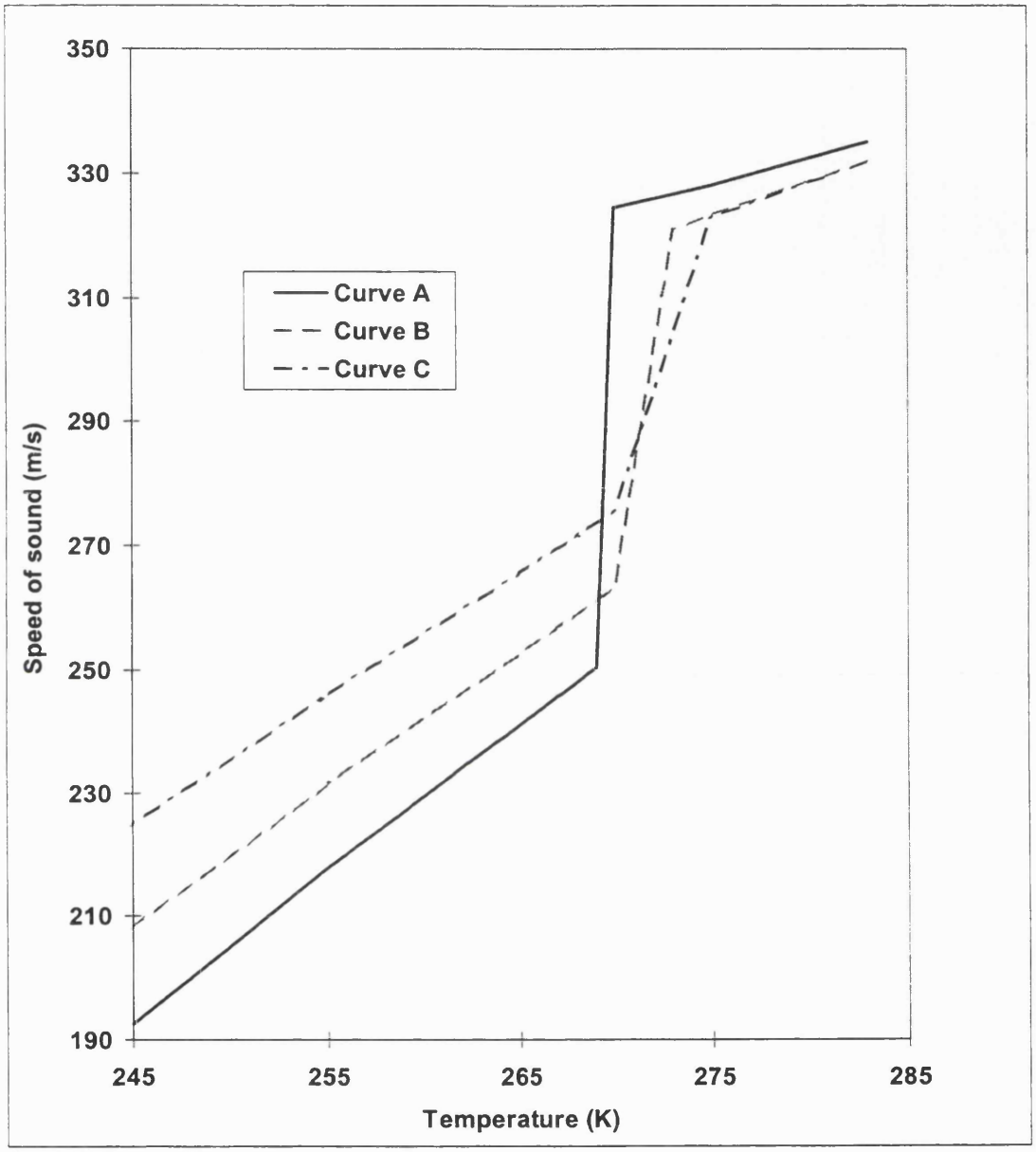

Figure 5.8.2: Variation of speed of sound with temperature along various isobars for the Piper Alpha mixture

Curve A: P = 80 Bar
Curve B: P = 70 Bar
Curve C: P = 60 Bar

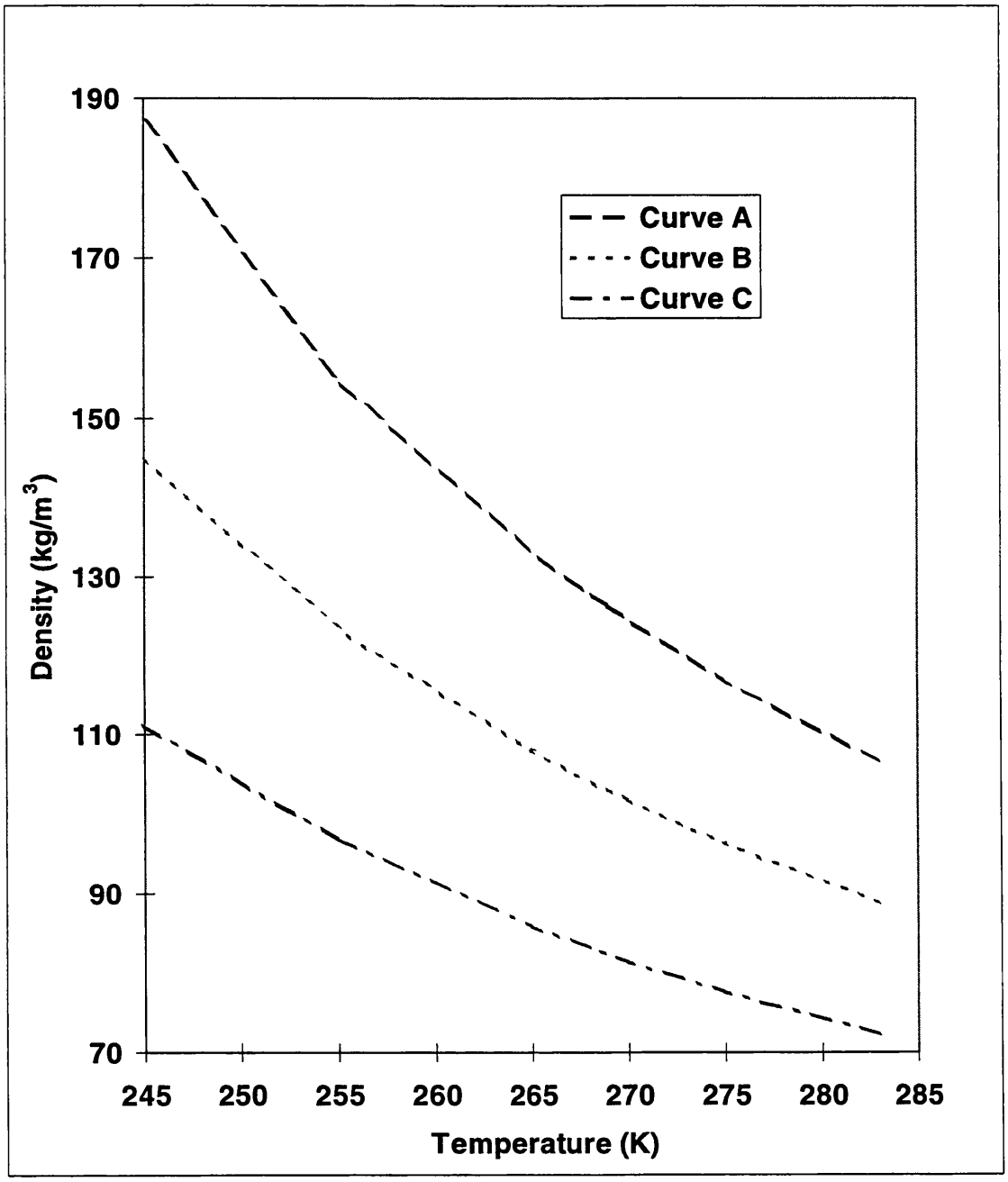

Figure 5.8.3: Variation of predicted fluid density for a range of temperatures along various isobars for the Piper Alpha mixture.

Curve A: P = 80 Bar
Curve B: P = 70 Bar
Curve C: P = 60 Bar

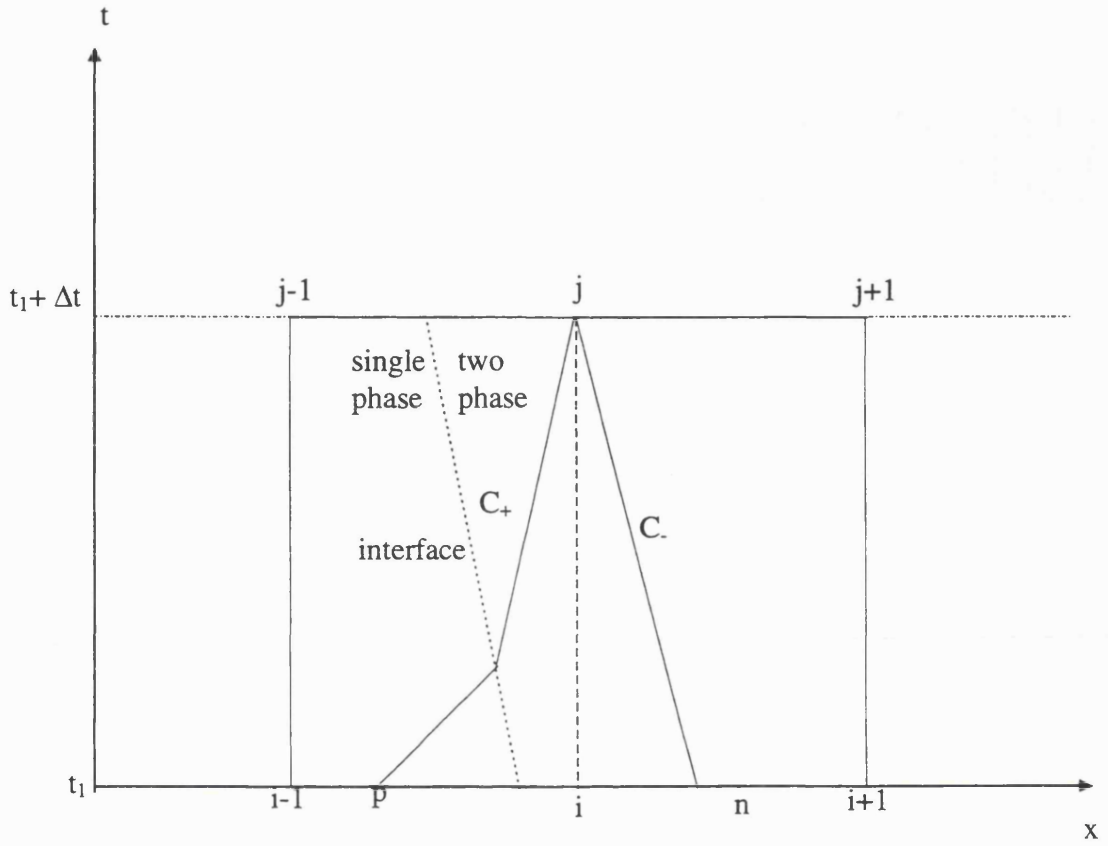

Figure 5.8.4: Refraction effect of single phase/two phase interface on characteristic lines

The propagation velocity of the positive Mach line is greater in a single phase than in a two phase mixture so that the gradient ($\Delta t/\Delta x$) will be steeper in two phase flow than in single phase flow. The reverse is true for the negative Mach line.

Secondly, other fluid properties may change significantly across an interface so the compatibility equations have to account for the presence of an interface (Nakamura et. al., 1975). The added complexity of the mathematical modelling that is necessary to fully account for this phenomena is avoided in this study by using a small enough

Δt to effectively minimise the error caused by the refraction of characteristic lines. This is explained below.

The maximum possible Δt, Δt_{max} in keeping with the CFL criterion is given by equation 4.6.1. In the CNGS models a Δt that is 90% of this maximum permissible is taken for all tests performed (see chapter 4). For a permanent gas model, this criterion is valid as sound velocity variations are linear. To understand the effect of taking a smaller Δt, it is first necessary to look at the effect Δt has on the characteristic lines.

For both first and second order solutions, the values of the velocity, u, and speed of sound, a, need to be calculated a priori before the locations of points p and n can be calculated (see sections 4.4.1 and 4.4.2 for the first and second order solutions respectively). In the first order solution for example, in order to calculate the location of point p, i.e. is the point of intersection of the positive Mach line on the previous time line, the following two equations, as shown in chapter 4 but repeated here for reference, are solved simultaneously for u_p and a_p,

$$u_p\left(1+\frac{u_i-u_{i-1}}{x_i-x_{i-1}}\Delta t\right)+\frac{u_i-u_{i-1}}{x_i-x_{i-1}}\Delta t a_p = u_i \qquad (4.4.13)$$

$$a_p\left(1+\frac{a_i-a_{i-1}}{x_i-x_{i-1}}\Delta t\right)+\frac{a_i-a_{i-1}}{x_i-x_{i-1}}\Delta t u_p = a_i \qquad (4.4.14)$$

Once u_p and a_p are known, the location of x_p is calculated from,

$$x_p = x_i - \Delta t\left(u_p + a_p\right) \qquad (5.8.1)$$

Using a smaller Δt has the effect of pushing the location of x_p closer to that of x_i where the exact conditions are known and so flow values are likely to be close to those at x_i, thus minimising interpolation errors. This effect is illustrated in figure 5.8.5.

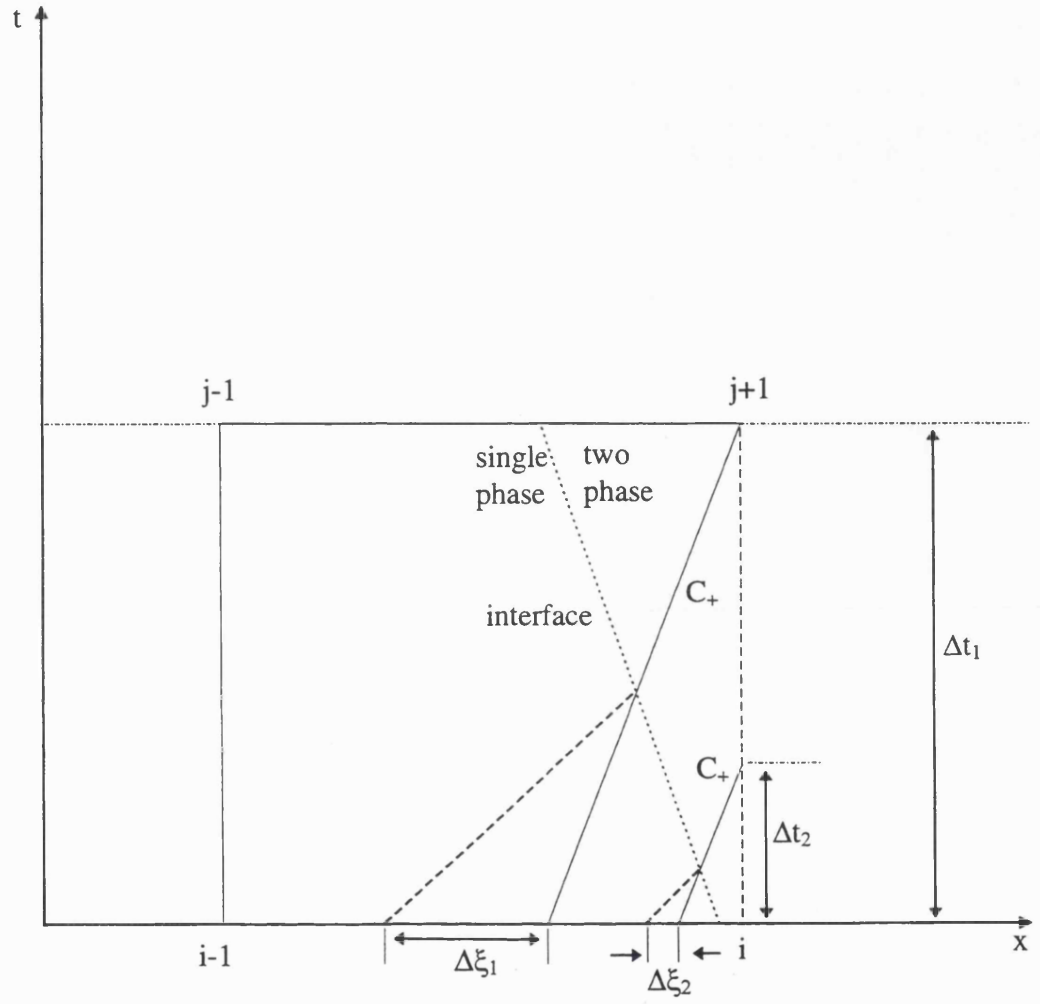

Figure 5.8.5: Effect of smaller Δt on resulting accuracy of prediction of point p

The broken lines indicate the refracted characteristics whilst the straight characteristic line denotes the first order solution.

Δt_2 is smaller than Δt_1 and results in a smaller interpolation error $\Delta \xi_2$.

Quantification of errors caused by presence of the phase transition interface is carried out in the following manner. A cell is located where the node at x_i has a two phase condensate whereas the node at x_{i-1} has a single phase gas. The values of u_p and a_p are calculated for a chosen Δt from equations 4.4.13 and 4.4.14 and the corresponding location of x_p is calculated from equation 5.8.1. Once x_p is found, the pressure, temperature and density are calculated from linear interpolation. The interpolated values of pressure and temperature are used to perform an isothermal flash calculation and the calculated results for bulk mixture density and speed of sound are compared with the interpolated values to check accuracy. This procedure is repeated for several different Δt's satisfying the CFL criteria.

Figure 5.8.6 elucidates the above by showing the effect of % of maximum permissible Δt on the % errors in density (Curve A) and speed of sound (Curve B) predictions. Errors in the prediction of density through interpolation are consistently higher, up to 60% of maximum permissible Δt after which there is a sudden increase in the errors associated with the linear interpolation calculation of speed of sound. The generally higher errors associated with the linear interpolation prediction of fluid density can be attributed to its overall non-linear variation with pressure and temperature as shown in figure 5.8.3.

The sudden increase in errors pertaining to the calculation of speed of sound is a consequence of the refraction of the Mach line at the phase transition interface. If the same Δt as used in the permanent gas model (i.e. 90% of maximum permissible, Δt_{max}) is to be used then errors of about 33% and 16% can be expected for the calculation of speed of sound and density respectively. It must be stressed that this error is only for the cell containing the interface between different phases which in most cases of pipeline depressurisation would account for only one cell on any given time level. The data in figure 5.8.6 indicate that an unacceptably small Δt is required in order to reduce the error introduced by calculating density using linear interpolation to agreeable levels.

The error arisen in the determination of density through linear interpolation can of course be eliminated by calculating it directly via an isothermal flash. In itself, this

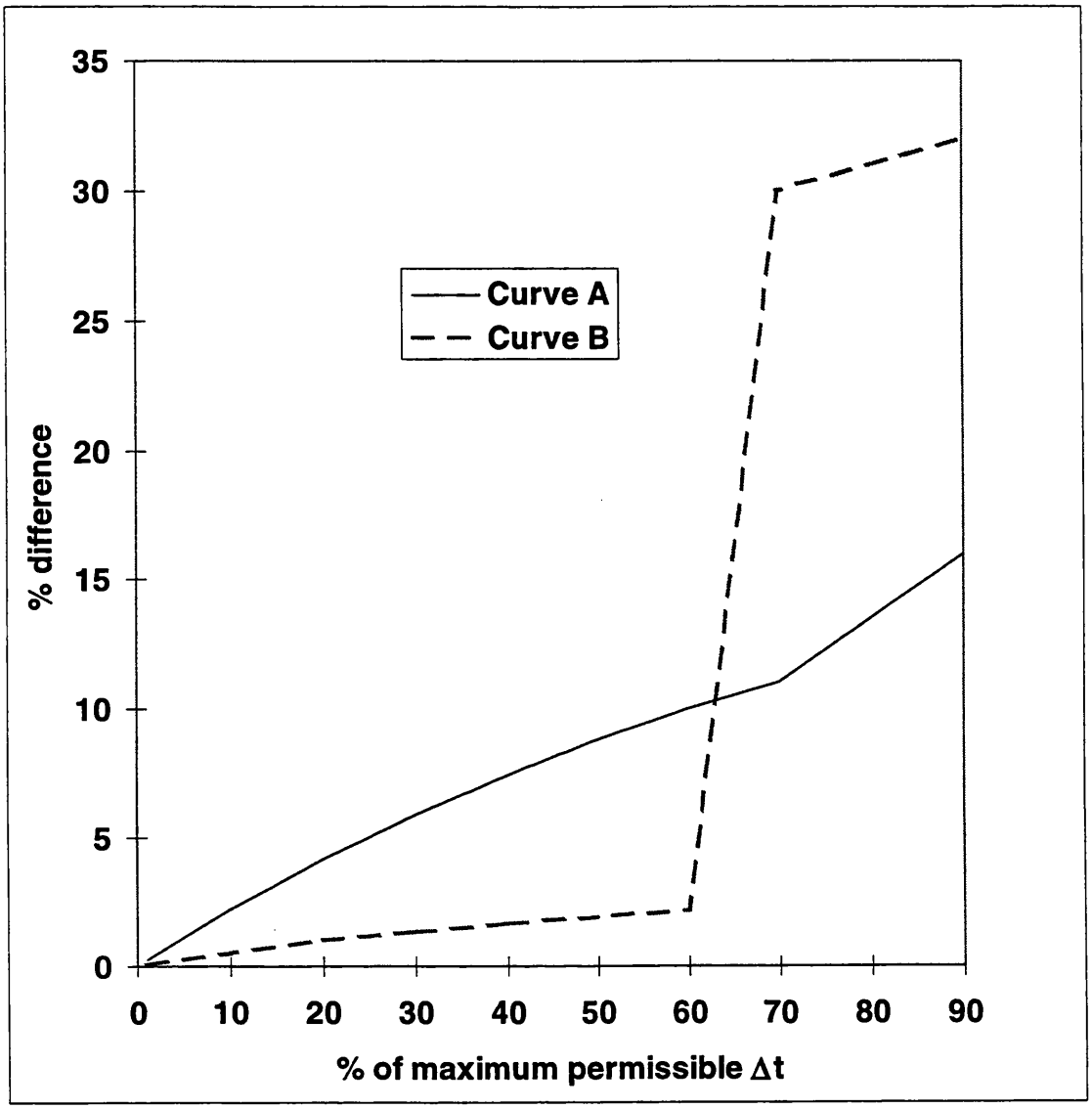

Figure 5.8.6: The effect of % of maximum permissible Δt on the % errors in density and speed of sound predictions (Piper Alpha mixture).

Curve A: Density
Curve B: Speed of sound

would give rise to an increase in CPU as compared to obtaining density using linear interpolation. However, our experience has shown the fact that the much larger Δt that can now be afforded gives rise to a significant overall reduction in CPU.

The error in the calculation of speed of sound remains, since it is obtained by simultaneous solution of equations 4.4.13 and 4.4.14 for point p, and equations 4.4.15 and 4.4.16 for point n. However, the discrepancy is minimised by utilising a small Δt. For point, o (figure 4.4.2), however, since the value of acoustic velocity is not needed to find x_o, it is calculated by performing a flash calculation.

With regards to other cells away from the phase transition cell, the errors associated with calculating speed of sound at a given cell using linear interpolation are not expected to be as significant as inferred from figure 5.8.2. These can be anything up to a maximum of 1-3% for $\Delta t = 0.9 \times \Delta t_{max}$ depending on proximity to the rupture plane. The discrepancy is significantly lower for smaller Δt's (<1%). However, the cumulative effect of such errors can become significant thus giving rise to spurious results especially in the late time regime.

The effect of Δt is also particularly acute at the rupture plane in terms of maintaining the choking condition for homogeneous flow, u = a (see section 5.5.2 for details). The rupture plane calculation is unique in that it is the only occasion when flash and flow calculations are coupled so that the thermodynamic speed of sound is compared with the outflow velocity obtained from the flow equations (compatibility equations). When using a $\Delta t = 0.9 \times \Delta t_{max}$, the predicted outflow velocity is underestimated in respect to the predicted sound velocity by anything up to about 40%. It is necessary to reach a $\Delta t = 0.1 \times \Delta t_{max}$ before the choking condition can accurately be satisfied (underestimation is less than 1%). The choice of Δt to uphold the choking condition will very much depend on the mixture present. Thus for any new mixture, a calculation needs to be done to check the optimum Δt.

Figure 5.8.7 shows the effect of two different Δt's on release rate profiles for the Piper Alpha FBR. Curve A shows the results obtained from the CNGS-HEM model with $\Delta t = 0.9\Delta t_{max}$ whereas Curve B shows the results obtained using a $\Delta t = 0.1\Delta t_{max}$.

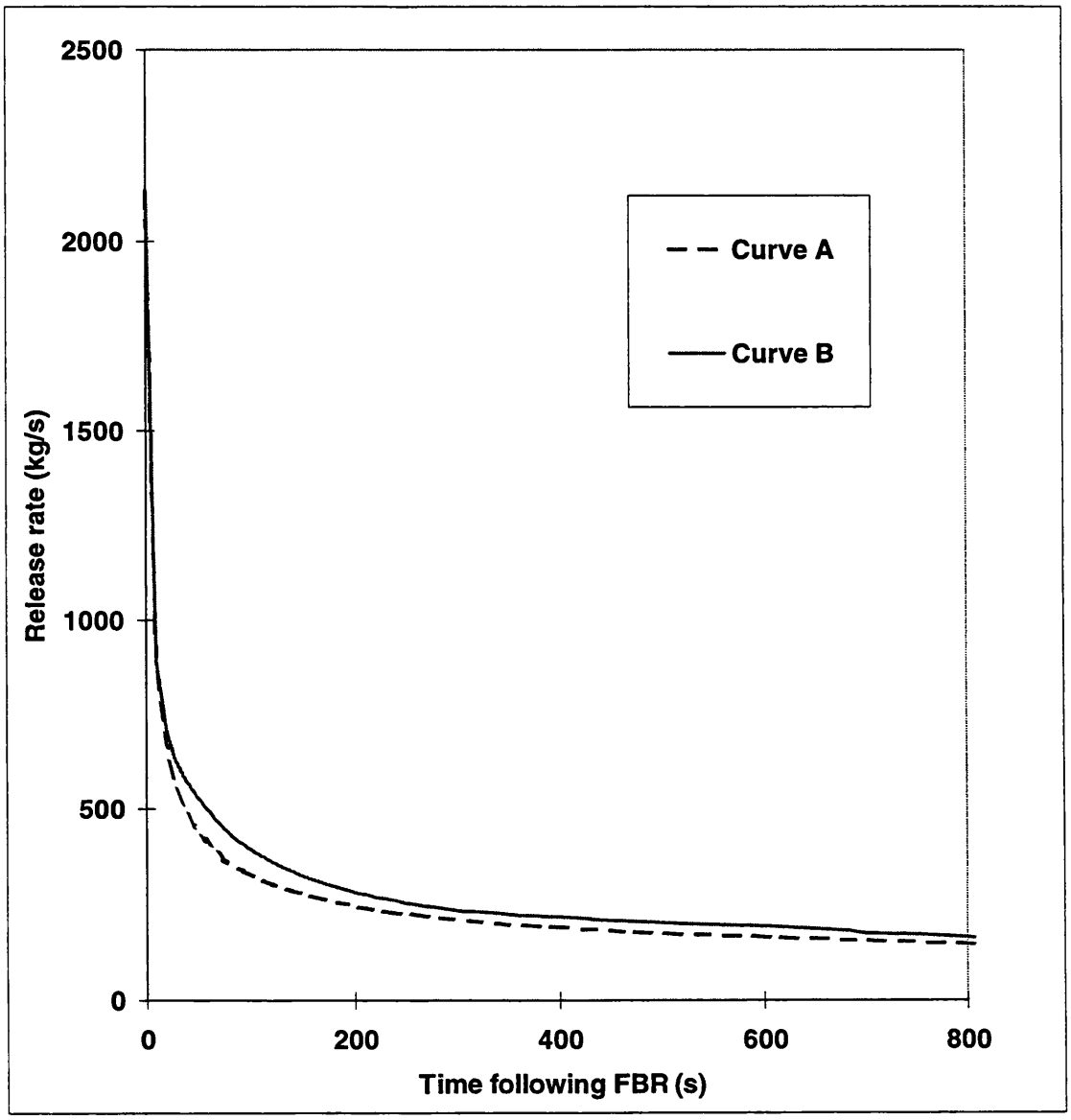

Figure 5.8.7: Release rate profiles for different Δt settings (Piper Alpha mixture).
Δx_3 = 500m, Δx_2 = 100m, Δx_1 = 20m
Curve A; $\Delta t = 0.9\Delta t_{max}$, CPU time = 7.5 hours
Curve B; $\Delta t = 0.1\Delta t_{max}$, CPU time = 40 hours

When necessary, the outflow velocity at the rupture plane is replaced by the thermodynamic sound speed.

Using a large Δt (Curve A) gives rise to an underestimation of release rate due to the discrepancies mentioned above. The significant increase in CPU is due to the fact that the model with $\Delta t = 0.1\Delta t_{max}$ has to perform nine times as many calculations as compared with $\Delta t = 0.9\Delta t_{max}$ to reach a specific time. However, CPU times are less than this ratio for the former due to better convergence in the fast transient region near the rupture plane. In fact for $\Delta t = 0.1\Delta t_{max}$, we find that just one iteration of the corrector step is needed before convergence is obtained. $\Delta t = 0.9\Delta t_{max}$ requires at least two.

Greater accuracy can be expected if a smaller Δt is employed, but this will lead to an even greater increase in CPU time. For relatively short pipelines, an even smaller Δt becomes more practical. For the Piper Alpha simulation, $\Delta t = 0.1\Delta t_{max}$ provides a good accuracy (see section 5.9) in a reasonable time scale for the purposes of this study.

The scenario might arise in some cases where the interface reaches the closed end boundary and a single phase exists throughout the pipeline. It should then be possible to use a larger Δt (within the CFL criterion) since the added restriction placed by the presence of a fluid interface is lifted. This would then require the construction of a variable grid with different time steps.

5.9 VALIDATION OF CNGS-HEM

5.9.1 Rupture of Piper to MCP-01 subsea line

Figure 5.9.1 shows the predicted intact end pressure/time history for the Piper Alpha to MCP-01 subsea line.

Also shown are the measured data taken during release on the night of the disaster; Curve A. Curves B,C, and D show the results predicted by CNGS-HEM (section 5.6 and 5.8), CNGS-HEM-CF and CNGS (section 4.6.1) respectively.

CNGS-HEM-CF refers to the HEM with a constant friction factor of 0.00324 as is also the case in the ideal gas model, CNGS. All the models considered here have the following grid spacings, Δx_3=500m, Δx_2=100m, and Δx_1=20m, and for the HEM $\Delta t = 0.1\Delta t_{max}$ which corresponds to a time step of 0.103 seconds.

The CNGS-HEM makes provision for a flow dependent friction factor by utilising the Chen (1979) friction factor equation. No data is provided for the roughness of the pipe, and hence the value corresponding to that for carbon steel (ε=0.004mm) (Perry and Green, 1997) is used in this study.

The largest discrepancy is obtained from the ideal gas model which demonstrates the importance of accurate prediction of real fluid effects in any study regarding FBR of pipelines containing multi-component fluids. However the difference in CPU times is staggering (1.5 minutes compared to 6 days). Hence for the particular system studied for a quick reasonable estimate of the effects of FBR, a permanent gas model ma be useful.

Very good agreement is obtained using the CNGS-HEM (Curve B) as opposed to the CNGS-HEM-CF (Curve C). This proves the importance of accurate prediction of friction factor for long pipelines. The results for CNGS-HEM shows a slight deflection at about 1518s. This corresponds to the onset of condensation at the closed end as indicated in figure 5.9.2. The formation of the liquid phase has a significant effect on friction factor because of increased viscous drag which is only accounted for by CNGS-HEM.

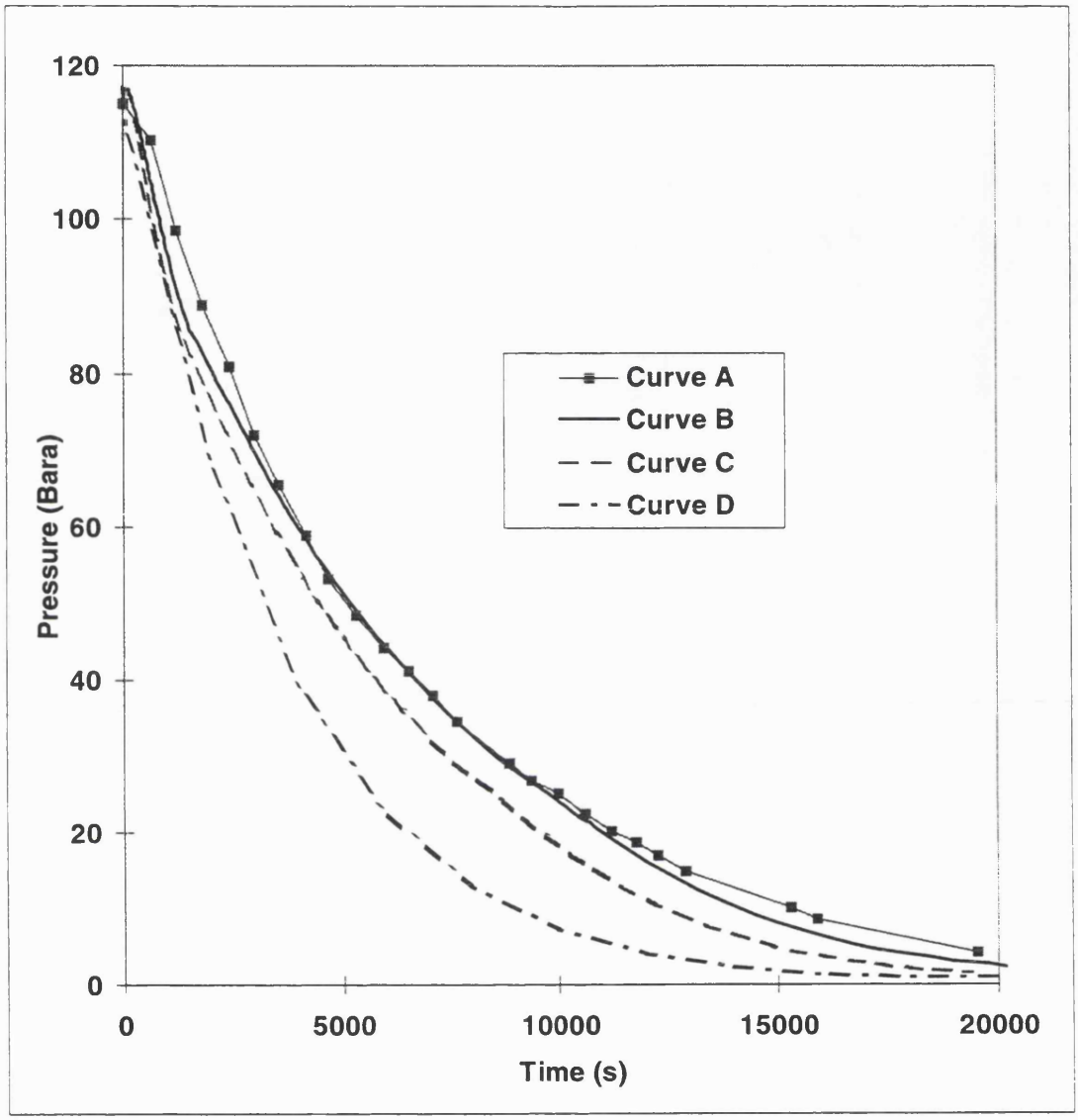

Figure 5.9.1: Comparison of intact end pressure (Piper Alpha)
$\Delta x_3 = 500m$, $\Delta x_2 = 100m$, $\Delta x_1 = 20m$

Curve A: Measurement
Curve B; CNGS-HEM, CPU time = 6days
Curve C; CNGS-HEM-CF, CPU time = 5.5 days
Curve D; CNGS, CPU time = 1.5 minutes

Returning to figure 5.9.2, Curves A and B show the data obtained using the CNGS-HEM and Chen at. al.'s (1993) META-HEM respectively. It is interesting to note that the two sets of data are in good accord. The maximum liquid volume fraction is ca. 0.034 corresponding to a liquid mass fraction of about 15%. As the pipeline continues to depressurise, less inventory stays in the liquid phase and at about 10,100s following FBR the closed end is exposed to gas only.

Figure 5.9.3 shows the phase envelope for the Piper-Alpha mixture. It may be observed that the two-phase region covers a relatively wide range of pressures and temperatures. This is due to the fact that the mixture is made up of many components. For a mixture containing fewer components, the two-phase region can be expected to be narrower. The extent of two-phase flow formation during any depressurisation process is determined by the thermodynamic path followed by pressure and temperature.

Figure 5.9.4 shows the variation of release rate with time.

Curve A shows the data generated using the META-HEM whereas Curves B and C show the corresponding data using CNGS-HEM and CNGS respectively. The results of CNGS-HEM and META-HEM are in good agreement, with the latter predicting a slightly higher release rate. The discrepancy increases with depressurisation time. However both methods predict much higher release rates than the CNGS model.

5.9.2 FBR experiments using LPG at the Isle of Grain

The validation for Piper Alpha showed that the CNGS-HEM gives good accuracy when modelling FBR of pipelines containing a predominantly gaseous mixture. To test the applicability of the CNGS-HEM for a flashing liquid mixture, the experimental data of BP and Shell Oil Isle of Grain (Richardson and Saville, 1996, Chen, 1993) are used as a basis for comparison. Tests P40 and P42 (see section 5.6), in particular, are selected as they relate to FBR.

In both tests, a diaphragm covering the whole pipe cross-section is ruptured. The pertinent experimental conditions including pipeline dimensions, and material compositions as well as starting temperature and pressure were given in section 5.6.

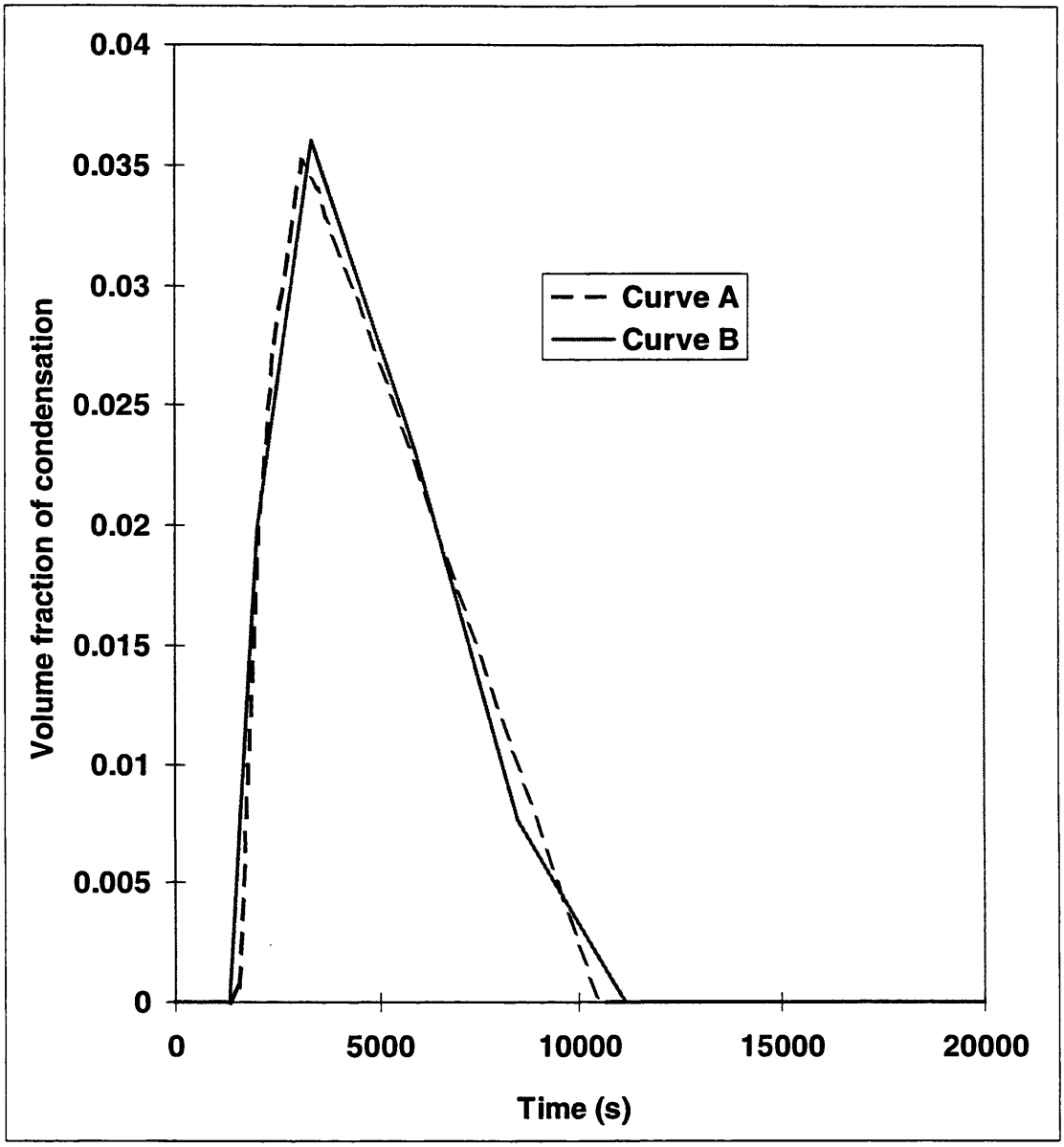

Figure 5.9.2: Comparison of condensation volume fraction at closed end of pipe (Piper Alpha)

Curve A: CNGS-HEM
Curve B: META-HEM

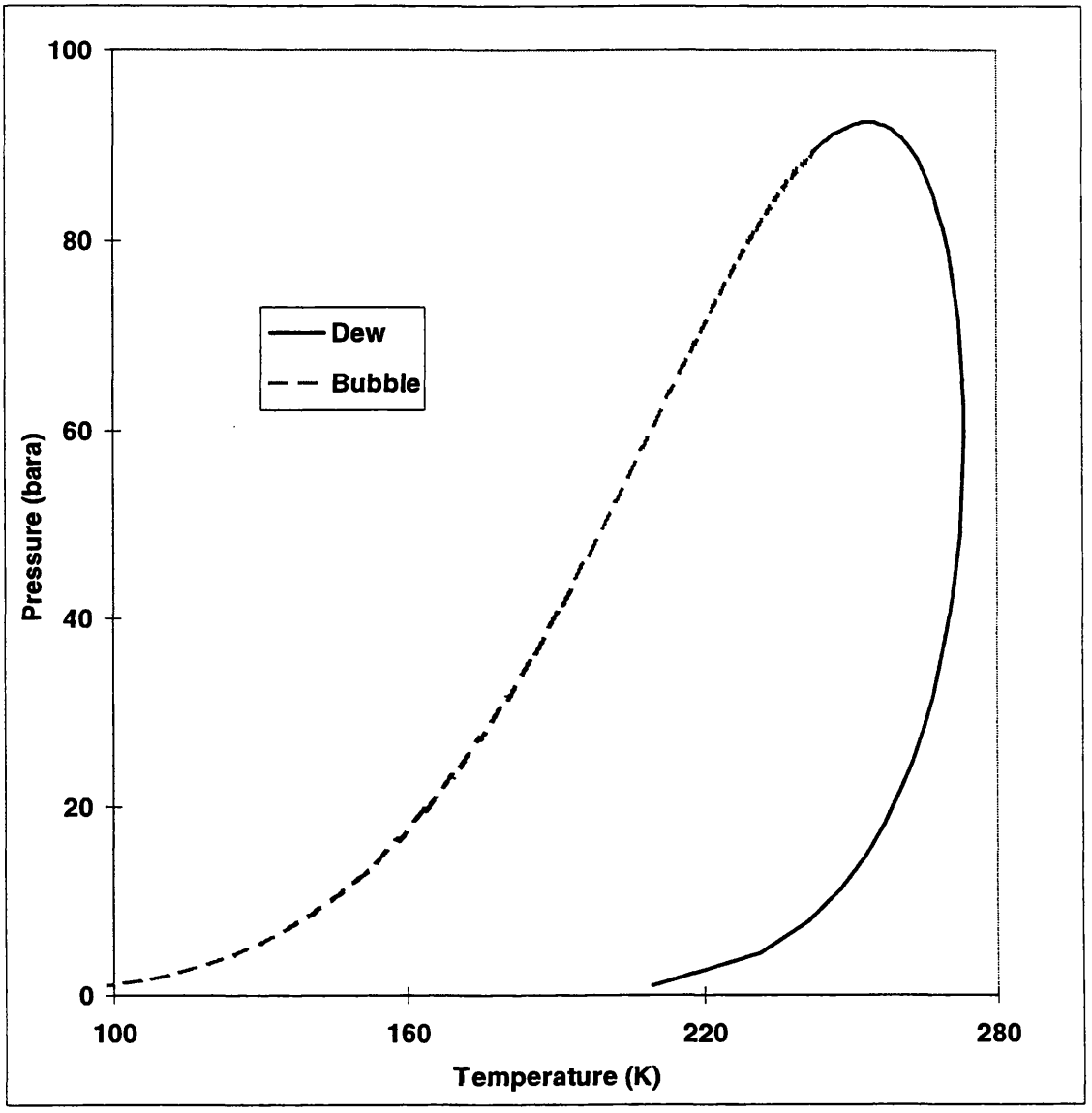

Figure 5.9.3: Phase envelope for the Piper Alpha mixture

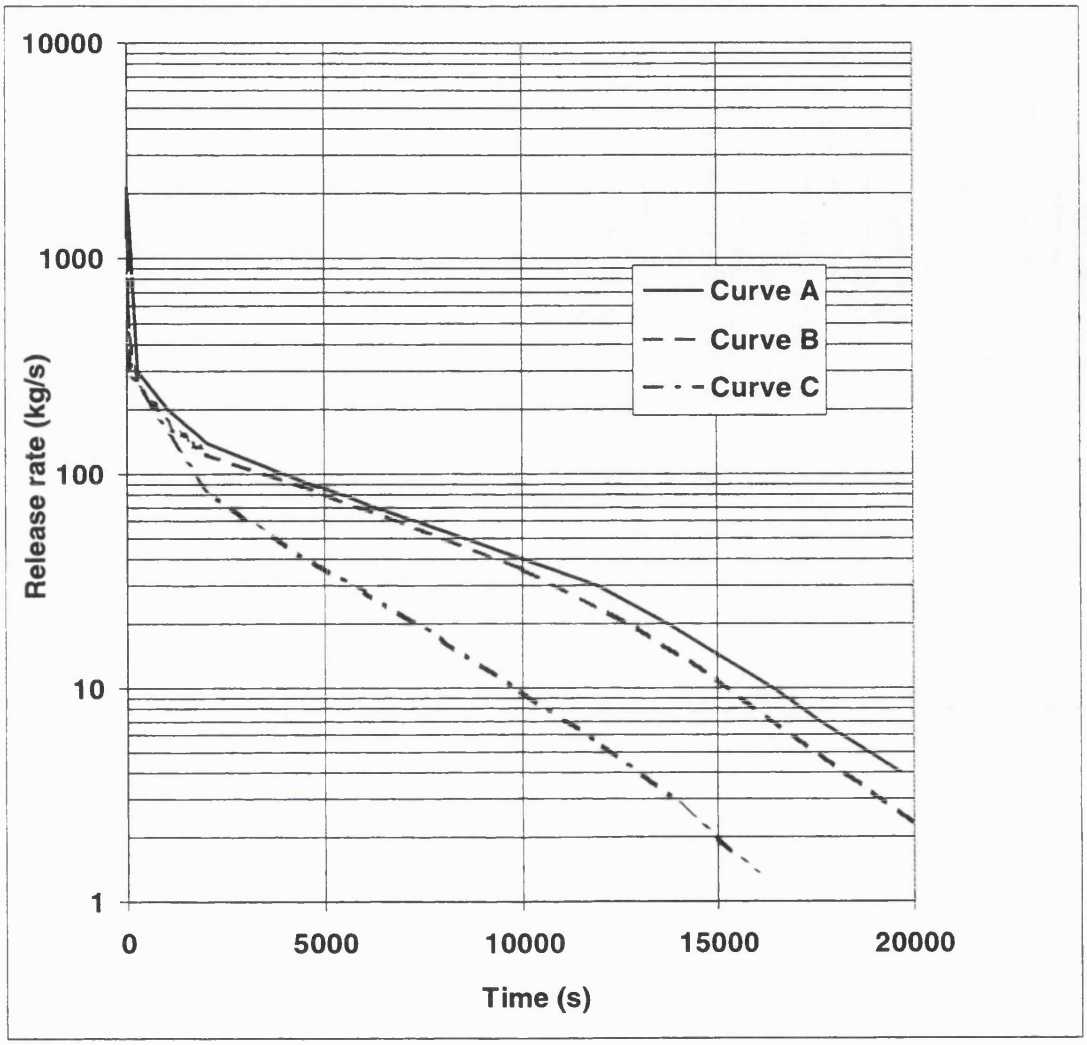

Figure 5.9.4: Comparison of predicted release rate of CNGS-HEM, META-HEM and CNGS (Piper Alpha).

Curve A: META-HEM
Curve B: CNGS-HEM
Curve C: CNGS

The same assumptions made by Chen (1993) are employed in this work, namely, constant wall heat transfer coefficient and pipe roughness scale of 100 W/m^2K and 0.05 mm respectively.

The results for Piper Alpha suggested that the calculation for friction factor based on flow dependent correlations is particularly sensitive to the presence of liquid. In view of this finding, it is decided here to test the results for both the Chen (1979) friction factor equation (see also section 5.4) and the Moody (Massey, 1983) approximation to the Colebrook equation (Perry and Green, 1997) (see also section 5.4). For reference purposes, the CNGS-HEM in conjunction with Chen's equation is denoted by CNGS-HEM-CH whilst CNGS-HEM-MC relates to the Moody-Colebrook correlation.

Figure 5.9.5 shows the results for prediction of open and closed end pressure-time histories for the LPG mixture. Curve A shows the measured data at the open end, Curve B shows the data at the closed end. Curves C and D on the other hand show open end predictions for CNGS-HEM-MC and CNGS-HEM-CH respectively, whereas Curves E and F show respective closed end predictions for CNGS-HEM-MC and CNGS-HEM-CH.

An extremely rapid initial decrease in pressure is recorded by measurement at the closed and open ends (Curves A and B). This is due to the speed of sound in a liquid mixture being much greater than that in a gas or a two-phase mixture (Wylie and Streeter, 1993; Thorley, 1991). The greater speed of propagation of disturbance following FBR will mean that depressurisation will be on a much faster scale in the liquid LPG mixture. The rapid decrease corresponds to a very short period of expansion of the compressed liquid propane followed almost immediately by flashing of the liquid propane.

The rate of drop in pressure is expected to decrease with an increase in pipeline length due to the more significant frictional and inertial effects.

A slight undershoot can be noticed in both measured open and closed end pressure data (Curves A and B). This can most probably be attributed to non-equilibrium effects such as delayed bubble nucleation arising from the rapidity of the pressure

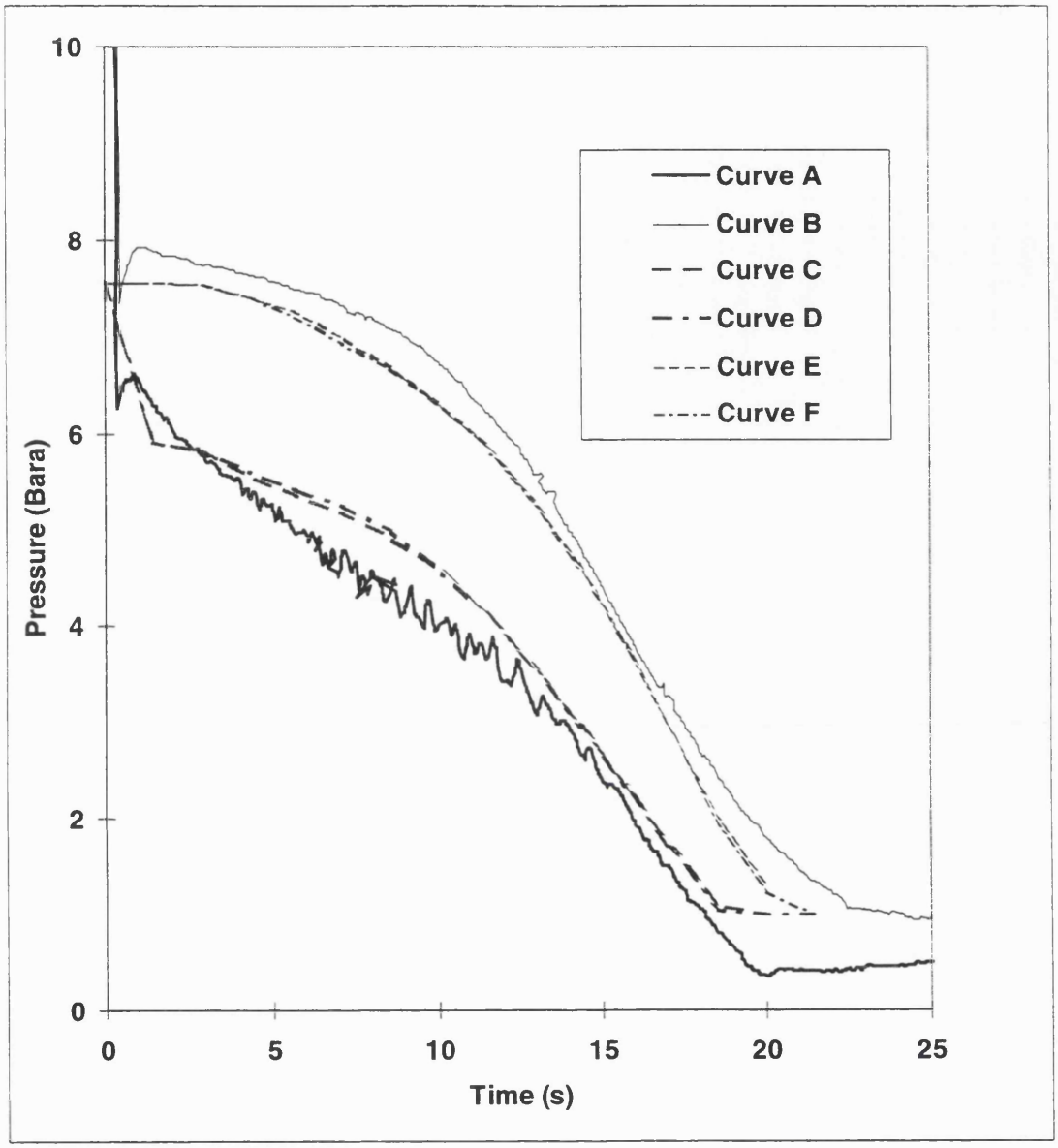

Figure 5.9.5: Pressure time profiles at closed and open ends for test P40 (LPG)
For both CNGS-HEM: $\Delta x_3 = 20m$, $\Delta x_2 = 4m$, $\Delta x_1 = 0.8m$; CPU time = 1.4 hours

Curve A: Measurement (Open End)
Curve B: Measurement (Closed End)
Curve C: Open End, CNGS-HEM-MC
Curve D: Open End, CNGS-HEM-CH
Curve E: Closed End, CNGS-HEM-MC
Curve F: Closed End, CNHS-HEM-CH

decrease, and possibly due to reflection of expansion waves in the compressed liquid off the closed end of the pipe.

Once the transition to saturated liquid is reached, the pressure at the closed end remains approximately at the saturation pressure for a further 12 s, gradually dropping to atmospheric pressure in the subsequent 10 s indicating the possibility of thermodynamic equilibrium in this region.

Referring to the theoretical predictions, the initial undershoot due to the transition from liquid to two-phase flow is not predicted since the calculation procedures start with the fluid at the saturation pressure. However, both models on the whole provide reasonably accurate predictions of the pressure/time histories. The CNGS-HEM-MC gives slightly better agreement and is therefore chosen as the preferred method in all subsequent simulations in this study.

Referring to figure 5.9.5, the finite difference between model and experimental data may be attributed to a number of reasons including the uncertainty associated with the measurement of pressure or precise information on the fluid composition. In the former case, it is interesting to note that the final open end pressure is well below atmospheric pressure (see Curve A).

It should also be pointed out that the composition of 95 mole% propane and 5 mole% butane as used in this study is an approximate one for commercial LPG. The actual composition is not known precisely, but the mixture usually containes propane and other low molecular weight hydrocarbons, such as butane and ethane.

Figure 5.9.6 shows the effect of addition of a small amount of ethane on the LPG depressurisation profiles. The new LPG composition is taken to be 94.5 mol% propane, 4.95 mol% butane and 1 mol% ethane.

It is interesting to note that even a small change in composition gives rise to a relatively large change in the pressure profiles. The addition of a light hydrocarbon hastens the depressurisation process. The converse would be expected if a heavier hydrocarbon was chosen. Also the saturation pressure is dictated by the mixture composition which will have a significant effect on the pressure profiles, especially

so at the closed end where the liquid mixture stays at the saturation pressure for a comparatively long time.

Another possible source of error is the fact that cubic equations of state such as Peng-Robinson tend to under-estimate liquid densities (Reid et. al., 1986). This could have a noticeable effect on the mass and momentum transfer phenomena and hence the pressure/time profiles.

Uncertainty in the pipe roughness can also lead to spurious pressure profile predictions. Chen (1993) showed the effect of this on pressure profile predictions and found that the higher the pipe roughness, the slower is the depressurisation rate. He concludes however that uncertainty in the roughness length scale is less than that of the rupture mechanism and therefore uses a roughness scale of 0.05mm for all his simulations.

Figure 5.9.7 shows the predicted (Curves A and B) and measured temperature profiles (Curves C and D) at the closed and open ends for test run P40. The predicted temperature profiles show similar trends as those observed above for pressure profiles when compared to experimental data. The open end predictions are slightly higher whereas the closed end predictions are slightly lower than measured data. Open end temperatures are overestimated between 2 and 10 seconds with a maximum discrepancy of about 5 °C.

A significant and rapid rise in the measured temperature at the open end (Curve A) can be noticed towards the end of the depressurisation process. The rise corresponds to the cessation of two-phase flow with the consequent onset of gas phase flow at the rupture plane, and is probably a reflection of different heat transfer rates from the wall to the fluid. The CNGS-HEM-MC cannot reproduce this trend because a constant heat transfer coefficient is used. Hence further improvement of the model in this late time regime can be obtained by introducing correlations to account for fluid state dependent heat transfer rate.

The slight levelling of the temperature immediately before the subsequent rise corresponds to the moment when the flow at the rupture plane ceases to be choked, i.e. when the pressure reaches atmospheric pressure for the HEM.

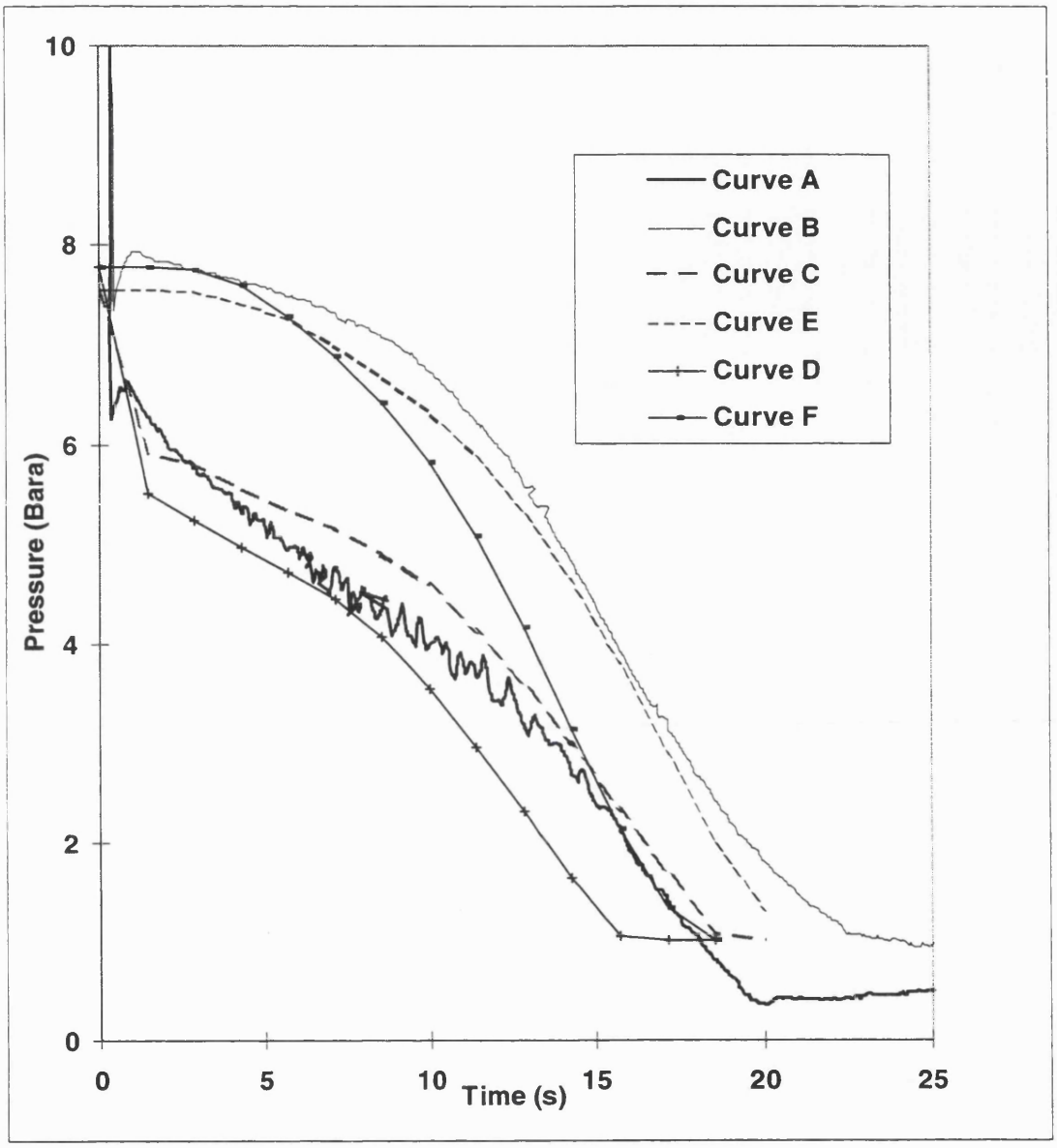

Figure 5.9.6: Effect of the addition of 1 mol% ethane on pressure-time profiles at open and closed ends for test P40 (LPG).

Curve A: Measurement (Open End)
Curve B: Measurement (Closed End)
Curve C: Open End, CNGS-HEM (2 component LPG mixture)
Curve D: Open End, CNGS-HEM (2 component + 1mol% ethane LPG mixture)
Curve E: Closed End, CNGS-HEM (2 component LPG mixture)
Curve F: Closed End, CNHS-HEM (2 component + 1mol% ethane LPG mixture)

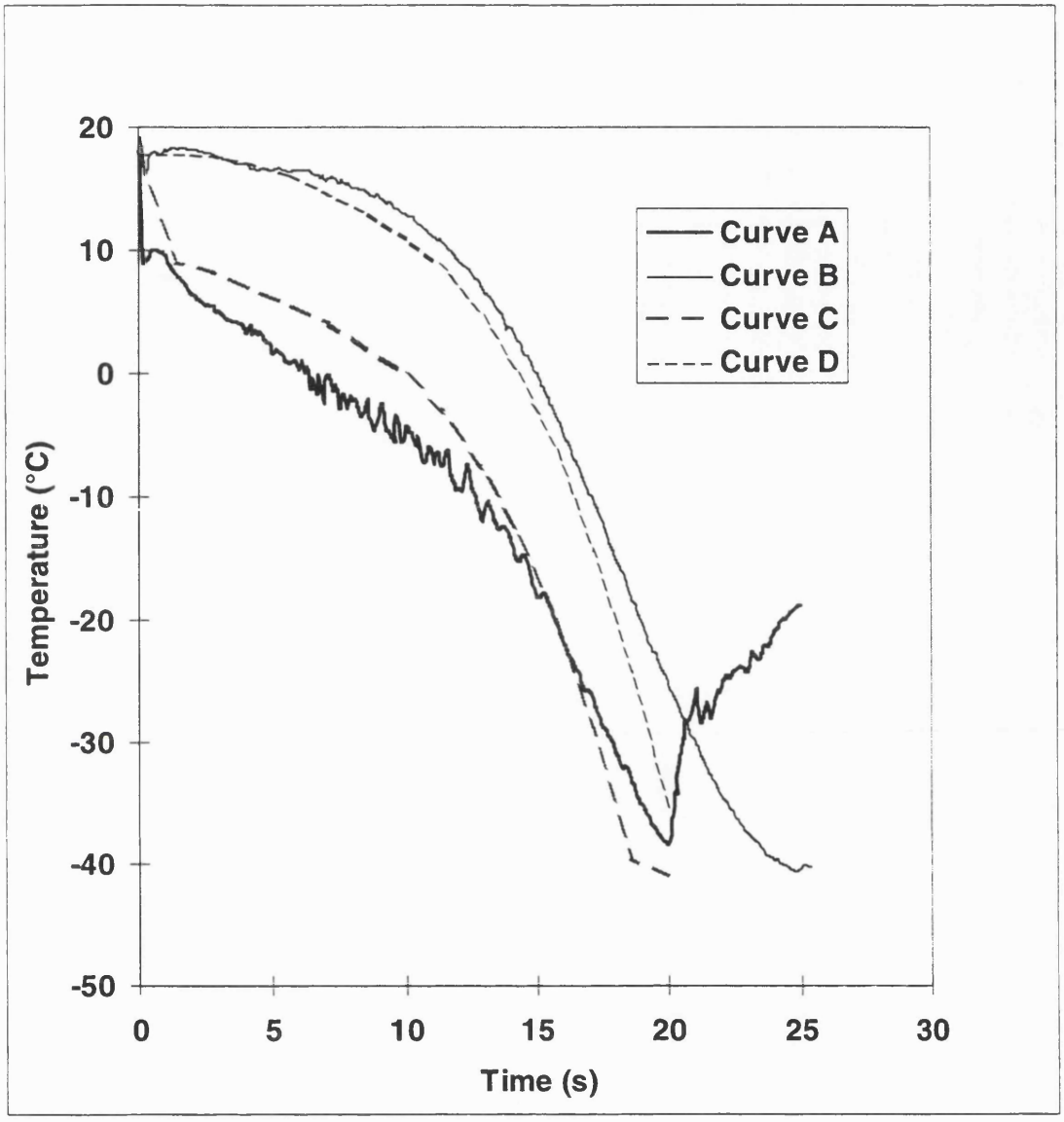

Figure 5.9.7: Temperature-time profiles at the open and closed ends for test P40 (LPG) $\Delta x_3 = 20m$, $\Delta x_2 = 4m$, $\Delta x_1 = 0.8m$; CPU time = 1.4 hours

Curve A: Measurement (Open End)
Curve B: Measurement (Closed End)
Curve C: CNGS-HEM (Open End)
Curve D: CNGS-HEM (Closed End)

Figure 5.9.8 shows the comparisons for total line inventory during depressurisation for test run P40. Curve A shows the load cell values whereas Curves B and C show the predictions using Chen's (1993) META-HEM and the current CNGS-HEM respectively. Both models overestimate line inventory and give very similar results.

Figure 5.9.9 shows model predictions for release rate/time data for run P40. Curve A shows the results for CNGS-HEM whereas Curve B shows the results for META-HEM. CNGS-HEM gives higher predictions for release rate. Figure 5.9.10 shows release rate predictions for run P42. The same trend is observed in this case. Unfortunately no experimental data exists to allow comparison. Since the release rate is dependent on outlet velocity and fluid density at the rupture plane, it is worth comparing the predictions for both these parameters by the respective models.

Figure 5.9.11 shows the predictions for flow velocity/time at the rupture plane for run P42. CNGS-HEM (Curve A) gives lower velocity predictions than META-HEM, and therefore CNGS-HEM must give higher predictions for density than META-HEM in order to produce the higher release rates observed. A direct comparison cannot be made for density since such data at the rupture plane is not presented for META-HEM by Chen (1993).

A disagreement in density prediction is a consequence of different pressure and temperature predictions. This is especially exaggerated for a LPG mixture since the phase envelope is very narrow, so even a small difference in pressure and temperature prediction can lead to the mixture being close either to the dew point curve or to the bubble point curve. Figure 5.9.12 shows the phase envelope for the LPG mixture. The existence of a very narrow area for two-phase flow means that the depressurisation process follows a very fine line from the bubble point curve to the dew point curve.

Figures 5.9.13 and 5.9.14 show the pressure and temperature profiles using CNGS-HEM for test P42. In both figures, Curves A and B are the measurement data at the open and closed ends respectively, whereas Curves C and D are the corresponding data obtained using CNGS-HEM.

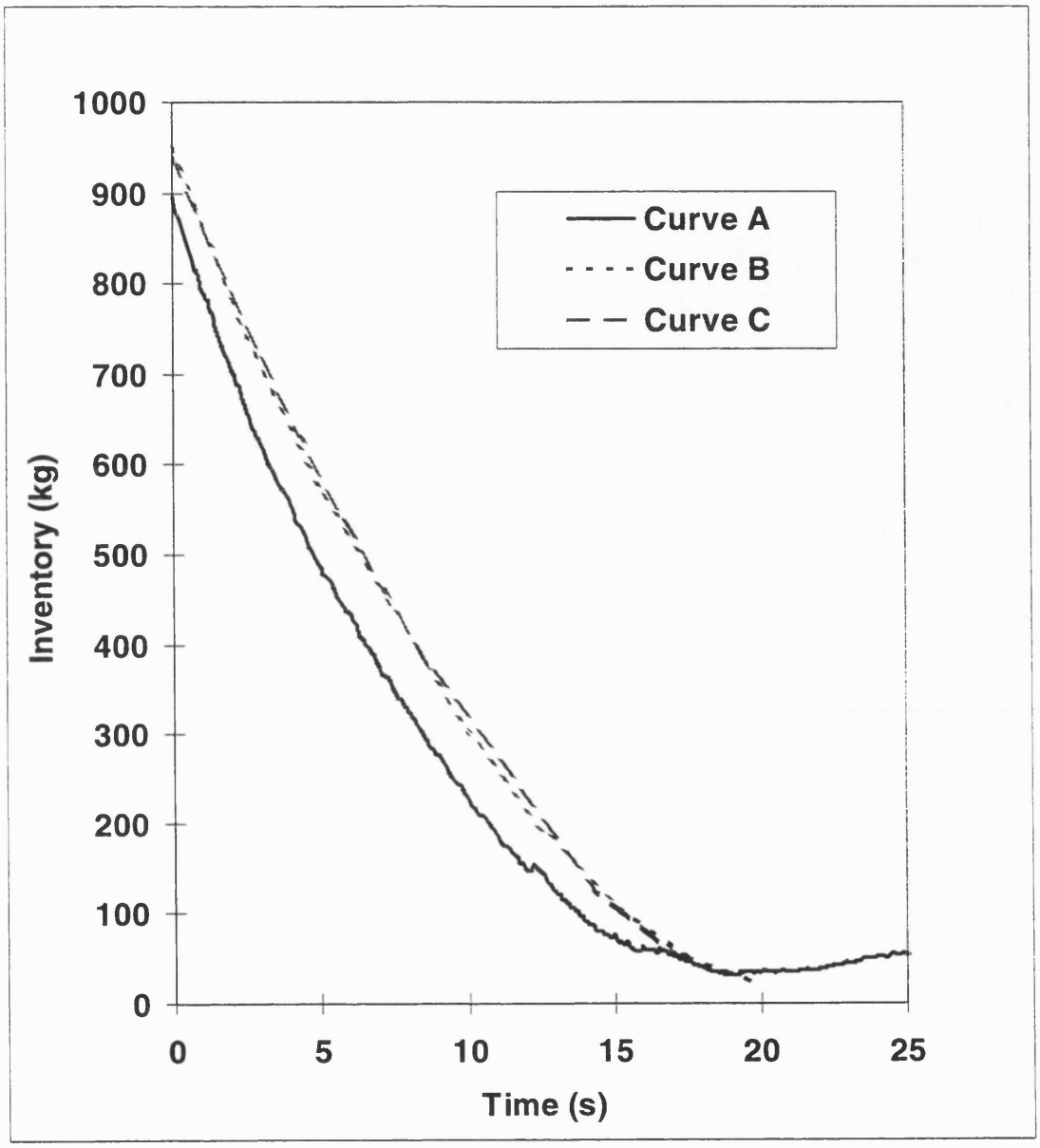

Figure 5.9.8: Comparison of total line inventory predictions with test P40 measurements (LPG)

Curve A: Measurement
Curve B: META-HEM
Curve C: CNGS-HEM

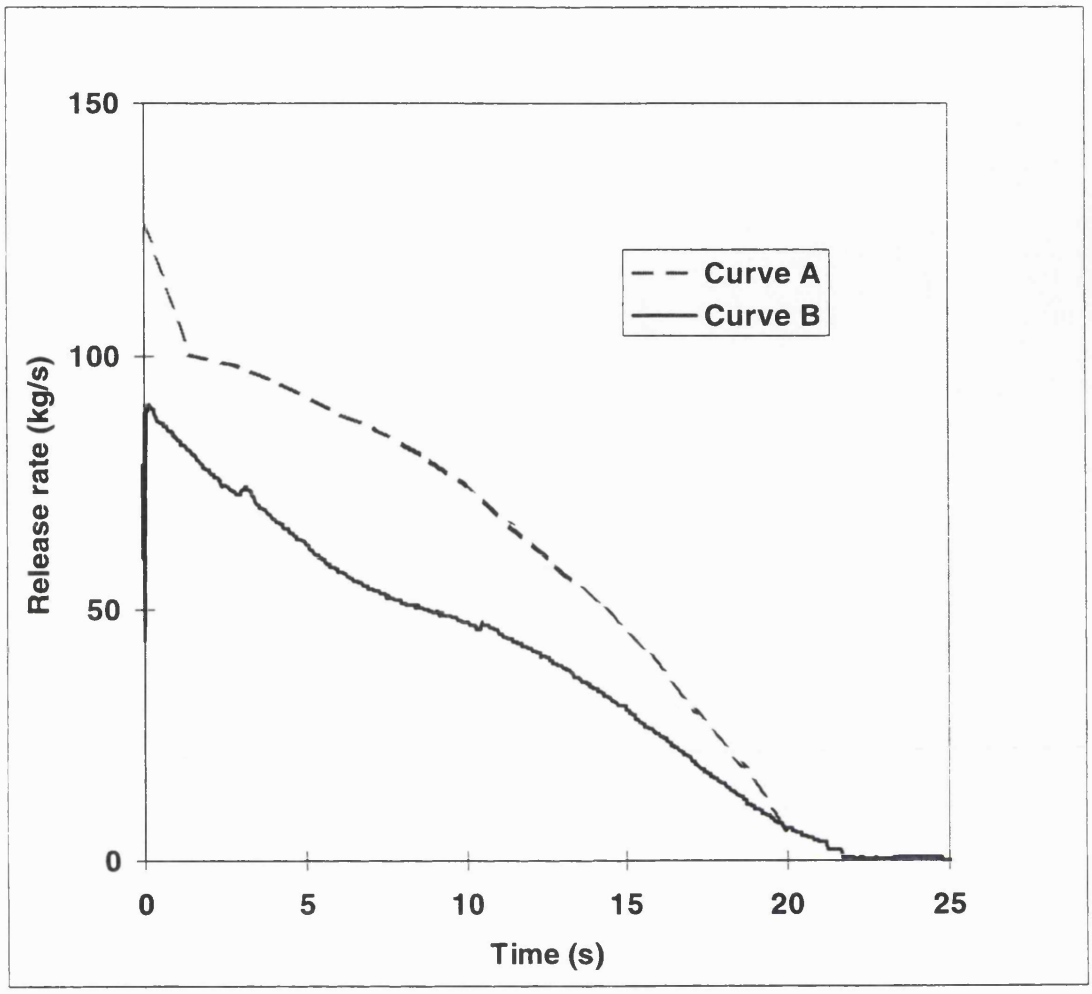

Figure 5.9.9: Comparison of predictions of release rate for test P40 (LPG)

Curve A: CNGS-HEM
Curve B: META-HEM

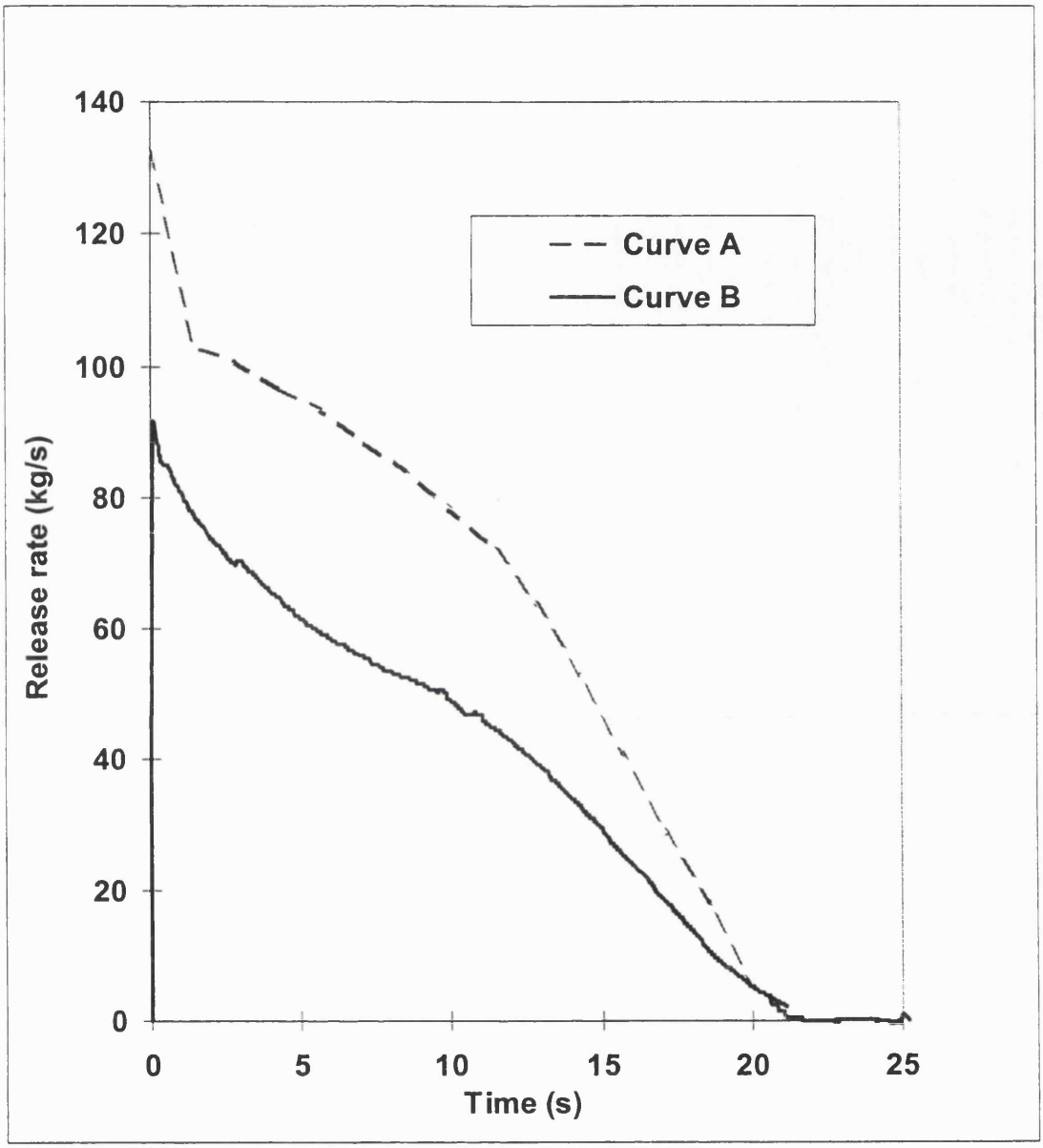

Figure 5.9.10: Comparison of predictions of release rate for test P42 (LPG).

Curve A: CNGS-HEM
Curve B: META-HEM

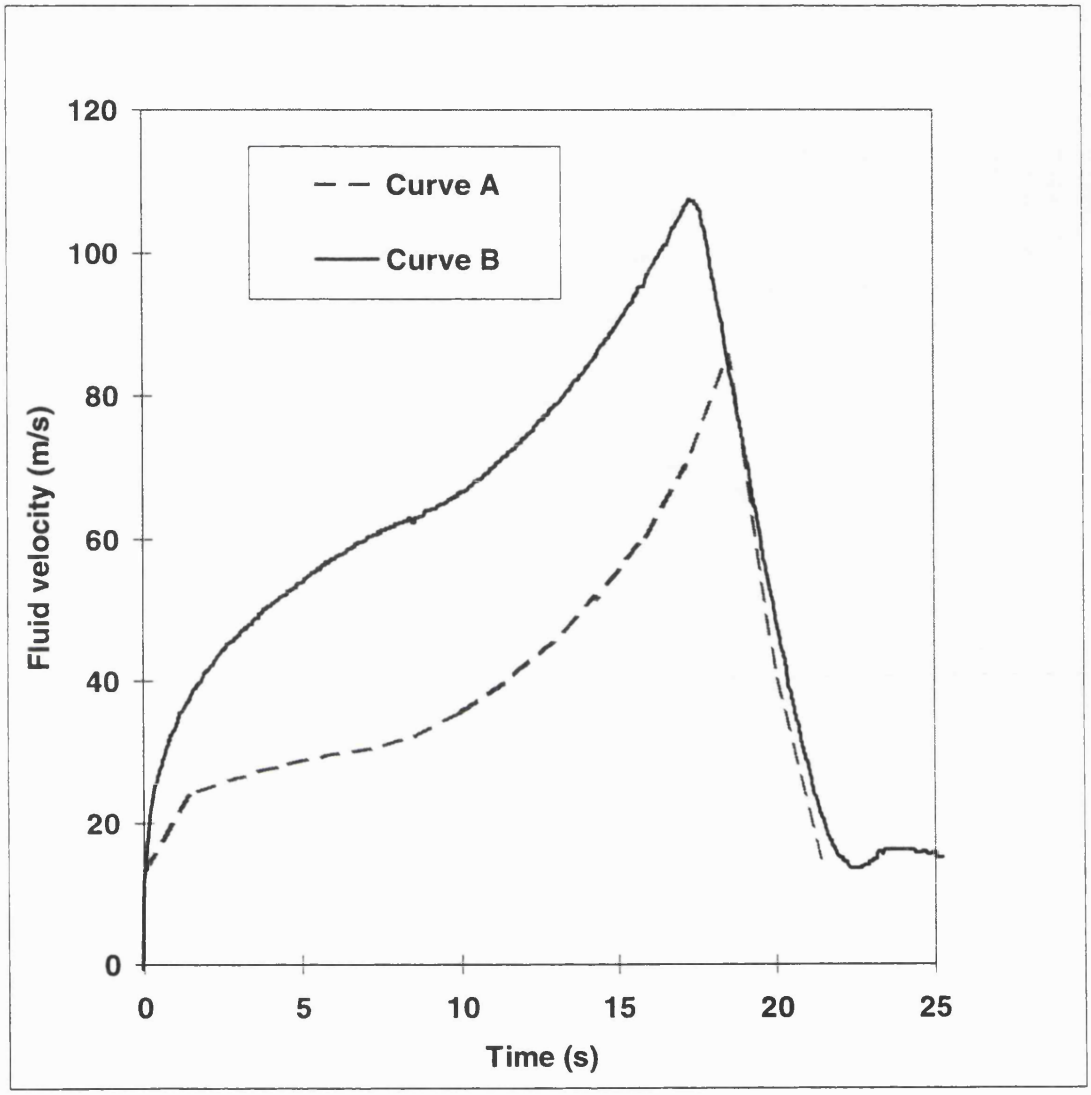

Figure 5.9.11: Comparison of predictions of flow velocity at the rupture plane for test P42 (LPG)

Curve A: CNGS-HEM
Curve B: META-HEM

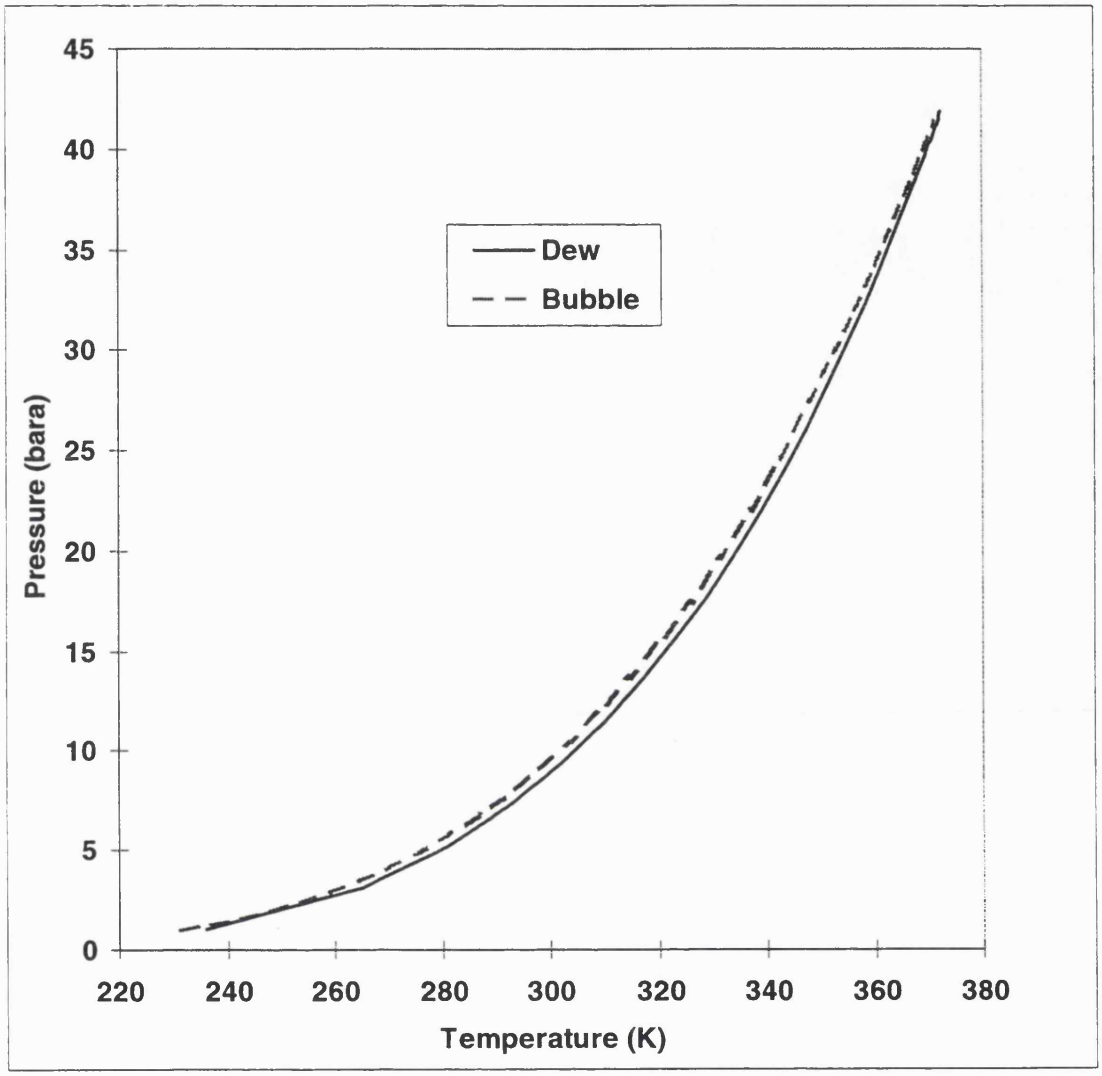

Figure 5.9.12: Phase envelope for LPG mixture

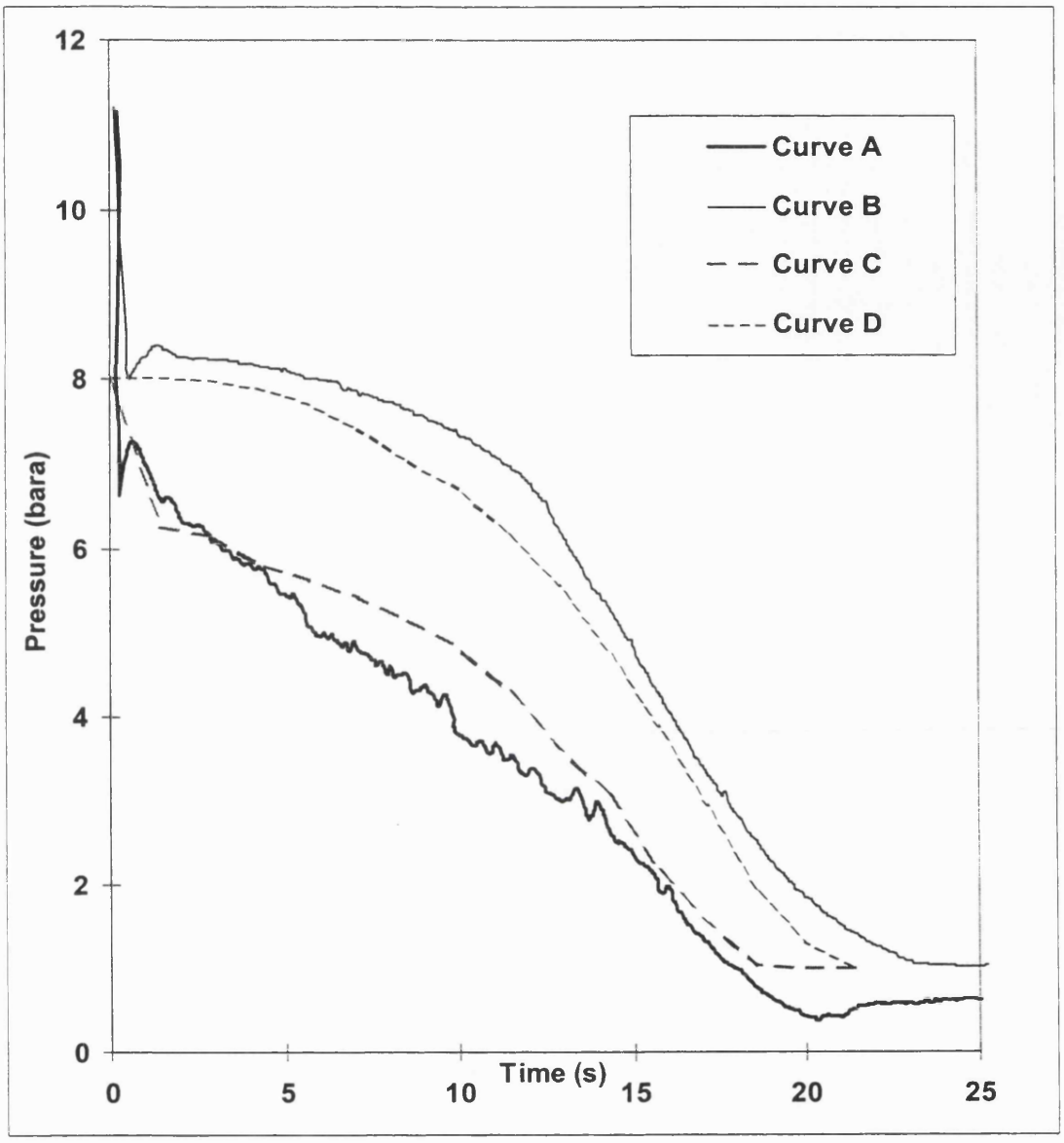

Figure 5.9.13: Pressure-time profiles at open and closed ends for test P42 (LPG); $\Delta x_3 = 20m$, $\Delta x_2 = 4m$, $\Delta x_1 = 0.8m$; CPU time = 1.4 hours

Curve A: Measurement (Open End)
Curve B: Measurement (Closed End)
Curve C: Open End, CNGS-HEM
Curve D: Closed End, CNGS-HEM

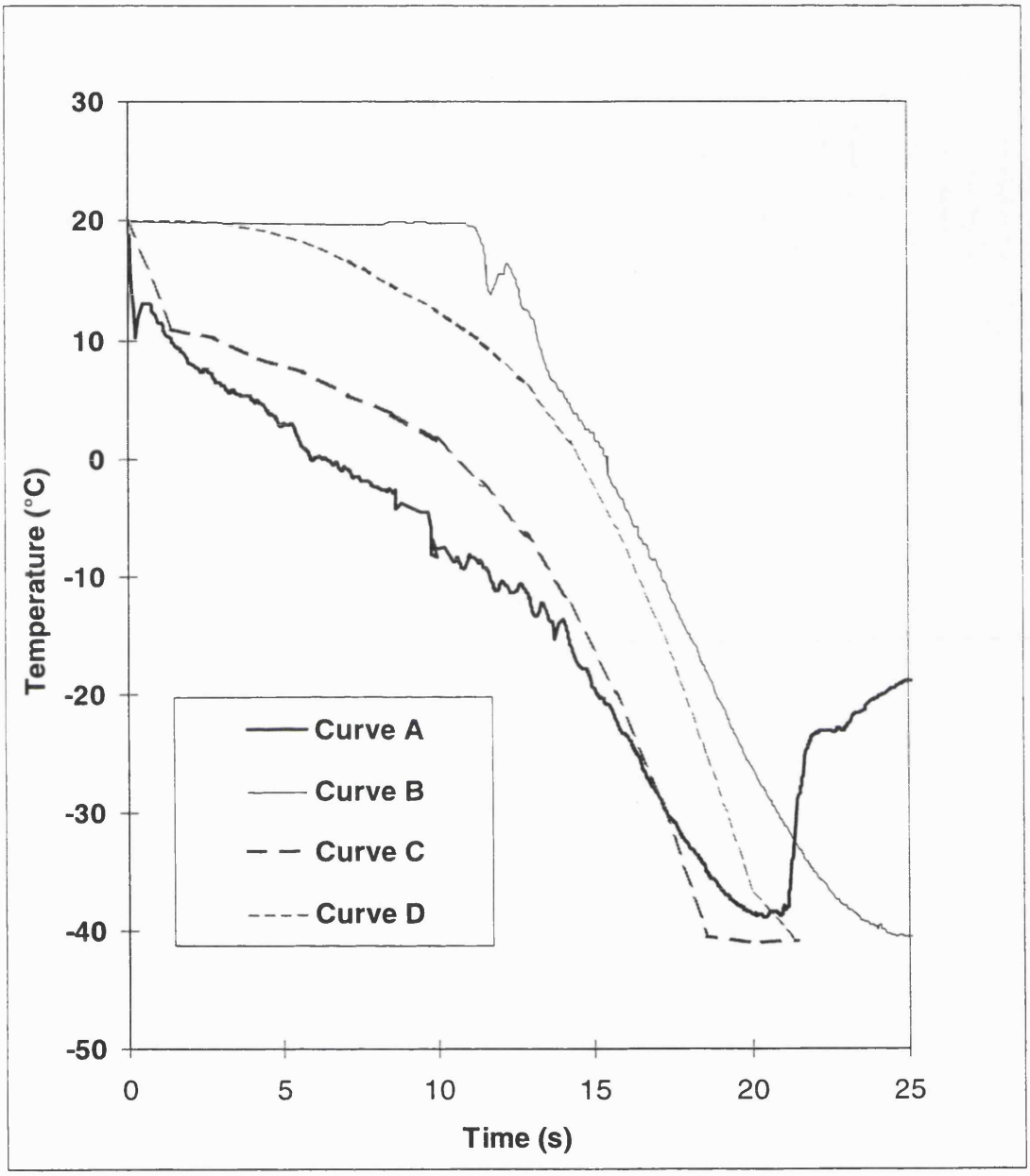

Figure 5.9.14: Temperature-time profiles at open and closed ends for test P42 (LPG)
Δx_3 = 20m, Δx_2 = 4m, Δx_1 = 0.8m; CPU time = 1.4 hours

Curve A: Measurement (Open End)
Curve B: Measurement (Closed End)
Curve C: Open End, CNGS-HEM
Curve D: Closed End, CNGS-HEM

As occurred in test P40, the comparison of CNGS-HEM pressure and temperature profiles with measurement both show a slight over-estimate at the open end and an under-estimate at the closed end.

It is known (see sections 5.8.1 and 5.8.2) that the various interpolation techniques used to calculate fluid properties on the previous time line in MOC will lead to some smearing of the true solution. For multi-component fluids such as the Piper Alpha mixture with a wide phase envelope (see figure 5.9.3), any significant error may accrue only in the cell containing the gas/two-phase interface as shown in section 5.8.2 and hence excellent prediction of closed end pressure/time histories are obtainable (see figure 5.9.1).

Mixtures such as LPG exhibiting a narrow phase envelope, are especially sensitive in terms of magnitude of the density variation with pressure and temperature, and therefore accurate prediction of the latter parameters along each time line is essential for FBR simulations. Solution of the compatibility and characteristic equations in CNGS-HEM is an accurate way of predicting flow and fluid parameters at the various grid points, however inaccuracies arise when interpolation is performed to predict pressure and temperature variation in between grid points. Such errors can be expected to be especially acute for mixtures such as LPG. However the fact that the discrepancy between model and experimental data is not so great suggests that the assumptions made during interpolation are not too far off reality.

Figure 5.9.15 shows the comparisons for total line inventory for test run P42. Again CNGS-HEM and META-HEM agree very well with each other with both slightly over-estimating compared to measurement. It might be expected that higher release rate predictions as is the case with CNGS-HEM with respect to META-HEM would lead to significant under-estimation of total line inventory, but this is not the case as clearly illustrated in figures 5.9.8 and 5.9.15. This is because CNGS-HEM predicts less gas evolution than META-HEM which signifies higher density predictions throughout the pipeline and hence greater line inventories in spite of higher release rates (see figures 5.9.9 and 5.9.10).

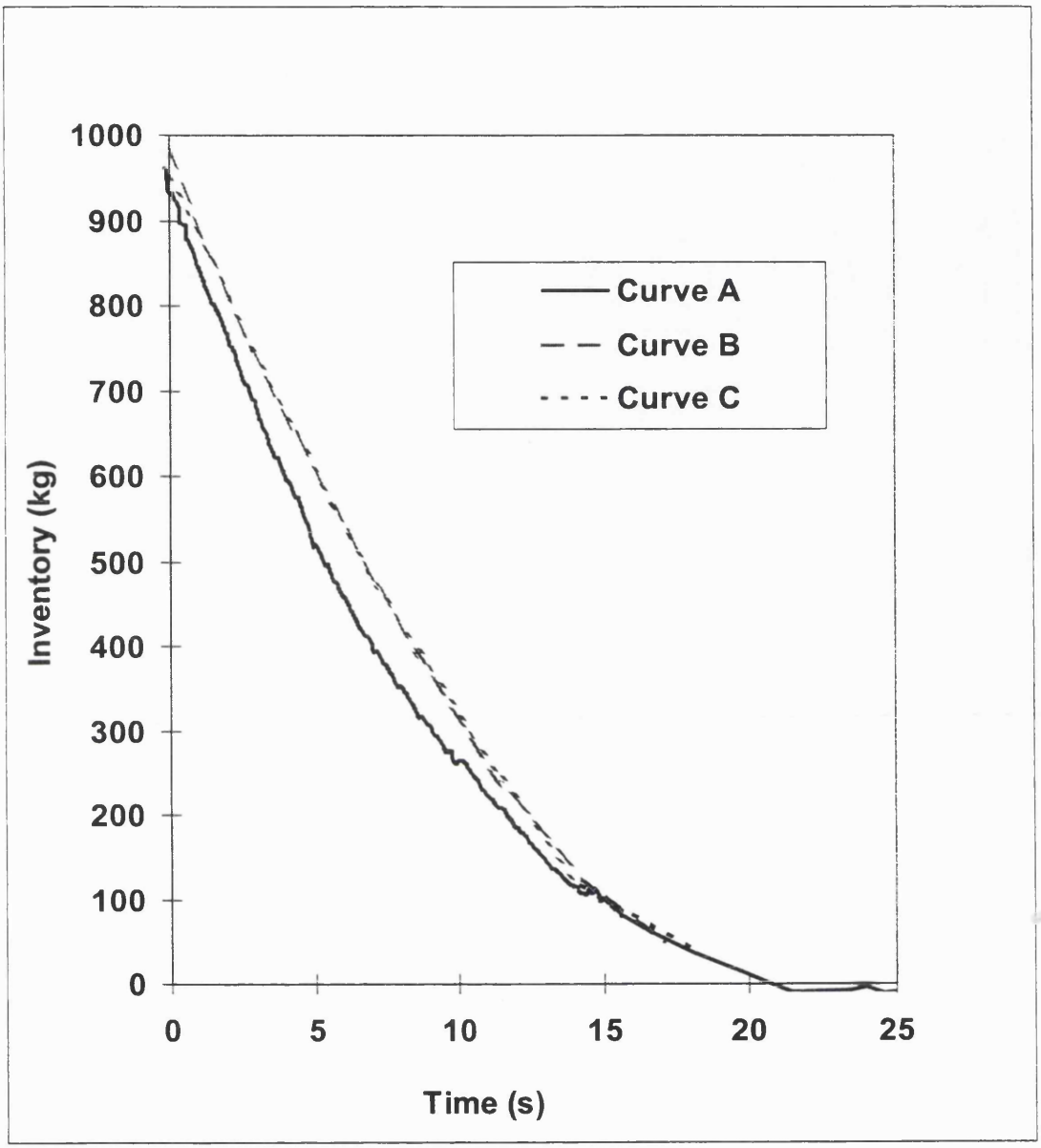

Figure 5.9.15: Comparison of total line inventory with test P42 measurements (LPG)

Curve A: Measurement
Curve B: CNGS-HEM
Curve C: META-HEM

Figure 5.9.16 shows the results of a comparison for the open end pressure made using CNGS-HEM (Curve B) and other models including META-HEM, MSM-CS, BLOWDOWN, and PLAC (Curves B,C,D, and E respectively) for the LPG mixture. The measurement data (load cell) is given by Curve A.

The BLOWDOWN model was developed by Richardson and Saville (1991), the MSM-CS model by Chen (1993) and the PLAC code by Hall et. al. (1993). The BLOWDOWN simulation for pipelines is based on quasi-steady state, equilibrium and homogeneous two-phase flow assumptions. The MSM-CS model takes into account the slip velocity between the two phases and thus incorporates the relevant hydrodynamic constitutive relations that accompany this effect. As a result, two momentum equations, one for each phase, are solved instead of just one in META-HEM. The MSM-CS is based on the same solution techniques as META-HEM.

PLAC is an extension of the nuclear reactor safety code TRAC in that it incorporates a flash calculation package, MULTIFLASH, to predict VLE data for hydrocarbon mixtures. In addition to this, the original critical flow boundary condition in TRAC is replaced by a homogeneous frozen flow model. It allows different temperatures for the two phases thus permitting thermal non-equilibrium since two energy equations are solved for each phase. This creates a dilemma as to which temperature should be used for the equilibrium phase behaviour, an inevitable problem in determining the phase behaviour of multi-component mixtures.

From figure 5.9.16 it is apparent that the best predictions are obtained from CNGS-HEM and META-HEM. BLOWDOWN substantially under-estimates open end pressure because of the quasi steady flow assumption. MSM-CS gives almost the same predictions as BLOWDOWN. It is surprising that the former cannot provide a better prediction of the pressure profile at the open end. This could be due to the use of unrealistic hydrodynamic constitutive relations. Another possible reason is inaccuracy in prediction of wave propagation velocities.

PLAC also gives rise to poor predictions. It predicts a large drop in pressure of at least 2 bara at about 5 seconds after rupture and continues to drop thereafter. One of the reasons for this discrepancy might be due to the fact that no actual flash

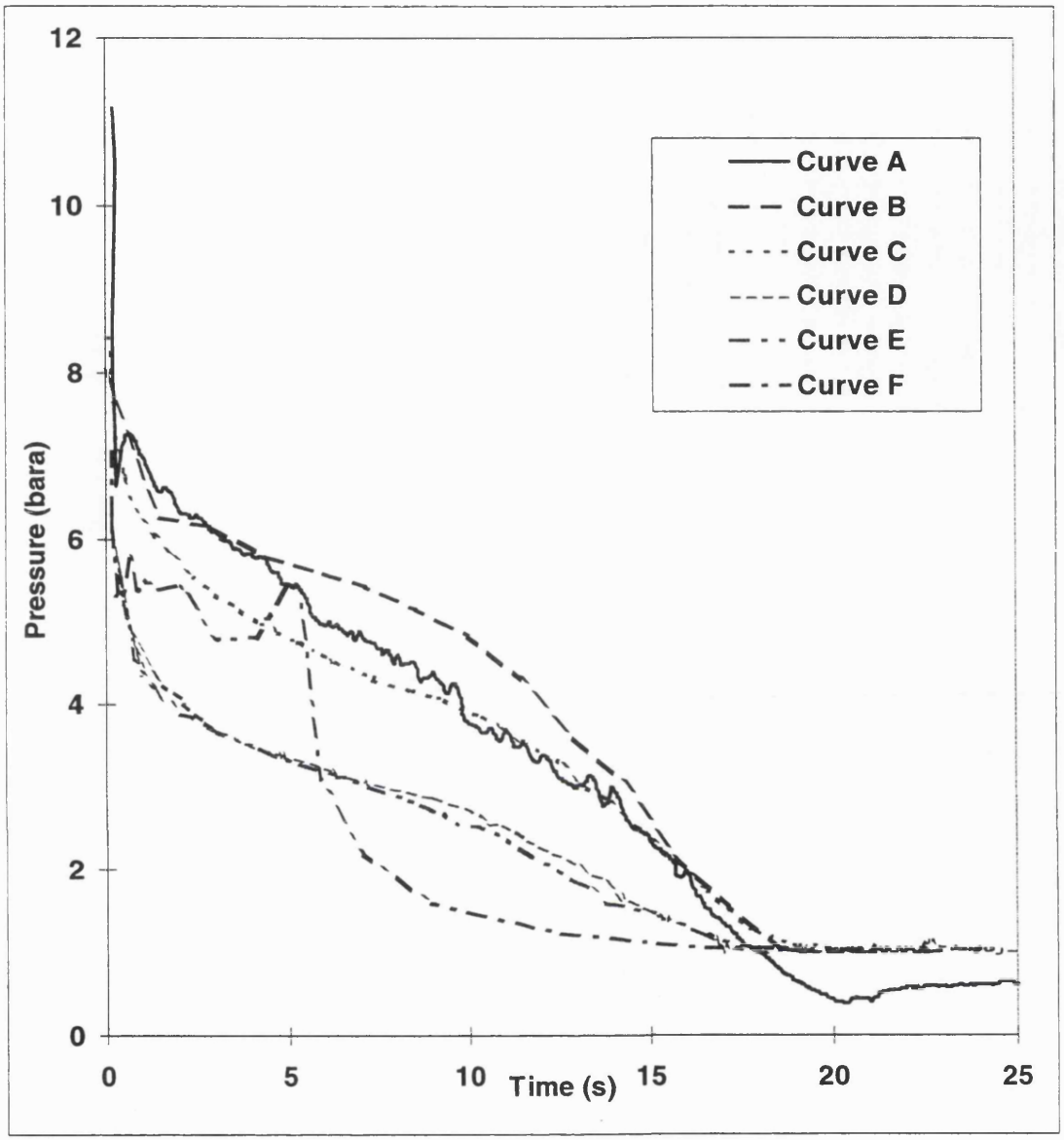

Figure 5.9.16: Pressure time profiles at the open end for test P42 (LPG).

Curve A: Measurement
Curve B: CNGS-HEM
Curve C: META-HEM
Curve D: MSM-CS
Curve E: BLOWDOWN
Curve F: PLAC

calculations are performed to determine fluid properties during the depressurisation. As discussed before, depressurisation profiles for mixtures such as LPG are especially sensitive to accurate thermodynamic prediction. In PLAC fluid physical properties are calculated at a given pressure and temperature in a cell by interpolation from look-up tables generated using the phase equilibrium package before transient flow calculations begin.

Chen (1993) shows by way of a comparison of total line inventory prediction for test P42 that the initial inventory from PLAC start at a much lower value (695 kg) than measurement (970 kg), and drops to less than 20% within 5 seconds (CNGS-HEM and META-HEM predictions are given in figure 5.9.15). The considerable under-estimation can be attributed to two possible reasons.

Firstly, too much gas formation is predicted in the pipeline by PLAC and hence lighter line inventory prediction. Hall (1993) take the initial state of the fluid as 80% liquid which means that PLAC starts transient flow calculations at a point that is already quite well into two-phase flow as opposed to near the saturation point. CNGS-HEM starts its calculations at the saturation point and gives good initial agreement, so the initial state of the fluid is in reality close to this point. A second reason could be due to over-estimation of the release rate by the homogeneous frozen critical flow boundary condition, but this would also be linked to the phase velocities calculated at the rupture plane as discussed earlier.

Figure 5.9.17 shows the results of a comparison for the closed end pressure made using CNGS-HEM (Curve B) and other models including META-HEM, MSM-CS, BLOWDOWN, and PLAC (Curves B,C,D, and E respectively) for the LPG mixture 9tast P42). The measurement data (load cell) is given by Curve A.

CNGS-HEM, META-HEM and BLOWDOWN give very similar predictions with MSM-CS doing less well and PLAC performing very poorly. As also occurred for the open end pressure predictions, PLAC shows a very sharp drop in pressure at the closed end at ca. 5 seconds and continues to drop at a much faster rate than the other models thereafter.

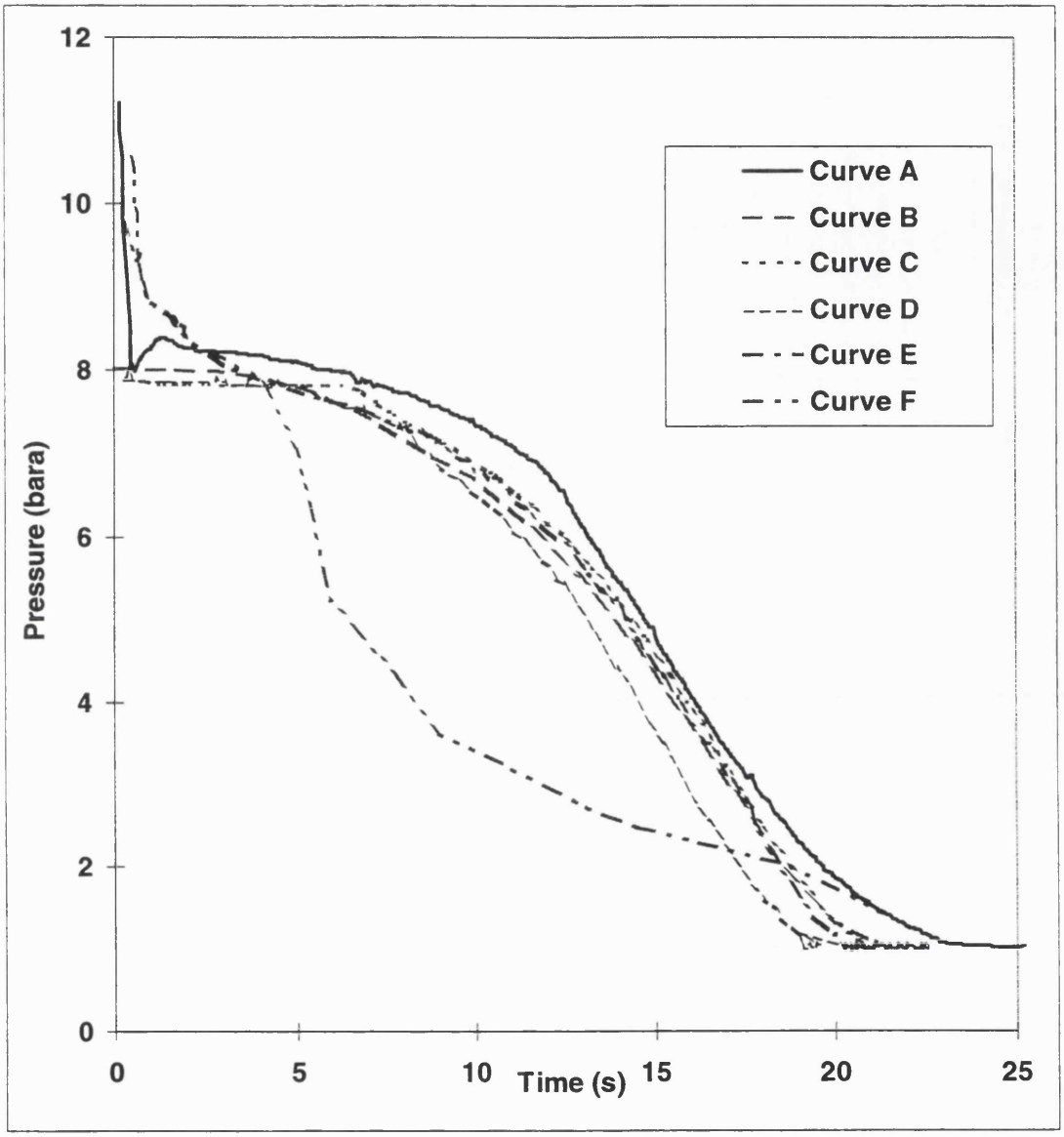

Figure 5.9.17: Pressure-time profile predictions at the closed end for the test P42

Curve A: Measurement
Curve B: CNGS-HEM
Curve C: META-HEM
Curve D: MSM-CS
Curve E: BLOWDOWN
Curve F: PLAC

From the above, it is clear that the CNGS-HEM provides relatively good predictions of the conditions following FBR. This demonstrates that such types of failures can be simulated effectively by using the method of characteristics together with the homogeneous equilibrium model as long as thermodynamic and phase behaviour predictions are accurate and applied rigorously.

5.10 CASE STUDY - ESDV/SSIV SHUTDOWN PIPER ALPHA

Having thus gained confidence in the use of CNGS-HEM, the proceeding sections illustrate the use of this model to study the dynamic response of ball and check valves following FBR of a pipeline containing a condensable gas or a two phase mixture. The simulations are performed in conjunction with the Piper Alpha mixture which exhibits a clear phase transition during depressurisation. In order to reduce CPU times, the analogous results based on assuming that the fluid behaves as an ideal gas are also presented and the resulting errors are quantified.

5.10.1 Fluid dynamics data

Most of the important points discussed in chapter 4 regarding pressure and velocity profiles generated following FBR of a pipeline containing an ideal gas are equally applicable for any real fluid mixture. In terms of valve closure dynamics, the difference between two-phase and single phase flows is the effect that the former have on activation times. For a check valve, this depends very much on its location relative to the position of flow reversal, whereas for ball valves, the activation times are essentially dictated by the rate of depressurisation within the pipeline. Both these phenomena are influenced directly by the rate of propagation of the expansion waves through the fluid medium away from the rupture plane.

The expansion wave velocity is calculated relative to the fluid motion and in all MOC numerical procedures is given by the right running Mach line (=u+a).

Figure 5.10.1 shows the predictions for expansion wave velocities over the first 360 metres of pipeline as measured from the rupture plane. Curves A and B show the results at t=0 and t= 0.6 s respectively following FBR for the two phase mixture whereas Curves C and D show the corresponding data in the case of an ideal gas assumption.

As has already been discussed in section 5.8.2, a sudden drop in sound velocity occurs due to the onset of two phase flow. This obviously leads to a reduction in the

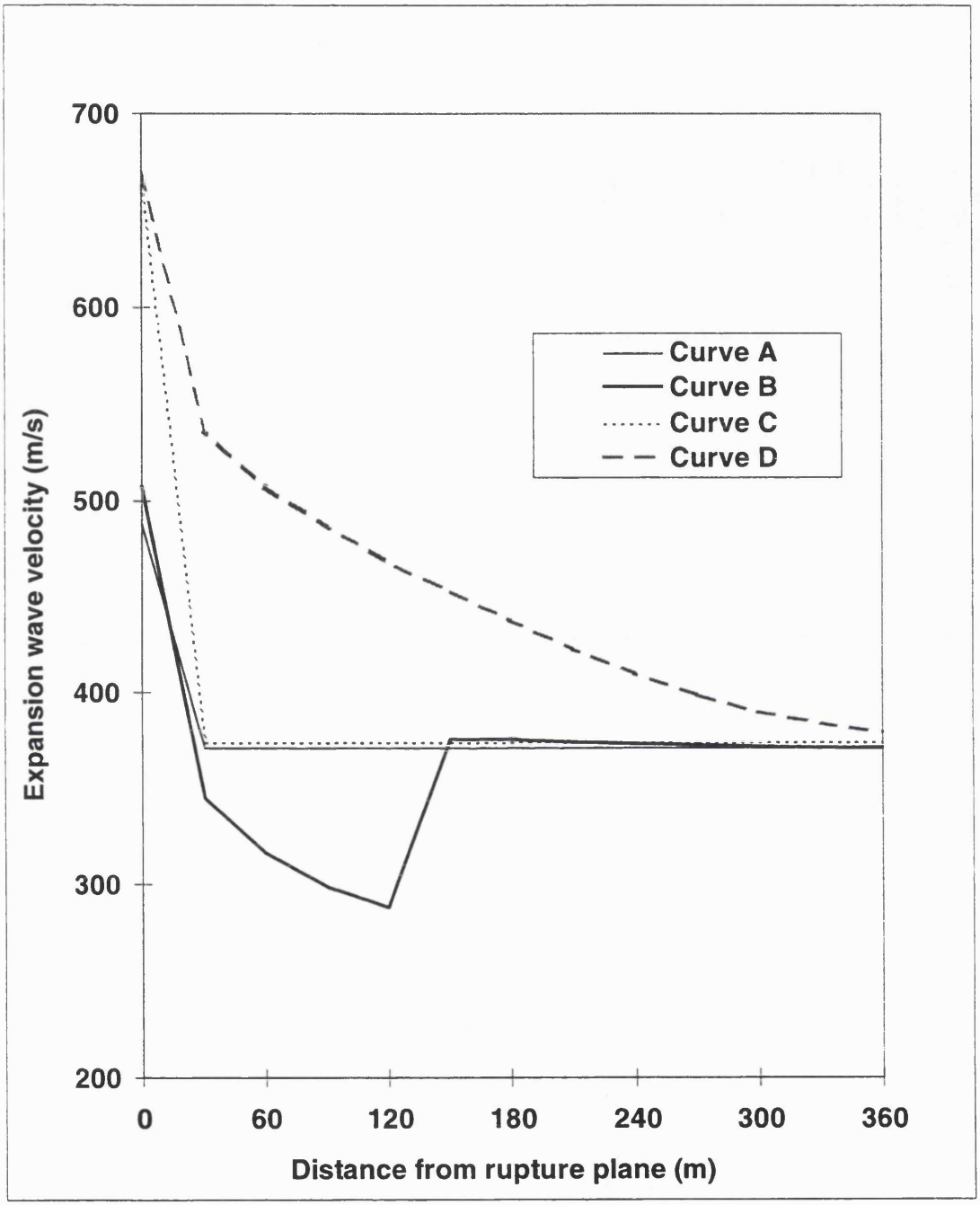

Figure 5.10.1: Predictions for the expansion wave velocities over the first 360 m of pipeline as measured from the rupture plane (Piper Alpha mixture).

Curve A: Two-phase; t = 0s following FBR
Curve B: Two-phase; t = 0.6 s following FBR
Curve C: Ideal gas; t = 0s following FBR
Curve D: Ideal gas; t = 0.6s following FBR

expansion wave velocity as compared to that for the permanent gas. At t=0, this effect is only noticed at the rupture plane (cf. Curves A and C).

At t = 0.6 s however, the phase transition interface has moved about 120m (Curve B) from the rupture plane. Over this distance, the presence of a two phase mixture results in a relatively large difference in expansion wave velocities between the two phase and ideal gas scenarios (Curves B and D). The sharp rise in expansion wave velocity at 120 m (Curve B) corresponds to the point in the pipeline where gas phase exists and hence in this region the difference between the two models is less pronounced. Finally, the results from the two models converge because the fluid in the rest of the pipeline is stationary.

Clearly, the presence of a two-phase mixture will affect the ESDV activation time. Figure 5.10.2 shows the variation of fluid velocity with distance from the rupture plane at different times for the Piper Alpha mixture. Curves A-C show the results from the two phase model at 9.23, 27.69, and 46.15 s respectively whereas Curves D to F show the corresponding results for an ideal gas.

The ideal gas model predicts faster fluid velocities than the two-phase model, a result of higher sound velocity predictions. This will in turn lead to faster activation times for a check valve. Taking the example of a check valve placed 6.1 km from the rupture plane, the two-phase model predicts an activation time of ca. 9.23 s whereas the ideal gas model predicts an activation time of ca. 8.6 s. These are obtained by determining the times corresponding to zero flow velocity at the given location.

Figure 5.10.3 shows the variation of pressure with distance at different times for the Piper Alpha mixture. Curves A - C show the results for the two phase model at 9.23, 27.69, and 46.15 s respectively whereas Curves D - F show the corresponding results for an ideal gas.

The ideal gas gives larger pressure drops leading to faster depressurisation rate predictions with the effect increasing with time. These profiles are necessary in determining activation times for a ball valve. For example, for a ball valve placed at the same distance as the check valve (6.1 km) from the rupture plane and triggered to initiate shutdown on sensing a pressure drop of greater than 10 bara, the corresponding activation time are 7.5s (gas phase) are 9.23 s (two phase)

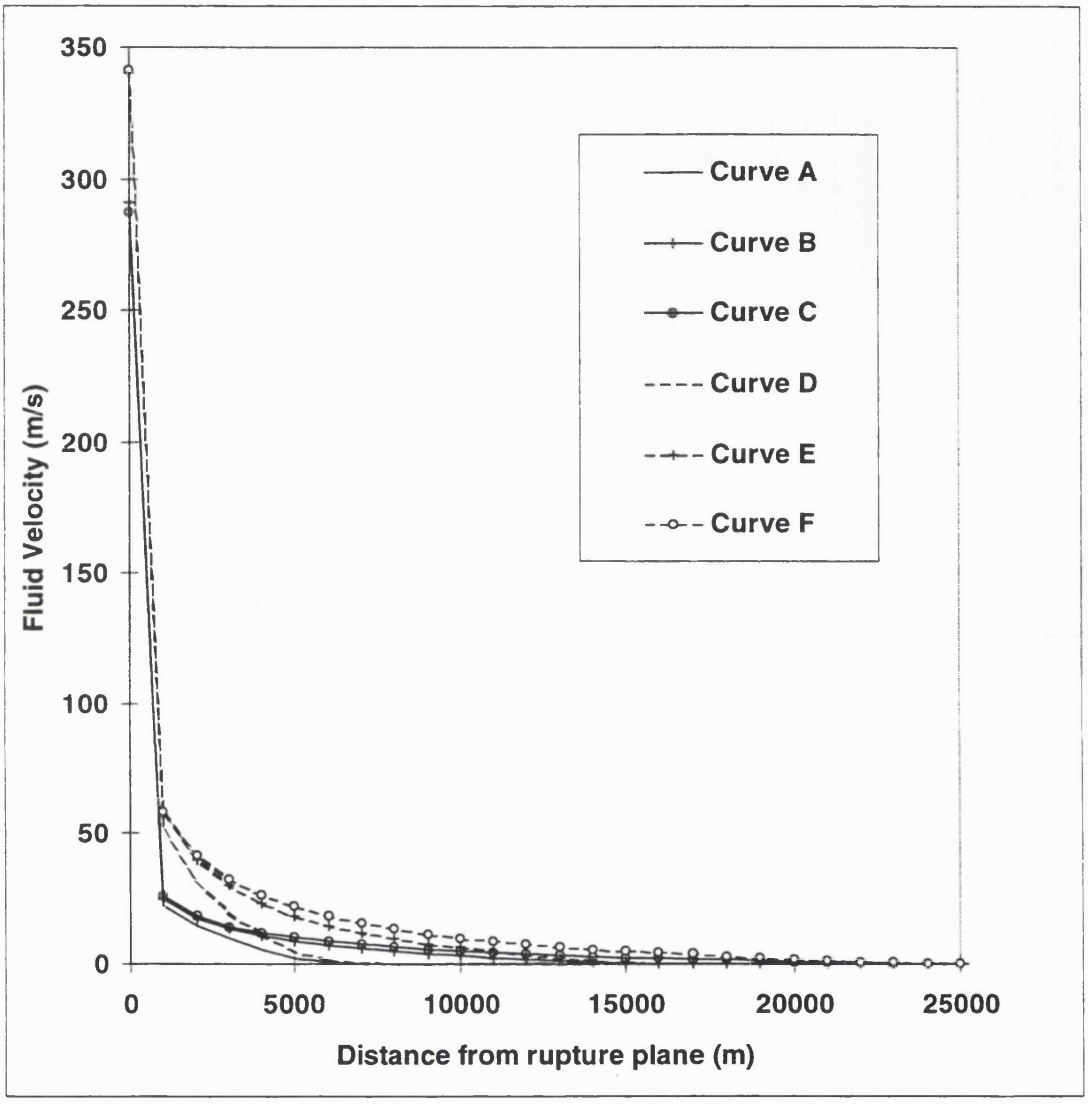

Figure 5.10.2: Variation of fluid velocity with distance from the rupture plane at different times subsequent to FBR (Piper Alpha mixture).

Curve A: Two-phase; t = 9.23 s
Curve B: Two-phase; t = 27.69 s
Curve C: Two-phase; t = 46.15 s
Curve D: Ideal gas; t = 9.23 s
Curve E: Ideal gas; t = 27.69 s
Curve F: Ideal gas; t = 46.15 s

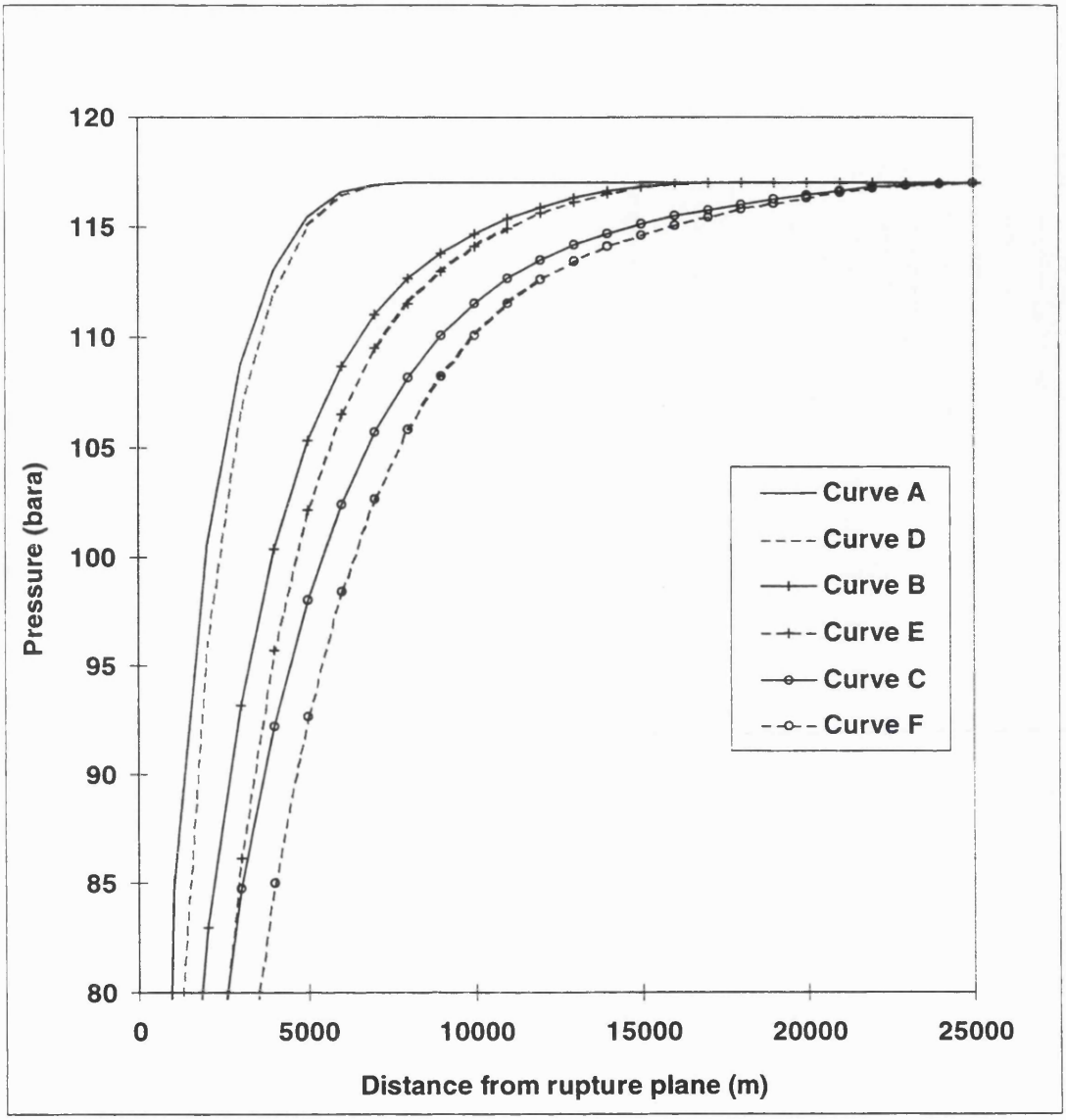

Figure 5.10.3: Variation of pressure with distance from the rupture plane at different times subsequent to FBR (Piper Alpha mixture).

Curve A: Two-phase; t = 9.23 s
Curve B: Two-phase; t = 27.69 s
Curve C: Two-phase; t = 46.15 s
Curve D: Ideal gas; t = 9.23 s
Curve E: Ideal gas; t = 27.69 s
Curve F: Ideal gas; t = 46.15 s

respectively. For both ball and check valves, the difference in activation times between the two models can be expected to be more noticeable the further the valves are placed from the rupture plane.

On the other hand, although the differences between the gas phase and two-phase activation times are small, for the high momentum flows that occur as a result of FBR, approximation of real behaviour with an ideal gas assumption could lead to significant under-estimations in inventory loss calculations.

5.10.2 Mass release data

The general trends observed from the ideal gas model are expected to be applicable for two-phase flows, namely, that a check valve offers a better degree of protection as compared to a ball valve when either is placed in close proximity to the rupture plane, and that at long distances the difference in performance between the two valves becomes insignificant. However, a considerable under-estimation in the release rate and hence the calculated inventory loss will result if the ideal gas model is used as opposed to two phase.

Figure 5.10.4 shows the variation of release rate with time subsequent to valve closure for various arbitrary delays in shut-down. The ESDV is placed 300m from the rupture plane. Curves A and B respectively show the results obtained using the two-phase model for valve shutdown taking place 1.37 and 6.47 s after the passage of flow reversal. Curves C and D show the corresponding results for an ideal gas.

It is clear from the data that the predicted release rate in the case of the two-phase mixture is significantly higher than that for the gas following emergency isolation of the pipeline. Pipeline depressurisation times are also longer.

For example, in the case of a 1.37 s delay in shutdown, complete evacuation of the isolated section of the ideal gas pipeline takes ca. 10 s (Curve C). The corresponding evacuation time for the two-phase mixture is ca. 16 s (Curve A). Similar differences can be observed for a closure delay of 6.47 s.

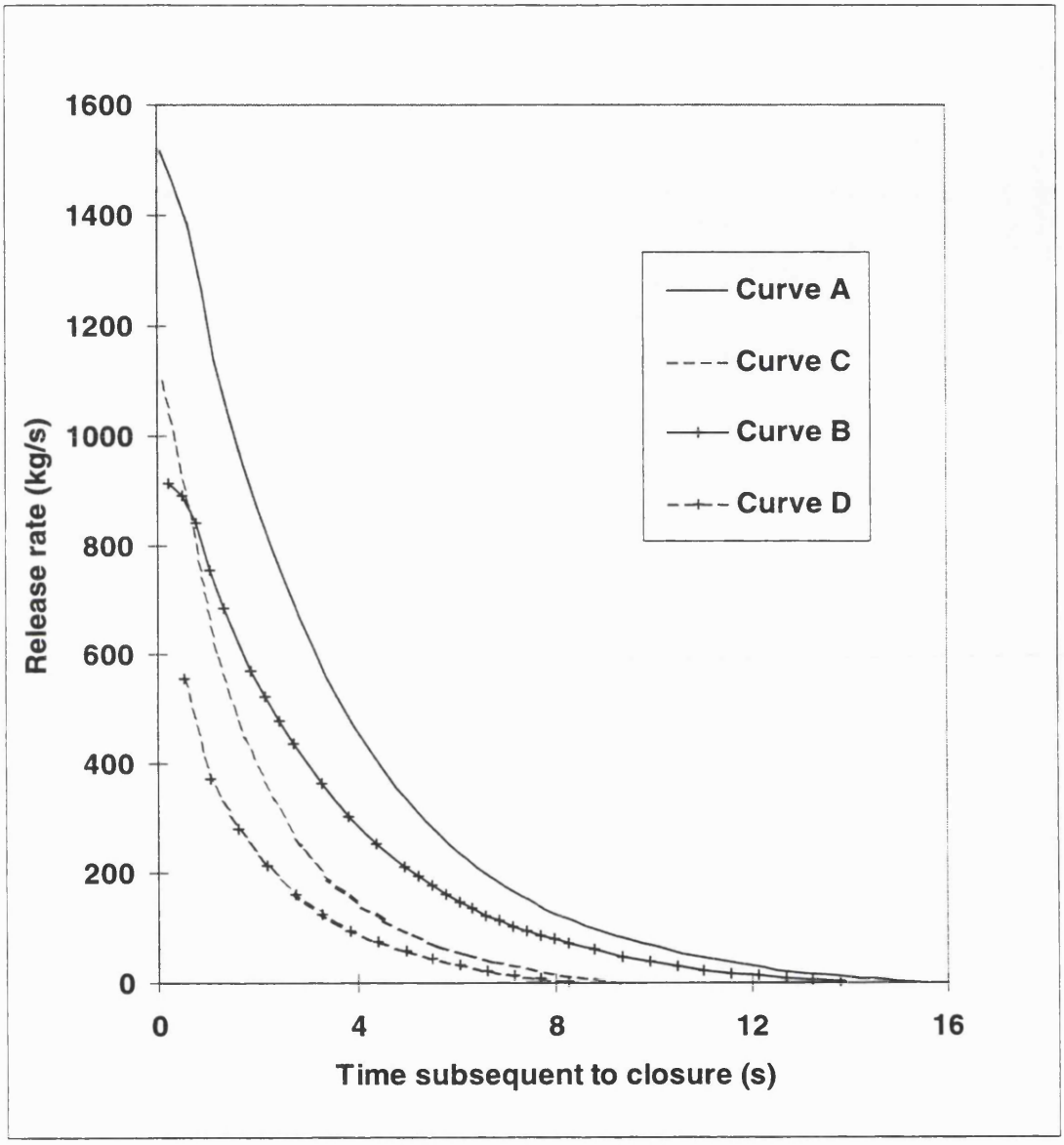

Figure 5.10.4: Variation of release rate with time subsequent to check valve closure for arbitrary delays in shutdown (Piper Alpha mixture).

Curve A: Two-phase; valve closure delay after the passage of flow reversal = 1.37 s
Curve B: Two-phase; valve closure delay after the passage of flow reversal = 6.47 s
Curve C: Ideal gas; valve closure delay after the passage of flow reversal = 1.37 s
Curve D: Ideal gas; valve closure delay after passage of flow reversal = 6.47 s

The combination of the higher flow rate and the slower depressurisation rate for the two-phase mixture clearly indicate that the total inventory released prior to pipeline isolation will be greater than that for the gas pipeline. For the ranges tested, this is regardless of the delay in valve closure.

5.10.3 Pressure/Time history

Figure 5.10.5 shows the effect of time delay in valve closure following the passage of flow reversal on the pressure/time history at the upstream side of a check valve placed 300 m from the rupture plane. Curves A-D show the data for the two-phase mixture whereas Curves E-H relate to the gas system. The data is taken for a shorter pipeline (5 km) in order to reduce the CPU time. The general conclusions reached are however not expected to be affected.

As foreseen, when the valve shuts immediately on sensing flow reversal, i.e. at t=0 s, no pressure oscillation is predicted by either model (Curves A and E).

From our experience, the pressure peaks associated with expansion waves always slightly precede the loci of flow reversal (see section). As a result, when instantaneous shutdown of check valve occurs at the position of flow reversal (Curves A and E), there is a slight pressure differential across the valve. However, this disturbance quickly disappears due to frictional effects before being able to reflect from the intact end thus not giving rise to pressure oscillations. The larger the time delay, the greater is the resulting pressure differential impinging on the upstream valve face and the greater the consequent disturbance oscillating within the isolated section.

The upstream pressure predicted from the two phase model is always larger than that from the gas phase; the difference becoming more pronounced with the delay in valve closure. The latter is due to the increase in the volume fraction of liquid with the passage of time prior to valve closure, and also due to increasing non-linearity in fluid properties as a result of the increasing magnitude of the pressure disturbance.

The magnitude of the observed pressure peaks in figure 5.10.5 are however alarming.

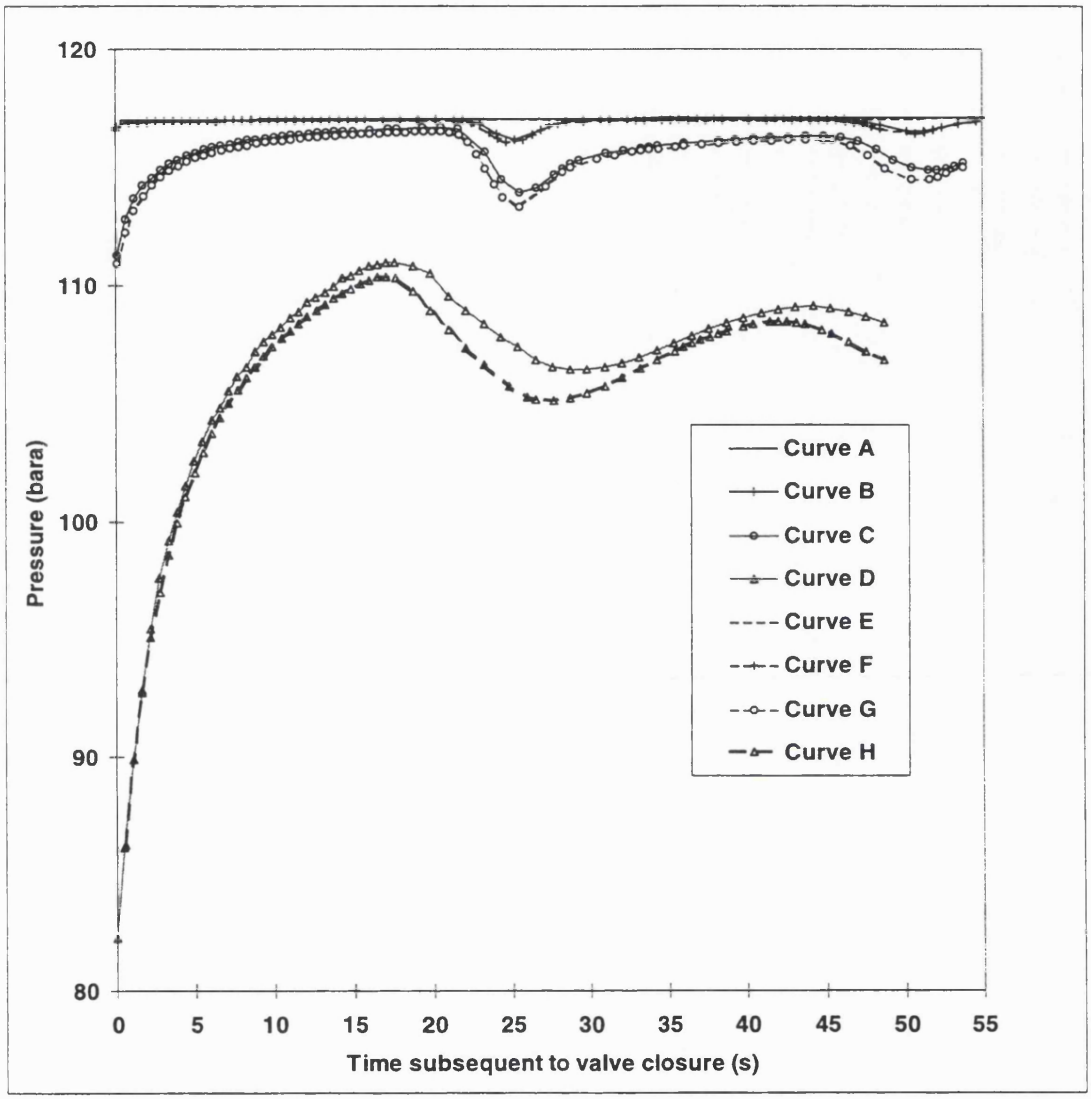

Figure 5.10.5: The effect of time delay in valve closure following the passage of flow reversal on the pressure-time history at the upstream side of a check valve placed 300m from the rupture plane (Piper Alpha mixture).

Curve A: Two-phase; time delay = 0s
Curve B: Two-phase; time delay = 0.57s
Curve C: Two-phase; time delay = 1.37s
Curve D: Two-phase; time delay = 6.47s
Curve E: Ideal gas; time delay = 0s
Curve F: Ideal gas; time delay = 0.57s
Curve G: Ideal gas; time delay = 1.37
Curve H: Ideal gas; time delay = 6.47s

For example, a delay of 6.47 s in valve closure results in a pressure rise of almost 30 bara on the upstream side of the valve. This could have serious consequences in practice.

Figure 5.10.6 shows the results for the effect of pipeline length on the upstream pressure-time history of a check valve, placed 300m from the rupture plane (Piper Alpha mixture). The valve is assumed to close 1.37 seconds after the passage of flow reversal. Curves A - C show the results obtained using the two phase model for pipeline lengths of 1, 5 and 54 km respectively. Curves D - F show the corresponding results for the ideal gas model.

As noted in chapter 4, the shorter the pipeline the greater is the frequency and magnitude of oscillation since the pressure waves are reflected to and fro between the closed walls at either end in considerably smaller time periods. The differences between the results predicted from the ideal gas and two-phase models become more pronounced the shorter the pipeline since the subsequent large changes in pressure can lead to considerable and frequent changes in fluid properties which can only be detected accurately by a two-phase model. For long pipelines, both models give similar results because of a reduction in the frequency of pressure oscillations.

Figure 5.10.7 shows the upstream ball valve pressure-time histories for different closure rates for the Piper Alpha mixture. Curves A and B show the two-phase model results for closure rates of 2.54 and 5.08 cm/s respectively whereas Curves C and D show the corresponding data for the ideal gas assumption. As before, the valve is assumed to activate on sensing a pressure drop of 10 bara below the normal operating pressure (117 bara).

As expected, both the ideal gas and two phase models show that the faster is the valve closure rate, the greater is the accrual of line pressure. Closure times after activation are 16.5 seconds for valve closure at 2.54 cm/s and 8.25 seconds for a closure rate of 5.08 seconds.

As the valve starts to close the pressure continues to drop at the valve location while the aperture diameter is still comparable to that of the pipe. On approaching the halfway stage of closure, the pressure then starts to build up with the two-phase model predicting higher pressures than the ideal gas. The observed faster initiation

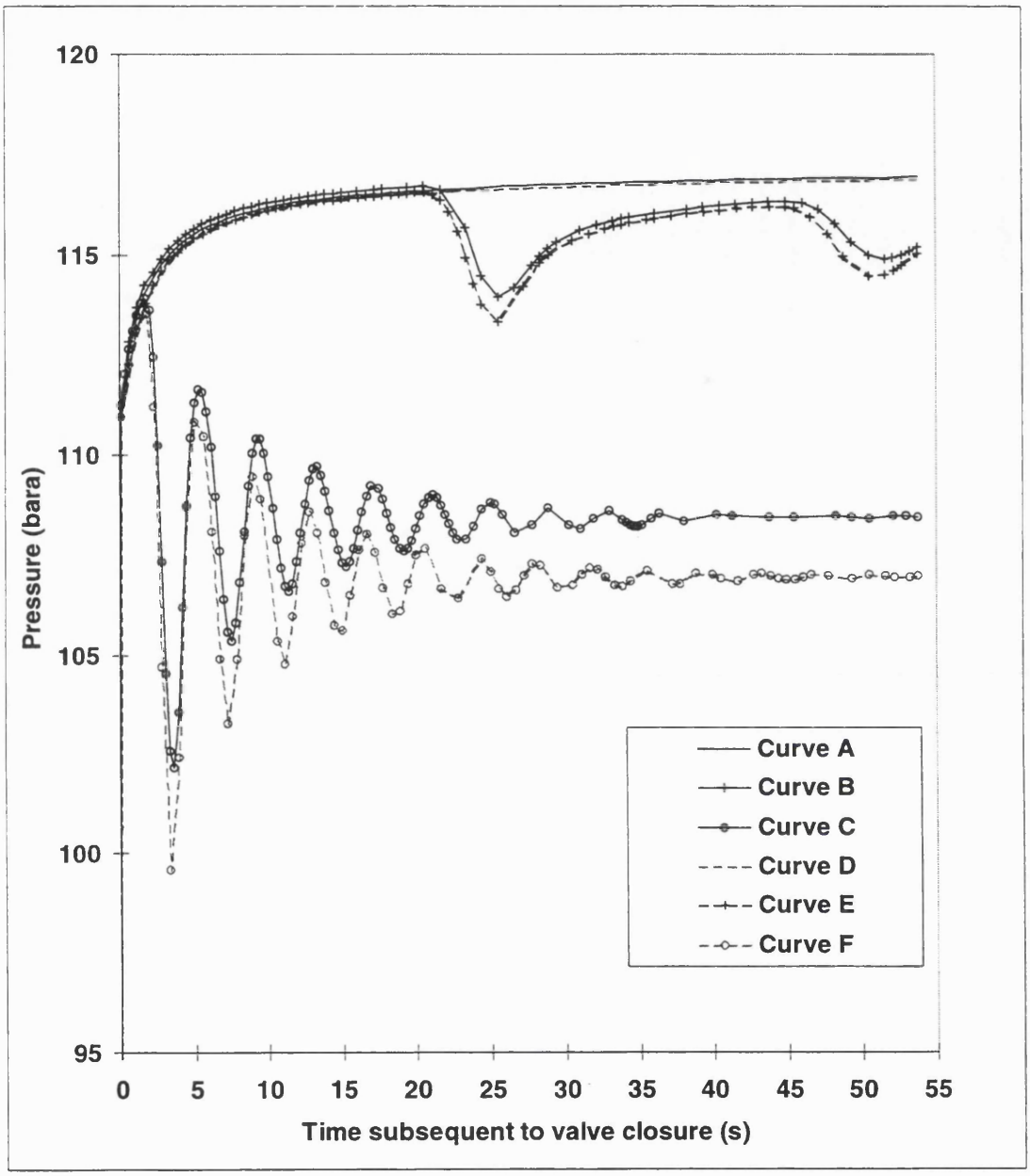

Figure 5.10.6: The effect of pipeline length on the upstream pressure-time history of a check valve, placed 300m from the rupture plane. Check valve shuts 1.37 s after the passage of flow reversal (Piper Alpha mixture).

Curve A: Two-phase; pipeline length = 54km
Curve B: Two-phase; pipeline length = 5km
Curve C: Two-phase; pipeline length = 1km
Curve D: Ideal gas; pipeline length = 54km
Curve E: Ideal gas; pipeline length = 5km
Curve F: Ideal gas; pipeline length = 1km

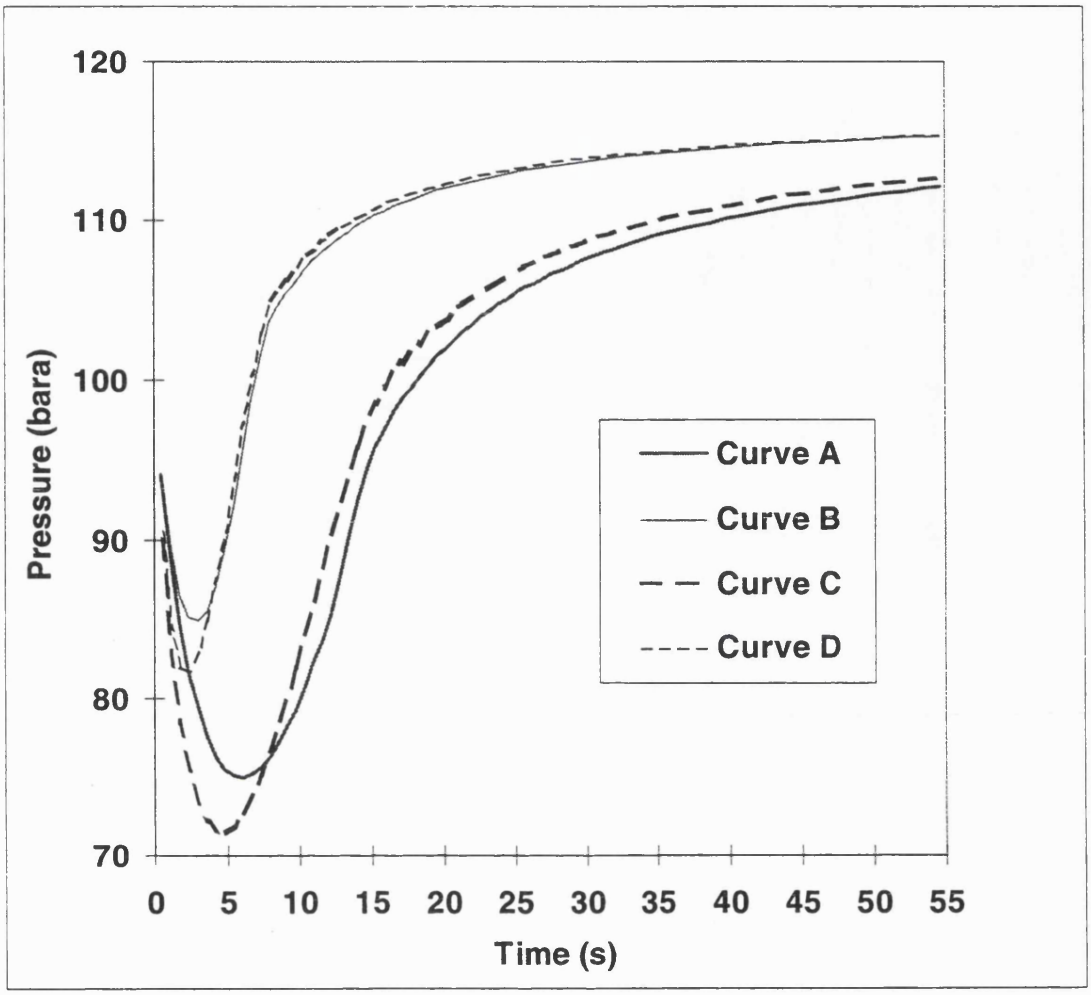

Figure 5.10.7: Upstream Ball Valve pressure-time histories for different closure rates (Piper Alpha mixture)

Curve A: Two-phase, 2.54 cm/s
Curve B: Two-phase, 5.08 cm/s
Curve C: Ideal gas, 2.54 cm/s
Curve D: Ideal gas, 5.08 cm/s

time for this pressure increase in the case of the ideal gas can be attributed to the fact that wave velocity predictions are larger in this case. When the valve crosses the halfway stage, the continuing pressure rise is steeper in the ideal gas than the two phase model and the former goes on to give higher line pressure predictions, even after the valve fully shuts. This result is surprising considering that up to now, the results for check valve closure have indicated that the ideal gas model predicts lower valve face pressures.

Figure 5.10.8 shows the pressure variation with time at the downstream side of the ball valve during closure for the Piper Alpha mixture. Curves A and B show the two-phase model results for closure rates of 2.54 and 5.08 cm/s respectively whereas Curves C and D show the corresponding results for an ideal gas.

In this case, there is a significant difference between the ideal gas and the two phase models with the latter predicting much higher pressures. Hence the pressure drop across the valve is much greater in the ideal gas than in the two phase model. This in turn gives rise to faster depressurisation rates and as a result contributes to the lower inventory loss predictions as discussed in section 5.10.2.

5.10.4 Pressure Surge

Figure 5.10.9 shows the pressure surge versus time delay predictions obtained using the two-phase (Curve A) and ideal gas models (Curve B). Pressure surge data were calculated using equation 4.7.1 shown again below,

$$\Delta P = \rho\left(a u_r + u_r^2\right) \qquad (4.7.1)$$

It is surprising to note that the ideal gas model predicts much higher pressure surge despite its lower density. Figure 5.10.10 shows the variation of fluid density at the valve location with time as predicted from the two phase (Curve A) and the ideal gas

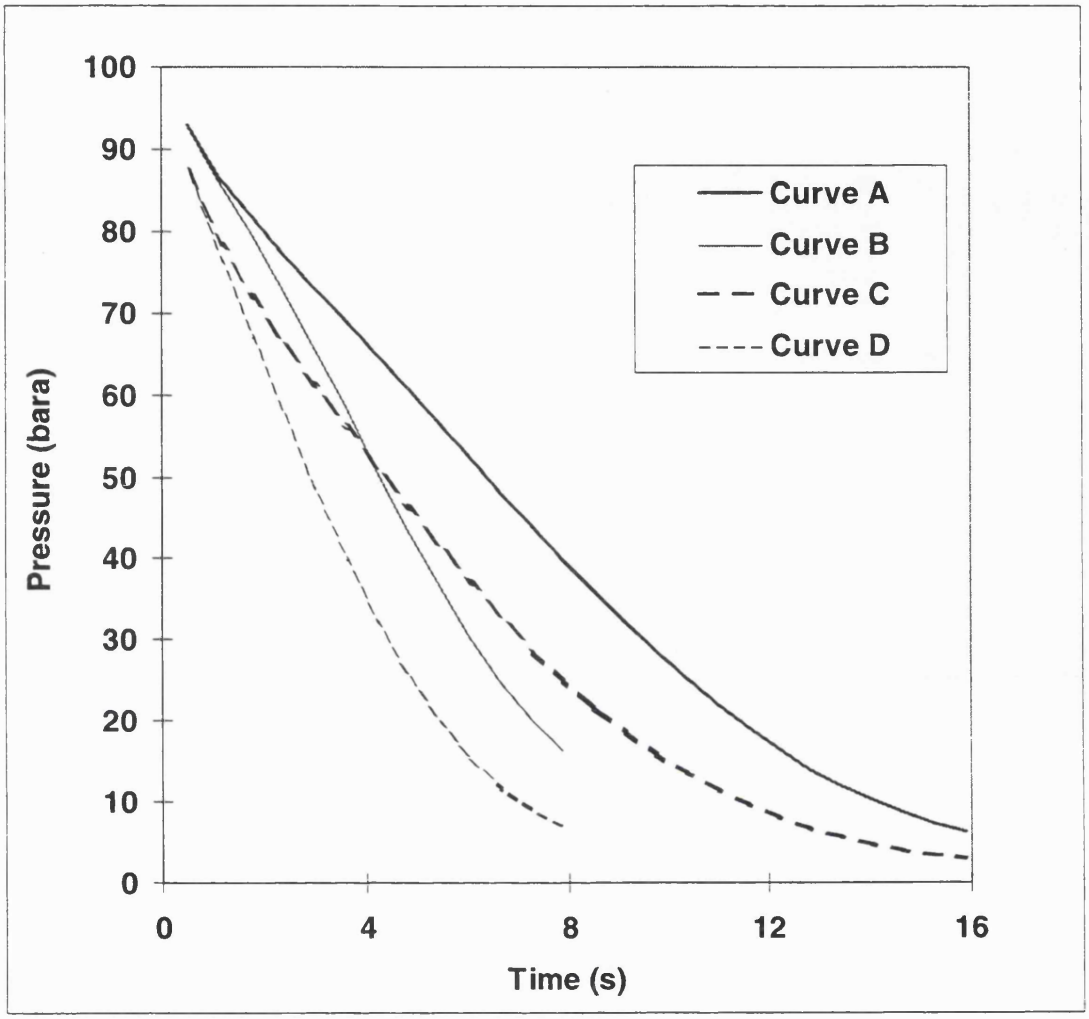

Figure 5.10.8: Downstream Ball Valve pressure-time histories for different closure rates (Piper Alpha mixture).

Curve A: Two-phase, 2.54 cm/s
Curve B: Two-phase, 5.08 cm/s
Curve C: Ideal gas, 2.54 cm/s
Curve D: Ideal gas, 5.08 cm/s

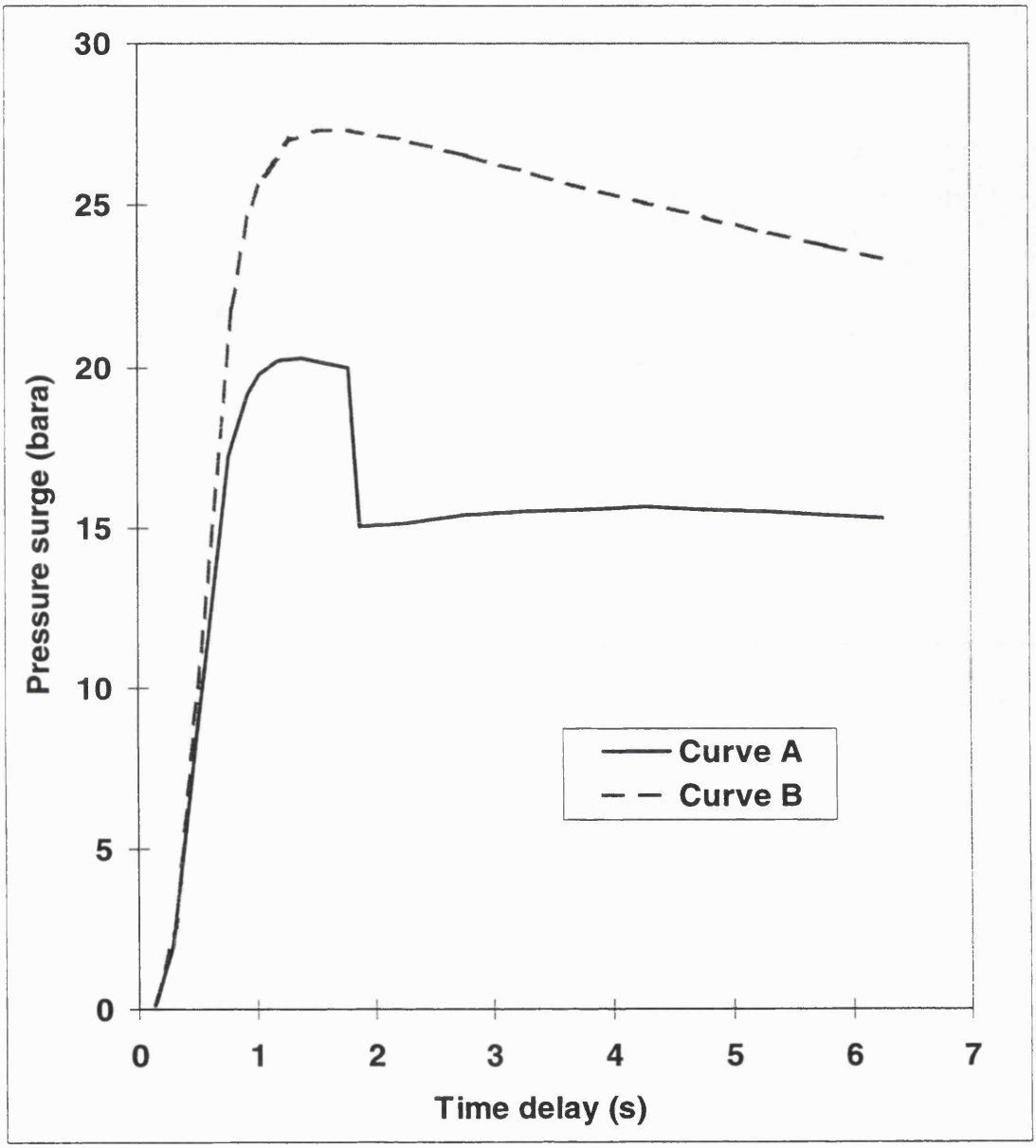

Figure 5.10.9: Variation of pressure surge at various valve closure time delays following the passage of flow reversal (Piper Alpha mixture).

Curve A: Two-phase
Curve B: Ideal gas

models (Curve B). As expected a large difference in density prediction is obtained, the two phase giving larger density values.

The lower pressure surge observed in the case of the two phase mixture is due to the overriding effect of the terms u_r^2 and $u_r a$ in equation 4.7.1, both being much higher in the case of the ideal gas assumption as opposed to the two-phase model, as shown in figures 5.10.11 and 5.10.12.

The sudden drop in the term $u_r a$ shown in figure 5.10.12 which also affects the pressure surge data at the same time corresponds to condensation effects.

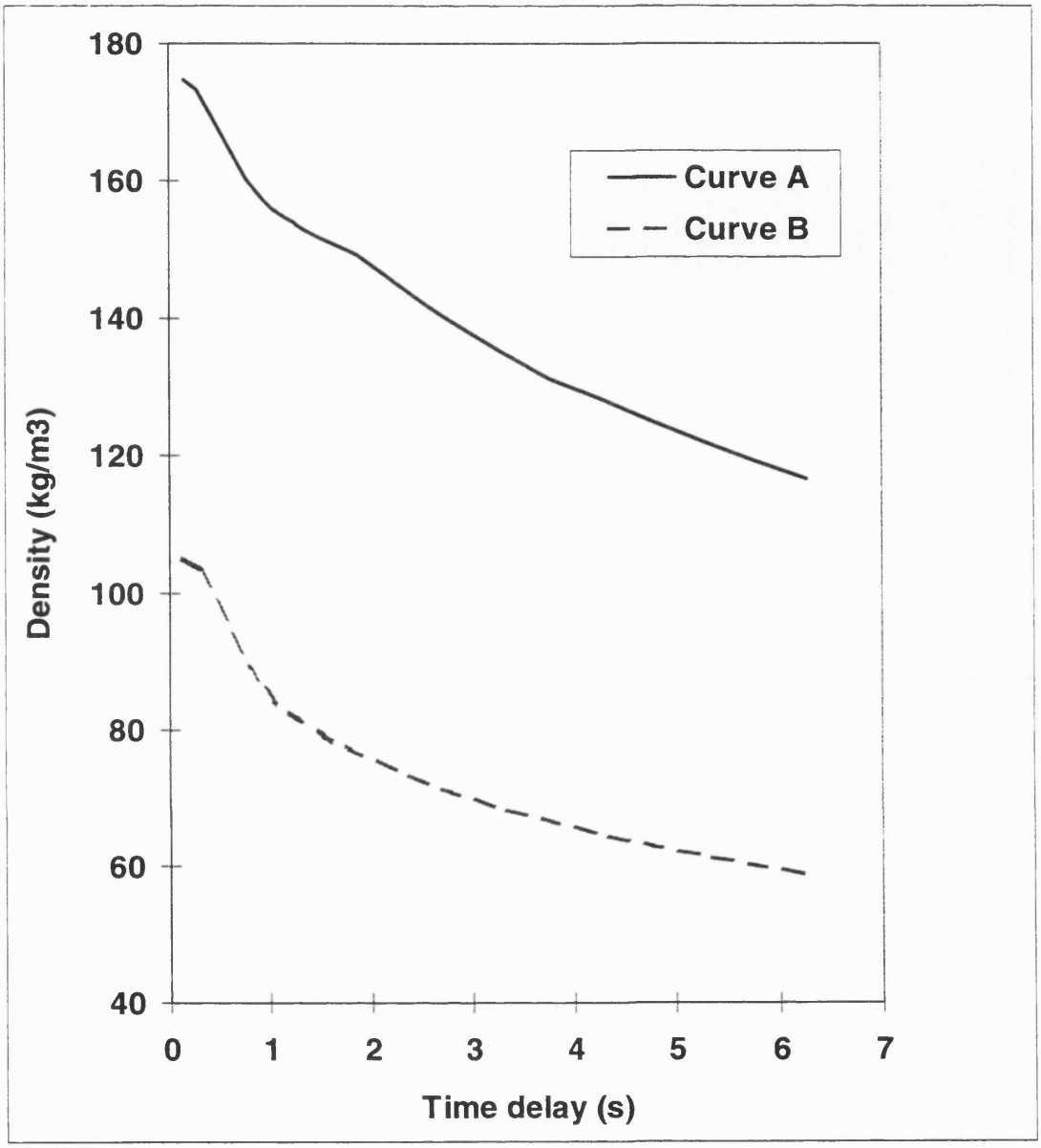

Figure 5.10.10: Variation of fluid density at the valve location for various closure time delays subsequent to the passage of flow reversal (Piper Alpha mixture).

Curve A: Two-phase
Curve B: Ideal gas

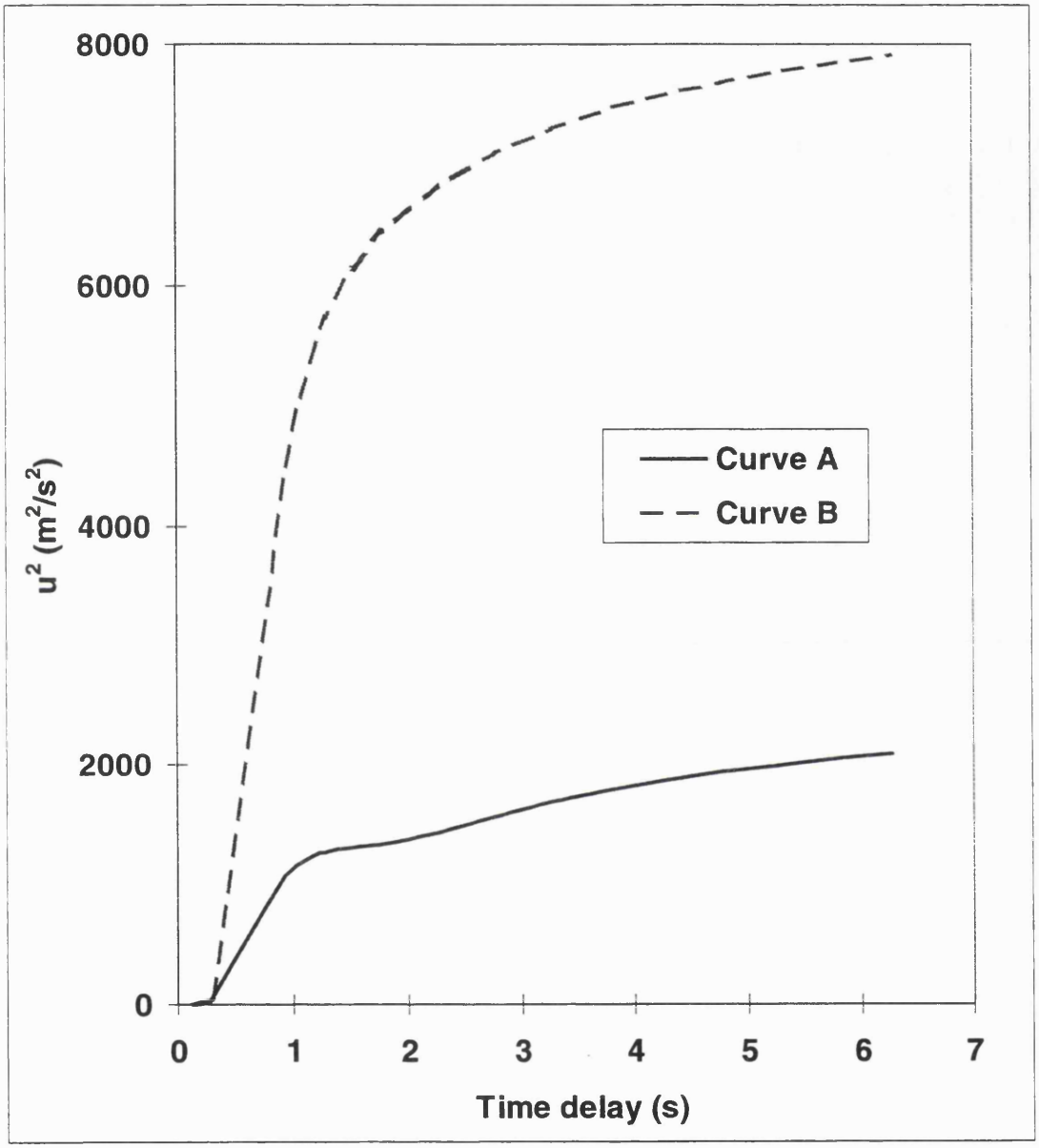

Figure 5.10.11: Variation of the term, u^2, at the valve location for various closure time delays subsequent to the passage of flow reversal (Piper Alpha mixture).

Curve A: Two-phase
Curve B: Ideal gas

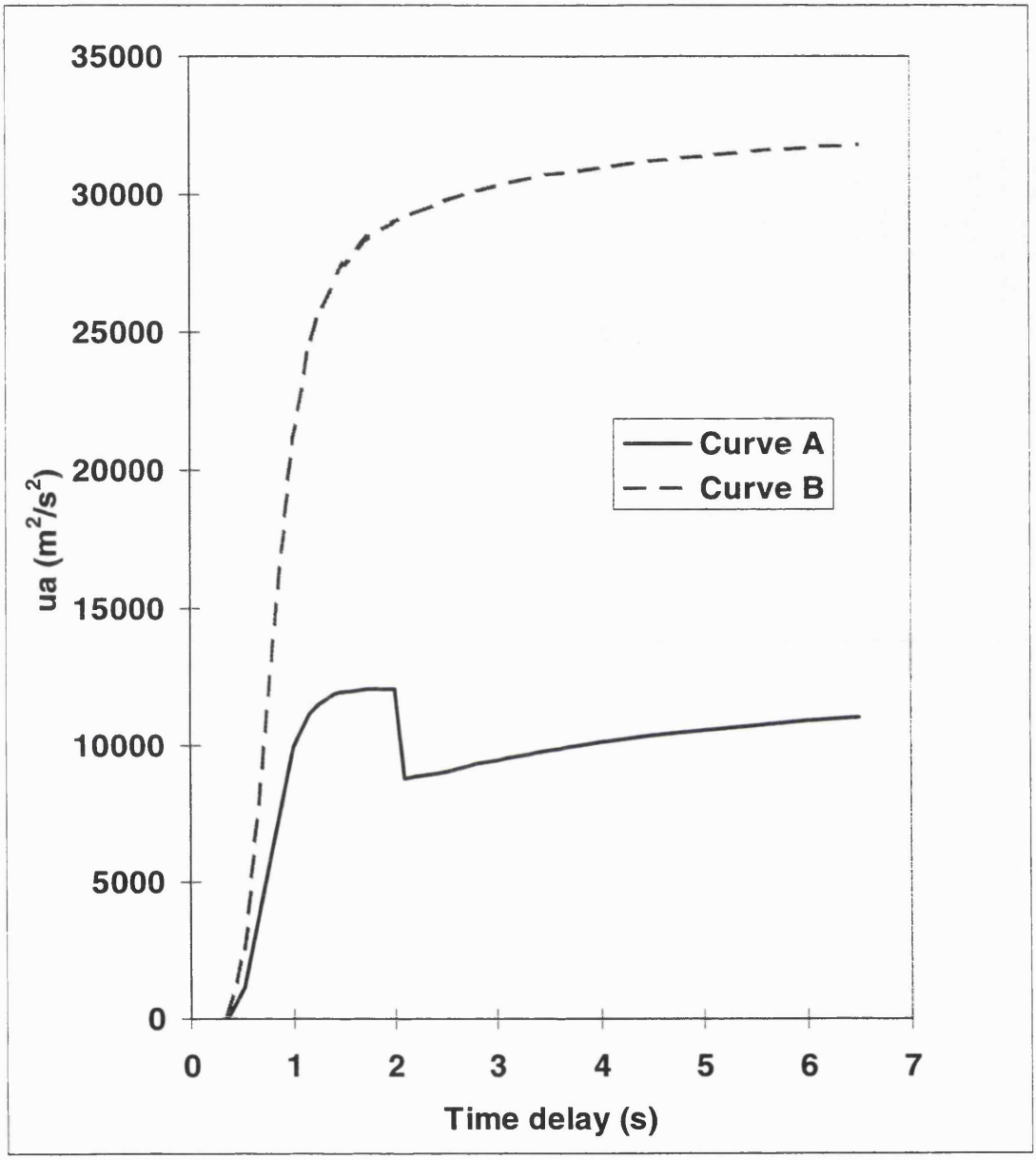

Figure 5.10.12: Variation of the term, ua, at the valve location for various closure time delays subsequent to the passage of flow reversal (Piper Alpha mixture).

Curve A: Two-phase
Curve B: Ideal gas

5.11 CONCLUDING REMARKS

In this chapter, the ideal gas model based on the method of characteristics and relying on a specified time intervals grid for numerical discretisation (CNGS) as proposed in chapter 4 has been developed to deal with two-phase flows (CNGS-HEM). Subsequent optimisation and validation with field data have also been made for condensable gas (Piper Alpha) and flashing liquid (LPG) flows in long pipelines (>=100m). The conclusions that can be drawn are as follows:

- The use of curved characteristics at the rupture plane for real fluid flows enables use of large Δx's without sacrificing global accuracy, yet at the same time allowing fast CPU times
- Significant error can be eliminated by performing isothermal flash calculations to determine fluid densities in between grid points instead of relying on interpolation techniques. The elimination of this error contributes to much greater stability of the model as divergent oscillations in pressure and density as noticed by Picard and Bishnoi (1989) are not prevalent
- The magnitude of each time step is restricted by the phase transition boundary and the satisfaction of the choking boundary condition for homogeneous fluid flow (u=a).
- The results of CNGS-HEM for the Piper Alpha simulation show excellent agreement with measured data pertaining to intact end pressures. Comparison of other data such as volume fraction of condensation and release rate with Chen's (1993) META-HEM also show good agreement. A comparison of the efficiency of the CNGS-HEM with META-HEM with respect to CPU times is not possible since they are run on different computers. META-HEM takes about 6 weeks on a DEC station to profile 20000 s of depressurisation. CNGS-HEM takes 6 days on a DEC Alphaserver 8400 5/440 running at 440MHz.
- CNGS-HEM gives good agreement when modelling pressure, temperature and total line inventory variations with time for FBR of a pipeline containing a LPG

- mixture. CNGS-HEM also compares very favourably with META-HEM, however two-fluid models such as MSM-CS (Chen, 1993) and PLAC perform surprisingly poorly in comparison. This backs up the findings of Chen (1993) that the fluid can be taken to be at thermal and mechanical equilibrium during the depressurisation process. Thermal non-equilibrium is insignificant except for the very early stages of depressurisation when processes such as delayed bubble nucleation may be prominent
- CNGS-HEM predicts higher release rates for the LPG FBR experiments than META-HEM although velocities at the rupture plane exhibit the opposite trend. This is due to CNGS-HEM predicting higher fluid densities than META-HEM, signifying a smaller rate of gas evolution
- Models such as PLAC that use interpolation techniques during the transient depressurisation calculations to calculate mixture properties are generally faster than more complete models such as CNGS-HEM, but can result in considerable inaccuracy for certain types of mixtures, especially those with a very narrow phase envelope
- The dynamic response of both ball and check valves are affected by making the assumption of ideal gas. The ideal gas assumption predicts higher fluid and expansion wave velocities leading to faster activation times for both types of valves. The ideal gas model also fails to detect the reduction in expansion wave velocity due to the onset of two-phase flows.
- Pipelines containing two-phase fluids can be expected to be more susceptible to delayed emergency shutdown than those containing just gas.
- The ideal gas model can significantly under-estimate release rate and total depressurisation time thus yielding under-estimations with respect to inventory loss predictions. This can have damaging consequences when performing the safety case for any installation.
- For check valves, the two-phase model predicts higher upstream valve pressures with respect to the ideal gas model. The difference between the two models increases with valve closure time delay due to increasing real fluid effects.

☞ The pressure surge in a two-phase mixture can be expected to be smaller than that in a gas phase. This is due to the lower velocity and speed of sound predictions in two-phase flows.

CHAPTER 6: CONCLUSIONS AND SUGGESTIONS FOR FUTURE WORK

6.1 CONCLUSIONS

This thesis describes the development and application of a mathematical model based on the Method of Characteristics to describe the fluid dynamic effects subsequent to full-bore rupture (FBR) of a high pressure pipeline. The study also includes simulation and analysis of ESDV dynamic response, particularly for ball valves and check valves following FBR.

In chapter 2, the Navier-Stokes equations are simplified to the Euler equations. This is done based on the assumptions of homogeneous equilibrium and viscid-inviscid fluid flow together with negligible heat conduction effects within the fluid.

By making the assumption of homogeneous flow, a single momentum equation is sufficient for both phases and likewise with respect to the energy equation for the assumption of thermodynamic equilibrium between the two phases. As a result of these assumptions, the equations obtained for a real fluid are similar to those obtained for an ideal gas.

The use of the derived thermodynamic relations require prior knowledge of the state (gas, liquid or two-phase) of the mixture This is provided by the Michelsen stability criterion which thus allows accurate tracking of the phase boundary transition.

In chapter 3, the hyperbolic nature of the Euler equations of flow is shown in terms of the characteristic wave solutions. Various numerical techniques for the solution of the Euler equations are reviewed and based on this, the method of characteristics using a specified time (ST) interval grid is chosen for the following reasons:

- discontinuities in the initial value may propagate along the characteristics, making it easy to handle
- no additional smoothing parameter is needed to control overshoot and oscillation as is the case with second or higher order explicit finite difference schemes

- the boundary conditions are properly posed
- boundary conditions may be introduced at predefined times in the ST grid approach. This feature makes the ST method useful in modelling the dynamic effects of ESDV closure at various locations within the pipeline by choosing an appropriate grid spacing.

In chapters 4 and 5, it is found that a proposed modification to the classical ST method of characteristics gives the same accuracy of results as the classical ST method but for a given run, CPU time for the former is less than a tenth of the latter. This is because in the new procedure, no iteration is needed to calculate the locations of the initial points. The validity of this approach is tested by comparison of this model's results (CNGS) with the classical approach for the Piper Alpha FBR scenario, assuming that the mixture always stays in the gas phase. Good agreement is also obtained with the Wave Tracing Method, based on a characteristic grid type solution, of Chen et. al. (1993).

It is also shown that the use of a nested grid is essential if underestimation of the release rate is to be avoided and if accuracy in the fast transient region near the rupture plane is not to be compromised. For a given pipeline, although the number of elements in a nested grid scheme is greater than that for a simple grid scheme, the CPU time for the former is faster due to accelerated convergence near the rupture plane.

In the case of ideal gases, the use of curved characteristics makes little difference to accuracy as compared to the first order linear solution. However the CPU time is significantly longer. For real fluids, the use of curved characteristics at the rupture plane enables use of large Δx's without sacrificing global accuracy, yet at the same time allowing fast CPU times

The inclusion of heat transfer effects is necessary if the late time regime is to be modelled accurately. The effects of a fire surrounding a pipeline can only be modelled if the model includes heat transfer from the surroundings.

In chapter 5, the CNGS is further developed so as to handle two-phase flows (CNGS-HEM). Subsequent optimisation and validation with field data have also been carried

out for condensable gas (Piper Alpha) and flashing liquid (LPG) flows in long pipelines (>=100m). The conclusions that can be drawn are as follows:

- Significant error can be eliminated by performing isothermal flash calculations to determine mixture fluid densities in between grid points instead of relying on interpolation techniques. The elimination of this error contributes to much greater stability of the model as divergent oscillations in pressure and density as noticed by Picard and Bishnoi (1989) are not prevalent.

- The magnitude of each time step is restricted by the phase transition boundary and the satisfaction of the choking boundary condition for homogeneous fluid flow (u=a).

- The results of CNGS-HEM for the Piper Alpha simulation show excellent agreement with measured data pertaining to intact end pressures. Comparison of other data such as volume fraction of condensation and release rate with Chen's (1993) META-HEM also show good agreement. A comparison of the efficiency of the CNGS-HEM with META-HEM with respect to CPU times is not possible since they are run on different computers. META-HEM takes about 6 weeks on a DEC station to profile 20000 s of depressurisation. CNGS-HEM takes 6 days on a DEC Alphaserver 8400 5/440 running at 440MHz.

- CNGS-HEM gives good agreement when modelling pressure, temperature and total line inventory variations with time for FBR of a pipeline containing a LPG mixture. CNGS-HEM also compares very favourably with META-HEM. However two-fluid models such as MSM (Chen, 1993) and PLAC perform surprisingly poorly by comparison. This backs up the findings of Chen (1993) that the fluid can be taken to be at thermal and mechanical equilibrium during the depressurisation process. Thermal non-equilibrium is insignificant except for the very early stages of depressurisation when processes such as delayed bubble nucleation may be prominent.

- CNGS-HEM predicts higher release rates for the LPG FBR experiments than META-HEM although velocities at the rupture plane exhibit the opposite trend. This is due to CNGS-HEM predicting higher fluid densities than META-HEM, signifying a smaller rate of gas evolution.

☞ Models such as PLAC that use interpolation techniques during the transient depressurisation calculations to calculate mixture properties are generally faster than more complete models such as CNGS-HEM, but can result in considerable inaccuracy for certain types of mixtures, especially those with a very narrow phase envelope.

With regards to the valve closure simulations in chapters 4 and 5, the following conclusions can be drawn,

i. The dynamic response of both check valves and ball valves following FBR depends primarily on their proximity to the rupture plane and the flow reversal propagation speed. As the latter is directly related to the velocity of sound in the fluid medium relative to the escaping fluid,

   a) pipelines containing gases are expected to be more susceptible to delayed emergency shut-down compared to those containing liquids. This however should be balanced against the higher pressure surges expected in liquid pipelines. On the other hand, pipelines containing two-phase fluids can be expected to be more susceptible to delayed emergency shutdown than those containing just gas.

   b) shut-down delay is expected to be longer when rupture occurs during 'normal' flow as compared to that occurring during 'shut-in'. This is because in the former the expansion wave propagation velocity, which directly affects the valve activation time, is decelerated due to the normal flow of gas in the opposite direction.

ii. The dynamic response of both ball and check valves are affected by making the assumption of ideal gas. The ideal gas assumption predicts higher fluid and expansion wave velocities leading to faster activation times for both types of valves. The ideal gas model also fails to detect the reduction in expansion wave velocity due to the onset of two-phase flows.

iii. In the case of a check valve, the amplitude and frequency of upstream pressure fluctuations following emergency shut-down are directly related to,

   a) gas flow reversal velocity at the time of valve closure

b) valve proximity to the rupture plane

c) pipeline length

d) fluid compressibility

The two-phase model predicts higher upstream check valve pressures with respect to the ideal gas model. The difference between the two models increases with valve closure time delay due to increasing real fluid effects. Pipelines incorporating ball valves are generally less susceptible to pressure surges or oscillations depending on closure rate.

iv. No pressure surge is expected in the case of a check valve closing instantaneously upon sensing flow reversal. However, even in the case of a very short delay (ca 2s), a relatively large build-up in the pressure surge to a maximum value can be expected. It then diminishes in magnitude for larger closure delays.

v. The pressure surge in a two-phase mixture can be expected to be smaller than that in a gas phase. This is due to the lower velocity and speed of sound in two-phase flows.

vi. In terms of limiting the amount of released inventory following emergency shut-down, a check valve offers a far better degree of performance as compared to a ball valve when either is placed at close proximity of the rupture plane. At longer distances however, the difference in performance becomes insignificant.

vii. The ideal gas model can significantly under-estimate release rate and total depressurisation time thus yielding under-estimations with respect to inventory loss predictions. This can have serious implications when performing the safety case for any installation.

viii. A deceptively simple argument that the total amount of inventory released following FBR is equal to that present in the isolable section of the pipeline prior to ESD may give rise to gross underestimates particularly in the case of ball valves placed in close proximity of the rupture plane.

In conclusion, the results of this thesis demonstrate the importance of analysing the effect of fluid flow behaviour following full bore pipeline rupture on the dynamic response of emergency shutdown valves. The general conclusions reached however, are applicable to the range of parameters tested in the present study. Although, they may serve as a useful starting point, a comprehensive analysis is recommended in conjunction with the particular system under investigation. This is particularly the case for pipelines containing two-phase mixtures. The MOC has been shown to be a powerful tool in allowing such type of analysis.

6.2 SUGGESTIONS FOR FUTURE WORK

ESDV dynamic simulation studies in flashing liquid flows

ESDV dynamic simulations in this study have been performed in conjunction with a condensable gas mixture. The techniques used to date should be applied to simulate the effect of flashing liquid flows such as LPG on the various parameters tested, e.g. inventory loss, pressure surge, pressure oscillation and valve activation times.

Use of variable Δt depending on flow conditions

The use of a Δt that is only 10% of the maximum permissible according to the CFL criterion has been shown to be necessary for accurate prediction of fluid parameters across the phase transition interface. Further investigation needs to be performed to clarify if the Δt can be increased when the whole pipeline contains the same phase. The same test also needs to be performed with respect to satisfying the choking condition at the rupture plane during the late time regime.

Use of an implicit-explicit method of characteristic scheme

The possibility exists to model the characteristic curve refraction across the phase transition interface as a result of different fluid compressibility (Nakamura et. al., 1975) within the confines of an implicit MOC. The drawback of this methodology is that it can only be applied when the acoustic effect is not so important, i.e. for Mach numbers less than 0.5. However this method should be suitable for internal flows far from the rupture plane. The advantage of this method is that it is implicit so that fluid parameter interpolations occur along the temporal axis instead of the spatial axis. An investigation of the use of this method in conjunction with the method proposed in this thesis needs to be performed with the potential of further reduction in CPU time.

Use of interpolation techniques for the calculation of fluid properties

Since a significant proportion of CPU time is spent performing flash calculations, it is envisaged that great reduction in CPU time is likely if flash calculations can be avoided wherever possible. In the slow transient region that exists the further one gets from the rupture plane in any long pipeline, fluid thermodynamic properties tend to vary much less drastically than in the fast transient region. Therefore, the prediction of fluid properties based on various interpolation techniques ought to be tried as an alternative to always performing flash calculations. Numerical tests need to be conducted to assess the impact on accuracy of using a variety of interpolation techniques that are available.

More accurate prediction of liquid density

It is well known that the use of cubic equations of state lead to under prediction of liquid mixture densities. The use of a volume correction factor such as that proposed by Peneloux et. al. (1982) as well as other equations of state on density predictions require further investigation. This obviously will have an effect on release rate profiles.

Effect of pipe elevation and fluid structure interaction

The effect of pipe elevation on fluid transients needs to be addressed. Pipe elevations can lead to interesting effects such as slugging which have detrimental effects with regards sudden surges in flowrate at the downstream end.

In the present study, the pipelines have been assumed to be rigid. Often the risers linking subsea wellhead clusters to semi-submersibles or sometimes floating production storage and off-loading systems (FPSO's) are flexible pipes and as a result are prone to the phenomenon of fluid structure interaction. The effect of this with regards to transient fluid flow predictions in flexible pipes needs to be studied.

Other transient flow scenarios

The present model can easily be extended to deal with transient fluid flow in pipe networks, and can also be used to study the effect of other equipment such as pumps and compressors in line.

REFERENCES

Adewumi, M.A. and Zhou, J., "Simulation of transients in natural gas pipelines", *SPE Production and Facilities, SPE 31024*, pp. 202-208, 1996.

Adewumi, M.A., Zhou, J., and Nor-Azian, N., "Transients in wet gas pipelines", *ASME, Fluids Engng. Div.*, Vol. 236, No.1, pp.695-700, 1996.

Allaire, P. E., *Basics of the Finite Element Method: Solid Mechanics, Heat Transfer and Fluid Mechanics*, Wm. C. Brown Publishers, Dubuque, Iowa, 1985.

Ames, W. *F., Numerical Methods for Partial Differential Equations,* 2nd ed., John Wiley & Sons, New York 1977.

Ansari, J. S., "Influence of Including Radial Flow on the Solution of Unsteady Pipe Flow Equations", *Transactions of the ASME*, Paper No. 72-FE-28, 1972.

Assael, M.J., Martin Trusler, J.P, Tsolakis, T., *Thermophysical Properties of Fluids*, Imperial College Press, 1996.

Basset, A.B., *A treatise on Hydrodynamics*, Dover Pub. Ltd., New York, 1961.

Batchelor, G. K., *An Introduction to Fluid Dynamics*, Cambridge University Press, 1992.

Beauchemin, P. and Marche, C., "Transients in Complex Closed-Conduit Systems: Second-Order Explicit Finite Difference Schemes", in "Unsteady Flow and Fluid Transients", Bettess, R. and Watts, J. (Ed.), A. A. Balkema, Rotterdam, pp. 31-39, 1992.

Bedford, A., *Hamilton's Principle in Continuum Mechanics,* Pitman Pub. Ltd., London, 1985

Bell, R.P., "Isopleth Calculations for Ruptures in Sour Gas Pipelines", *Energy Processing/Canada*, pp.36-39. 1978.

Bendiksen, K. H., Malnes, D., Moe, R., and Nuland, S., "The Dynamic Two-Fluid Model OLGA: Theory and Application," *SPE Production Eng.*, pp. 171, May 1991.

Bendiksen, K. H., and Moe, R., "Transient Simulation of 2D and 3D Stratified and Intermittent Two-Phase Flows. PART I: Theory", *Int. J. Num. Meth. Fluids*, Vol. 16, pp. 461, 1993.

Bhallamudi, M. S., and Chaudhry, M. H., "Analysis of Transients in Homogeneous Gas-Liquid Mixtures", in *"Proceedings of the 6th Int. Conf. on Pressure Surges"*, Thorley, A. R. D. (Ed.), BHRA, pp. 343-348, 1990.

Bisgaard, C. Sorensen, H. H. and Spangenberg, S., "A Finite Element Method for Transient Compressible Flow in Pipelines", *Int. J. Num. Meth. Fluids*, 7, pp. 291-303, 1987.

Boldy,A,P., Personal Communication, 1997.

Bond, J., *IChemE Accidents Database*, 1996.

Botros, K. K., Jungowski, W. M. and Weiss, M. H., "Models and Methods of Simulating Gas Pipeline Blowdown", *Can. J. Chem. Eng.*, Vol. 67, pp. 529-539, 1989.

Brent, R.P., *Algorithms for Minimization Without Derivatives*, Prentice Hall, 1973.

Budny, D.D., Wiggert, D.C., and Hatfield, F.J., "Energy Dissipation in the Axially-Coupled Model for Transient Flow", in Thorley, A.R.D., (Ed.), "*Proc. of the 6th Int. Conf. on Pressure Surges*", BHRA, pp.15-26, 1990.

Cebeci, T., and Bradshaw, P., *Physical and Computational Aspects of Convective Heat Transfer*, New York: Springer Verlag, 1984.

Chapman, D.R., "Computational Aerodynamics, Development and Outlook", *AIAA J.*, Vol. 17, pp.1293-1313, 1979.

Chen, C.R., Richardson, S.M., and Saville, G., "Numerical Simulation of Full-Bore Ruptures of Pipelines Containing Perfect Gases", *Trans.IChemE.*, Vol.70, Part B., pp.59-69, 1992.

Chen, J.R., "Modelling of Transient Flow in Pipeline Blowdown Problems", *PhD. Thesis*, University of London, 1993.

Chen, J. R., Richardson, S. M., and Saville, G., "A Simplified Numerical Method for Transient Two-Phase Flow", *Proc. 1993 IChemE Research Event,* Birmingham, 1993, See also *Trans. IChemE,* Vol. 71, Part A, p. 304, 1993.

Chen, J. R., Richardson, S. M., and Saville, G., "Modelling of two-phase Blowdown From Pipelines - I, A Hyperbolic model Based on Variational Principles", *Chem. Eng. Sci.*, Vol. 50, No. 4, pp.695-713, 1995.

Chen, J. R., Richardson, S. M., and Saville, G., "Modelling of two-phase Blowdown From Pipelines - II, A Simplified Numerical Method for Multi-Component Mixtures", *Chem. Eng. Sci.*, Vol. 50, No.13, pp.2173-2187, 1995.

Chen, N.H., "An Explicit Equation for Friction Factor in Pipe", *Ind. Eng. Chem. Fund.*, Vol. 18, No. 3, pp.296-297, 1979.

Cheng, L.C., and Bowyer, J.M., "Tube-Transient Compressible Flow Code", in Papadakis, C., and Scarton, H., (Eds.), "*Fluid Transients and Acoustics in the Power Industry*", Proceedings of the Winter Annual Meeting of the ASME, pp.31-35, 1978.

Courant, R., Friedrichs, K.O., and Lewy, H., "Über die Partiellen Differenzengleichungen der Mathematisches Physik", *Math. Ann.*, Vol. 100, pp. 32-74, 1928.

Courant, R., Isaacson, E., and Reeves, M., 'On the solution of non-linear hyperbolic differential equations by finite differences.' *Comm. on Pure and Applied Mathematics*, Vol. 5, pp.243-55, 1952.

Cronje, J. S., Bishnoi P. B., and Svrcek., W. Y., "The Application of the Characteristic Method to Shock Tube Data That Simulate a Gas Pipeline Rupture", *Can. J. Chem. Eng.*, Vol. 58, p. 289, 1980.

Cullen,W.D., *The public inquiry into the piper alpha disaster,* Dept. of Energy, HMSO, 1990

Edward, A. R., and O'Brien, T. P., "Studies of Phenomena Connected with the Depressurization of Water Reactor" *J. Br. Nucl. Energy Soc.*, 9, 125 1970.

Egely, G., and Saha, P., "A Study of Momentum Transfer in Two-Fluid Formulation of Two-Phase Flow", in Veziroglu, T.N., and Bergles, A.E., (Eds.) "*Multi-Phase Flow and Heat Transfer III. Part A: Fundamentals*", Elsevier Science Publ. pp. 79-101, 1984.

Eichinger, P., and Lein, G., "The Influence of Friction on Unsteady Pipe Flow", in Bettess, J., and Watts, J., "*Unsteady Flow and Fluid Transients*", Balchema, Rotterdam, pp.41-50, 1992.

Fannelop, T. K. and Ryhming, I. L., "Massive Release of Gas From Long Pipelines", *J. of Energy*, Vol. 6. Part 2, pp. 132-140, 1982.

Fashbaugh, R. H., and Widawsky, A., "On the Difference Methods for Shock Wave Propagation in Variable Ducts Including Wall Friction", Naval Civil Engineering Laboratory, Port Heneme, California/ASME, 1972.

Flatt, R., "A Singly-Iterative Second Order Method of Characteristics for Unsteady Compressible One-Dimensional Flows", *Comm. in Applied Num. Meth.*, Vol. 1, pp. 269-274, 1985.

Flatt, R., "On the Application of Numerical Methods of Fluid Mechanics to the Dynamics of Real Gases", *Forschung im Ingenieurwesen*, Vol. 51, No. 2, pp. 41-52, in German (English translation: British Gas Translation No. T07823/BG/LRS/LRST817/86), 1985.

Flatt, R., "Unsteady Compressible Flow in Long Pipelines Following a Rupture", *Int. J. Num. Meth. Fluids*, Vol. 6, pp..83-100, 1986.

Flatt, R., "Unified Approach of Calculation of Monophase and Biphase/Homogeneous Flows of Condensable Pure Fluids", *Revue Entropie*, No. 149, pp. 48-55 (French), 1989.

Flatt, R., "Derivation of the Conservation Equations for Unsteady Quasi-One Dimensional Flow of Real Gases Through Non-Rigid Non-Constant-Area Ducts", Swiss Federal Institute of Technology, Lausanne (unpublished), 1993.

Flatt, R., "The Basic Relation of the γδ Method", Swiss Federal Institute of Technology, Lausanne (unpublished,), 1993.

Flatt, R. and Trichet, J. C., "CFD Oriented Thermodynamics for Single and 2Phase/Equilibrium Flows of Real Gases", *EUROMECH Colloquium 331: Flow With Phase Transition*, Gottingen, 1995.

Foothills Pipe Lines (Yukon)Ltd, "Final Report on the Test Program at the Northern Alberta Burst Test Facility", *Report No. 18031*, 1981.

Friedel, L., "Improved Friction Pressure Drop Correlations for Horizontal and Vertical Two-Phase Flow", *Proc. European Two-Phase Flow Group Meeting,* Ispra, Italy, 1979.

Glaister, P., "An efficient Shock-Capturing Algorithm for Compressible Flows in a Duct of Variable Cross-Section", *Int. J. Num. Meth. Fluids*, Vol. 18, pp. 107-122, 1994.

Guy, J.J., "Computation of unsteady gas flow in pipe networks", *Proc. of Symp. of Efficient Methods for Practising Chemical Engineers*, Symposium Series No. 23, London, Instn. Chem. Engrs. pp.139-145, 1967.

Hall, A. R. W., Butcher G. R. and Teh C. E., "Transient Simulation of Two-Phase Hydrocarbon Flows in Pipelines", *Proc. European Two-Phase Flow Group Meeting,* Hannover, June 6-10, 1993.

Hanel, D., and Schroder, W., "An unfactored implicit scheme with multigrid acceleration for the solution of the Navier-Stokes equations", *Computers & Fluids*, Vol.15, No.3, pp.313-336, 1987.

Heath,M.J. and Blunt, J.C., 'Dynamic simulation applied to the design and control of a pipeline network', *Inst. Gas Eng. J.,* Vol. 9, No. 4, pp.261-279, 1969.

Hirose, M., "Frequency-Dependent Wall Shear in Transient Fluid Flow: Simulation of Unsteady Turbulent Flow", *MSc. Dissertation*, Massachusetts Institute of Technology, 1971.

Hirsch, C., *Numerical Computation of Internal and External Flows*, Vols. 1 & 2, J. Wiley & Sons, 1995.

HMSO, *A Guide to Offshore Installation (Safety case) Regulations*, 1992.

HMSO, *The Offshore Installations Emergency Pipeline Valve Regulations, Statutory Instruments*, 1989.

Holmboe, E. L. and Rouleau, W. T., "The Effect of Viscous Shear on Transients in Liquid Lines," *ASME J. Basic Eng.,* 89, 174 1967.

Holt, M., *Numerical Methods in Fluid Dynamics*, 2nd Edition, Springer-Verlag, Berlin, 1984.

Hsu, Y-Y., and Graham, R.W., *Transport Processes in Boiling and Two-Phase Systems*, Hemisphere Publishing Corporation, 1976.

Huang, W. and Sloan, D. M., "A New Pseudospectral Method With Upwind Features", *IMA. J. of Num. Anal.,* Vol. 13, pp. 413-430, 1993.

Idsinga, W., Todreas, N., and Bowring, R., "An Assessment of Two-Phase Pressure Drop Correlations for Steam Water Systems", *Int. J. Multiphase Flow*, Vol. 3, pp. 401-413, 1979.

Iserles, A., *Numerical Analysis of Differential Equations*, Cambridge University Press, Cambridge, 1996.

Jones, D.G., and Gough, D.W., "Rich Gas Decompression Behaviour in Pipelines", *AGA-EPRG Linepipe Research Seminar IV*, Duisberg, British Gas, Report No. ERS E 293, 1981.

Kagawa,T, Matsumoto, N., and Furukawa, S., "High Speed and Accurate Computing Method of Frequency Dependent Friction in Laminar Pipe Flow for Characteristics Method", JSME, Vol. 49, (447), pp. 26- 38 (Japanese), 1983.

Kieffer, S.W., "Sound speed in liquid-gas mixtures: water-air and water-steam", *Journal of Geophysical Research*, Vol. 82, No. 20, pp. 2895-2904, 1977.

Kimambo, C. Z. M., and Thorley, A., "Computer Modelling of Transients Ruptured High Pressure Natural Gas Pipelines: A Review of Experimental and Numerical Studies", C502/003, IMECHE, 1995.

Knox, H.W., Atwell, L.D., Angle, R., Willoughby, R., and Dielwart, .J., "Field Verification of Assumptions for Modelling Sour Gas Pipelines and Well Blowouts", *Petroleum Society of CIM*, Paper No. 80-31-46, 1980.

Koetzier, H., Kruisbrink, A.C.H., and Lavooij, C.S.W., "Dynamic behaviour of large non-return valves", in *Proc. of the 5th International Conference on Pressure Surges*, Hannover, F.R. Germany: 22-24 Sept., BHRA, pp.237-243, 1986.

Kunsch, J.P., Sjøen, K., and Fannelop, T.K., "Loss Control by Subsea Barrier Valve for Offshore Gas Pipeline", *23rd Annual Offshore Tech. Conf.*, Houston, Texas, OTC 6616, 1991.

Kunsch, J.P., Sjøen, K., and Fannelop, T.K., "Simulation of Unsteady Flow, Massive Releases and Blowdown of Long High Pressure Pipelines", *Int. Gas Conf.*, Cannes, France, 1995.

Kutler, P., "A perspective of theoretical and applied computational fluid Dynamics", *AIAA Paper 83-0037*, AIAA 21st Aerospace Sciences Meeting, 1983.

Lang, E., "Gas Flow in Pipelines Following a Rupture Computed by a Spectral Method", *J. Appl. Maths and Physics* (ZAMP), Vol. 42, pp. 183-197, 1991.

Lang, E., and Fannelop, T.K., "Efficient Computation of the Pipeline Break Problem", in Dodge, F.T., and Moody, F.J., (Eds.), "*Fluids Transients in Fluid Structure Interaction*", FED 56, ASME, pp. 115-123, 1987.

Lavooij, C.S.W, and Tijsseling, A.S., "Waterhammer with Fluid-Structure Interaction", *App. Scientific Research*, Vol.47, No.3, pp.273-285, 1990.

Lavooij, C.S.W, and Tijsseling, A.S., "Fluid-Structure Interaction in Liquid-Filled Piping Systems", *J. of Fluids and Structures*, Vol.5, No.5, pp.573-595, 1991.

Lax, P.D., 'Weak solutions of non-linear hyperbolic equations and their numerical computation' *Comm. on Pure and Applied Mathematics*, Vol. 7, pp.159-93, 1954.

Lax, P.D., and Wendroff, B., 'Difference schemes for hyperbolic equations with high order of accuracy.' *Comm. on Pure and Applied Mathematics*, Vol. 17, pp.381-98, 1964.

Le Balleur, J.C., "Progres Dans le Calcul del'Interaction Fluide Parfait-Fluide Visqueux", *AGARD Conf. Proc. CP 351 on Viscous Effects in Turbo Machines*, 1983.

Lee, C.L., Jocson, A.T., and Hsu, S.T., "On the dynamic performance of large check valves", in *Unsteady Flow and Fluid Transients*, Bettess & Watts (eds), Balkema pub. pp.365-369, 1992.

LeVeque, R. J., *Numerical Methods for Conservation Laws,* Birkhauser, Basel, 1990.

Liepman, H. W., and Roshko, A., *Elements of Gasdynamics*, John Wiley & Sons, 1957.

Liou, M.S., and Steffen, C.J., "A new flux splitting scheme", *J. of Comput. Phys.*, Vol.107, No.1, pp.23-39, 1993.

Lister, M., "The Numerical Solution of Hyperbolic Partial Differential Equations by the Method of Characteristics", in Ralston A., and Wilf, H.S., (Eds.), *"Mathematical Methods for Digital Computers"*, John Wiley & Sons, pp.165-179, 1960.

Lyczkowski, R. W., D. Gidaspow, C. W. Solbrig and E. D. Hughes, "Characteristics and Stability Analysis of Transient One-Dimensional Two-Phase Flow Equations and Their Finite Difference Approximations", *Nucl. Sci. Eng.*, Vol. 66, p. 378, 1978.

Lyczkowski, R. W., R. A. Grimesey and C. W. Solbrig, "Pipe Blowdown Analyses Using Explicit Numerical Schemes", *AIChE Symp. Ser.* 74, No. 174, 129, 1978.

MacCormack, R.W., "The Effect of Viscosity in Hypervelocity Impact Cratering", *AIAA Paper 69-354*, 1969.

Massey, B. S., *Mechanics of Fluids,* Van Nostrand Reinhold Co. Ltd., Wokingham 1983.

Michelsen, M.L., "The Isothermal Flash Problem. Part I. Stability", *Fluid Phase Equil.*, Vol. 9, pp.1-19, 1982.

Michelsen, M.L., "The Isothermal Flash Problem. Part II. Phase-Split Calculation", *Fluid Phase Equil.*, Vol. 9, pp.21-40, 1982.

Michelsen, M.L., "Multi-Phase Isenthalpic and Isentropic Flash Algorithms", *Fluid Phase Equil.*, Vol. 33, pp.13-27, 1987.

Morrow, T., Southwest Research Institute, San Antonio, Texas, "Private Communication", 1997.

Morton, K.W., and Mayers, D.F., Numerical Solution of Partial Differential Equations, Cambridge University Press, Cambridge, 1994.

Nakamura, S., Berger, M.A., and Spencer, A.C., "One-Dimensional Implicit Characteristic Method For Compressible Two-Phase Coolant Flow", *Proc. of the Conf. on Comp. Methods in Nuclear Eng.*, NTIS conf-750413, American Nuc. Soc., April 15-17, 1995.

Oliemans, R. V. A., "Modelling of Two-Phase Flow of Gas and Condensate in Horizontal and Inclined Pipes", Paper presented at the *6th ASME Annual Pipeline Engineering Symposium*, Dallas., 1987.

Olorunmaiye, J.A., and Imide, N.E., "Computation of Natural Gas Pipeline Rupture Problems Using the Method of Characteristics", *J. of Hazardous Materials*, Vol.34, pp.81-98, 1993.

Osiadacz, A., 'Optimal numerical methods for simulating dynamic flow of gas in pipelines', *Int. J. Num. Methods in Fluids*, 3, pp.125-135, 1983.

Osiadacz, A. J. and Yedroudj, M., "A Comparison of a Finite Element Method and a Finite Difference Method for Transient Simulation of a Gas Pipeline", *Appl. Math. Modelling*, Vol. 13, pp 79-85, 1989.

Otwell, R. S., Wiggert, D. C., and Hatfield, F. J., "The Effect of Elbow Restraint on Pressure Transients", *J. of Fluids Eng.*, Vol. 107, No. 3, ASME, 1985.

Padmanabhan, M., Ames, W.F., and Martin, C.S., "Numerical analysis of pressure transients in bubbly two-phase mixtures by explicit-implicit methods", *J. Eng. Maths.* Vol. 12, No. 1, pp.83-93, 1978.

Pandolfi, M., "Computation of Steady Supersonic Flows by a Flux-Difference Splitting Method", *Computers & Fluids*, Vol.13, No.1, pp.37-46, 1985.

Pandolfi, M., and Botta, N., "Upwind formulations for the Euler equations in steady supersonic flows", *AIAA J.*, Vol.27, No.3, pp.293-298, 1989.

Peneloux, A., Rauzy, E., and Freze, R., "A Consistent Correction for Redlich-Kwong-Soave Volumes", *Fluid Phase Equil.*, Vol. 8, pp. 7-23, 1982.

Peng, D., and Robinson, D. B., "A New Two-Constant Equation of State," *Ind. Eng. Chem. Fund.*, 15, 59, 1976.

Perko, H.D., "Check valve dynamics in pressure transient analysis", in "*Proc. of the 5th Int. Conf. on Pressure Surges*, Hannover, F.R. Germany: 22-24 Sept., BHRA, pp.229-236. 1986

Perry, R.H., and Green, D.W., *Perry's Chemical Engineers Handbook*, 7th Edition, Mc graw Hill, 1997.

Philbin, M. T., and Govan, A. H., "PipeLine Analysis Code", *UKAEA Report AEA-APS 0031*, 1990.

Picard, D. J., and Bishnoi, P. R., "Calculation of the Thermodynamic Sound Velocity in Two-Phase Multi-Component Fluids", *Int. J. Multiphase Flow*, Vol. 13, No. 3, pp 295-308, 1987.

Picard, D.J., and Bishnoi, P.R., "The Importance of Real-Fluid Behaviour and Non-Isentropic Effects in Modelling Compression Characteristics of Pipeline Fluids for Application in Ductile Fracture Propagation Analysis", *Can. J. Chem. Eng.*, Vol. 66, pp. 3-12, 1988.

Picard, D. J., and Bishnoi, P. R., "The Importance of Real-Fluid Behaviour in Predicting Release Rates Resulting From High Pressure Sour-Gas Pipeline ruptures", *Can. J. Chem. Eng.*, 67, pp. 3-9, 1989.

Press, H.W., Teukolsky, S.A., Vetterling, W.T., and Flannery, B.P., *Numerical Recipes in Fortran*, 2nd Edition, Cambridge University Press, 1994.

Pulliam, T.H., and Steger, J.L., "Implicit Finite Difference Simulations of Three-Dimensional Flows", *AIAA Paper 78-10*, 16th Aerospace Sciences Meeting, 1978.

Rachford, H.H. Jr., and Dupont, T., "A Fast Highly Accurate Means of Modelling Transient Flow in Gas Pipeline Systems by Variational Methods", *Soc. Pet. Eng., J.*, Vol. 14, pp.165-178, 1974.

Rachid, F. B. F, and Stuckenbruck, S., "Transients in Liquid and Structure in Viscoelastic Pipes", in Thorley, A. R. D. (Ed.), "Proc. of the 6th Int. Conf. on Pressure Surges", BHRA, pp.69-84, 1990.

Richardson, S. M., and Saville, G., "Blowdown of Pipelines", *Soc. Pet. Engineers, SPE 23070*, pp. 369-377, 1991.

Richardson, S. M., and Saville, G., "Blowdown of LPG Pipelines", *Process Safety and Environmental Protection: Trans. of the Institution of Chem. Engineers, Part B*, Vol.74, No.4, pp.235-244, 1996.

Reid, R.C, Prausnitz, J.M., and Sherwood, T.K., *The properties of Gases and Liqiuds*, 4th Edition, McGraw-Hill Book Company, 1986.

Richtmyer, R.D., "Difference Methods for Initial-value Problems", *Interscience Tracts in Pure and Applied Mathematics*, No. 4, Interscience Publishers, Inc., New York, 1957.

Rund, H., *The Hamilton-Jacobi Theory in The Calculus of Variations,* Van Nostrand Reinhold Co. Ltd., London, 1966.

Salmon, R., "Hamiltonian Fluid Mechanics," *Ann. Rev. Fluid Mech.,* 20, 225, 1988.

Schlichting, H., *Boundary Layer Theory*, New York: McGraw-Hill, 1971.

Sens, M., Jouve, P. and Pelletier, R., "Detection of a Break in a Gas Line", *Proc. of the 11th Int. Gas Conf.*, Moscow, Paper No. IGU/C37-70, in French, (English Translation: British Gas, Translation No. BG. TRANS 4910). 1970

Shimida, M., "Time Marching Approach for Pipe Steady Flows", *J. Hydraul. Div., ASCE*, Vol. 114, No. HY11, pp. 1301-1320, 1988.

Shin, Y. W., "Two-Dimensional Fluid Transient Analysis by the Method of Characteristics", in "*Fluid Transients and Acoustics in the Power Industry*", Papadakis C. and Scarton H. (Ed.), ASME, New York, pp. 179-185, 1978.

Simpson, A.R., and Bergant, A., "Interesting lessons from column separation experiments", in *7th International Conference on Pressure Surges and Fluid Transients in Pipelines and Open Channels*, Ed. A. Boldy, BHR Group Conference Series, No. 19, 1996.

Smith, J.M., Van Ness, H.C., and Abbott, M.M., "Introduction to Chemical Engineering Thermodynamics", 5th Edition, McGraw Hill Chem. Eng. Series, 1996

Soave, G., "Equilibrium Constants From a Modified Redlich-Kwong Equation of State", *Chem. Eng. Sci.,* Vol. 27, pp.1197-1203, 1972.

Stadtke, H., and Holtbecker, R., "Hyperbolic Model for Inhomogeneous Two-Phase Flow", *Proc. Third Int. Conf on Multiphase Flow '91,* Tsukuba, Japan, September 24-27, 1991.

Steger, J.L., "Implicit Finite Difference Simulations of Flows About Arbitrary Geometries", *AIAA J.* Vol. 16, pp. 679-686, 1978.

Steger, J.L., and Warming, R.F., "Flux Vector Splitting of the Inviscid Gas-Dynamic Equations With Application to Finite Difference Methods", *J. Comp. Physics*, Vol. 40, pp. 263-293, 1981.

Stittgen, M. and Zielke, W., "Fluid Structure Interaction in Flexible Curved Pipes", in "*Proc. of the 6th Int. Conf. on Pressure Surges*", Thorley, A. R. D. (Ed.), BHRA, pp. 101-120., 1990.

Suwan, K., and Anderson, A., "Method of Lines Applied to Hyperbolic Fluid Transient Equations", *Int. J. Num. Meth. Eng.*, Vol. 33, pp. 1501-1511, 1992.

Swaffield, J.A., and Boldy, A.P., *Pressure Surge in Pipe and Duct Systems*, Ashgate Publishing Limited, Vermont, USA, 1993.

Taylor, B.A., "The Flow in Pipelines Following Catastrophic Failure", *British Gas Internal Report LRS 338*, 1978.

Thomas, J.L., Van Leer, B., and Walters, R.W., "Implicit flux-split schemes for the Euler equations", *AIAA J.*, Vol.28, No.6, pp.973-974, 1990.

Thorley, A.R.D., "Check valve behaviour under transient flow conditions: A state-of-the-art review", *Transactions of the ASME, Journal of Fluids Engineering,* Vol.111, pp. 178-183, 1989.

Thorley, A.R.D., *Fluid transients in pipeline systems: a guide to the control and suppression of fluid transients in liquids in closed conduits*, D & L George, Barnet, England, 1991.

Thorley, A.R.D., and Tiley, C.H., "Unsteady and Transient Flow of Compressible Flows in Pipelines - A Review of Theoretical and Some Experimental Studies", *Int. J. of Heat and Fluid Flow*, Vol.8, No.1, pp.3-15, 1987.

Tiley, C.H., "Pressure Transients in a Ruptured Gas Pipeline With Friction and Thermal Effects Included", *PhD Thesis*, City University, London, 1989.

Trikha, A. K., "An Efficient Method for Simulating Frequency-Dependent Friction in Transient Liquid Flow", *ASME J. Fluid Eng.*, Vol. 97, p. 97 1975.

Tullis, J.P., Streeter, V.L., and Wylie, E.B., "Waterhammer Analysis with Air Release", *Proc. of the 2nd Int. Conf. on Pressure Surges*, BHRA, Bedford, England, Sept. 22-24, 1976.

Van Deen, J. K., and Reintsema, S.R., "Modelling of High Pressure Gas Transmission Lines", *App. Math. Modelling*, Vol.7, No.4, pp.268-273, 1983.

Van Leer, B., "Towards the Ultimate Conservative Difference Scheme IV. A New Approach to Numerical Convection", *J. Comput. Physics.*, Vol. 23, pp. 276-299, 1977.

Vardy, A.E., "On the Use of the Method of Characteristics For the Solution of Unsteady Flows in Networks", in *Proc. 2nd Int Conf on Pressure Surges and Fluid Transients*, London, 22-24 Sep., Paper H2, 1977.

Vardy, A.E., and Brown, J.M.B., "Transient, Turbulent, Smooth Pipe Friction", *J. Hydr. Res.*, Vol. 33, pp. 435-456, 1995.

Vardy, A.E., and Brown, J.M.B., "On turbulent, unsteady, smooth-pipe friction", *Proc. 7th Int Conf on Pressure Surges and Fluid Transients*, Harrogate, 16-18 April, pp289-311, BHRA Group, 1996.

Vardy, A.E., and Chen, L.I., "Rapidly Attenuated Waterhammer and Steel Hammer", Paper A1, in *Proc. of the 4th International Conference on Pressure Surges*, BHRA, Bath, England, pp. 1-12, 1983.

Vardy,A.E., KuoLun, H., and Brown, J.M.B., "Weighting function model of transient turbulent pipe friction", *J. of Hyd. Res.*, Vol.31, No.4, pp.533-544, 1993.

Welty, J. R., Wicks, C.E., and Wilson, R.E., *Fundamentals of Momentum, Heat, and Mass Transfer*, 3rd Edition, J. Wiley & Sons, 1984.

White, F.M, *Fluid Mechanics*, 2nd Ed., McGraw Hill, New York, 1988.

Wiggert, D.C., and Sundquist, M.J., "The Effect of Gaseous Cavitation on Fluid Transients", *J. Fluids Eng., ASME*, pp. 79-86,1979.

Wood, D. J., and Funk, J. E., "A Boundary Layer Theory for Transient Viscous Losses in Turbulent Flow", *ASME J. Basic Eng., Vol. 92, p. 865,* 1970.

Wylie, E.B., "Advances in Use of MOC in Unsteady Pipeline Flow", in *Proc. of the 4th Int. Conf. on Pressure Surges*, BHRA, Bath, England, 1983.

Wylie, E.B., and Streeter, V.L., *Fluid Transients*, McGraw-Hill Inc., USA, 1978.

Wylie, E.B., and Streeter, V.L., *Fluid Transients in Systems*, Prentice-Hall, New Jersey, USA, 1993.

Wylie, E.B., Personal Communication, 1997.

Wylie, E.B., Stoner, M.A., and Streeter, V.L., "Network System Transient Calculations by Implicit Methods", *Soc. Pet. Eng. J., Trans. AIME*, Vol. 11, pp. 356-362, 1971.

Yigang, C., and Jing-Chao, S., "An Efficient Approximate Expression For Transient Flow of High Viscous Fluid in Hydraulic Pipelines", in *Proc. of the 6th Int. Conf. on Pressure Surges*, BHRA, pp. 15-26, 1990.

Zha, G.C and Bilgen, E, "Numerical-solutions of Euler equations by using a new flux vector splitting scheme", *Int. J. Num. Methods in Fluids*, Vol.17, No.2, pp.115-144, 1993.

Zha, G.C and Bilgen, E, "Numerical study of 3-dimensional flows using unfactored upwind-relaxation sweeping algorithm", *J. of Comput. Phys.*, Vol.125, No.2, pp.425-433, 1996.

Zielke, W., "Frequency-Dependent Friction in Transient Pipe Flow", *ASME J. Fluid Eng.*, Vol. 90, p. 109, 1968.

Zigrang, D.J., and Sylvester, N.D., "A Review of Explicit Friction Factor Equations", *J. Energy Res. Tech., Trans. ASME*, Vol. 107, No. 2, pp. 280-283, 1985.

Zucrow, M.J., and Hoffman, J.D., *Gas Dynamics*, Vols. I and II, New York; John Wiley and Sons, 1976.